DRL-58-DRD-SC 7

9950-797

DOE/JPL 954373 - 81/19
Distribution Category UC-63

SILICON INGOT CASTING - HEAT EXCHANGER METHOD MULTI-WIRE SLICING - FIXED ABRASIVE SLICING TECHNIQUE

Phase III - Phase IV

Silicon Sheet Growth Development for the
Large Area Sheet Task of the Low-Cost Solar Array Project

FINAL REPORT

BY

FREDERICK SCHMID AND CHANDRA P. KHATTAK

Covering Period from December 15, 1978 to June 30, 1981
JPL Contract No. 954373

CRYSTAL SYSTEMS INC.
Shetland Industrial Park, 35 Congress Street, Salem, Mass. 01970

DRL-58-DRD-SE-7

DOE/JPL 954373 - 81/19
Distribution Category U-63

SILICON INGOT CASTING - HEAT EXCHANGER METHOD (HEM)

MULTI-WIRE SLICING - FIXED ABRASIVE SLICING TECHNIQUE (FAST)

PHASE III AND PHASE IV

Silicon Sheet Growth Development for the
Large Area Sheet Task of the
Low-Cost Solar Array Project

FINAL REPORT

by

Frederick Schmid and Chandra P. Khattak

Covering Period from December 15, 1978 to June 30, 1981

Report Issued: December 1982

JPL Contract No. 954373

CRYSTAL SYSTEMS, INC.
35 Congress Street
Salem, MA 01970

The JPL Low-Cost Solar Array Project is sponsored by the U. S. Department of Energy and forms part of the Solar Photovoltaic Conversion Program to initiate a major effort toward the development of low-cost solar arrays. This work was performed for the Jet Propulsion Laboratory, California Institute of Technology by agreement between NASA and DOE.

This report contains information prepared by Crystal Systems, Inc., under JPL subcontract. Its content is not necessarily endorsed by the Jet Propulsion Laboratory, California Institute of Technology, National Aeronautics and Space Administration or the U. S. Department of Energy.

PREFACE

This Final Report covering Phases III and IV of JPL Contract No. 954373 has three parts:

Part I - Silicon Ingot Casting - Heat Exchanger Method (HEM)

Part II - Multi-Wire Slicing - Fixed Abrasive Slicing Technique (FAST)

Part III - Papers and Publications.

The technical reports comprising Parts I and II are completely independent. Part III pertains to both HEM and FAST.

ACKNOWLEDGMENT

Frederick Schmid was Program Manager and Dr. Chandra Khattak was Principal Investigator for the HEM/FAST Program carried out under JPL Contract No. 954373. JPL Technical Monitors during Phase III and Phase IV were Dr. Katherine Dumas, Dr. James Liu and Dr. Andy Morrison.

The authors acknowledge the significant contributions many individuals have made to the work reported on in this volume. Technical personnel directly involved with the project were:

Dr. Metin Basaran
John Lesiczka
Lawrence Lynch
Anthony Pasquale
Maynard Smith

Special thanks are expressed to Peter Johnson, who served as Contract Administrator, and to Vernon Kousky for assistance with technical and design requirements. Merle Larson of JPL was Contract Negotiator Specialist for both Phase III and IV of the Program.

Appreciation is expressed to Peggy Hawes for coordinating production of technical reports, and to all of the administrative, technical and clerical personnel at Crystal Systems who contributed to the success of this Program.

PART I

SILICON INGOT CASTING - HEAT EXCHANGER METHOD (HEM)

PART I

TABLE OF CONTENTS

I-ii INTENTIONALLY BLANK

PART I

LIST OF FIGURES

PART I

LIST OF TABLES

PART I

ABSTRACT

At the conclusion of the present program it has been demonstrated that directional solidification by the Heat Exchanger Method (HEM) is a viable approach for directional solidification of silicon ingots to be used for terrestrial solar cell applications. Some of the significant advances made during this phase of the program have been:

Ingot size -- 34 cm x 34 cm x 17 cm - 45 kg
Useable material yield - > 90%
Solar cell efficiency averaged over the whole ingot - 85% of control CZ (35 kg ingot)
Very uniform resistivity over the boule
Cycle time for 36 kg ingots - 56 hours

Some of the problems encountered have been growth rate decrease with increased ingot height, silicon carbide precipitates, and high dislocation density in HEM material. The silicon carbide is attributed to backstreaming of oil vapors from the vacuum pump; the high dislocation density is associated with the thermal history of the boule.

Using solar metallurgical meltstock nearly single crystal structure has been achieved with one HEM directional solidificiation. Solar cells fabricated using this meltstock have shown up to 12.33% conversion efficiency.

The projected add-on cost of HEM processing using the best simultaneous achievements is $\$17.39/m^2$--well within the allocation of $\$18.15/m^2$ for 1986 goals.

I-x INTENTIONALLY BLANK

PART I

SILICON INGOT CASTING - HEAT EXCHANGER METHOD (HEM)

1.1 INTRODUCTION

The adaptation of the Heat Exchanger Method (HEM) for growth of silicon crystals was started in November 1975. Within the two-year Phase I of the DOE/JPL contract #954373 the proof of concept was established. In the one-year Phase II program square cross-section ingots were grown with a high degree of single crystallinity. In Phase II, 10 cm x 10 cm cross-section 3.3 kg ingots were solidified.

During the one-year Phase III program, the process was scaled up to 22 cm x 22 cm cross-section, 16.5 kg ingot. This increase in mass of ingots by a factor of 5 did not show any deterioration in the quality of material and the 90% degree of single crystallinity was maintained. At this time the limits of size capability of the laboratory furnace was reached.

The Phase IV period involved design, fabrication and testing of a prototype furnace capable of directional solidification of 30 cm cube ingots. No problems were encountered with such a large production unit. The concept of using unpurified graphite parts[1] and removing the impurities during initial bakeout at high temperatures was established and has been used routinely without degradation of the silicon material quality. Using this furnace the size of the ingots was scaled up to 34 cm x 34 cm x 17 cm, 45 kg mass. During the entire scaleup period involving different size crucibles the heat treatment to develop a graded structure in crucibles was optimized. This prevented cracking of silicon ingots during the cooldown cycle.[2]

The concept of welding flat plate silica crucibles to solidify silicon ingots with very square corners was established.[3] Even though this approach gives a very high yield of square silicon ingots, it may not lend itself to an easy production process. A one-piece molded crucible with square corners was developed to solidify silicon ingots with 32 cm square cross-section. Using these crucibles more than 90% yield of usable material has been demonstrated.[4]

The unique feature of submerged solid-liquid in the HEM allows use of low-purity meltstock. It has been demonstrated that nearly single crystal structure can be achieved with one HEM directional solidification using solar metallurgical meltstock. Solar cells fabricated using a double HEM solidification have shown 12.33% conversion efficiency.[5]

While scale-up in size was in progress, very limited characterization was carried out on HEM material. Two complete boules, approximately 36 kg in mass, were delivered to JPL for characterization. It was found that the resistivity was very uniform throughout the ingot and the average oxygen concentration was lower than found in CZ material. The overall efficiency in one 35 kg ingot of the usable material averaged throughout the ingot was 85% of the control cell CZ material. It was established that the large grain polycrystalline HEM is comparable in efficiency to the single crystal HEM material. This first thorough characterization of the non-optimized HEM material demonstrates that the HEM material has great promise for use in the solar cell industry.

HEM material is substantially monocrystalline; it is not completely single crystal because there is a subtle heat flow problem associated with solidification and movement of such a large interface. Another problem is silicon carbide precipitates have been observed in HEM material. The silicon carbide has been attributed to backstreaming of oil vapors from the vacuum pump. The high dislocation density seen in

some material can be explained by the thermal history of the ingot; however, the complete cycle for HEM processing needs to be optimized.

Projected add-on cost calculations using IPEG analysis and best simultaneous achievements have shown that HEM processing will be $\$17.39/m^2$. This compares with the allocation of $\$18.15/m^2$.

1.2 CRYSTAL GROWTH

1.2.1 Heat Exchanger Method (HEM)

The Heat Exchanger Method (HEM) is a crystal growth process which is being used for commercial production of large sapphire and silicon crystals. It is a simple directional solidification technique in which an ingot is solidified in a crucible by controlling the thermal gradients in the solid and liquid without moving the crucible, heat zone or crystal.

A typical furnace setup is shown in Figure 1. The crucible with the seed centered at the bottom is loaded with meltstock and placed on top of the heat exchanger. After evacuation to about 0.1 torr, heat is supplied by the graphite heater and the charge is melted. The seed is prevented from melting by forcing gaseous helium through the heat exchanger. After sufficient meltback of the seed is achieved, growth is advanced by increasing the flow of helium and thereby decreasing the heat exchanger temperature. The liquid gradients are controlled by the furnace temperature while those in the solid by the heat exchanger temperature. The HEM is the only crystal growth process in which independent liquid and solid gradients are achieved during most of the crystal growth stage without any movement. After the crystal is grown it is still in the heat zone and can be annealed and cooled at a controlled rate to relieve solidification stresses. This unique capability allows the growth of very large crystals without cracking due to thermal stresses associated with such large sizes.

Another distinguishing feature of the HEM -- compared with other crystal growth processes such as CZ, EFG and Dendritic Web -- is the submerged solid-liquid interface. It is submerged beneath the surface and is surrounded by the melt. There are two distinct advantages associated with the positio[illegible]f the interface. Firstly, the light impurities, and

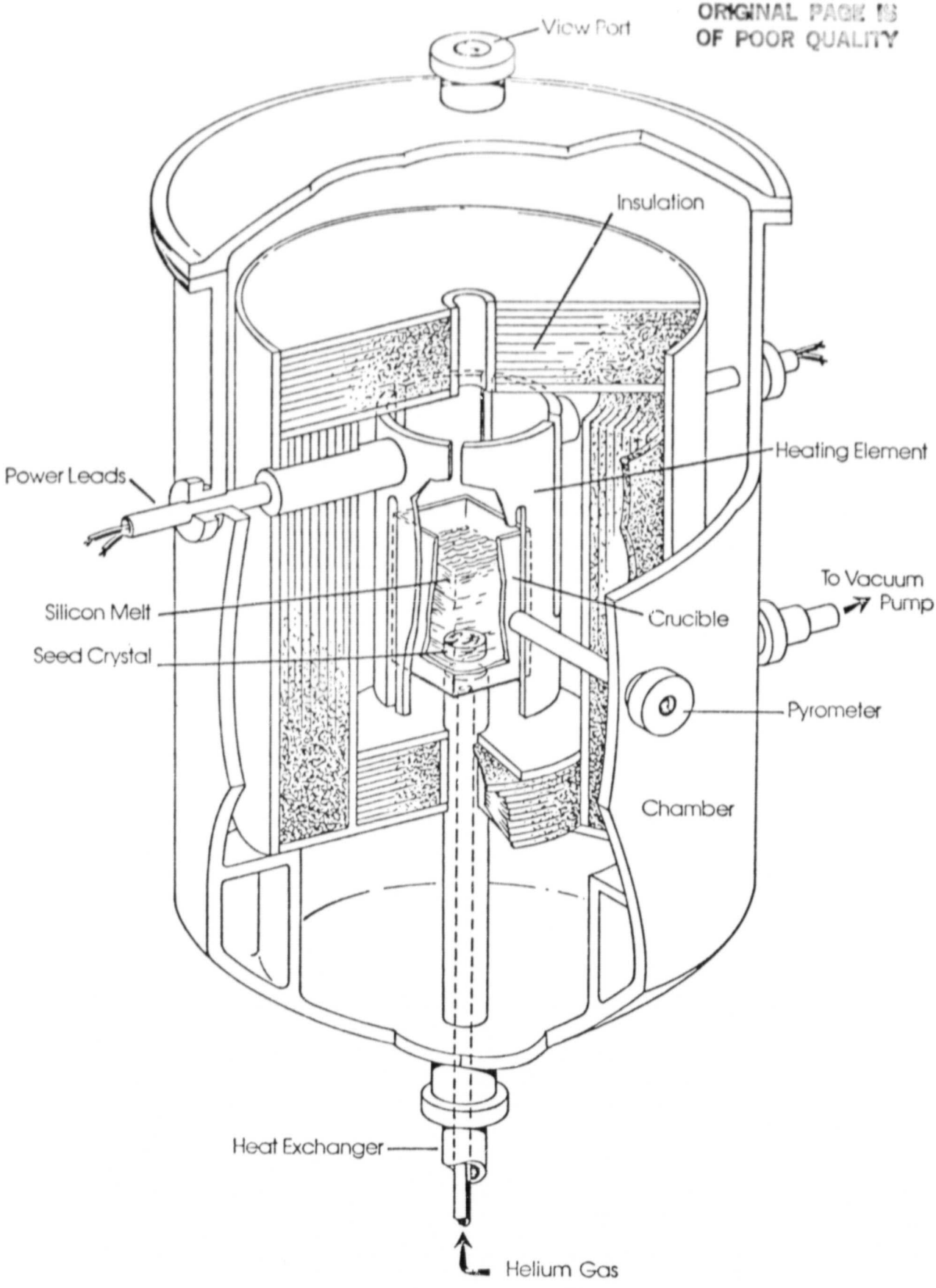

Figure 1. Schematic of HEM Furnace

even heavier impurities because of their particle morphology, float to the surface of the melt and do not disturb the growing solid-liquid interface.[6] Secondly, the temperature gradients at the interface in HEM are uniform because of the surrounding liquid mass. In other crystal growth processes the interface is at the melt surface where the local gradients vary sufficiently to cause solidification and remelting of the crystal.[7] These features are partly responsible for HEM material showing consistently better solar cell performance as compared to CZ using lower-purity meltstocks.[8]

In casting or Bridgman techniques[9,10] the first material to solidify is near the walls of the crucible and the last material to freeze containing the segregated impurities is in the region near the center and top surface of the ingot. This contaminated material cannot be easily removed without affecting the yields considerably. In comparison, the HEM crystals are grown from the inside out so that the last material to solidify is near the crucible wall. To maintain dimensional accuracy in production, trimming of the ingot can remove only the outer impure material.

In addition to the foregoing advantages, other technical advantages of HEM are as follows:

(i) Purification of meltstock by directional solidification

(ii) Square shaped crystals are grown

(iii) Simplicity of equipment and process

(iv) Ability to produce square ingots[11] to produce high array-packing efficiency of solar cells

(v) The submerged solid-liquid interface ensures no steep gradients; hence, less solidification stresses are set up in the growing crystal

(vi) Scale-up can use the same equipment for various sizes of crystals

(vii) Because of vacuum operation the average oxygen content in HEM silicon is lower than CZ-grown material[4]

(viii) Solar cells fabricated from the best HEM silicon have shown comparable performance to CZ cells[11]

Besides the above technical advantages, the economic advantages of HEM are low-cost equipment, labor, energy and expendable materials.

1.2.2 Silicon Crystal Growth by HEM

In November 1975 HEM was chosen by DOE/JPL for adaptation to grow silicon crystals for terrestrial photovoltaic applications. This choice was made mainly because of the potential low cost of the process. Within a period of two years technical feasibility was established.[11] It was demonstrated that square silicon crystals of 10 cm x 10 cm cross-section can be produced with over 90% single crystallinity. The solar cell performance of the best HEM material was comparable to that of Czochralski-grown silicon.

During Phase III of the program (December 1978 through December 1979) emphasis was placed on scale-up in the size of the ingots and evaluation of material quality. Phase IV of the program (December 1979 through June 1981) involved establishing technology readiness, characterization of the ingots and studying the utilization of the boules.

It has been demonstrated[4] that large, square cross-section ingots up to 45 kg in mass with dimensions of approximately 34 cm x 34 cm x 17 cm can be solidified by HEM. The overall efficiency of the usable material averaged throughout one 35 kg ingot is 85% of the control cell CZ material using baseline cell processing techniques. Further, it has been seen that large grain polycrystalline HEM is comparable in efficiency to the single crystal HEM material.

Previous work[11] had demonstrated growth of 15-cm diameter and 10 cm x 10 cm square ingots of up to 3.3 kg. Initial scale-up efforts during the current period were focussed on 20-cm diameter ingots pending custom fabrication of square cross-section crucibles. Figure 2 shows a 6.3 kg, 20-cm diameter ingot solidified by HEM in run 315-C (details in Appendix I-A.)

One of the advantages of HEM is its simplicity. This allows easy scale-up in size and use of different shapes of crucibles. Figure 3 shows the first ingot cast in a

Figure 2. View of ingot cast in run 315-C

17 cm x 17 cm size, 4.5 kg, in run 329-C. The next scale-up attempt was to 8.1 kg, 17 cm x 17 cm cross-section. The ingot is shown in Figure 4 as removed from the furnace with the adherent silica layer as cast in run 331-C.

The first ingot of 22 cm x 22 cm cross-section, 10.5 kg, was cast in run 354-C. Figure 5 shows the ingot after removal of the delaminated silica crucible. The largest size ingot produced by HEM in 22 cm x 22 cm cross-section was 18 cm high and weighed 16.5 kg. A number of such ingots were directionally solidified and a typical example is shown in Figure 6 from run 365-C.

During the one-year period of Phase III the ingot size was scaled up from approximate dimensions of 10 cm x 10 cm x 12 cm, 3.3 kg, to 22 cm x 22 cm x 18 cm, 16.5 kg -- an increase by a factor of 5. This scale-up is also apparent from the size of the crucibles used. Figure 7 shows the three sizes of crucibles used during this scale-up.

So far all the ingots were grown using the same experimental furnace. A new furnace was necessary to solidify larger square cross-section ingots. A prototype furnace was designed and fabricated to solidify ingots up to dimensions 30 cm x 30 cm x 30 cm. A microprocessor control was incorporated to program the furnace temperature and the helium flow. An overall view of this new furnace is shown in Figure 8. After an initial evaluation experiment with a 17 cm x 17 cm cross-section ingot was directionally solidified in this furnace (Run 41-02). Figure 9 shows the ingot as removed from the furnace with the adherent silica layer.

The next larger ingot solidified was 20 kg in mass with a 34 cm x 34 cm cross-section. A view of this ingot cast in run 41-15 is shown in Figure 10. Keeping the cross-section the same, the largest ingot produced by HEM was 45 kg. Figure 11 shows three views of a 34 cm x 34 cm x 16.7 cm ingot cast in run 41-25. A similar ingot produced in run

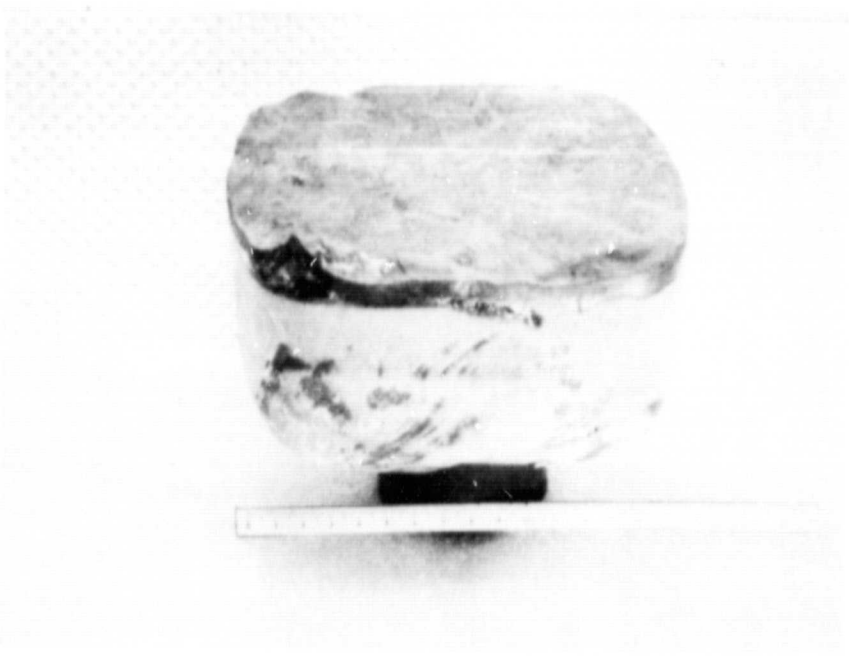

Figure 3. 17 cm x 17 cm square ingot cast by HEM in run 329-C

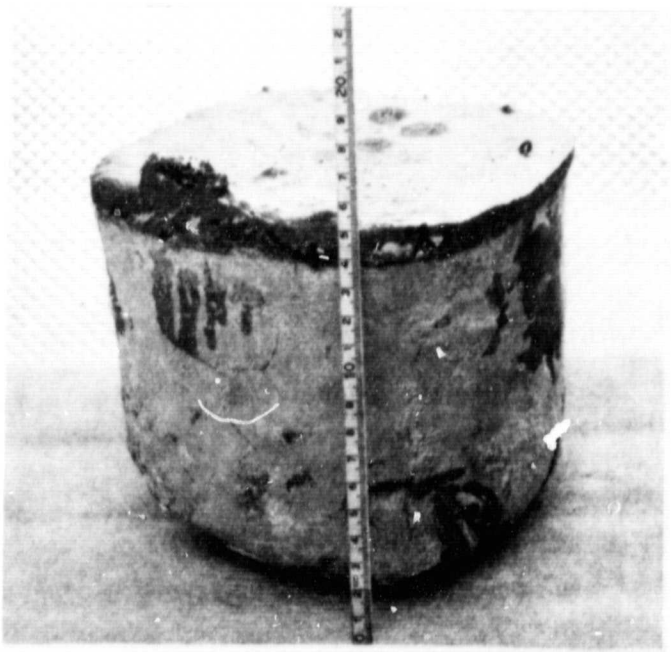

Figure 4. A view of 8.1 kg square ingot as removed from crucible

Figure 5. 10.5 kg, 22 cm square ingot after removal of attached silica

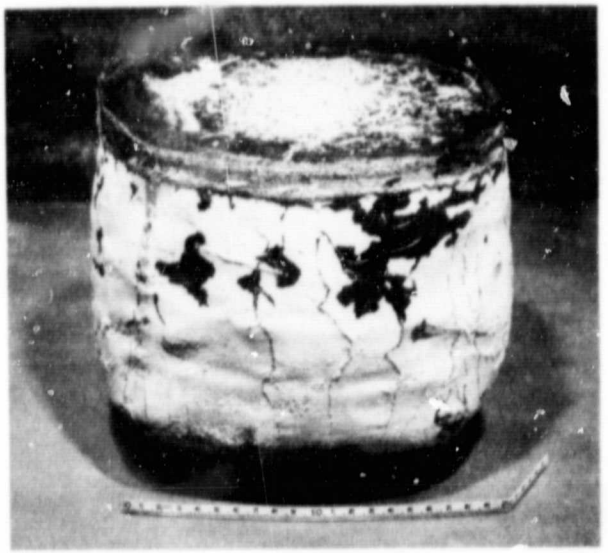

(a)

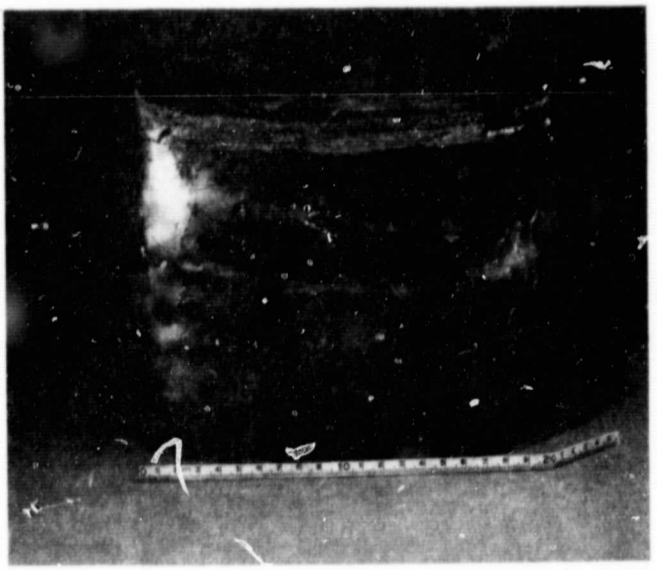

(b)

Figure 6. A 22 cm x 22 cm x 18 cm (16.3 kg) crystal solidified by HEM (run 365-C) (a) as removed from crucible and (b) after removal of adherent silica

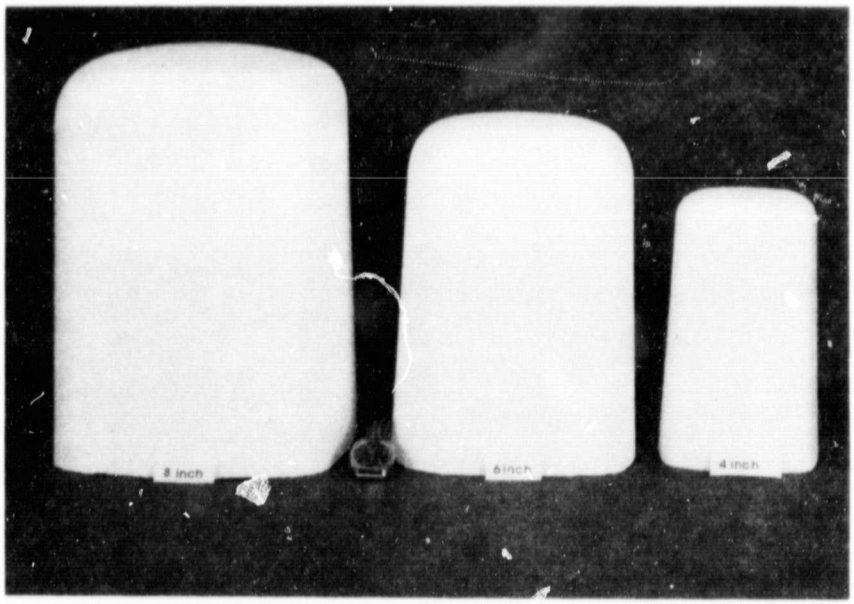

Figure 7. Square crucibles used during scale-up by HEM--22 cm x 22 cm, 17 cm x 17 cm, and 10 cm x 10 cm cross-section

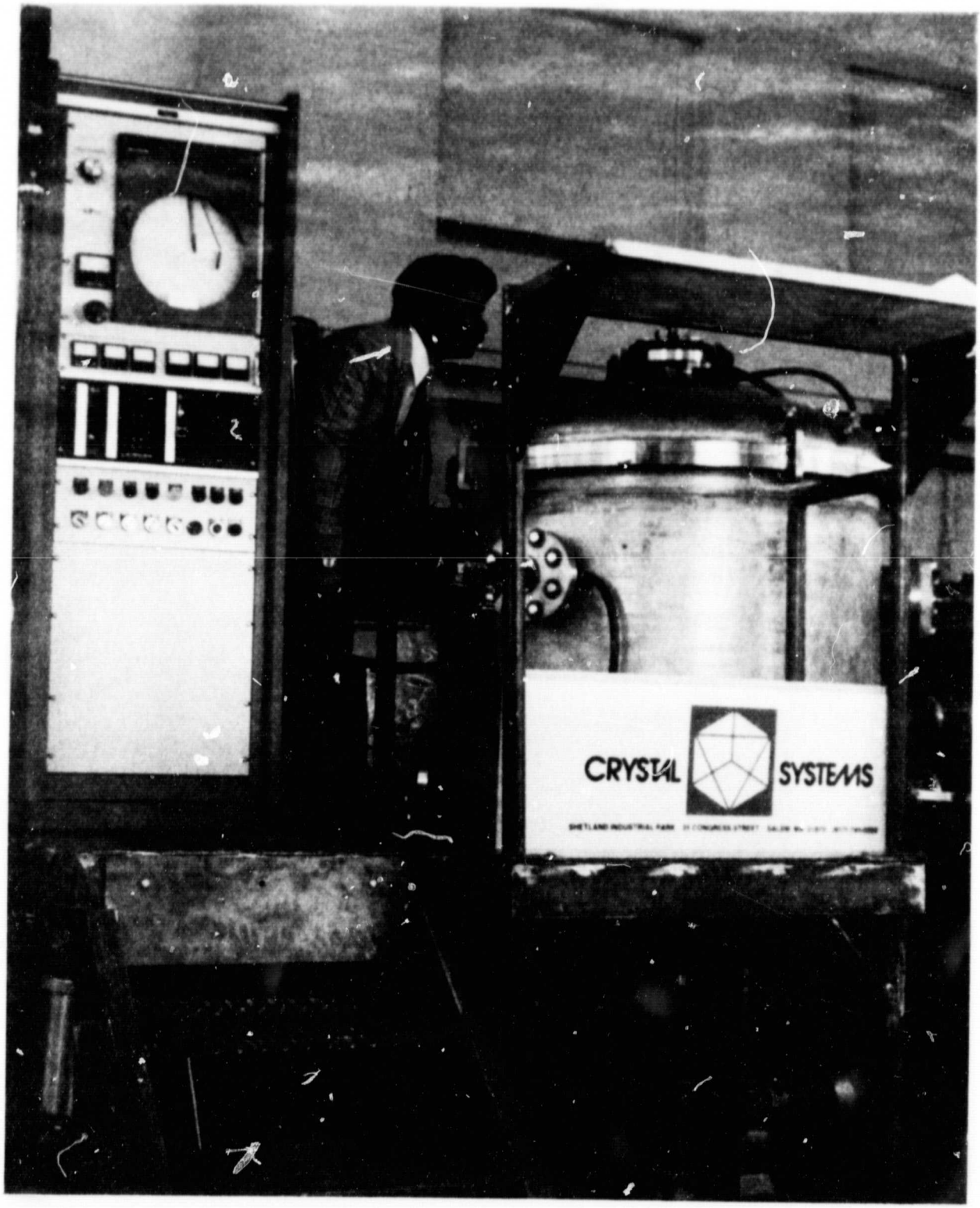

Figure 8. An overall view of the new furnace

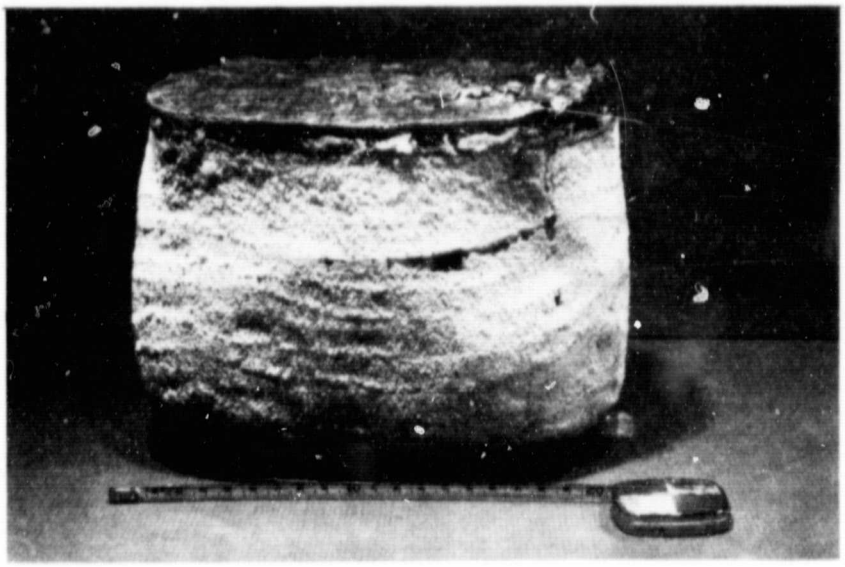

Figure 9. A 14.5 kg silicon ingot cast in run 41-02 in the new furnace

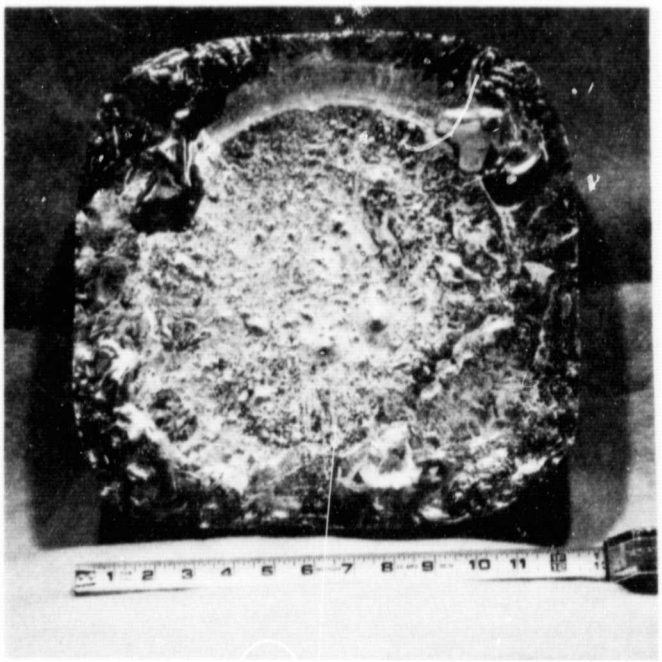

Figure 10. A view of the 34 cm x 34 cm cross-section ingot weighing 20 kg cast in run 41-15C

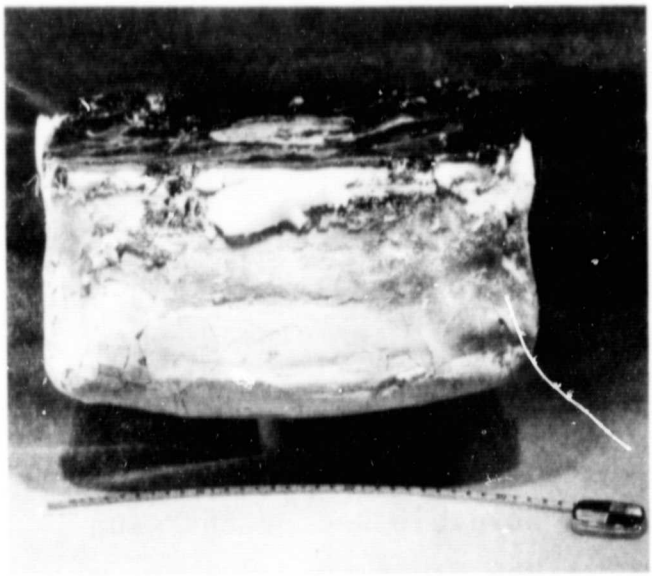

Figure 11. Three views of the 34 cm x 34 cm x16.7 cm, 45 kg ingot cast in run 41-25C; (a) side view showing some attachment of crucible near top surface; (b) bottom showing no delamination problems; and (c) top showing minor cracking along one side where crucible attached.

(a)

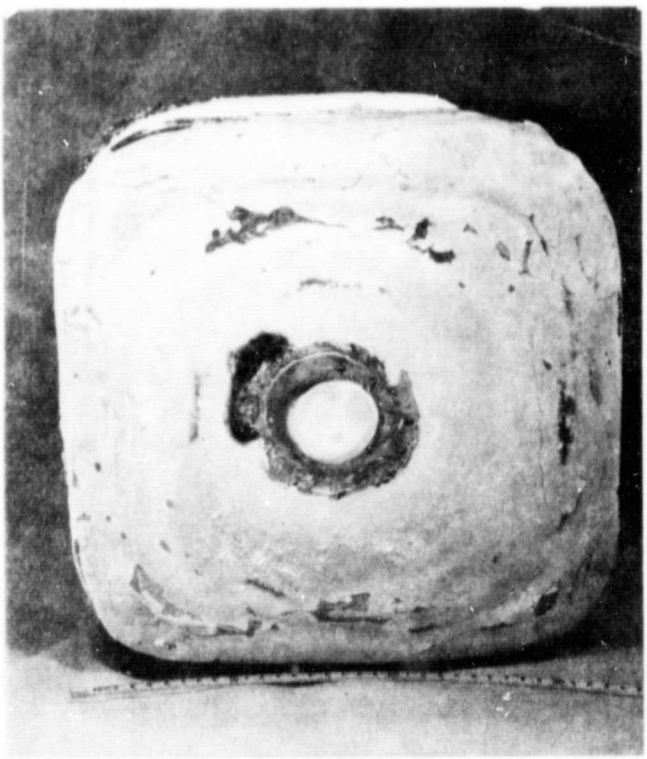

(b)

(c)

41-28 is shown in Figure 12. Figure 13 shows a 45 kg ingot produced in a crucible with square corners. The approximate dimensions of this ingot are 32 cm x 32 cm x 19 cm.

The graded silica crucibles[11] used in HEM are rather fragile when put in the furnace. During the meltdown cycle the crucible sinters and, therefore, gains strength. When large ingots were produced all the meltstock was loaded initially in the crucible. Point loading of the crucible because of sharp corners of meltstock caused the crucible to crack during the meltdown cycle prior to sintering to full density. This problem could be solved by fabricating supports to conform to the shape of the curcible and/or charging meltstock into the crucible after it has sintered. Rather than pursue further enlargement in size of the ingots it was mutually agreed by JPL and Crystal Systems to freeze the ingot size at 35 kg, 32 cm x 32 cm cross-section and emphasize characterization of the ingots. The 35 kg size was chosen because it was sufficient to meet the add-on cost goals of the DOE program for 1986. Six ingots were produced at Crystal Systems for characterization. Two views of a typical ingot are shown in Figure 14.

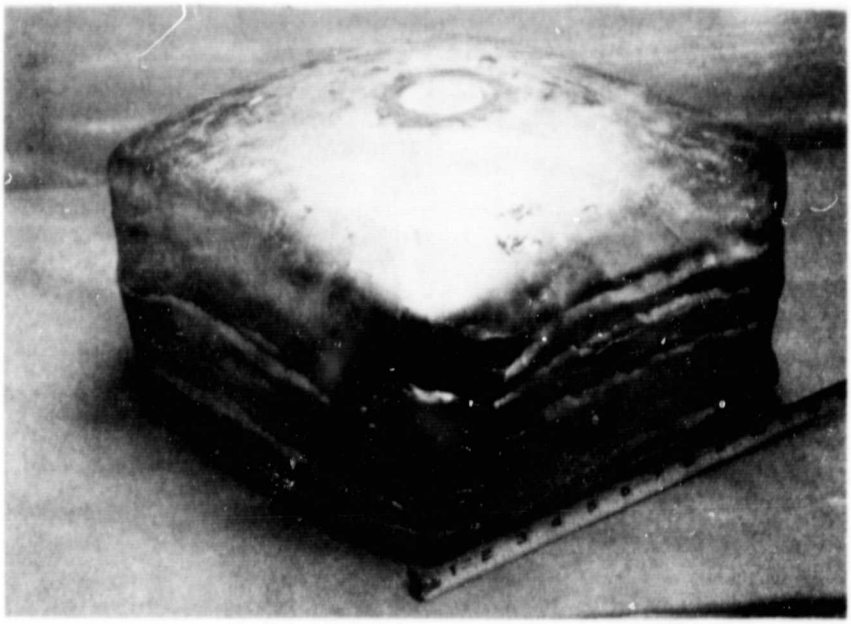

Figure 12. A view of the 34 cm x 34 cm x 16.7 cm high, 45 kg ingot cast by HEM in run 41-28C.

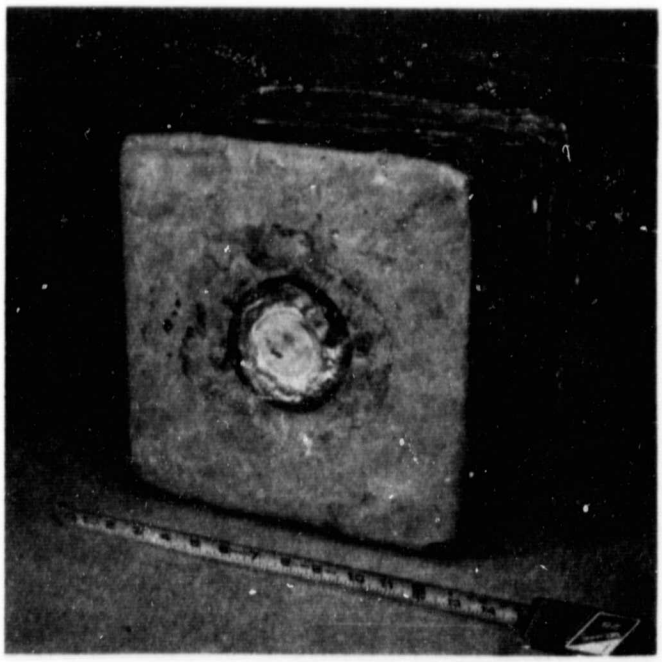

Figure 13. A 45 kg ingot cast in run 41-34C.

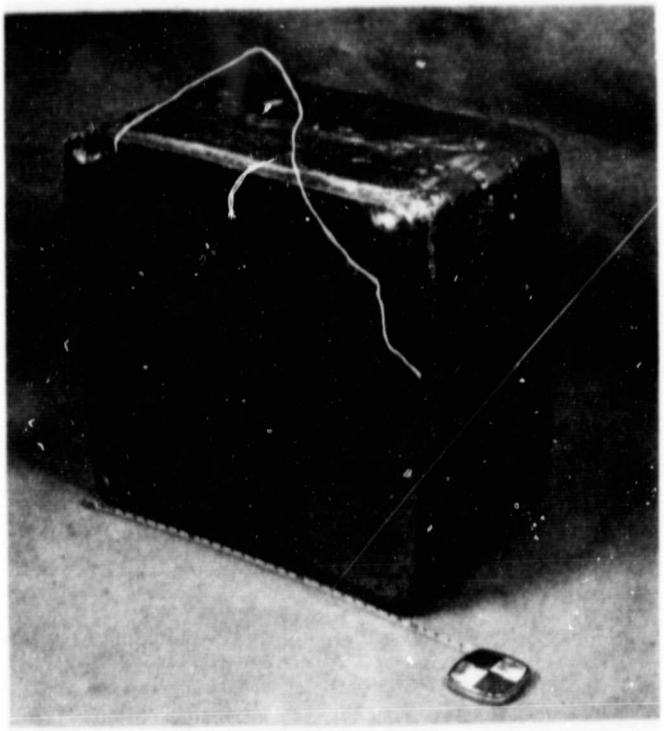

(a)

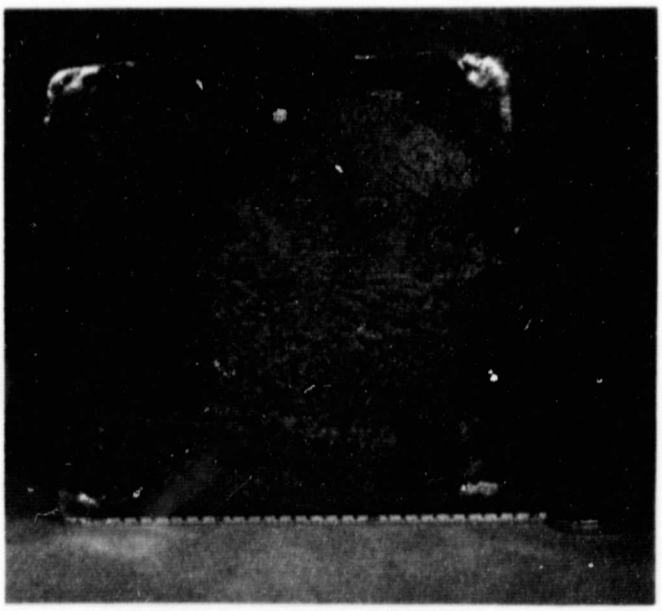

(b)

Figure 14. Two views of 32 cm x 32 cm cross-section, 35 kg ingot cast in the improved design crucible with better shape factor: (a) an isometric view; (b) the top surface of ingot showing last material to freeze is in the corner.

1.3 CRUCIBLE DEVELOPMENT

In HEM directional solidification of silicon, the ingot is solidified in the crucible; hence, a suitable crucible is necessary which can contain molten silicon without contamination of the melt as well as allow solidification and removal of the ingot. Silica is the best material for containment of silicon and is the standard of the semiconductor industry; however, the ingot cracking problem associated with solidifying silicon in silica crucibles is well known in literature.[12,13] The emphasis of the present program has been on using graded silica crucibles even though vitreous graphite as crucible material has also been evaluated.

1.3.1 Molded Crucibles

The crucibles used for HEM directional solidification of silicon ingots are slip cast crucibles which are calcined to give enough strength for handling. These crucibles are then heat treated to develop a graded structure which prevents cracking of the silicon ingots.

During the initial stages emphasis of the program was on increasing the size of the ingots. Heat treatment of the crucibles was optimized for each size crucible to prevent cracking of the ingot. Figure 7 shows three of the sizes of crucible used. These molded crucibles were of square cross-section with rounded corners; hence, the cross-section of the ingot was "squarish." It was shown that during HEM solidification there were no problems in flowing silicon into the corners.

As the size of the ingot increased and processing developed it was important to pay attention to yields of square material from the as-grown ingots. It was found that the corner radii affected the yields considerably. It was felt that the crucible at high temperatures could be deformed to the shape of the retainer and thereby improve the shape

factor. Thick molybdenum sheets were welded to form a rigid retainer. Figure 15 shows this attempt in run 41-05. The ingot had a squarer shape because of flattening of sides, but the corners were still rounded. The thermal expansion of molybdenum and stresses due to expansion of silicon on solidification caused deformation of the molybdenum sheets.

Efforts were also made to use thick graphite plates to form a tight box around the crucible and thereby improve the shape factors of ingots. No bulging of the sides occurred and very flat sides of the ingot were achieved. Figures 16 and 17 show 16 cm x 16 cm and 22 cm x 22 cm ingots, respectively, produced using this approach.

When the size of the crucibles was increased to 34 cm x 34 cm cross-section, the bottom of the crucible was contoured and the sides had a curvature and taper for ease of fabrication of such large size in slip casting. A graphite plate with a contour similar to the bottom of the crucible was necessary to provide support to the crucible. Because of taper in the crucible the graphite flat plates forming a box around the crucible provided support only near the top of the crucible; in this area the loading on the crucible because of meltstock is less than the lower part of the crucible. Further, the ingots cast were still squarish. In view of the above a square crucible was developed. This crucible has a flat bottom with no curvature and minimal taper on the sides; the corners also have a smaller radius. This crucible is shown in Figure 18 in comparison with the earlier design. An ingot cast in the new crucible is shown in Figure 19. This ingot has shown a boule utilization of more than 86% of square material after cropping from the sides, bottom and top of the ingot and sectioning into nine bars.

Figure 15. An 8 kg ingot cast in a crucible supported by moly sheets to prevent bulging (Run 41-05)

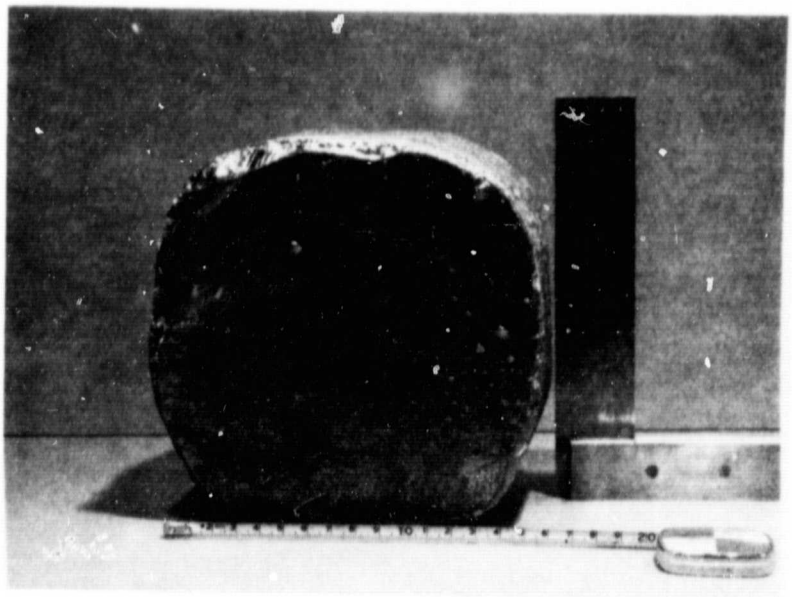

Figure 16. An ingot cast in a squarish crucible supported by graphite plates (Run 41-11)

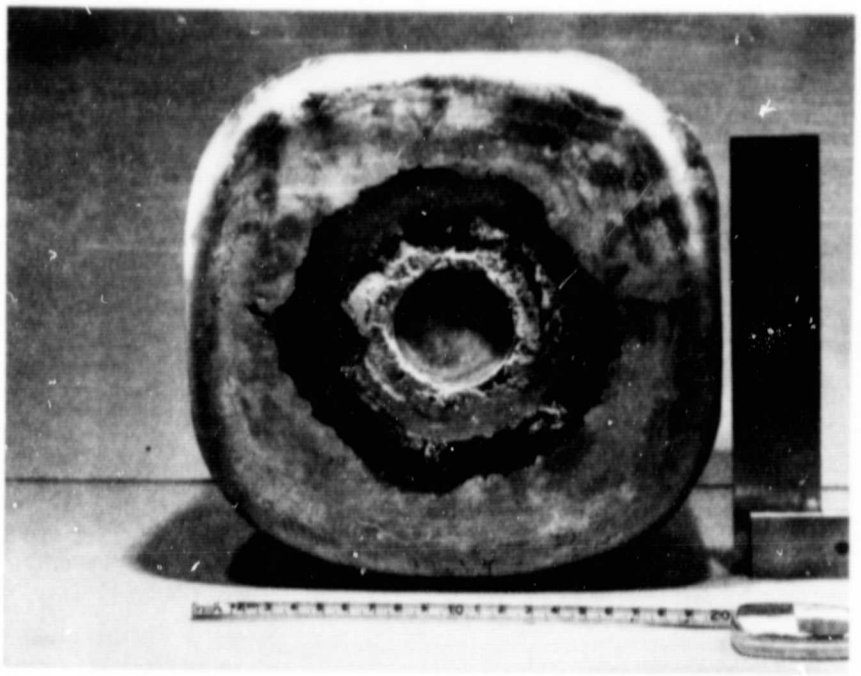

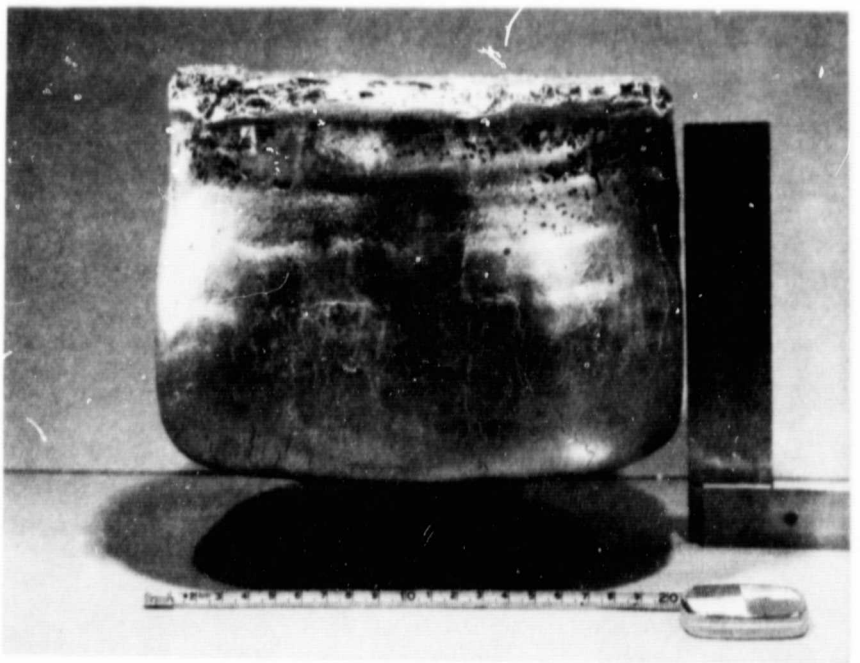

Figure 17. Two views of an ingot cast in a squarish crucible supported by graphite plates (Run 41-12)

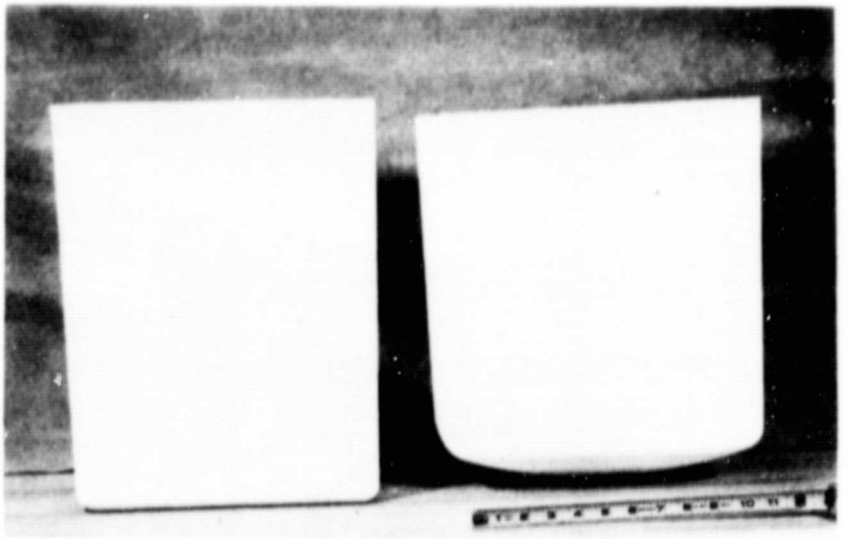

(a)

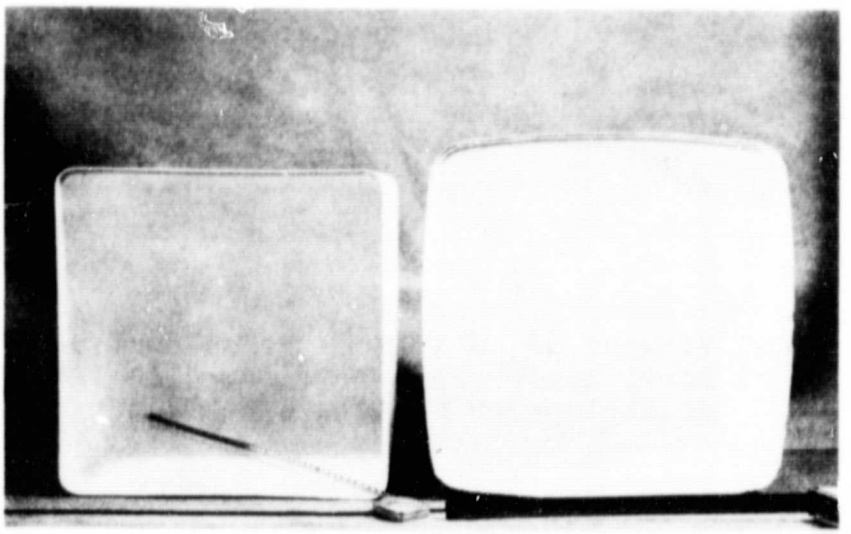

(b)

Figure 18. Views of the two crucibles used to cast 30 cm x 30 cm cross-section ingots. The crucible on the left is the new design (a) view of the side, (b) view of cross-section.

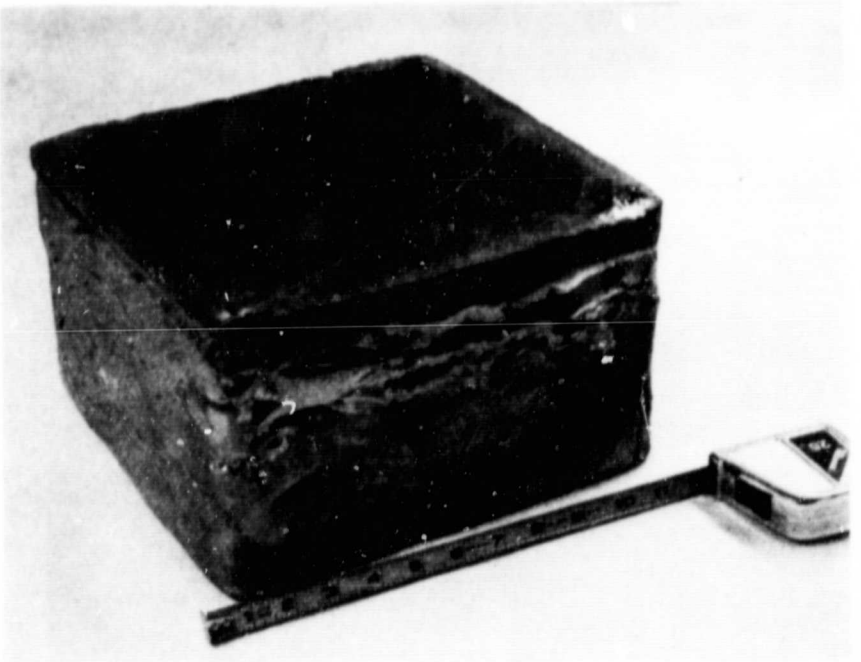

Figure 19. View of 32 cm x 32 cm cross-section, 35 kg ingot cast in improved design crucible with better shape factor

1.3.2 Flat Plate Crucibles

Another approach to obtain square ingots was to fabricate a crucible by welding five flat plates to form a box. The first such crucible was used in run 40-04 with a small amount of silicon to check the stability of the welded areas for silicon containment. No problems were encountered with respect to silicon leakage and a view of the crucible after use is shown in Figure 20. A second such experiment with approximately 5 kg silicon was performed in run 40-07 using thick molybdenum plates for retainer. The ingot still in the crucible is shown in Figure 21(a) and after removal of crucible in Figure 21(b). Sharp corners of the ingot are clearly evident and there was no problem of flowing silicon into the corners. The sides of the crucible show bulging, thereby indicating a need for a more rigid container.

In another experiment, run 41-09, a flat plate welded crucible was supported by ½-inch thick graphite plates. This approach resulted in a really square cross-section ingot. The ingot in the crucible is shown in Figure 22(a) and after removal of the crucible in Figure 22(b). Very sharp corners and a square shape without any bulging on the sides are evident in this ingot.

This approach works satisfactorily and gives a very high boule utilization for square material. It is, however, necessary to develop a low-cost technique for welding flat plates to form a crucible.

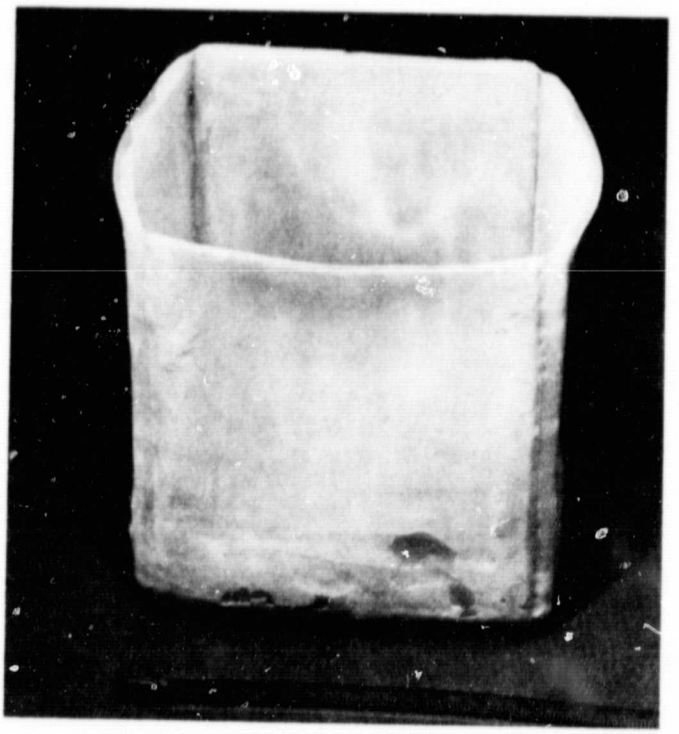

Figure 20. A view of the welded flat plate crucible after use in run 40-04

(a)

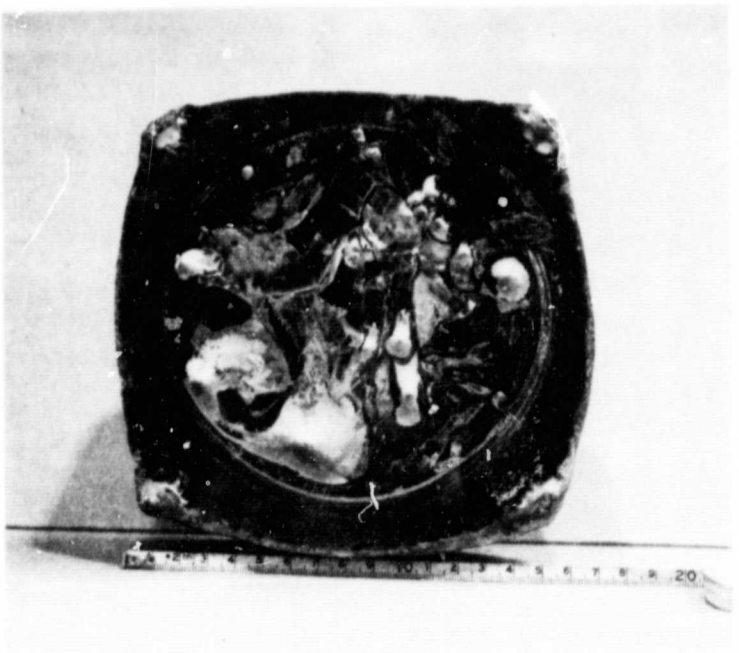

(b)

Figure 21. A 5 kg ingot cast in a crucible fabricated from flat plates (a) ingot in the crucible; (b) ingot removed from crucible

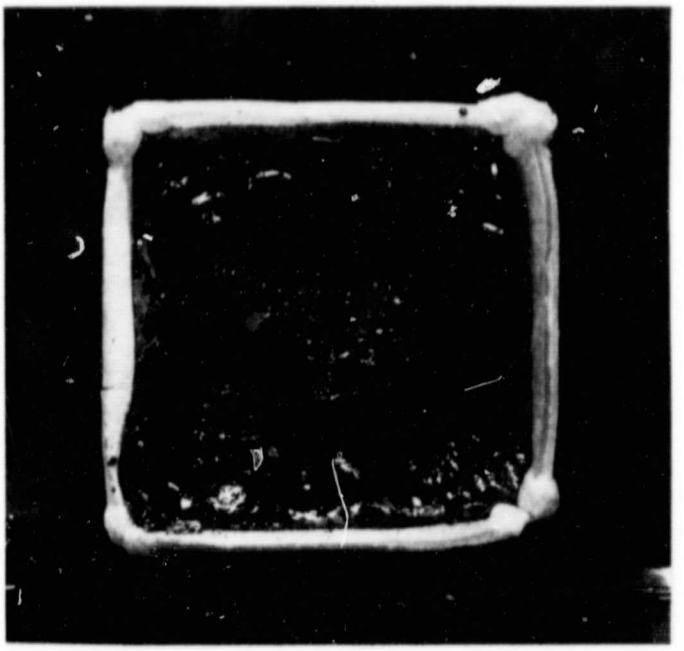

(a)

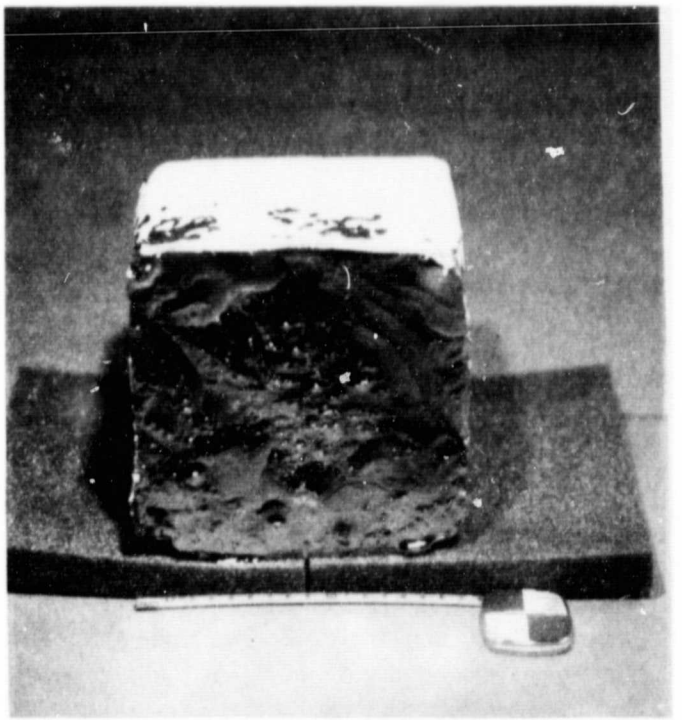

(b)

Figure 22. A 9.5 kg ingot cast in a crucible supported by graphite plates. Very sharp corners and a square shape with no bulging on sides evident (run 41-09). (a) Ingot in crucible; (b) After removal from crucible.

1.3.3 Vitreous Graphite Crucible

In run 40-09 a vitreous graphite crucible was tested to directionally solidify silicon by HEM. No problems were encountered and an uncracked ingot was solidified as shown in Figure 23. This was, as expected, because the differential thermal expansion coefficient between graphite and silicon is not as high as with silica and silicon.

The ingot showed a tenacious attachment to the crucible due to the SiC interfacial layer formed between the ingot and crucible. This boule could not be removed from the crucible without destroying the crucible.

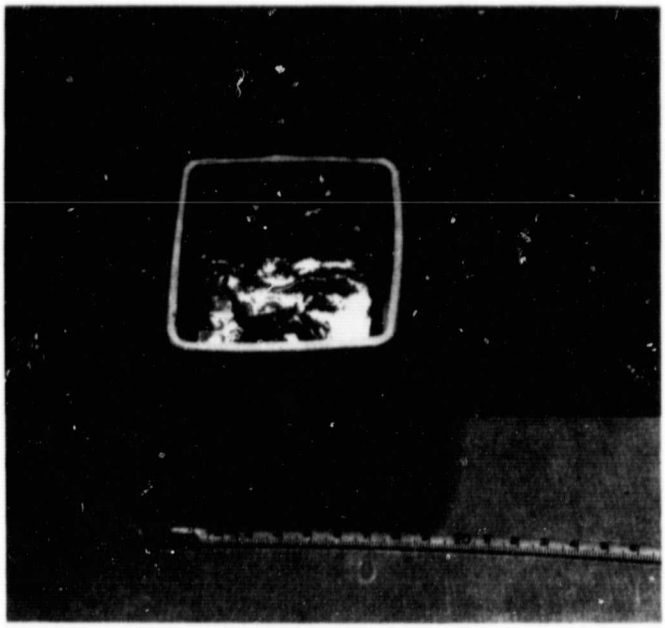

Figure 23. An ingot cast in a vitreous graphite crucible (Run 40-09A)

1.4 HEAT FLOW

A crystal growth process is essentially controlled extraction of heat. The quality of crystal grown and degree of crystallinity are, therefore, strongly dependent upon heat flow considerations. The balance of the heat input and heat extraction has to be maintained so that the solid-liquid interface is smooth and maintains the melt temperature isotherm. In order to prevent polycrystallinity, at no point in the melt aside from the solid-liquid interface should the temperature drop significantly below the solidification temperature. This may be accomplished by high superheat temperatures of the melt; however, the high conductivity of liquid silicon as compared with solid silicon[14] transfers most of the heat to the interface, thereby preventing rapid growth.[15] Further, solidification of very large interface has only recently been demonstrated and the heat flow problem can at best be studied qualitatively only in this time period.

1.4.1 Experimental

Experience with silicon growth by HEM has shown[15] that rapid solidification can only be achieved when the superheat in the melt is held to a minimum. The heat of fusion of silicon[14] necessitates this criterion. The ingots where high solidification rates were achieved were those where temperature was held at 3°C superheat--the minimum the control instrumentation could maintain.

In run 41-54 and 41-56 attempts were made to measure the melt temperature and position of the interface in a 20 cm x 20 cm cross-section crucible. These measurements were taken at two positions -- near the central region and near the edge of the crucible. Quartz tubes were dipped into the melt to establish the interface and the thermocouples contained in the tubes were used to measure the temperature at various levels of the melt. The experiment was carried

out in the usual manner when the meltstock was melted and a melt-back of the seed was achieved; the seed was prevented from melting by forcing helium gas through the heat exchanger. Approximately 9 cm of melt height was contained in the crucible. Solidification was achieved by increasing the flow of helium gas through the heat exchanger.

The solidification interface at the two positions is shown in Figure 24 as a function of time. It can be seen that while sufficient solidification progressed in the central area very little growth was achieved near the edge of the crucible. The shape of the interface indicates that the last material to solidify is along the wall of the crucible. Temperature movements at various positions of melt level during the growth cycle showed that the solidification occurred under very low superheat, approximately 1 to 3°C. The gradients in the liquid were very minimal.

A thermocouple placed within the heat exchanger showed that temperature was 1350°C with minimal helium flow and decreased to 800°C as the helium flow was increased.

Optical pyrometers sighted on the crucible wall were also used to measure temperature. The upper pyrometer corresponded to the melt level and the bottom pyrometer to the crucible bottom. During solidification the temperatures of the pyrometers corresponded to the following equations:

$$T = 1415 - 0.567 \times t \qquad (1)$$

$$T = 1413 - 0.345 \times t \qquad (2)$$

where equations(1) and (2) corresponded to upper and lower pyrometers respectively.

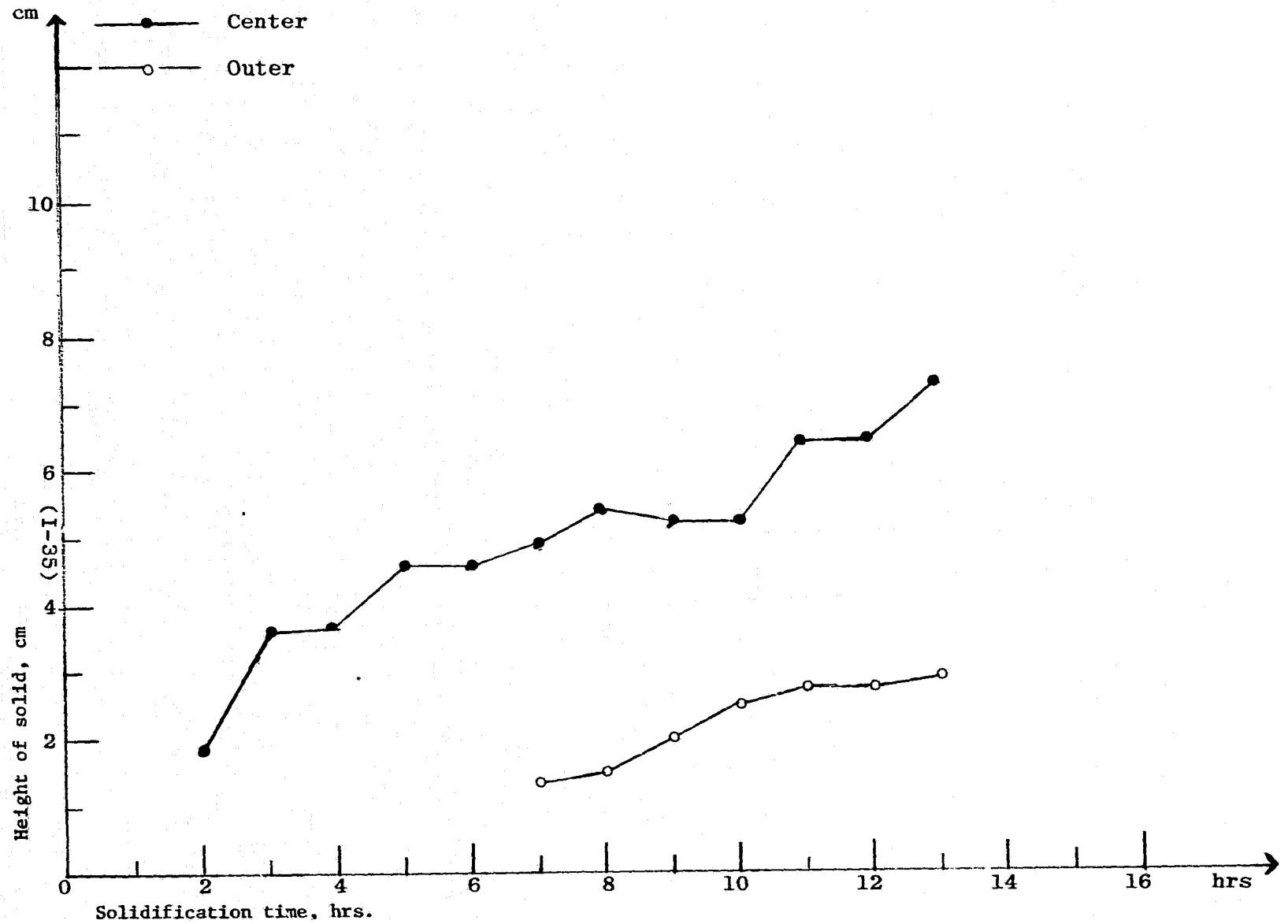

Figure 24. Interface positions for central (●) and near crucible wall (○) regions

1.4.2 Theoretical Analysis

The heat flow analysis of solidification of silicon by HEM was carried out by solving the heat conduction equation in cylindrical coordinates. Finite difference technique and the alternating direction implicit method[16] were used. Truncation errors were further reduced by the application of the Crank-Nicelson Method. A similar analysis was already carried out for the solidification of steel by Electroslag Remelting.[17] The difference in the present work, however, was the movement of interface in two dimensions due to the concentration of heat extraction only to the heat exchanger area.

Partial differential heat conduction equation in cylindrical coordinates is as follows:

$$\frac{\partial T}{\partial t} = \alpha \left(\frac{\partial^2 T}{\partial x^2} + \frac{\partial^2 T}{\partial r^2} + \frac{1}{r} \frac{\partial T}{\partial r} \right)$$

where α = $k/(\rho C_p)$, thermal diffusivity in cm^2/sec
ρ = density in gms/cm^3
k = thermal conductivity in $cals/(cm\ sec\ ^oC)$
T = temperature in ^oC
t = time in sec
x = distance in the axial direction in cm
r = distance in the radial direction in cm

The analysis was carried out for a 20 cm diameter crucible of 0.75 cm wall thickness placed on a 2.5 cm diameter heat exchanger. The grid arrangement used is shown in Figure 25 ; the grid size could be varied in the i and j direction independently in the analysis.

The melt temperature, rate of decrease of heat exchanger temperature, etc., were changed and effect studied. An example is shown below when the initial heat exchanger

temperature prior to growth was 1350°C and temperature was decreased linearly to 800°C in 5 hours, the melt temperature at start of growth was 1415°C. The initial conditions (t=o) used in the computer program corresponding to the grid arrangement of Figure 25 were:

$$T(i, j) = 1350 \qquad i=1,\ j-1,\ 21$$

$$T(i, j) = 1415 \qquad i=12,\ N;\ j=1, N_s$$

$$i=1,\ 11;\ j=22,\ N_s$$

$$T(i, j) = T(11, j) - \frac{1}{0.5}\ [0.5 - x(i)][T(11, j) - T(i, j)]$$

$$i = 2,\ 10;\ j = 1,21$$

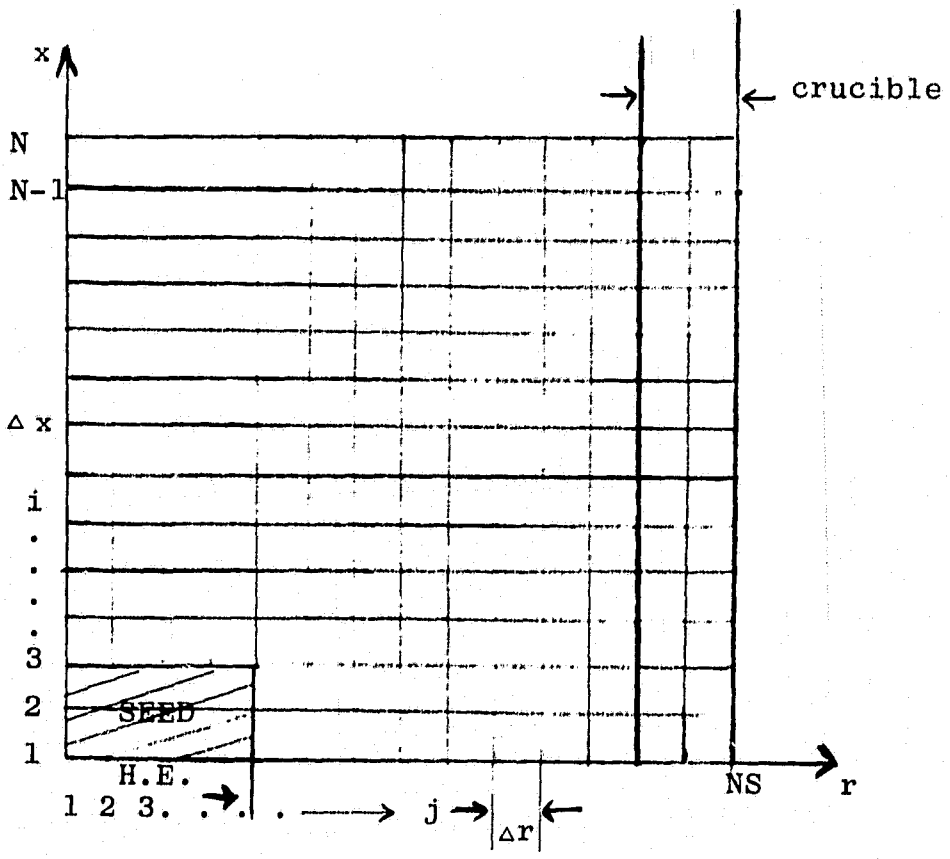

Figure 25. Mold dimension and grid arrangement

The boundary conditions (t>o) were determined by the following equations for the case outlined above:

$$T(i,j) = 1350 - 110t \qquad i=1,\ j=1,21$$

$$T(i,j) = 1415 - 0.345t \qquad i=1,\ j=22,\ N_s$$

$$T(i,j) = T(N,\ N_s) - \frac{1}{5}\,[5-x(i)][T(N_1N_s) - T(2,N_s)] \qquad i=2,N;\ j=N_s$$

$$T(i,\ j) = 1415 \qquad i=N,\ j=1,\ N_s-1$$

It was assumed that latent heat of fusion, H, can be taken into account by adjusting the specific heat, C_p, as follows:

$$C'_p = C_p + \frac{H}{\Delta T} \qquad (4)$$

where C'_p is adjusted specific heat, ΔT is the solidification range that latent heat is taken. In the study ΔT was assumed $2^{\circ}C$.

Thermal Properties of Silicon and Silica

A. Silicon

a. Thermal conductivity of silicon in the solid and liquid state near the melting point is 0.075 and 0.160 cal/cm sec°C respectively.[14] At room temperature[18] this is 0.331 cal/cm sec°K. Assuming an exponential change in conductivity, from these values the conductivity in the solid between melting point and room temperature was calculated as

$$k = 0.4555\ e^{-0.00107T} \qquad (5)$$

b. Heat capacity of silicon in the solid form was calculated from known values[19] at different temperature:

at 25°C C_p = 0.168 cal/gm°K
at 1411°C C_p = 0.227 cal/gm°K

Assuming that C_p changes linearly, it was found

$$C_p = 0.155 + 4.26 \times 10^{-5}T \quad \text{for 25 to 1411°C}$$

Heat capacity in the liquid state is 0.160 cal/gm°K.

c. Density of silicon is as follows:
in solid state, ρ = 2.34 g/cc
in liquid state, ρ = 2.51 g/cc

d. Latent heat of fusion is 431 cal/gr.

B. Silica Crucible
Conductivity, k = 0.0033 cal/cm sec °C
Heat capacity, $C_p = 14.40 + 2.04 \times 10^{-3}T$
Density, ρ = 2.2 g/cc

Using the above values thermal diffusivity of silicon and silica crucible were calculated as follows:

a. For silicon

$T \leqslant 1410°C \quad \alpha = 3600/e^{0.00107T}\ (0.79714 + 2.19 \times 10^{-4})$ cm²/hr

$T > 1412°C, \quad \alpha = 933.48$ cm²/hr

$1410 < T \leqslant 1412°C, \quad \alpha = 0.8085$ cm²/hr

b. For silica crucible

$\alpha = 3600/(9600 + 1.36T)$ cm²/hr

Results

The simplistic approach of theoretical analysis did not work satisfactorily. The temperature profile in the silicon was calculated; after some time into the growth cycle, computing terminated because of inherent constraints applied. Review of the data showed that the boundary conditions were putting undue limitation on the calculations. For example, the temperature of silicon near the crucible wall was computed to be lower than the melt in the center even at distances away from the interface. This is contradictory to experimental observation. It is possible that this is because of input of measured temperatures on the crucible wall. In the experimental setup these measurements are made off the graphite retaining box; during meltdown high temperatures are achieved so that the crucible is heated to these high temperatures. When the furnace temperature is reduced the silica crucible being an insulator would not give up heat readily and would, therefore, keep the melt in the vicinity at a higher temperature. The temperature of the melt near the crucible wall is, therefore, dependent on the prior history which is not possible to incorporate in such a simplistic approach in the computer model.

1.4.3 Two-inches diameter heat exchanger

In a typical HEM furnace a 1-inch diameter molybdenum heat exchanger is used. It was thought that a 2-inch diameter tube would extract heat more rapidly and thereby give higher growth rates. A practical problem encountered in this approach was that molybdenum tubes are extruded only up to 1-inch diameter size. Larger sizes have to be fabricated by machining which makes it prohibitively expensive

especially in large lengths.

In order to reduce costs it was decided to weld a 2-inch diameter molybdenum cap onto a stainless steel tube so that in the lower portion the temperatures would be compatible with use of stainless steel. The transition joint between molybdenum and stainless steel was designed and a high temperature solder was used to make up the assembly. Initially a 4- inch long molybdenum cap was used. The fabricated assembly was leak-tested and used in the HEM furnace, for example, in run 41-29. During meltdown stage sudden vacuum change of the chamber necessitated aborting the experiment. Examination of the heat exchanger after the run showed leakage at the molybdenum-stainless steel joint.

Another attempt was made in using a similar approach but with an 8-inch long molybdenum cap. It was felt that at this level the furnace temperature would be low enough to maintain the integrity of the joint. Again similar problems of leaking at the joint were ecnountered. Even though the furnace temperature at the level of the solder joint is low enough, the hot helium gas from the top of the heat exchanger is not sufficiently cooled by the time it reaches the transition area. In view of this, the effect of the 2-inch heat exchanger could not be studied.

1.4.4 Effect of Insulation

At the start of the present period only 3.3 kg ingots of 10 cm x 10 cm size were being cast by HEM. In less than two years the size was scaled up to 45 kg with 34 cm x 34 cm cross-section. This amounts to an increase by more than an order of magnitude. During this period the emphasis has been mainly on increase in size. Towards the end of the program

the size was fixed at 35 kg and emphasis was placed on quality of the material for solar cell applications. One of the criteria was the degree of single crystallinity. This parameter is strongly dependent on the heat flow. A simple approach to affecting this is by changing the insulation around the crucible.

In run 41-41 the crucible was insulated on the sides and bottom with graphite felt. Under these conditions the heat input was mainly from the top surface of the melt during the growth stage. Towards the end of the growth cycle there was a small leak from the crucible. Figure 26 shows the crystallinity of the ingot. The top surface corresponds to the shape of the interface and is fairly flat.

In run 41-48 there was no insulation on the sides of the crucible. Under these conditions there is some heat input through the crucible wall as well as from the top surface of the melt. The crystallinity of this ingot is shown in Figure 27. Towards the end of the cycle growth was achieved by freezing from the top surface. The curved nature of the interface can be seen in the figure. It can be seen that near the crucible wall there is a curvature to the interface as compared with 41-41. This change is because of additional heat input from the sides of the crucible. The altered change in shape of the interface produced better crystallinity; however, liquid entrapment in the corners caused breaking of ingot in these areas.

In run 41-51 only the corners of the crucible were insulated because they are nearest to the heater and in that area direct heat input can be reduced to prevent liquid entrapment without degradation of crystallinity, as shown in Figure 29. The liquid entrapment problem was improved but not eliminated. Even though, in principle, insulating the corners of the crucible should help, in a near equilibrium

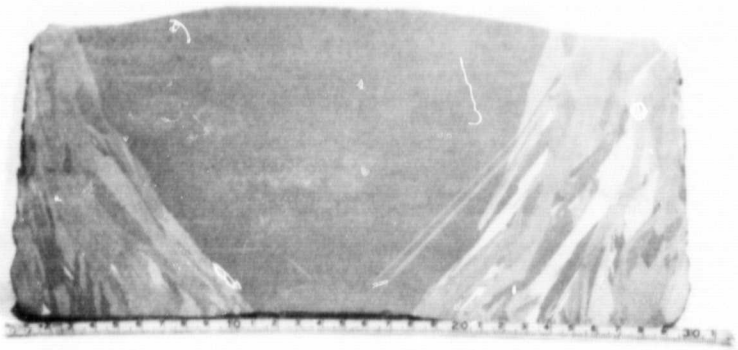

Figure 26. Cross-section of ingot cast in run 41-41

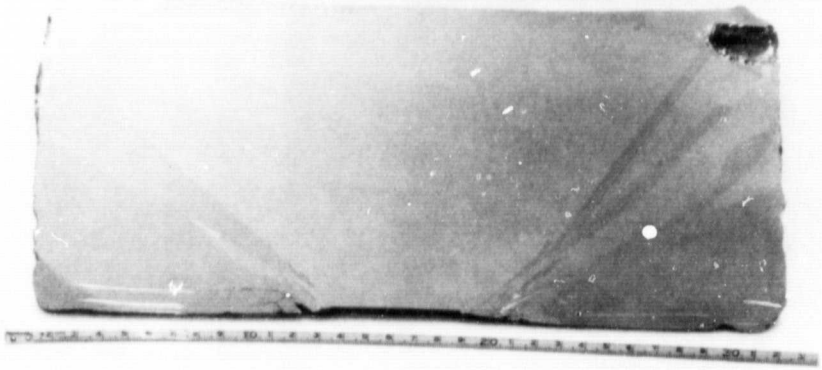

Figure 27. Ground and etched cross-section of ingot cast in run 41-48

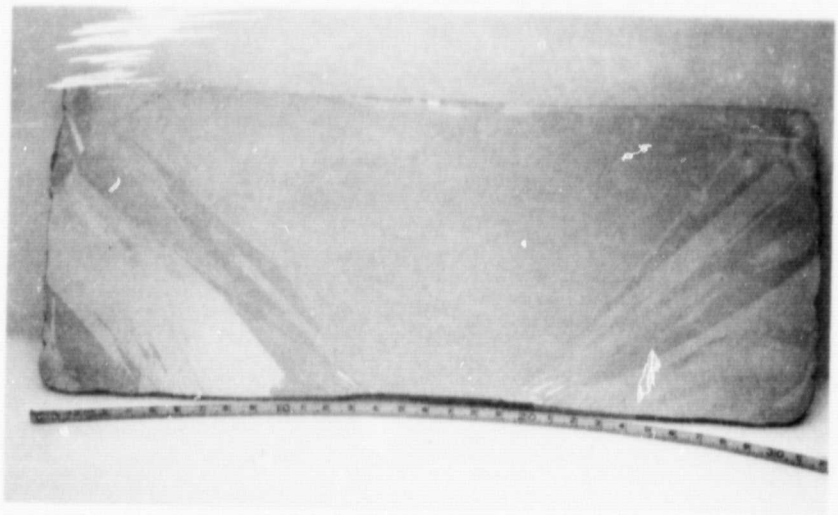

Figure 28. Ground and etched cross-section of ingot cast in run 41-51

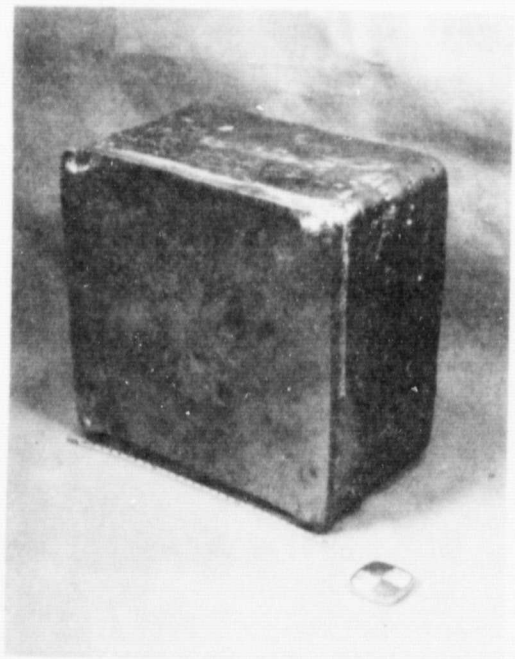

Figure 29. View of an ingot with no problem of broken corners when the crucible edge is not adjacent to the heater

situation achieved during crystal growth there is little improvement.

In ingots where liquid has been entrapped in the corners of the ingot the crucible is less than $\frac{1}{4}$ inch away from the heater. In such close proximity the distance of the interface from the heat exchanger is large; hence, the heating influence overrides the cooling effect; under these conditions directional solidification cannot be achieved and only freezing occurs and liquid is entrapped. When the heater is more than about one-half inch away from the crucible no liquid entrapment problems have been encountered; for example in run 41-31 (Figure 29).

1.4.5 Reduce Cooldown Time

The HEM furnace is very well insulated, hence the heat losses are minimized. While this is an advantage during the meltdown and solidification cycle of the crystal it prolongs the cooldown cycle. The silicon ingots solidified by HEM (up to 34 cm square cross-section) cannot be cooled rapidly because the temperature difference between the core and surface of the ingot will cause cracking due to thermal shock. At the present time it takes approximately 24 to 36 hours after solidification before the furnace is sufficiently cooled so that the ingot can be taken out.

In order to reduce the cooldown time without changing the insulation characteristics of the furnace, it was intended to introduce a gas to enhance cooling of the ingot. The cooldown is rather rapid at high temperatures and becomes progressively slower at low temperatures. In run 41-52 argon gas was introduced into the chamber approximately 24 hours after solidification prior to opening the chamber. The cooldown time was shortened; however, the ingot was cracked. It is felt that when argon was introduced the surface

temperature of the ingot was reduced rapidly causing cracking due to thermal shock.

In run 41-55 argon was introduced into the chamber at about 1400°C prior to start of cooldown cycle. No cracking of the ingot was observed; however, the cooldown time was not affected significantly.

Since helium gas has a higher thermal conductivity than argon and the gas ambient has to be introduced at high temperature, it was felt that helium should be used. In run 41-57 this procedure was adopted but the ingot cracked, probably due to sudden temperature change of the surface of the ingot.

In order to shorten the cooldown by introducing a gas ambient, it is necessary to correlate the ingot temperature with type of gas and rate of backfilling. This work could not be carried out within the present scope of the program. It has been demonstrated that backfilling of the chamber can be carried out without cracking the ingot.

1.5 LOW-PURITY MELTSTOCK

1.5.1 Background

An important feature of the HEM is that the crystal growth takes place from the bottom of the crucible to the top. Therefore, impurities which float on the surface of the melt do not interfere with the growing solid-liquid interface. Usually low-purity meltstocks have high carbon content and are coated with an oxide layer. On melting, the silica and silicon carbide float to the surface of the melt.

Most impurities in silicon have a distribution coefficient significantly less than unity;[20] therefore, during directional solidification these impurities are rejected to the melt and will eventually pile up in the last material to freeze. For HEM growth, this material is along the crucible wall. Cast ingots will have to be sectioned to maintain dimensional accuracy; hence, during the sectioning operation the contaminated material will be removed. In a typical casting process, the control of the solidification interface, if any, is only marginal and growth takes place from the sides to the center; thereby the last material to freeze is in the central region. Another important feature of HEM is the enlargement of the interfacial area as growth proceeds. Thus the effect of pile-up of impurities at the melt interface is minimized and constitutional supercooling is suppressed.

The segregation coefficient is a sensitive function of the impurity content and growth rate. As the concentration of impurities increases it is necessary to decrease the growth rate in order to achieve the same segregation effects. In the HEM crystal growth, because of segregation, impurities are rejected to the melt, consequently increasing their concentration in the liquid. As growth proceeds, the impurity level in the melt increases; however, the

distance of the solid-liquid interface from the heat exchanger also increases. The linear advancement of the interface is slowed. The HEM, therefore, has a built-in feature to compensate for the increased impurity rejection to the melt with slower growth rate.

One of the low-cost silicon meltstock approaches funded by DOE was silicon produced by the Direct Arc Reactor[21]. This meltstock was made by the carbonaceous reduction of silica in a submerged arc furnace similar to that used for the production of metallurgical silicon. Control of raw materials has made it possible to keep B and P contents low; however, use of a small experimental furnace has resulted in a very high carbon content (~20 times more than in commercial MG silicon). The experimental solar metallurgical silicon was tapped from the arc furnace in air at about 1700°C and, therefore, contained carbon, silicon carbide and silica as part of the sample. Material from two batches was used for evaluation. Emission spectrographic analysis of these two batches is shown in Table I. Meltstock from batch 1 was only crushed and screened to remove fines, whereas that from batch 2 was further acid-etched in order to reduce the oxide layer on the silicon. The latter material was further hand-sorted to remove obvious pieces of carbon and/or silicon carbide. Both batches of solar metallurgical are described later--unetched sample is from batch 1, while etched sample is from batch 2.

1.5.2 Directional Solidification

Run 353-C was carried out using solar metallurgical silicon meltstock from batch 2. Operational parameters were kept similar to runs using high-purity meltstock. Considerable amount of contaminants were seen floating on the surface of the melt throughout the solidification. This HEM ingot did not show any signs of cracking as seen in Figure 30. A ground and etched section of this ingot is shown in Figure 31. It can be seen that a very high degree of single crystallinity has been

TABLE I. Analysis of solar metallurgical silicon produced in two batches. All values are in ppm

Impurity	Batch 1	Batch 2
Al	100	70
B	3	3
Ca	40	50
Cr	10	10
Cu	5	5
Fe	50	80
Mn	10	10
Mo	10	10
Ni	10	10
P	7	3
Ti	10	10
V	10	10
Zr	10	10

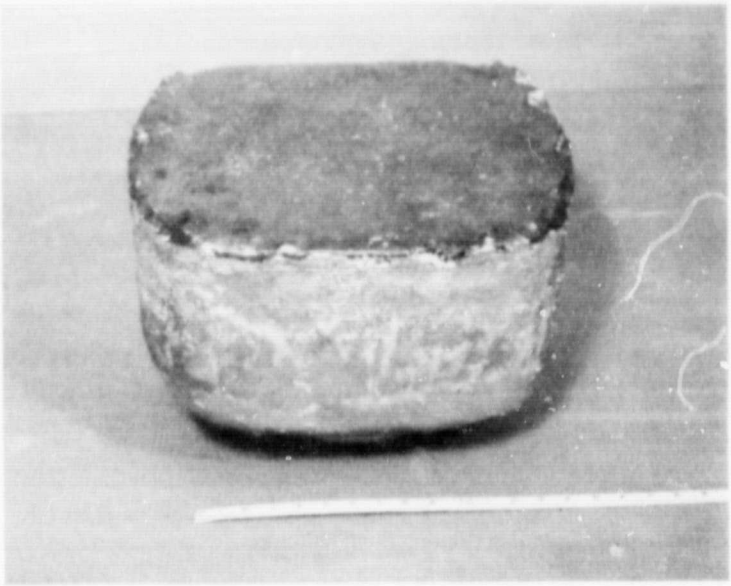

Figure 30. A 5.5 kg, 16 cm x 16 cm cross-section ingot cast in run 353-C using upgraded metallurgical silicon

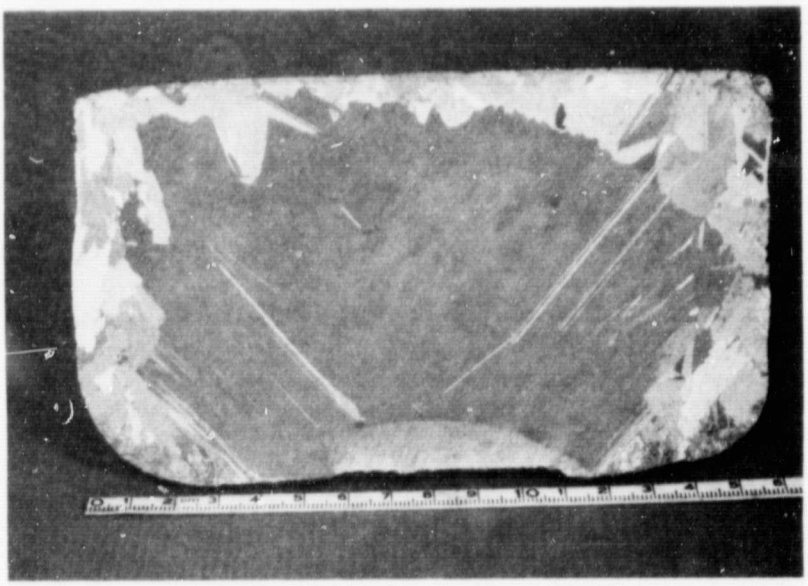

Figure 31. Cross-section of the ingot shown in Figure 30.

achieved. Macroscopic examination of the surface shows dark precipitates on the surface of the melted-back seed. These precipitates were identified as SiC by x-ray diffraction.[5] The precipitates did not disturb the interface. With the Czochralski method, where the interface is on the melt surface, single crystallinity could not be achieved during the first pull using this meltstock.[21] This demonstrates the stability of the submerged interface.

Two samples from the ingot were analyzed for impurities using Spark Source Mass Spectrographic Technique; one of the samples was taken from the middle of the ingot while the second was taken from the edge. The results are shown in Table II. A review of the data shows that significant purification and effective segregation have been achieved. Most of the impurities in the central region were below detectibility limits. The resistivity of the ingot was measured to be between 0.15 and 0.20 ohm-cm.

The main problem encountered in the directional solidification of solar metallurgical grade silicon was the presence of SiC particles that are known to cause shunting of solar cells.[22] Double HEM solidification reduced the SiC particles considerably.

1.5.3 Directional Solidification with Slagging

The high carbon content of solar metallurgical silicon meltstock results in the formation of silicon carbide in the melt. Since SiC is denser than silicon, most of it sinks to the bottom of the melt. However, because of particle morphology, some particles float or are suspended in the melt and are incorporated in the structure. Reaction

Table II. Spark-source Mass Spectrographic analysis of two samples from an HEM solidified ingot using solar metallurgical silicon. All values are ppba.

Impurity	Position in ingot		Impurity	Position in ingot	
	Middle	Edge		Middle	Edge
Ag	<6	<6	Nb	<3	<3
Al	1000	600	Ni	<30	<30
B	8000	-	P	3000	-
Co	<10	<10	Pd	<10	<10
Cr	<5	10	Sn	<5	<5
Cu	20	20	Ta	<10	30
Fe	<30	800	Ti	5	20
Mg	<5	50	V	<3	3
Mn	<5	400	W	<3	<3
Mo	<10	50	Zn	<5	<5
Na	3	40	Zr	<20	<20

of SiC with silica can reduce the SiC particles.[5] Some of the reactions that proceed to the right in an HEM environment are:[23,24]

$$SiC + 2SiO_2 \rightarrow 3SiO + CO$$
$$SiC + SiO_2 \rightarrow SiO + CO + Si$$
$$2SiC + SiO_2 \rightarrow 3Si + 2CO$$
$$SiC + SiO_2 \rightarrow 2Si + CO_2$$
$$SiC + SiO_2 \rightarrow C + 2SiO$$

In these cases a gaseous species will be formed leading to removal of SiC. Further, formation of the gaseous species causes stirring of the melt. This phenomenon enhances the reactions between SiC and SiO_2 further by creating a kinetically favorable environment. Furthermore, SiC particles that do not have contact with silica but which have contact with gases will float up even though their density is higher than silicon. All these phenomena were expected to reduce the SiC content in silicon.

In order to study this effect unetched solar metallurgical silicon with the adherent silica was used as meltstock in runs 40-01, 40-03, 40-05, 40-11 and 40-12.[23] Directional solidification by HEM was carried out in run 40-01 whereas in other runs high purity silica powder was added to the crucible along with the meltstock. A cross-section of the ingot in run 40-01 is shown in Figure 32. A comparison of this figure with Figure 31 shows that the SiC particles are considerably reduced. The structure of the ingot produced in run 40-12 as a result of better slagging with silica powder is shown in Figure 33. The whole ingot shows a nearly single structure. At the melted-back seed interface there is a high concentration of large SiC particles which cause formation of some twins; otherwise the structure is quite clean.

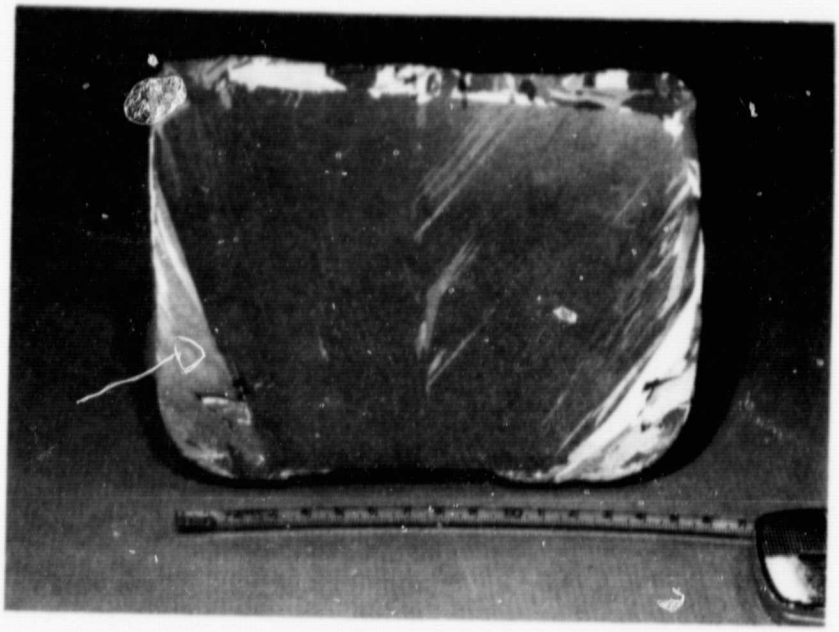

Figure 32. Polished and etched cross-section of ingot from run 40-01 using solar metallurgical silicon

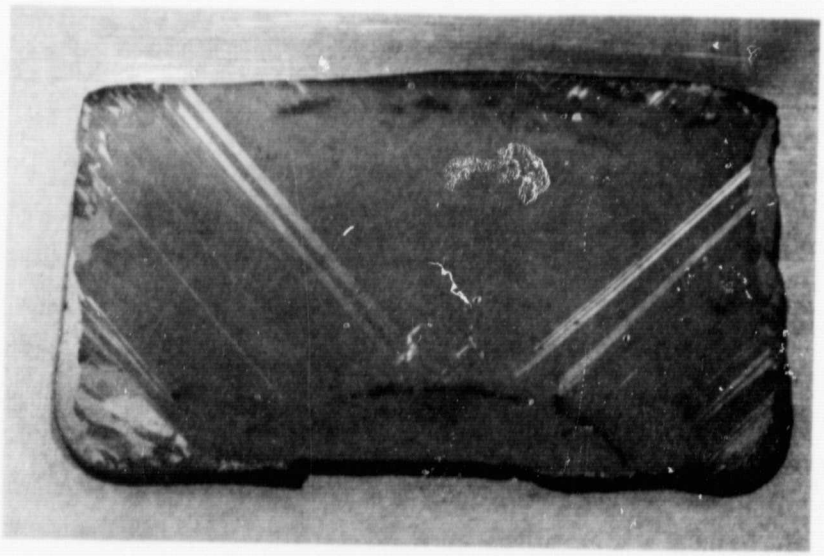

Figure 33. Structure of an ingot as a result of better slagging (Run 40-12)

1.5.4 Solar Cell Performance

Test solar cells (2 cm x 2 cm) were fabricated from a double HEM solidified ingot using standard cell processing procedures at Spectrolab, Inc. The range of conversion efficiency of the 22 cells processed and tested was 3.8-12.3 per cent (AM1) with two cells above 12% and 12 above 8%. The remaining showed shunting effects. The current-voltage characteristic of the best cell is shown in Figure 34.

1.5.5 Conclusion

Solidification of solar metallurgical silicon by HEM has shown that nearly single-crystal ingots can be produced. The use of Czochralski technique had produced single-crystal structure only on the second pull. The main problem encountered for photovoltaic applications wasthe SiC particles dispersed in the structure. These particles sink to the bottom of the melt since they are heavier than molten silicon. However, because of particle morphology some particles float or are even suspended in the melt. SiC does not break down the structure but causes shunting of the devices. It has been shown that concentration of the particles is reduced by slagging techniques. The source of these contaminants is the high carbon content of the melt-stock which is associated with a small furnace operated under experimental conditions. Solar cells fabricated from double HEM solidified solar metallurgical silicon have shown conversion efficiencies up to 12.33% (AM1).

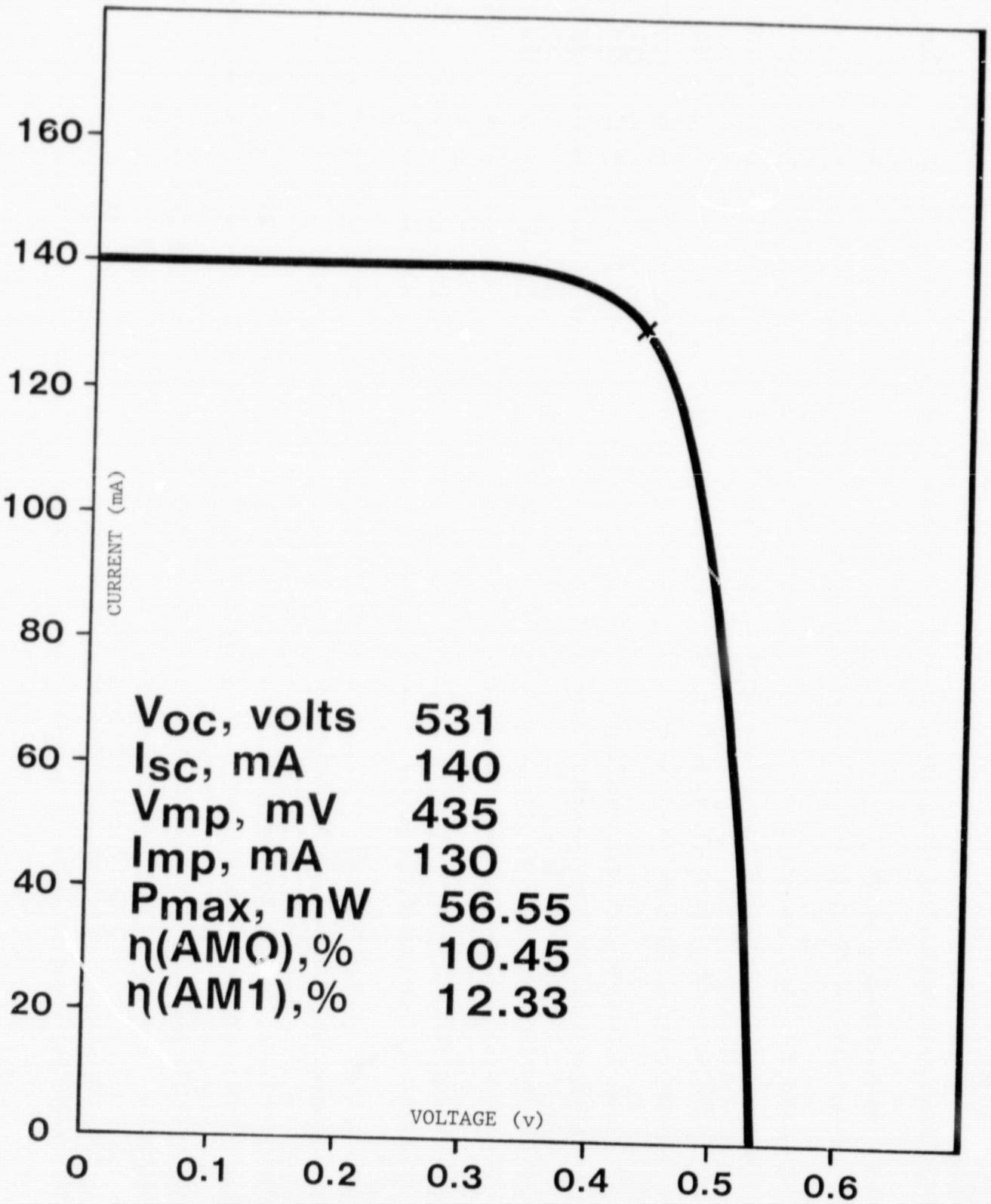

Figure 34. Solar cell data (AMO) on 2 cm x 2 cm HEM cast UMG silicon

1.6 CHARACTERIZATION

1.6.1 Crystal Structure

During Phase II 15-cm diameter and 10 cm x 10 cm x 10 cm ingots were directionally solidified by HEM. Nearly 90% single crystallinity was demonstrated.[11] Sequential scale-up steps were taken during the latter half of the program and ingots of 20-cm diameter, 16 cm x 16 cm, 22 cm x 22 cm, and 34 cm cross-section were cast.

Work on 20-cm diameter ingots was carried out for a short period before square crucibles were received from vendor. Initial attempts with these round crucibles produced single crystal structure in the central area with large grains near the periphery. An example from run 305 is shown in Figure 35.

Solidification of 16 cm x 16 cm cross-section ingots also produced large grains near the crucible wall and single crystal structure in the central area. Figure 36 shows the structure of an ingot cast in run 351. During this run the furnace power was decreased towards the end of the solidification cycle while there was still some molten silicon. This has resulted in very large grains near the top surface. In run 349 single crystal structure was achieved all the way to the top surface of the ingot (Figure 37). In order to establish that the structure of the surface parallel to the growth direction is representative of the entire ingot a slab was sectioned perpendicular to the growth direction. This structure from run 338 is shown in Figure 38. It can be seen that the material shows more than 90% single crystallinity.

The structure similar to that achieved with 16 cm x 16 cm cross-section ingots was also obtained in the first run at 22 cm x 22 cm square cross-section ingots (run 354). This is shown in Figure 39.

Further attempts were made to scale up the ingot size to 32 cm x 32 cm cross-section. Figure 40 shows the structure of a 35-kg ingot case in run 41-41. It can be seen that the

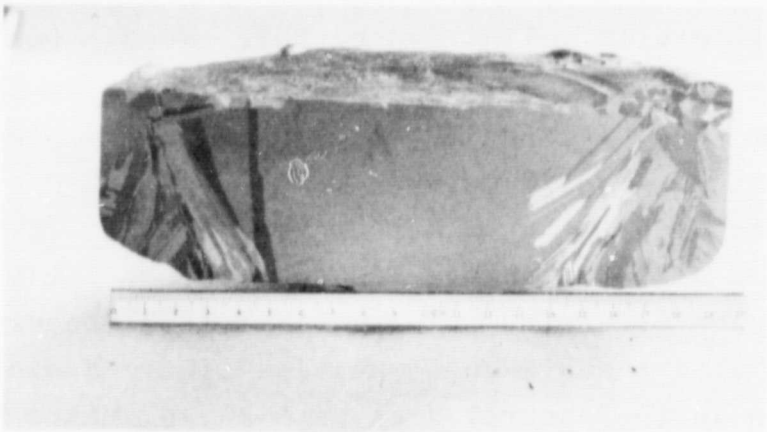

Figure 35. An example of crystallinity achieved in 20 cm diameter ingot

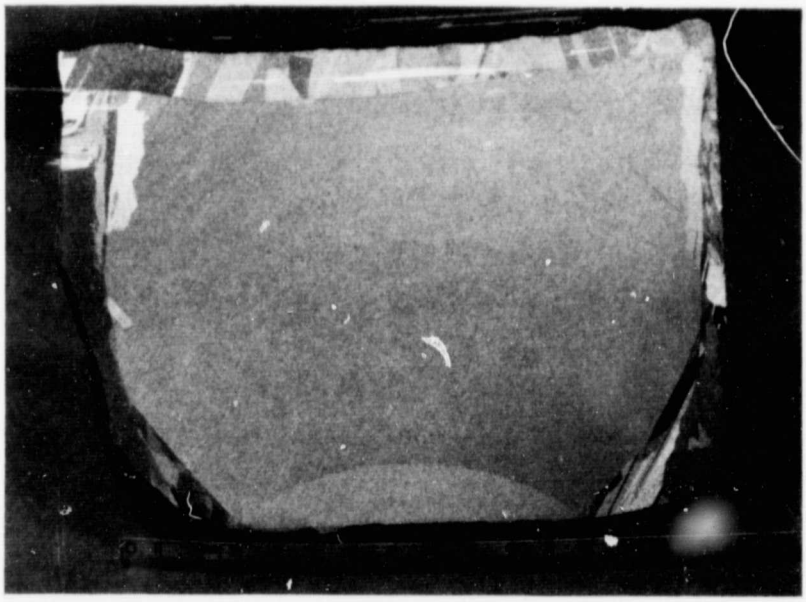

Figure 36. Crystal structure of ingot cast in run 351-C

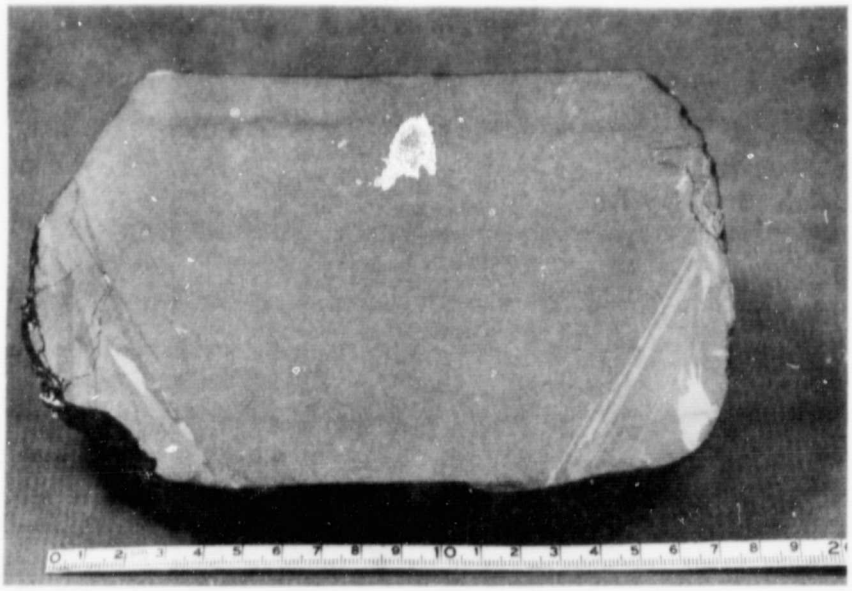

Figure 37. Polished and etched section of ingot cast in run 349-C

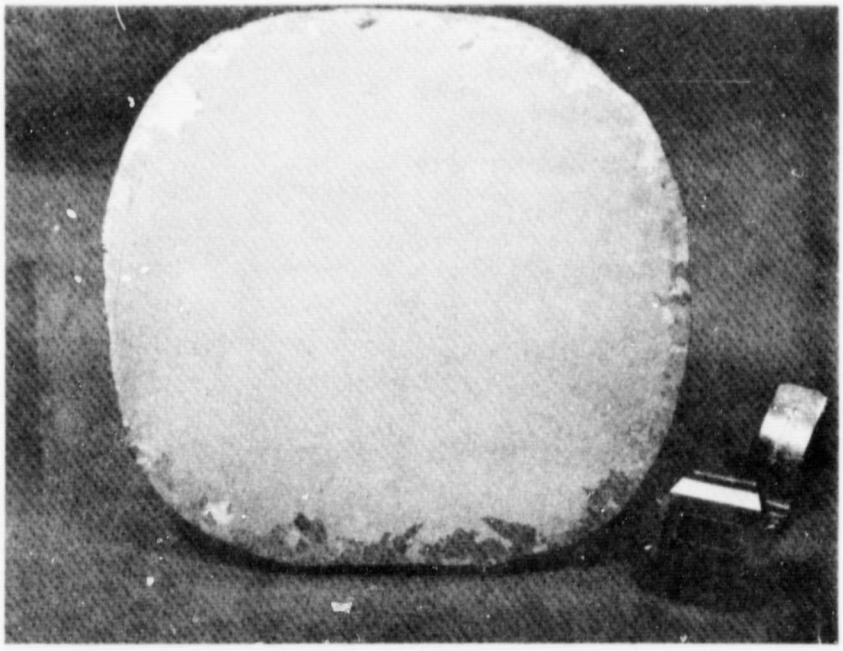

Figure 38. Polished and etched slab sectioned perpendicular to growth direction showing cross-section and crystallinity

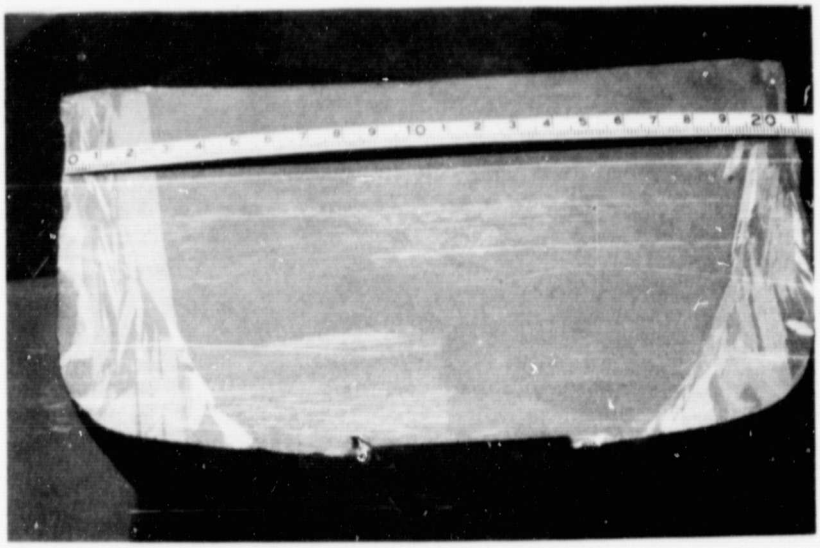

Figure 39. Polished and etched section cf 22 cm x 22 cm cross-section ingot cast in run 354-C

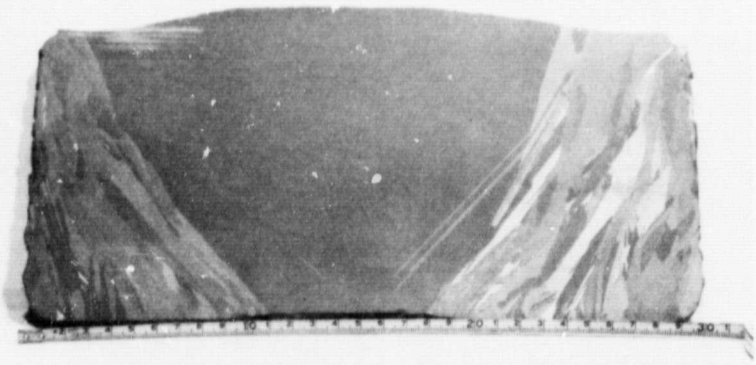

Figure 40. Cross-section of ingot cast in run 41-41

percentage of single crystal area has decreased even though the nature of single crystal central region and large grains on sides has been maintained. In this configuration the heat flow in the HEM furnace has changed substantially because the corners of the crucible are very close to the heating element. The bottom of the crucible was quite cold; hence, crystal growth was initiated off the crucible bottom rather than off the solid-liquid interface. This has resulted in large-grained columnar growth as can be seen by the orientation of the grains.

With the size of the ingots maintained constant attempts were made to improve the single crystallinity of the ingots. Significant improvements of the structure were observed as shown in Figure 41 for run 41-48. It can be seen that breakdown in single crystallinity was restricted to an area of the melted back seed in contact with the crucible. Nucleation at this point caused a few very large grains to be formed.

It is felt that complete single crystal structure can be achieved. The problem has been reduced to optimization of heat flow at the edge of the seed in contact with the crucible. The HEM technology for silicon crystal growth has been scaled up in size over a short period to a stage where it is unique in solving problems of heat flow for very large solidification fronts. A careful analysis of this problem is necessary to solve this problem.

1.6.2 Resistivity Measurements

Measurement of resistivity of HEM-solidified ingots has shown that the boules are of homogeneous resistivity. Data were taken with a four-point probe on an ingot slab. An example of the grid arrangement and the resistivity values are shown in Figure 42a and 42b. The resistivity decreases slightly along the solidification direction; however, the change is so low that in general the ingot can be considered

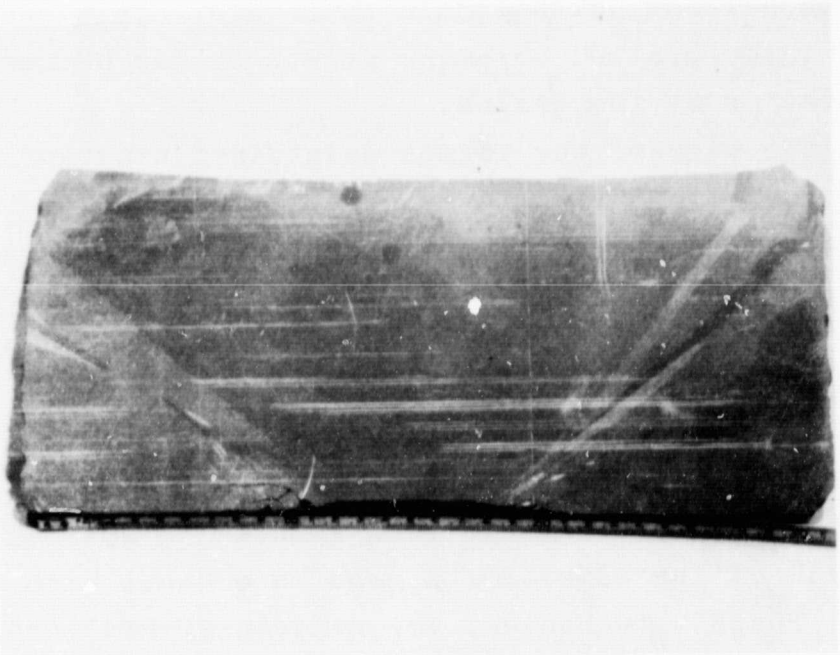

Figure 41. Ground section of ingot 41-48 showing breakdown in crystallinity is very limited

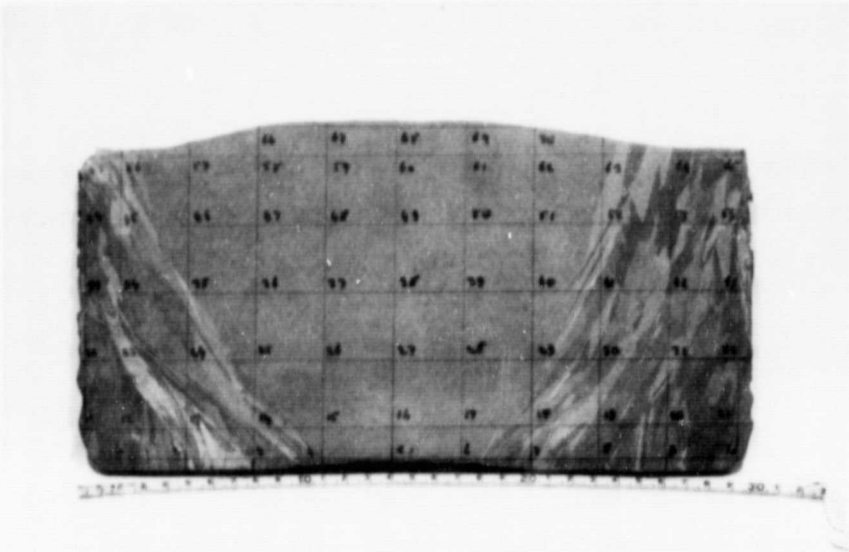

Figure 42a. Grid pattern on cross-section of ingot cast in run 41-41 corresponding to points for resistivity values shown below

	(a)	(b)	(c)	(d)	(e)	(f)	(g)	(h)	(i)	(j)	(k)
(a)				1.31	1.17	1.18	1.28	1.27			
(b)	1.66	1.20	1.19	1.17	1.34	1.29	1.23	1.25	1.24	1.20	1.40
(c)	1.36	1.29	1.34	1.40	1.39	1.46	1.49	1.38	1.29	1.38	1.25
(d)	1.45	1.44	1.45	1.47	1.48	1.58	1.53	1.40	1.48	1.44	1.37
(e)	1.60	1.44	1.49	1.53	1.58	1.57	1.60	1.52	1.62	1.44	1.55
(f)	1.55	1.47	1.55	1.59	1.50	1.52	1.51	1.58	1.59	1.56	1.63
(g)		1.45	1.58	1.47	1.55	8.55	1.66	1.69	1.75	1.57	1.55

Figure 42b. Resistivity data in Ω-cm

having homogeneous resistivity. Some resistivity decrease with solidification is to be expected because the segregation coefficient of boron is less than unity.

1.6.3 Carbon and Oxygen Analysis

Carbon and oxygen analyses were carried out on samples from two ingots--41-41 and 41-48.[4] The vertical cross-sections from areas A, B and C (see Figure 43 for labels) of ingot 41-41 were measured for oxygen concentration. Figure 44 is a plot of the central vertical section (Section A) of ingot 41-41 showing the oxygen distribution from the top of the ingot to the bottom. As can be seen, the oxygen concentration is lowest on top and increases linearly to the bottom of the ingot from 6 to 27 ppma. A similar view of ingot 41-48 in Figure 45 indicates that the increase in oxygen concentration is more gradual and remains between 20-30 ppma for more than three quarters of the height of the ingot. The dissimilar solidification times (40 hours and 28.5 hours for 41-41 and 41-48 respectively) would account for the difference in the oxygen gradients between the two ingots. The oxygen concentration of the CZ grown ingots is approximately 30 ppma. The lower value for HEM ingots may be accounted for by the vacuum operation of HEM.

Other vertical sections were measured and showed the same results. This indicates that the oxygen concentration remains roughly constant in a plane perpendicular to the growth direction. Further confirmation of this result is seen in the oxygen data measured in the horizontal sections shown in Figure 46. For both ingots virtually no change occurred in the oxygen concentration in a horizontal plane from the center of the ingot out toward the edge. This also indicates that the growth interface remains fairly flat during the growth cycle. Table III is a summary of the oxygen content measured in various sections of both ingots. The

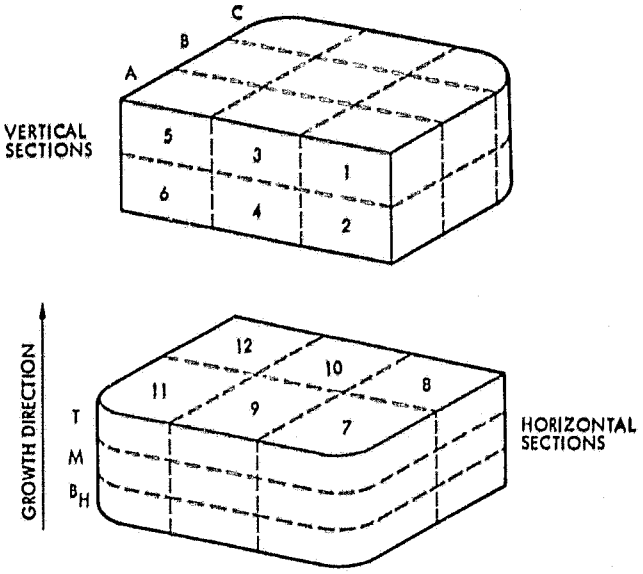

Figure 43. Ingot Map

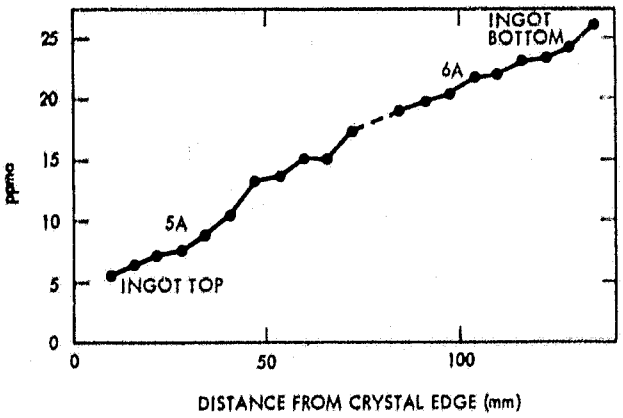

Figure 44. Oxygen distribution of vertical section A across ingot 1

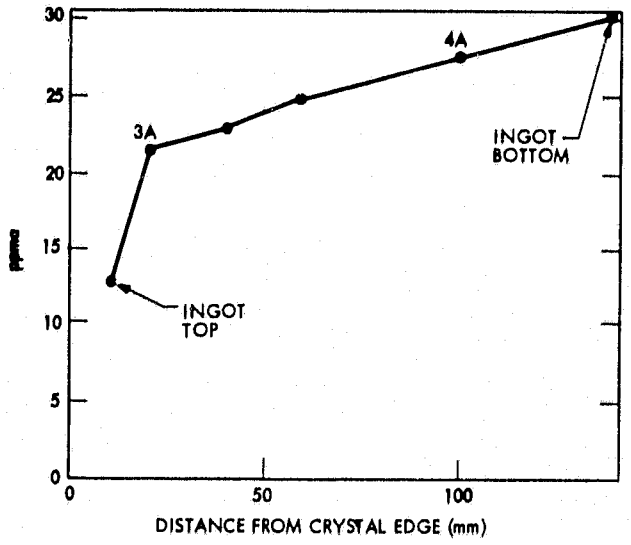

Figure 45. Oxygen distribution in vertical direction across ingot 2

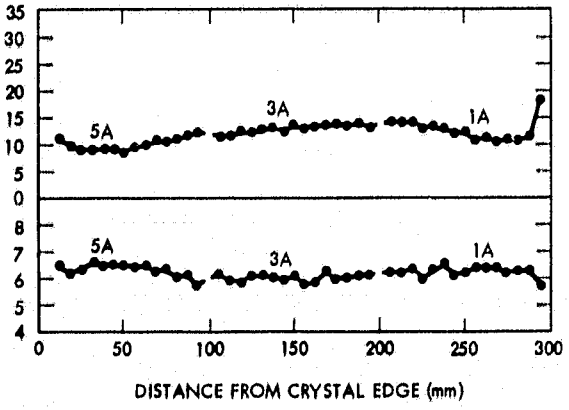

Figure 46. Horizontal distribution of oxygen and carbon across ingot 1

Table III. Oxygen and carbon concentrations as function of position within ingot 1 and 2

ID	Oxygen (ppma)	Carbon (ppma)
	Ingot 1	
1A	3-18	6.25
2A	20-26	6.65
3A	5-21	6.00
4A	23-33	6.48
5A	5-17	6.24
6A	19-26	6.32
1B	5-15	
2B	18-25	
3B	6-18	
4B	22-27	
9M	19-21	
10M	22-24	
	Ingot 2	
3A	13-24	
4A	25-30	
4C	25-33	
9M	24	
10M	24-25	
9T	8-45	
10T	21-19	

data are grouped by sections scanning from the top of the ingot down or from outer edge inward.

The carbon concentration (non-precipitate) was measured in ingot 41-41 and found to be distributed uniformly throughout the ingot. Figure 46 is a plot of the carbon concentrations in the horizontal directions and Figure 47 is a plot of the vertical distribution. The average concentration is approximately 6 ppma. These carbon results are also listed in Table III.

1.6.4 Silicon Carbide Precipitates

Silicon carbide precipitates have been observed in HEM-grown ingots.[5,25,26] One study[26] involving 72 samples from run 41-48 has shown the density of these precipitates to be between 5×10^4 to $1.3 \times 10^6/cm^2$ with most samples showing in the range of $10^5/cm^2$. Another analysis[5] shows an approximate density of $5 \times 10^7/cm^2$. The latter work measured the size of these precipitates to be submicron size; larger precipitates were substantially lower in density. Figure 48 is a photo of the submicron size precipitates.

The silicon carbide precipitates have been associated with backstreaming of oil vapors from the vacuum pump into the growth chamber. This resulted in a dull finish and many particulates on the top surface of the ingot. When a molecular sieve trap was used on the mechanical pump line a bright metallic sheen was observed on the surface of the ingot. This may not be responsible for all the contamination problems, but it does pinpoint a possible source of carbon.

1.6.5 Disclocation Density Measurements

HEM-solidified ingots have been characterized for dislocation density in two studies.[26,5] A study[26] of 72 samples from run 41-48 showed the dislocation density to be in the range of 50 to $2.5 \times 10^3/cm^2$ which is a rather low value. From a random sampling of material from 41-41 the dislocation

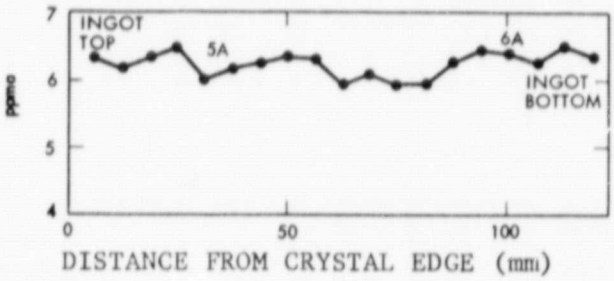

Figure 47. Carbon distribution in vertical direction across ingot 1

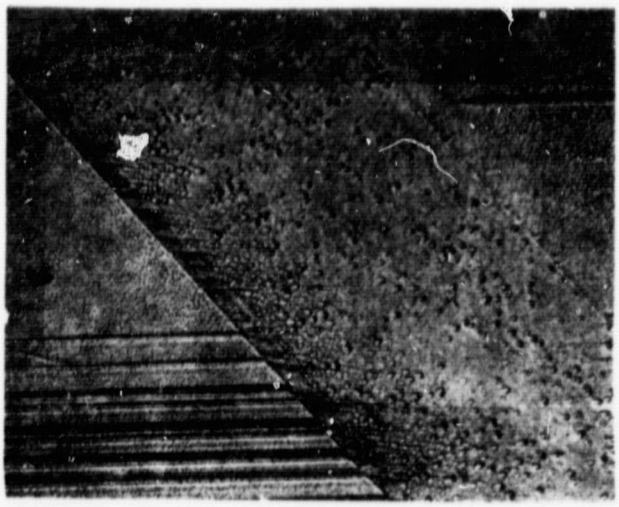

Figure 48. SiC Precipitates at 250X Magnification

density of approximately $10^6/cm^2$ was measured.[5] This dislocation network is independent of the crystal structure.

The large variation between the two studies may be accounted for by the thermal history of the two ingots. Ingot 41-41 was solidified in 40 hours whereas 41-48 in 28.5 hours. In the HEM process the crystal is still in the heat zone after solidification; hence, an annealing cycle can be incorporated to relieve the solidification stresses and lower the dislocation density.

1.6.6 Optimization of Solidification Time

The HEM cycle has not been optimized. Emphasis has been placed on increasing the size of the ingots. During the latter portion of the program it was decided to carry out solidification of 35 kg ingots and study the effect of processing parameters. The main purpose of these experiments was to develop an optimum cycle.

Initial emphasis was placed on optimization of the solidification cycle and degree of single crystallinity. Seven experiments were carried out and the solidification time is listed below:

Run No.	Solidification Time
41-41	40.0 hrs.
41-48	28.5
41-51	40.0
41-55	32.0
41-58	18.5
41-62	40.0
41-70	20.0

In the above data it is seen that the solidification time varies from 18.5 to 40 hours. Based upon experience it can be estimated that the following schedule will hold for the duty cycle for a 36 kg ingot other than the solidification time:

Meltdown time	8 hours
Stabilization	2 hours
Solidification	
Anneal cycle	3 hours
Cooldown time	24 hours

Using this scenario the cycle time for the above-mentioned ingots varied between 55.5 hours and 77.0 hours. Other variants, such as introducing a gas into the chamber and lowering the ingot in the heat zone after anneal cycle, could accelerate cooling of the ingot and thereby shorten the duty cycle. More work is necessary to shorten the cycle time for HEM processing.

1.6.7 Boule Utilization

One of the important parameters that strongly affects the economics of the process is boule utilization or percentage of usable material. Two ingots have been characterized[5] for this parameter. Ingot 41-41 was found to have >90% usable material while for 41-48 this value was lower (about 70%). The difference is accounted for by the fact that 41-41 was 32 cm square cross-section while 41-48 was 34 cm square cross-section. Even though this is a small difference in size it showed a large difference in yield. The heat zone in the experimental furnace unit was designed for 30 cm square crucibles. When 34 cm size ingots were cast, the proximinity of the edge of the crucible to the heating element caused problems

with solidification of silicon in the top corners. This material could not be solidified by the directional cooling of the heat exchanger; the temperature decrease of the furnace caused solidification of the top surface and consequently trapping of liquid silicon below the top layer. During cooldown cycle the corners were broken off resulting in poor yield. A slightly larger heat zone would eliminate this problem.

1.6.8 Solar Cell Performance

Ingots 41-41 and 41-48 were characterized for solar cell performance. Solar cell properties of short circuit current density (J_{sc}), open circuit voltage (V_{oc}), curve fill factor (C_{ff}) and cell efficiency (η) was measured in a number of vertical and horizontal sections. Approximately 150 (2 cm x 2 cm) solar cells from both the horizontal and vertical sections for a total of 300 cells were tested from each ingot. Both the single and polycrystalline material were processed.

The diffusion lengths (L_D) were measured by a surface photovoltage (SPV) method.[19] Individual L_D values along with the corresponding solar cell efficiencies for a vertical section from 41-41 are shown in Figure 49. The results for L_D vary widely between 5-70 μm with the overall average diffusion length of 34 μm. This compares with 82 μm L_D for control cells. A review of normalized efficiency shown in Figure 49 shows that the worst set of solar cells were those containing the seed area. This is not surprising because this CZ material was heated to high temperatures and cooled thereby affecting its lifetime. Table IV summarizes the average solar cell efficiency η for both ingots. The average values of the control cells are also listed. The ratio of the efficiency of the HEM material to that of the control cells

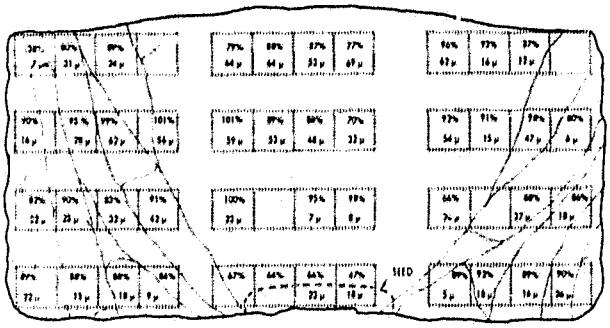

Figure 49. Normalized efficiency and diffusion length values for ingot 1, section A

Table IV. Average V_{oc}, J_{sc}, C_{ff} and normalized η values

Ingot 1						Ingot 2					
Section	V_{oc} (mv)	J_{sc} $\left(\frac{mA}{cm^2}\right)$	C_{ff} (%)	Normalized η (%)	Usable Material (%)	Section	V_{oc} (mv)	J_{sc} $\left(\frac{mA}{cm^2}\right)$	C_{ff} (%)	Normalized η (%)	Usable Material (%)
A	559	25.8	72	85	>90	A	545	27.4	75	90	88
B	563	26.4	70.1	90	>90	B	528	27.4	75	89	75
C	556	26.2	68.3	86	>90	C	540	27.1	72	84	48
Control	574	28.2	73			Control	578	29	75		
T	548	25.9	68	80	>90	T	538	26.5	60	79	39
M	566	27	73	90	>90	M	547	28.1	68	91	67
B_H	550	25.1	73	81	>90	B_H	529	26.5	68	83	89
Control	577	28.2	76			Control	577	28.0	70		

yields the normalized efficiency shown in the table. No optimization was done in the fabrication of these cells. The wafers were processed using only baseline procedures. The baseline process is $POCl_3$ diffusion for 0.3 to 0.4 μm junction, evaporated TiPdAg contacts and SiO antireflection coating.

The overall solar cell efficiency of the material from 41-41 and 41-48, when averaged over all the sections, is 85% of the CZ control cell material. The large grain polycrystalline areas of the HEM ingots have been shown to produce solar cells with efficiencies comparable to those made using the single crystal areas in the HEM material. This result suggests that it is not the grain boundaries that are limiting the quality of the material, but rather some other mechanism. The SiC precipitates are the likely limiting factors.

Since this is the first thorough characterization of the HEM material and since the process is still not optimized, these results indicate that the HEM material has great promise for use in the solar cell industry.

1.7 ECONOMIC ANALYSIS

Projected add-on cost of the HEM ingot casting process has been carried out using IPEG analysis.[27] Sensitivity of various assumptions have also been analysed.

The calculations have been made for a plant to produce 5×10^6 square meters of sheet per year. Production is on three shift basis, 345 days per year. Labor is $9 per hour with 4.7 persons to cover the three-shift cycle. Power is assumed to cost $0.06/kwh.

The following IPEG equation[27] was used:

$$\text{Price} = [(0.49 \times \text{EQPT}) + (110.61 \times \text{SQ FT}) + (2.14 \times \text{SLAB}) + (1.23 + \text{MATS}) + (1.23 \times \text{UTIL})]/\text{QUANTITY}$$

where

EQPT = total equipment costs

SQ FT = working area in square feel

SLAB = direct labor costs

MATS = direct materials costs

UTIL = utilities costs

All dollar numbers are in 1980 dollars.

The calculations have been carried out in two steps: (i) HEM casting of 36 kg ingots (Table V) and (ii) Band saw sectioning into nine 10 cm x 10 cm x 15 cm bars (Table VI).

Therefore, the total add-on price for HEM ingots is $16.30 plus $1.09, or $17.39/m^2. The product will be 10 cm x 10 cm blocks, cast by HEM and sectioned with a bandsaw. The add-on goal for this technology is $18.15/m^2. It can be seen that the HEM technology will meet the DOE price goals of 70¢ per watt with the demonstrated technological achievements.

The sensitivity of the assumptions is shown in Figures 50 through 53. The parameters varied are equipment

cost (Figure 50), Units/operator (Figure 51), Expendables/run (Figure 52) and Cycle time (Figure 53).

TABLE V. IPEG ANALYSIS FOR ASSUMPTIONS AND VALUE ADDED PRICE OF HEM CASTING OF 36 kg INGOTS OF 31 cm X 31 cm X 16 cm SIZE

	Estimate
Equipment cost per unit, $	35,000
Floor space per unit, sq ft	60
Labor, units/operator	10
Cycle time, hrs	56
Expendables/run, $	135
Add-on price, $/m^2	$16.30
Sectioning add-on (Table VI)	1.09/kg
Total add-on price, $/m^2	$17.39
Add-on goal, $/m^2	$18.15

TABLE VI. IPEG ANALYSIS FOR ASSUMPTIONS AND VALUE ADDED PRICE OF BAND SAW SECTIONING

	Estimate
Equipment cost per unit, $	20,000
Floor space per unit, sq. ft.	80
Labor, units/operator	1
Cycle time/boule, hrs.	2.5
Motor power, h.p.	3
Expendables/boule, $	5
Conversion ratio, m^2/kg	1
Add-on Price, $/$m^2$	$1.09

ORIGINAL PAGE IS
OF POOR QUALITY
GOAL
42.2
19
18
17
16
15
14
13
50
40
30
20
10
EQUIPMENT COST, $(1000)
VALUE ADDED PRICE, $/m²

Figure 50.

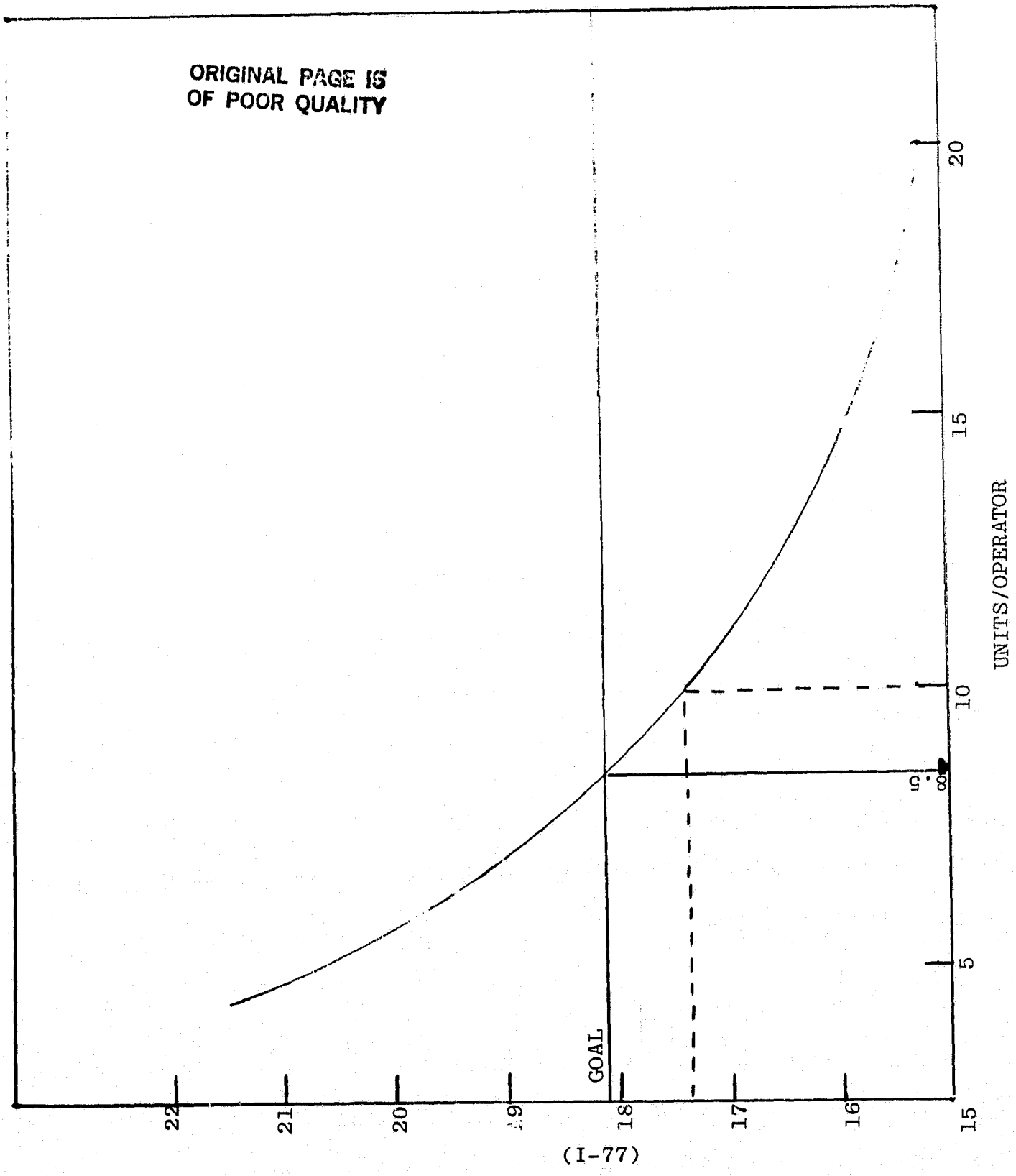
ORIGINAL PAGE IS
OF POOR QUALITY
UNITS/OPERATOR
20
15
10
8.5
5
GOAL
22
21
20
19
18
17
16
15
VALUE ADDED PRICE, $/m²

Figure 51.

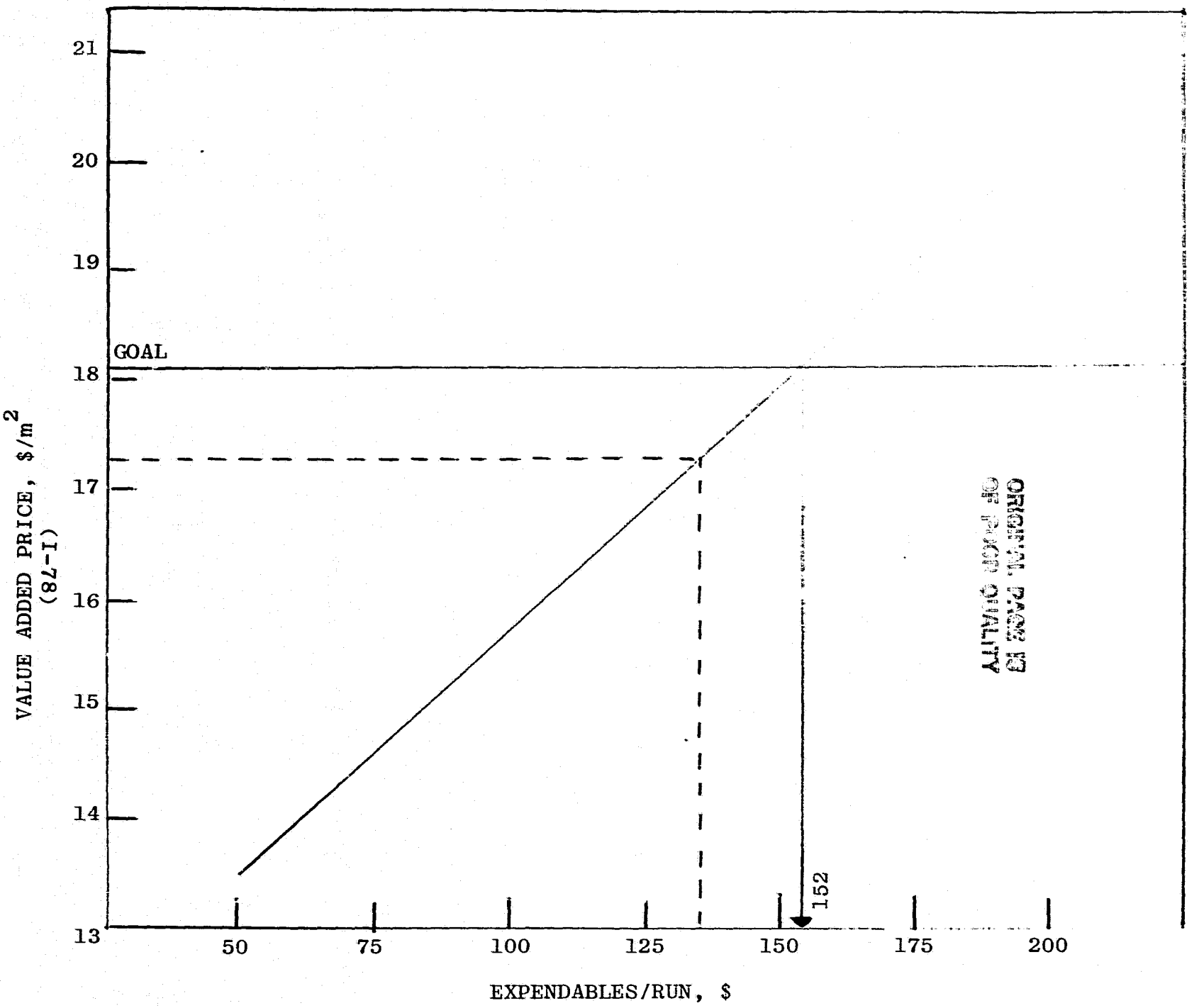
21
20
19
GOAL
18
17
16
15
14
13
VALUE ADDED PRICE, $/m2
(87-I)
50
75
100
125
150
175
200
EXPENDABLES/RUN, $
152

Figure 52.

ORIGINAL PAGE IS
OF POOR QUALITY

Figure 53.

1.8 SUMMARY

1. The HEM solidification of silicon ingots has been scaled up to 45 kg in mass with dimensions of approximately 34 cm x 34 cm x 17 cm.
2. A prototype furnace was designed and fabricated which is large enough to solidify 30 cm cube silicon ingots. A microprocessor programmer was incorporated for simultaneously controlling furnace temperature and the helium flow.
3. The heat treatment of silica crucibles to develop a graded structure for delamination during cooldown has been projected. No problems of ingot cracking were encountered during the scaleup to such large sizes.
4. A square cross-section crucible with sharp corners and flat sides has been developed which gives >90% yield of square material from a HEM cast ingot.
5. Flattening of sides of "squarish" crucibles using thick molybdenum sheets could not be accomplished. Significant progress was, however, achieved by using rigid graphite retainers.
6. The concept of using flat silica plates welded together to achieve square corners of ingots has been demonstrated.
7. No problems were encountered in casting silicon by HEM in vitreous graphite crucibles. The ingot was crack-free but tenaciously attached to the crucible.
8. Experimental measurements have shown that during crystal growth there are very shallow gradients within liquid silicon.
9. Mapping of interface has shown that the last material to solidify is near the wall of the crucible.
10. A 2-inch diameter heat exchanger could not be utilized because of leakage problems at the brazed molybdenum stainless steel joint.

11. The heat flow, though controlled by insulation parameters initially, was governed by steady state conditions towards the end of the solidification cycle.
12. Nearly single crystal structure was achieved with one directional solidification using solar metallurgical meltstock.
13. Large SiC particles were dispersed throughout the structure with particularly heavy concentration near the seed area and in the last material to solidify.
14. The SiC concentration in solar grade starting material ingots was reduced by double solidification
15. Addition of silica powder to the meltstock and/or silica coating on solar metallurgical meltstock reduced SiC particles.
16. The rejection of impurities using solar metallurgical meltstock was limited to the edge of the ingot.
17. It has been demonstrated that 12.33 per cent efficiency solar cells can be fabricated using HEM solidified solar metallurgical meltstock after double solidification.
18. The single crystallinity breakdown in 35 kg ingots is limited to the periphery of the seed in contact with the crucible.
19. The resistivity of HEM solidified ingots has been shown to be very uniform over the entire cross-section for 35 kg ingots.
20. The carbon content of HEM silicon is approximately 6 ppma.
21. The oxygen distribution in the horizontal direction is very uniform; however, it decreases along the growth direction. Typical values observed are lower than that for CZ material.
22. Silicon carbide precipitates have been observed in HEM material. They have been primarily associated with back streaming of oil vapors from the mechanical pump. A molecular sieve trap on the vacuum line has reduced the contamination.

23. The dislocation density in HEM material is associated with the thermal history of the ingot.
24. The overall efficiency of the useable material averaged throughout the ingot is 85% of the control CZ material using baseline processing.
25. The large grain polycrystalline HEM is comparable in efficiency to the single crystal HEM material.
26. Over 90% useable material has been demonstrated in HEM ingots.
27. The breaking of corners of ingots in some cases has been associated with trapping of liquid silicon. This is caused by the proximity of the corner to the heating element and can be prevented by using a slightly larger heat
28. A 56-hour duty cycle has been demonstrated for 36 kg ingots.
29. The cooldown time can be reduced by introducing argon or helium gas into the chamber after solidification. The add-on cost of HEM processing using IPEG analysis is $\$17.39/m^2$. This is lower than the allocation of $\$18.15/m^2$.

1.9 REFERENCES

1. F. Schmid and C. P. Khattak, JPL 954373, Crystal Systems, Quarterly Progress Report No. 2, Phase III (1979).

2. C. P. Khattak and F. Schmid, Proc. 13th IEEE Photovoltaic Specialists Conf., Washington, DC (1978).

3. F. Schmid and C. P. Khattak, JPL 954373, Crystal Systems, Quarterly Progress Report No. 1, Phase IV (1979).

4. K. A. Dumas, C. P. Khattak and F. Schmid, Proc. 15th IEEE Photovoltaic Specialists Conf., Kissimmee, FL (1981).

5. C. P. Khattak, F. Schmid and L. P. Hunt, Proc. 157th Meeting, Electrochemical Soc. (1980).

6. F. Schmid, M. Basaran and C. P. Khattak, Proc. 3rd E.C. Photovoltaic Conf., Cannes (1980).

7. K. M. Kim, A. F. Witt and H. C. Gatos, J. Electrochem. Soc. 119 (1972).

8. F. Schmid and C. P. Khattak, Optical Spectra (May, 1981).

9. D. Helmreich, Proc. 157th Meeting, Electrochemical Soc. (1980).

10. J. Fally and C. Guenel, Proc. 3rd E.C. Photovoltaic Conf., Cannes (1980).

11. F. Schmid and C. P. Khattak, JPL 954373, Crystal Systems, Final Report, Phase II (1979).

12. H. C. Torrey and C. A. Witner, Crystal Rectifiers, McGraw-Hill Book Co., NY (1948).

13. J. Hino and H. E. Stauss, J. Metals, 4 (1952).

14. Y. M. Shashkon and V. P. Grishin, Soviet Physics Solid State, 8 (February, 1966).

15. F. Schmid and C. P. Khattak, JPL 954373, Crystal Systems, Final Report, Phase I (1977).

16. M. N. Ozisik, Boundary Value Problems of Heat Conduction, International Textbook Co. (1968).

17. T. Z. Kattamis, M. Basaran and E. Chang, Proc. Conf. Heat and Mass Transfer in Metallurgical Systems, Dubrovnik, Yugoslavia (1979).

18. CRC Handbook of Chemistry and Physics, CRC Press, 61st ed.

19. Annual Book of ASTM Standards, ASTM, Philadelphia, PA (1979).

20. W. R. Runyan, Silicon Semiconductor Technology, McGraw-Hill Book Co., NY (1948).

21. L. P. Hunt and V. D. Dosaj, Dow Corning Corp., Final Report, JPL 954559 (1979).

22. C. V. Hari Rao, H. E. Bates and K. V. Ravi, J. Appl. Phys. 47 (1976).

23. F. Schmid and C. P. Khattak, JPL 954373, Crystal Systems, Quarterly Progress Report No. 2, Phase IV (1980).

24. F. Schmid, C. P. Khattak, T. G. Digges, Jr., and L. Kaufman, J. Electrochem. Soc., 126 (1979).

25. Materials Research, Inc., Technical Report MRI-283 (1981).

26. Materials Research, Inc., Technical Report MRI-285 (1981).

APPENDIX I-A

TABULATION OF HEAT EXCHANGER AND FURNACE TEMPERATURES

TABULATION OF HEAT-EXCHANGER AND FURNACE TEMPERATURES

RUN	PURPOSE	SEEDING		GROWTH CYCLE			REMARKS
		FURN. TEMP. ABOVE M.P. °C	H.E. TEMP. BELOW M.P. °C	RATE OF DECREASE H.E. TEMP. °C/HR.	RATE OF DECREASE FURN. TEMP. °C	GROWTH TIME IN HOURS	
301-C	Cast 20 cm diameter ingots	-	-	-	-	-	Run aborted due to distortion of crucible.
302-C	Cast 20 cm diameter ingots	-	-	-	-	-	Run aborted due to distortion of crucible.
303-C	Cast 20 cm diameter ingots	13	341	130	13	4.5	3.8 kg ingot cast.
304-C	Cast 20 cm diameter, 5.3 kg ingot	15	277	185	15	6.5	Some attachment of crucible.
305-C	Cast 20 cm diameter, 4.7 kg ingot	11	280	132	11	6.5	Very limited attachment. Good crystallinity.
306-C	Crucible development with 10 cm x 10 cm ingot	19	236	115	19	5.5	Very limited attachment. Very good crystallinity.
307-C	Crucible development with 10 cm x 10 cm ingot	3	223	170	3	7.5	Power failure at end of growth cycle. Good delamination of crucible and very good crystallinity.
308-C	Crucible development with 15 cm diameter ingot	<3	260	125	1	6.5	Attachment of crucible caused cracking.

. . . cont.

TABULATION OF HEAT-EXCHANGER AND FURNACE TEMPERATURES (Cont.)

RUN	PURPOSE	SEEDING		GROWTH CYCLE			REMARKS
		FURN. TEMP. ABOVE M.P. °C	H.E. TEMP. BELOW M.P. °C	RATE OF DECREASE H.E. TEMP. °C/HR.	RATE OF DECREASE FURN. TEMP. °C	GROWTH TIME IN HOURS	
309-C	Crucible development with 15 cm diameter ingot	<3	222	160	1	7.0	Attachment of crucible in localized area.
310-C	Crucible development with 15 cm diameter ingot	-	-	-	-	-	Run terminated as crucible cracked
311-C	Crucible development with 15 cm diameter ingot	5	254	132	5	6.8	Minimal attachment of crucible in localized areas.
312-C	Crucible development with 15 cm diameter ingot	13	252	122	13	8.6	Crucible attachment to ingot
313-C	Cast 20 cm diameter, 5.3 kg ingot	10	224	120	10	7.0	Crucible attachment in some areas.
314-C	Cast 20 cm diameter, 5.3 kg ingot	36	172	147	36	9.0	Crucible attachment in localized areas. Good crystallinity.
315-C	Cast 20 cm diameter, 6.3 kg ingot	4	168	154	4	7.0	Minimized crucible attachment in localized areas.
316-C	Crucible development with 15 cm diameter ingot	5	165	158	5	8.3	Attachment of crucible to ingot.

...cont.

TABLE I. TABULATION OF HEAT-EXCHANGER AND FURNACE TEMPERATURES (Cont.)

RUN	PURPOSE	SEEDING		GROWTH CYCLE			REMARKS
		FURN. TEMP. ABOVE M.P. °C	H.E. TEMP. BELOW M.P. °C	RATE OF DECREASE H.E. TEMP. °C/HR.	RATE OF DECREASE FURN. TEMP. °C	GROWTH TIME IN HOURS	
317-C	Improve solidification cycle	8	160	161	8	6.5	Controlling with power
318-C	Improve solidification cycle	< 3	110	234	0	6.8	Controlling with power
319-C	Improve solidification cycle	3	100	256	3	5.5	Controlling with power
320-C	Improve solidification cycle	3	152	226	3	6.3	Controlling with power
321-C	Improve solidification cycle	5	135	262	5	6.0	Controlling with power
322-C	Improve solidification cycle	< 3	165	258	0	4.8	Controlling with power
323-C	Improve uniformity of graded structure of crucible	< 3	213	237	2	4.5	Good crystallinity but attachment of crucible to ingot
324-C	Improve uniformity of graded structure of crucible	< 3	145	333	2	4.5	Crucible attached to ingot

(cont.)

TABULATION OF HEAT-EXCHANGER AND FURNACE TEMPERATURES (cont.)

RUN	PURPOSE	SEEDING		GROWTH CYCLE			REMARKS
		FURN.TEMP. ABOVE M.P. °C	H.E.TEMP. BELOW M.P. °C	RATE OF DECREASE H.E. TEMP. °C/HR.	RATE OF DECREASE FURN. TEMP. °C	GROWTH TIME IN HOURS	
325-C	Crucible development using lathe	< 3	145	416	0	4.5	Crucible attachment caused cracking
326-C	Crucible development using lathe	< 3	163	295	0	5.7	Crucible attachment caused cracking
327-C	Crucible development using lathe	4	133	346	4	4.0	Good crystallinity achieved
328-C	Crucible development using lathe	3	146	314	3	4.5	Good crystallinity achieved
329-C (1-89)	Cast 4.5 kg, 16 cm x 16 cm square ingot	< 3	135	29?	0	5.7	Crack-free ingot cast
330-C	Cast 16 cm x 16 cm square ingot	< 3	115	33?	0	6.0	Minor attachment in bottom area
331-C	Cast 8.1 kg, 16 cm x 16 cm square ingot	4	110	360	4	14.5	Minor attachment in bottom area
332-C	Cast 4.3 kg, 16 cm x 16 cm square ingot	4	96	246	3	5.75	Very good crystallinity
333-C	Cast 4.3 kg, 16 cm x 16 cm square ingot	< 3	95	362	0	6.00	Very good crystallinity

(cont.)

TABULATION OF HEAT-EXCHANGER AND FURNACE TEMPERATURES (cont.)

RUN	PURPOSE	SEEDING		GROWTH CYCLE			REMARKS
		FURN. TEMP. ABOVE M.P. °C	H.E. TEMP. BELOW M.P. °C	RATE OF DECREASE H.E. TEMP. °C/HR.	RATE OF DECREASE FURN. TEMP. °C	GROWTH TIME IN HOURS	
334-C	Cast 4.3 kg, 16 cm x 16 cm square ingot	4	93	274	4	6.5	Minor chipping of ingot
335-C	Cast 4.3 kg, 16 cm x 16 cm square ingot	15	109	308	15	6.75	Very good crystallinity
336-C	Cast 4.3 kg, 16 cm x 16 cm square ingot	-	-	-	-	-	Run terminated; reaction of Si with graphite pipe
337-C	Cast 8.2 kg ingot	-	-	-	-	-	Run terminated; Heat Exchanger failure
338-C	Cast 7.7 kg ingot	11	205	400	11	16.5	Minor chipping of ingot
339-C	Improve crucible delamination	< 3	96	380	0	5.3	Very good crystallinity.
340-C	Test effect of larger plug	< 3	101	340	0	6.5	Very good crystallinity.
341-C	Improve crucible delamination	< 3	102	356	0	6.75	Attachment of ingot to crucible.
342-C	Modified heat treatment of crucible	< 3	98	338	1	7.25	Non-uniform graded structure of crucible.
343-C	Test larger plug	< 3	110	354	2	6.5	Very good crystallinity.
344-C	Modified heat treatment of crucible	< 3	107	440	1	8.0	Non-uniform graded structure of crucible.

...cont.

TABULATION OF HEAT-EXCHANGER AND FURNACE TEMPERATURES (Cont.)

RUN	PURPOSE	SEEDING		GROWTH CYCLE			REMARKS
		FURN. TEMP. ABOVE M.P. °C	H.E. TEMP. BELOW M.P. °C	RATE OF DECREASE H.E. TEMP. °C/HR.	RATE OF DECREASE FURN. TEMP. °C	GROWTH TIME IN HOURS	
345-C	Cast 8.3 kg ingot	< 3	121	501	0	15.5	Very good crystallinity.
346-C	Cast 8.3 kg ingot	3	128	170	3	11.5	No "chipping" of ingot.
347-C	Improve crucible delamination	12	140	478	12	6.3	Partial delamination of crucible. Very good crystallinity.
348-C	Improve crucible delamination	4	132	413	4	6.25	Partial delamination of crucible. Very good crystallinity
349-C	Cast 6.5 kg ingot	< 3	112	389	1	10.75	Very good crystallinity.
350-C	Cast 7.5 kg ingot	3	128	370	3	11.3	Good crystallinity.
351-C	Cast 7.5 kg ingot	6	121	393	4	10.5	Good crystallinity. Limited attachment of crucible.
352-C	Improve crucible delamination	-	-	-	-	-	Run terminated due to helium pump malfunction.
353-C	Crystal growth of upgraded metallurgical silicon meltstock	< 3	113	420	0	7.75	No cracking of ingot. Single crystallinity achieved. Impurities segregated during directional solidification.

...cont.

TABULATION OF HEAT-EXCHANGER AND FURNACE TEMPERATURES (cont.)

RUN	PURPOSE	SEEDING		GROWTH CYCLE			REMARKS
		FURN. TEMP. ABOVE M.P. °C	H.E. TEMP. BELOW M.P. °C	RATE OF DECREASE H.E. TEMP. °C/HR.	RATE OF DECREASE FURN. TEMP. °C	GROWTH TIME IN HOURS	
354-C	Solidify 10.5 kg, 22 cm square ingot	< 3	111	353	0	9.8	No cracking of ingot. Very good crystallinity all the way to the top of the boule.
355-C	Solidify 8.1 kg 16 cm square ingot	4	91	478	4	10.0	No cracking of ingot.
356-C	Solidify 16 cm square ingot	4	93	450	-	-	Control instrumentation malfunction. Power shut down prematurely.
357-C	Optimize post-solidification cycle	11	109	484	11	6.7	Attachment of crucible in some areas.
358-C	Optimize post-solidification cycle	7	112	438	7	7.0	Very limited attachment of crucible.

...cont.

TABULATION OF HEAT-EXCHANGER AND FURNACE TEMPERATURES (Continued)

RUN	PURPOSE	SEEDING		GROWTH CYCLE			REMARKS
		FURN. TEMP. ABOVE M.P. °C	H.E. TEMP. BELOW M.P. °C	RATE OF DECREASE H.E. TEMP. °C/HR.	RATE OF DECREASE FURN. TEMP. °C	GROWTH TIME IN HOURS	
40-01	Directional solidification of UMG silicon	15	-	-	14	13.8	Nearly single crystal structure.
40-02	Interface monitoring during growth	18	-	-	18	12.0	Crack-free ingot cast.
40-03	Slagging of UMG silicon	19	-	-	8	12.5	Seed melted out. Very large grains formed.
40-04	Test welded crucible	11	-	-	10	11.25	No problem of silicon containment.
40-05	Slagging of UMG silicon	5	-	-	5	11.25	Nearly single crystal structure. Impurities segregated to bottom and top areas.
40-06	Test different form of silica crucible	8	-	-	8	4.4	Crucible attachment in some areas.
40-07	Use welded flat plate crucible	5	-	-	5	8.0	Crack-free ingot cast.
40-08	Test different form of silica crucible	19	-	-	19	12.0	Some attachment of crucible to ingot.
40-09	Test different form of silica crucible	18	-	-	14	12.0	Minor attachment limited to few areas in the bottom.

...cont.

TABULATION OF HEAT-EXCHANGER AND FURNACE TEMPERATURES (cont.)

RUN	PURPOSE	SEEDING		GROWTH CYCLE			REMARKS
		FURN.TEMP. ABOVE M.P. °C	H.E.TEMP. BELOW M.P. °C	RATE OF DECREASE H.E. TEMP. °C/HR.	RATE OF DECREASE FURN. TEMP. °C	GROWTH TIME IN HOURS	
40-09A	To use vitreous graphite as crucible	24	-	-	24	3.0	No ingot cracking but ingot attached to crucible.
40-10C	Test for another form of crucible	10	-	-	10	8.5	A thin layer of crucible attached to ingot and prevented cracking.
40-11C	Cast UMG silicon with slagging	18	-	-	1	7.5	Cut section shows large grain throughout ingot.
40-12C	Cast UMG silicon with slagging	14	-	-	6	7.8	Very clean cross-section. Nearly single crystal. SiC particles are either floated at the top of the ingot, or sink onto seed.
41-01C	Test new furnace	9	-	-	9	9.0	Good performance.
41-02C	Cast 20 x 20 cm square ingot in new furnace	7	-	-	7	21.0	Crack-free ingot.
41-03C	Cast 20 x 20 cm square ingot in new furnace	3	-	-	3	33.0	Crack-free ingot. Cross-section shows large grains due to insufficient melt-back of seed top surface.

...cont.

TABULATION OF HEAT-EXCHANGER AND FURNACE TEMPERATURES (cont.)

RUN	PURPOSE	SEEDING		GROWTH CYCLE			REMARKS
		FURN. TEMP. ABOVE M.P. °C	H.E. TEMP. BELOW M.P. °C	RATE OF DECREASE H.E. TEMP. °C/HR.	RATE OF DECREASE FURN. TEMP. °C	GROWTH TIME IN HOURS	
41-04C	Maintain square shape with heavy wall moly retainer	5	-	-	2	9.0	Crack-free ingot. Nearly single crystal structure.
41-05C	Maintain square shape with heavy wall moly retainer	6	-	-	6	16.0	Crack-free ingot.
41-06	High purity doped ingot	8	-	-	8	7.5	Ingot fractured due to crucible attachment
41-07	High purity doped ingot	9	-	-	1	12.0	No ingot cracking, no crucible attachment
41-08	Large ingot	3	-	-	1	15.0	Good large ingot, except distorted sides due to no rigid support
41-09	Test of welded plates	1	-	-	1	14.0	Flat sides, sharp corners, good ingot
41-10	Retain square shape	1	-	-	1	12.0	Sides of ingot are flat.
41-11	Retain square shape	4	-	-	1	14.0	Sides flat, corners rounded
41-12	Retain square shape	2	-	-	1	14.0	Good shape, flat sides.

...cont.

TABULATION OF HEAT-EXCHANGER AND FURNACE TEMPERATURES (Cont.)

RUN	PURPOSE	SEEDING		GROWTH CYCLE			REMARKS
		FURN. TEMP. ABOVE M.P. °C	H.E. TEMP. BELOW M.P. °C	RATE OF DECREASE H.E. TEMP. °C/HR.	RATE OF DECREASE FURN. TEMP. °C	GROWTH TIME IN HOURS	
41-13C	Improve square shape of ingot	14	-	-	11	34	Graphite box has held ingot to a square shape with flat sides
41-14C	Improve solidification	2			1	31	Profile does not show significant improvement across bottom
41-15C	Cast 34 cm x 34 cm cross-section ingot	14	-	-	4	6.5	First large 12-inch square ingot. No cracking.
41-16C	Cast 40 kg ingot	-	-	-	-	-	Run terminated as silicon leaked from crucible before start of growth cycle
41-17C	Test welded crucible	-	-	-	-	-	Run terminated during meltdown. Instrumentation malfunction.
41-18C	Test new plug design	39	-	-	1	27	No significant improvement in crystallinity
41-19C	Improve crystallinity across bottom of ingot	40	-	-	2	30	No significant improvement in crystallinity

...cont.

TABULATION OF HEAT-EXCHANGER AND FURNACE TEMPERATURES (cont.)

RUN	PURPOSE	SEEDING		GROWTH CYCLE			REMARKS
		FURN. TEMP. ABOVE M.P. °C	H.E. TEMP. BELOW M.P. °C	RATE OF DECREASE H.E. TEMP. °C/HR.	RATE OF DECREASE FURN. TEMP. °C	GROWTH TIME IN HOURS	
41-20C	Cast 45 kg ingot	45	-	-	33	8	Crucible leaked at crack in corner along wall. Final weight was 20 kg.
41-21C	Improve crystallinity across bottom of ingot	-	-	-	-	-	Run terminated during meltdown. Problems with cooling water system.
41-22C	Effect of solidification parameters	12	-	-	12	12.5	Single crystal growth not achieved throughout the height of ingot
41-23C	Effect of solidification parameters	4	-	-	3	32.0	Single crystal growth achieved to the top surface of ingot
41-24C	Use shallow gradients at bottom	25	-	-	27	21.5	Freezing occurred on top surface
41-25C	Cast 34 cm x 34 cm, 45 kg ingot	17	-	-	17	36.0	No solidification problems. Slight cracking near top periphery.

...cont.

TABULATION OF HEAT-EXCHANGER AND FURNACE TEMPERATURES (Cont.)

RUN	PURPOSE	SEEDING		GROWTH CYCLE			REMARKS
		FURN.TEMP. ABOVE M.P. ^{o}C	H.E.TEMP. BELOW M.P. ^{o}C	DECREASE OF H.E. TEMP. ^{o}C/HR.	DECREASE OF FURN. TEMP. ^{o}C	GROWTH TIME IN HOURS	
41-26C	Cast 34 cm x 34 cm, 45 kg ingot	-	-	-	-	-	Run terminated during melt-down. Cracking in a corner of the crucible.
41-27	Improve growth cycle	32	-	-	40	36.5	No significant improvement in solidification time.
41-28	Cast 34x34cm^2, 45 kg ingot	39	-	-	40	42	Good solid ingot
41-29	Cast 34x34cm^2, 45 kg ingot. Test 2"Ø heat exchanger.	-	-	-	-	-	Run aborted during meltdown.
41-30C	Test 32 cm x 32 cm crucible with 45 kg charge	-	-	-	-	-	Run aborted during meltdown.
41-31C	Test 32 cm x 32 cm crucible with 35 kg charge	9	-	-	9	28	Good solid ingot, flat sides
41-32C	Test welded crucible	10	-	-	12	5.5	
41-33C	Test 32 cm x 32 cm crucible with 45 kg charge	-	-	-	-	-	Run aborted during meltdown.

(I-98)

...cont.

TABULATION OF HEAT-EXCHANGER AND FURNACE TEMPERATURES (Cont.)

RUN	PURPOSE	SEEDING		GROWTH CYCLE			REMARKS
		FURN.TEMP. ABOVE M.P. °C	H.E.TEMP. BELOW M.P. °C	DECREASE OF H.E. TEMP. °C/HR.	DECREASE OF FURN. TEMP. °C	GROWTH TIME IN HOURS	
41-34C	Test 32 cm x 32 cm crucible with 45 kg charge	16	-	-	20	31	Good solid ingot, flat sides.
41-35C	Test 23 cm x 23 cm crucible with 15 kg charge	14	-	-	18	10	Freezing occurred on top surface
41-36C	Test 23 cm x 23 cm crucible with 15 kg charge	31	-	-	36	12	Food solid ingot, flat sides.
41-37 (I-99)	Improve crystallinity		-	-	-		Run aborted during meltdown due to the problem at the heat exchanger fitting
41-38	Improve crystallinity		24	42	25		Good crystallinity
41-39	Improve crystallinity		8	24	25		No seed meltback on top of seed
41-40	Improve crystallinity		6	22	27		No seed meltback
41-41	Cast 32 x 32 cm^2 35 kg ingot		15	33	40		Crucible leaked at crack on the wall. Final weight was 30.8 kg.

...cont.

TABULATION OF HEAT-EXCHANGER AND FURNACE TEMPERATURES (Cont.)

RUN	PURPOSE	SEEDING FURN.TEMP. ABOVE M.P. °C	GROWTH CYCLE DECREASE OF FURN.TEMP.°C	GROWTH TIME IN HRS.	REMARKS
41-42	Improve crystallinity at the bottom	37	29	24	
41-43	Improve crystallinity at the bottom	48	48	32	
41-44	Improve crystallinity at the bottom	62	64	31.5	
41-45	Improve crystallinity at the bottom	39	39	23	
41-46	Cast 32 x 32 cm^2 35 kg ingot	-	-	-	Run aborted after 17 hrs. of growth time due to crucible leakage
41-47	Improve crystallinity at the bottom	33	33	24	
41-48	Cast 32 cm x 32 cm^2 35 kg ingot	14	14	28.5	Ingot sent to JPL for characterization
41-49	Improve crystallinity at the bottom	33	33	14	
41-50	Improve crystallinity at the bottom	20	20	21	Oxygen sensor probe put in furnace

...cont.

TABULATION OF HEAT-EXCHANGER AND FURNACE TEMPERATURES (Cont.)

RUN	PURPOSE	SEEDING FURN.TEMP. ABOVE M.P. °C	GROWTH CYCLE DECREASE OF FURN.TEMP.°C	GROWTH TIME IN HRS.	REMARKS
41-51	Improvement of heat flow by insulating corners of crucible	6	8	40.0	No significant improvement in preventing trapping of liquid. Ingot sent to JPL.
41-52	Reduce cooldown time by introducing argon into chamber	35	35	14.0	Ingot cracked in half due to thermal stress
41-53	Improve crystallinity by using taller seed	38	40	22.0	Meltdown not sufficient around the seed
41-54	Measure temperature gradients in liquid	6	8	15.0	No large gradients in liquid. Probed position of interface during growth.
41-55 (I-101)	Reduce cooldown time by introducing argon into chamber at high temperatures	34	34	32.0	No cracking of ingot.
41-56	Determine shape of interface experimentally	17	19	15.0	Data reported in Heat Flow section
41-57	Reduce cooldown time by introducing He into chamber	31	36	21.0	Ingot cracked due to thermal stress
41-58	Improve solidification time in 35 kg ingot	30	37	18.5	Some freezing occurred from the top surface

...cont.

TABULATION OF HEAT-EXCHANGER AND FURNACE TEMPERATURES (Cont.)

RUN	PURPOSE	SEEDING FURN.TEMP. ABOVE M.P. °C	GROWTH CYCLE DECREASE OF FURN.TEMP. °C	GROWTH TIME IN HRS.	REMARKS
41-59	Improve solidification time in 35 kg ingot	2	4	33.0	Low temperature caused freezing; hence temperature was raised to prevent freezing.
41-62	Same as 41-59			40.0	
41-70	Same as 41-59			20.0	

D2

PART II

MULTI-WIRE SLICING -
FIXED ABRASIVE SLICING TECHNIQUE (FAST)

PART II

TABLE OF CONTENTS

PART II

LIST OF FIGURES

LIST OF TABLES

ABSTRACT

The Fixed Abrasive Slicing Technique (FAST) is a new slicing technique that has been developed to slice ingots more effectively. It has been demonstrated that 25 wafers/cm can be sliced from 10-cm diameter and 19 wafers/cm from 15-cm diameter ingots. Over 99% yield (222 out of a possible 224) has been demonstrated during slicing of 10-cm diameter ingots at 25 wafers/cm. The average thickness of wafers was 0.249 mm and the kerf was 0.151 mm. The surface damage of FAST sliced wafers was 3-5 μm. Slicing rates as high as 0.14 mm/min have also been demonstrated for 10-cm diameter ingots.

A laboratory, high-speed slicer was designed and fabricated for FAST slicing. The salient features of this machine were a light-weight reciprocating head with a longer stroke, a wider rocking angle for the workpiece and grooved guide rollers on either side of the workpiece for accurate alignment and guiding of wire blades.

The main emphasis of the program was on wire blade development. Initially impregnated blades were developed which showed high potential; however, this approach needs much more development. In order to evaluate and control the plating variables, an in-house electroplating facility was set up. The problems involved in electroplating diamonds on wires were the high surface area to volume ratio and the high, uniform concentration necessary for effective slicing. Besides setting up procedures to achieve the above requirements some of the technical problems solved were plating ductile nickel to prevent wire embrittlement and baking of steel-core wires after plating to prevent hydrogen embrittlement. Unique features developed in wire-blade development were electroplating diamonds only in the cutting edge of wires and electroforming techniques to plate diamonds in a

predetermined shape and form. These processes would yield lower kerf with large diamonds, longer life of wires and higher accuracy of guiding for the wires during slicing.

The FAST approach has shown potential and demonstrated salient features in laboratory. This has been achieved through process development. It is now necessary to evaluate the basic parameters of this slicing on a quantitative basis.

In large-scale production it is expected that the add-on cost of FAST slicing will be between $5.90 and $13.13 per square meter of silicon sheet.

VOLUME II

MULTI-WIRE SLICING - FIXED ABRASIVE SLICING TECHNIQUE (FAST)

2.1 INTRODUCTION

Silicon crystals have been sliced into wafers for the semiconductor industry by the Internal Diameter (ID) and Multiple Blade Slurry (MBS) techniques. While these processes were developed for semiconductor applications, they cannot be utilized, as they exist today, for photovoltaic applications. Unlike semiconductor devices where silicon material constitutes sometimes less than one per cent of the cost, the cost of silicon wafers comprises about half the cost of a solar panel. The wafering technique to produce silicon wafers from ingot is one of the important steps towards reducing costs for terrestrial photovoltaic applications. The slicing process must be low cost and must combine minimum kerf plus slice thickness to achieve high material utilization. With improved material utilization alone, the contribution of the cost of polysilicon and crystal growth for photovoltaic power generation, dollars per peak watt, is significantly reduced. Therefore, material utilization is critical for reducing costs to make photovoltaics a reality for terrestrial applications.

Besides being most developed and commercially available, the advantages of an ingot process towards making sheet are high throughput, purification of meltstock during growth, consistent quality, simple instrumentation and control; however, material utilization and kerf in slicing limits the low-cost potential. In fact, the justification for silicon ribbon

processes is based on the premise that slicing is costly and wastes material. As the cost of polysilicon meltstock is reduced to the goal of $14/kg kerf losses in slicing become less significant, but material utilization is still critical. The combination of an effective slicing process with an ingot process, such as the Heat Exchanger Method (HEM), allows the economical production of square shaped high conversion efficiency material to produce high power density modules at low cost.

The essential parameters for a slicing technique for photovoltaic applications are (i) low-cost process, (ii) low expendable costs, (iii) high material utilization, (iv) high quality product, and (v) high yield. There are three commercially used wafering processes, viz., ID, MBS and Multiple Wire Slurry (MWS) techniques. A comparison of the parameters for these wafering methods with FAST is shown in Table I. It can be seen that the advantages are low expendable material costs, low labor and high throughput in ID, low equipment and labors costs in MBS, and high material utilization in MWS. In the case of FAST all these advantages are retained.

TABLE I. A COMPARISON OF THE ESSENTIAL PARAMETERS OF WAFERING FOR DIFFERENT SLICING TECHNIQUES

Parameter	ID	MBS	MWS	FAST
Equipment costs	High	Low	High	Low
Labor supervision	Low	Low	High	Low
Throughput	High	Medium	Low	High
Expendable costs	Low	High	Very high	Low
Material utilization	Medium	Medium	High	High
Surface damage	High	Medium	Medium	Low

In the FAST process[1] a multiple-wire bladepack is stretched in a frame and reciprocated on rails. Diamond is fixed onto the wires and used as an abrasive for slicing silicon. Diamond has been demonstrated to be an effective abrasive for silicon via the ID process and, therefore, the expendable materials costs are kept low. The simplified equipment concept of reciprocating bladehead keeps the FAST slicer costs low and this has been proven by the MBS. The best material utilization of wire slicing[2] is also incorporated in FAST. This feature is possible with wire because once the wire cuts through it no longer contacts the workpiece, hence less clearance is necessary. This reduces kerf and also makes it possible to slice thinner wafers. In the MWS the silicon being sliced is completely lost when a wire breaks. For the FAST approach, a broken wire results in loss of two wafers it is contacting. In addition to the above advantages to FAST the surface damage of the sliced wafers is lower[3] than that reported for other slicing technologies.[4]

FAST is a new slicing technique that has been developed to slice ingots more effectively. Work has been carried out in three areas, viz., machine development, blade development and testing.

2.2 MACHINE DEVELOPMENT

The Fixed Abrasive Slicing Technique (FAST) is a new wafering method. The proof of concept of this method was established[1] with a machine designed for multi-blade slurry slicing. All the parameters for effective slicing such as low kerf, thin slices, etc., had been demonstrated for 4 cm x 4 cm silicon workpieces. Larger workpieces could not be sliced with the modified slurry machine. Based on the experience with a modified slurry slicer a laboratory high-speed slicer based on new concepts was designed, fabricated, assembled and tested.[5]

The high speed slicer, as shown in Figure 1, is a basic laboratory machine which could be modified, if necessary. The essential features are that it has a larger and lighter carriage so that higher speeds and longer stroke can be achieved. The wire carriage is an aluminum weldment that is reciprocated on air bearings. The carriage is moved back and forth by a link guided by a straight line motion mechanism which is crank actuated. By shifting the crank pin location on the guide mechanism, different stroke lengths can be obtained. Beneath the guide mechanism is a second crank which has a mass equal to the carriage weight attached to its end. This crank is driven out of phase with the carriage motion, and thus serves to damp the inertial loads of the system. The drive assembly is mounted separately from the bladehead frame to obtain vibration isolation. A view of the slicer after slicing a 10-cm diameter silicon ingot is shown in Figure 2. Initial slicing of 7.6-cm and 10-cm diameter workpieces at 19 wafers/cm with this slicer showed 97% yield.[5] These tests also proved that fixed diamond on wires give better performance at high speeds.

In order to achieve higher speeds it was necessary to lighten the reciprocating bladehead. The weight of the slurry slicer bladehead was about 200 pounds and a surface speed of 100 feet per minute was achieved. The high speed slicer was such that the blade carriage was twice as long and weighed half as much. Slicing tests were carried out at surface speeds of about 200 feet per minute.[5] Significant improvement of the cutting performance was seen at the higher speeds. To further increase speeds it was necessary to lighten the reciprocating carriage still further. A new 37 pound bladehead was designed and fabricated. Figure 3 shows two views of the new lightweight bladehead assembled in the slicer.

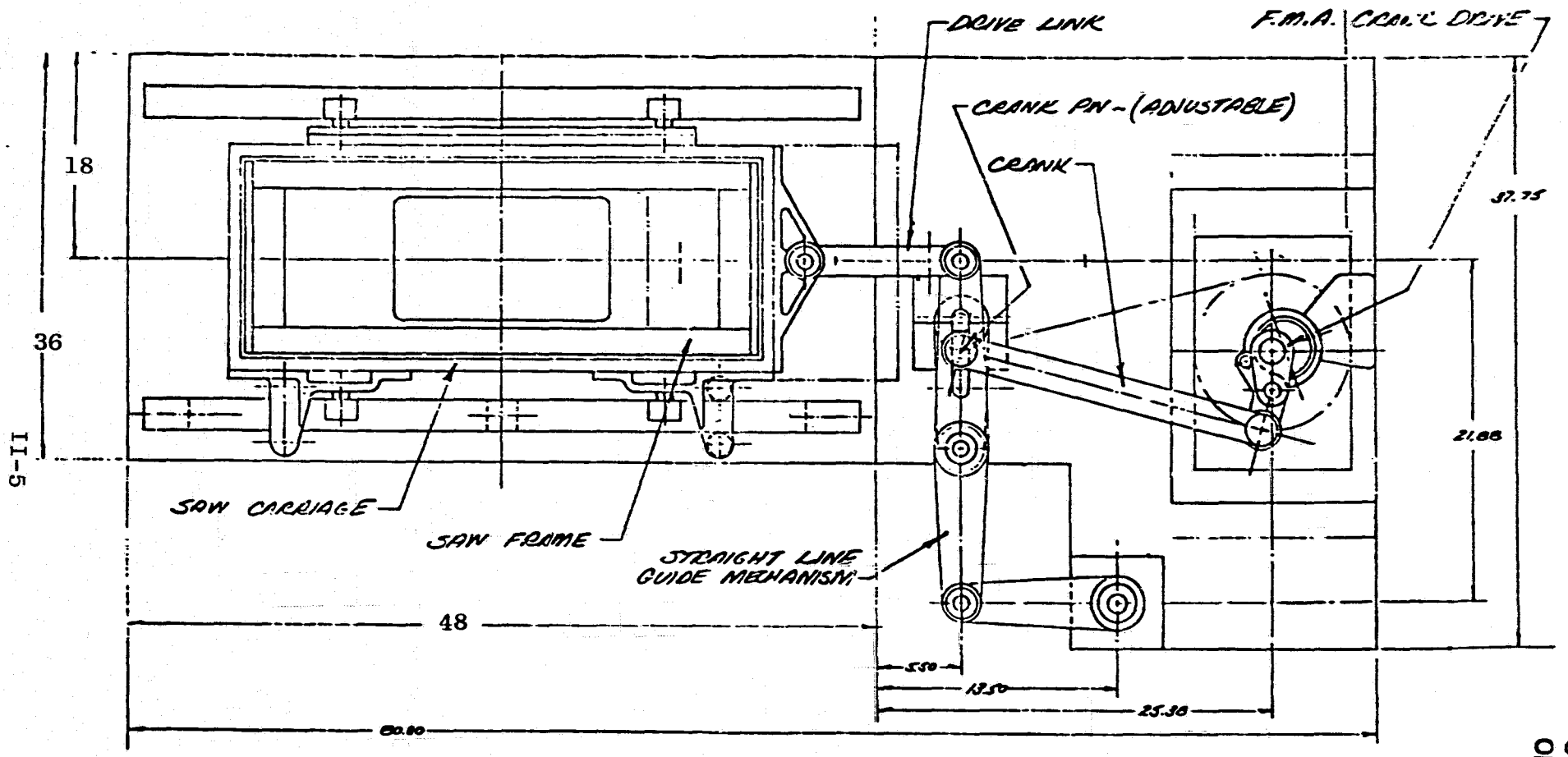

(All dimensions in inches)

Figure 1. Crystal Slicer - Plan View

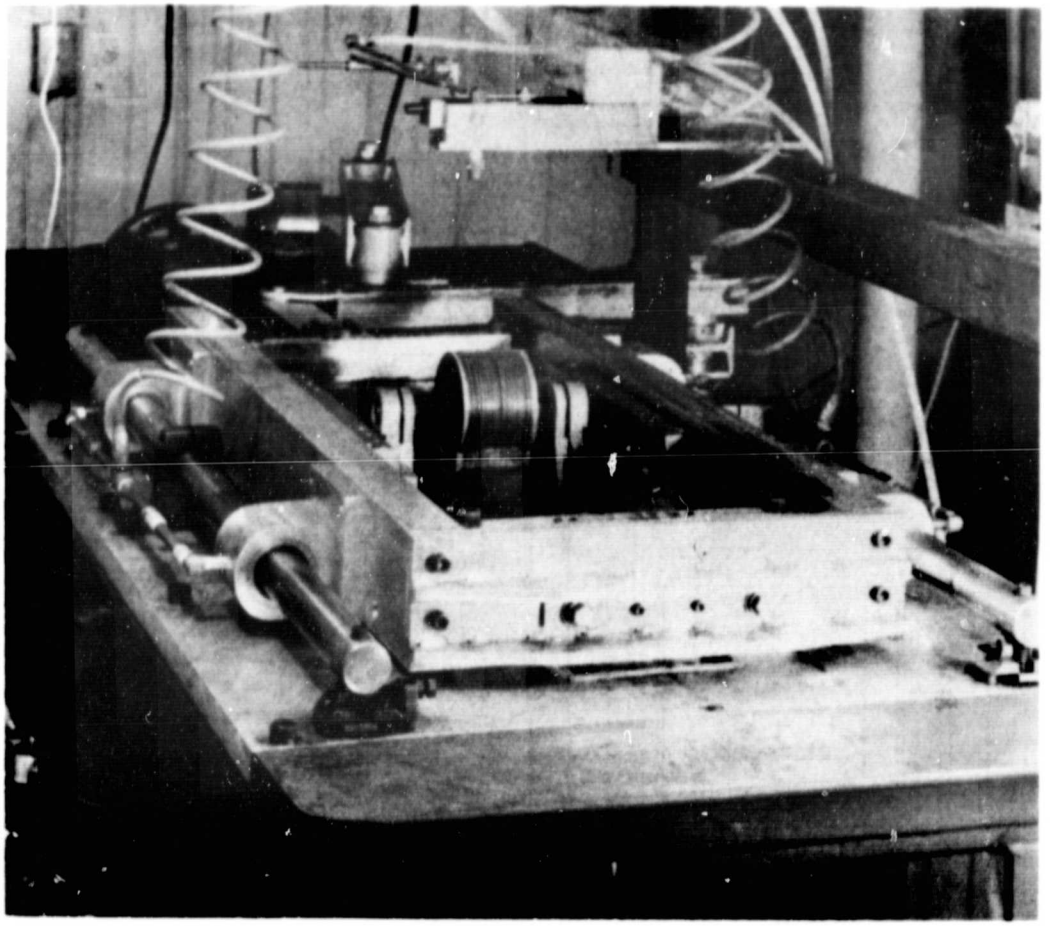

Figure 2. A view of the high-speed slicer after slicing a 10 cm diameter silicon ingot

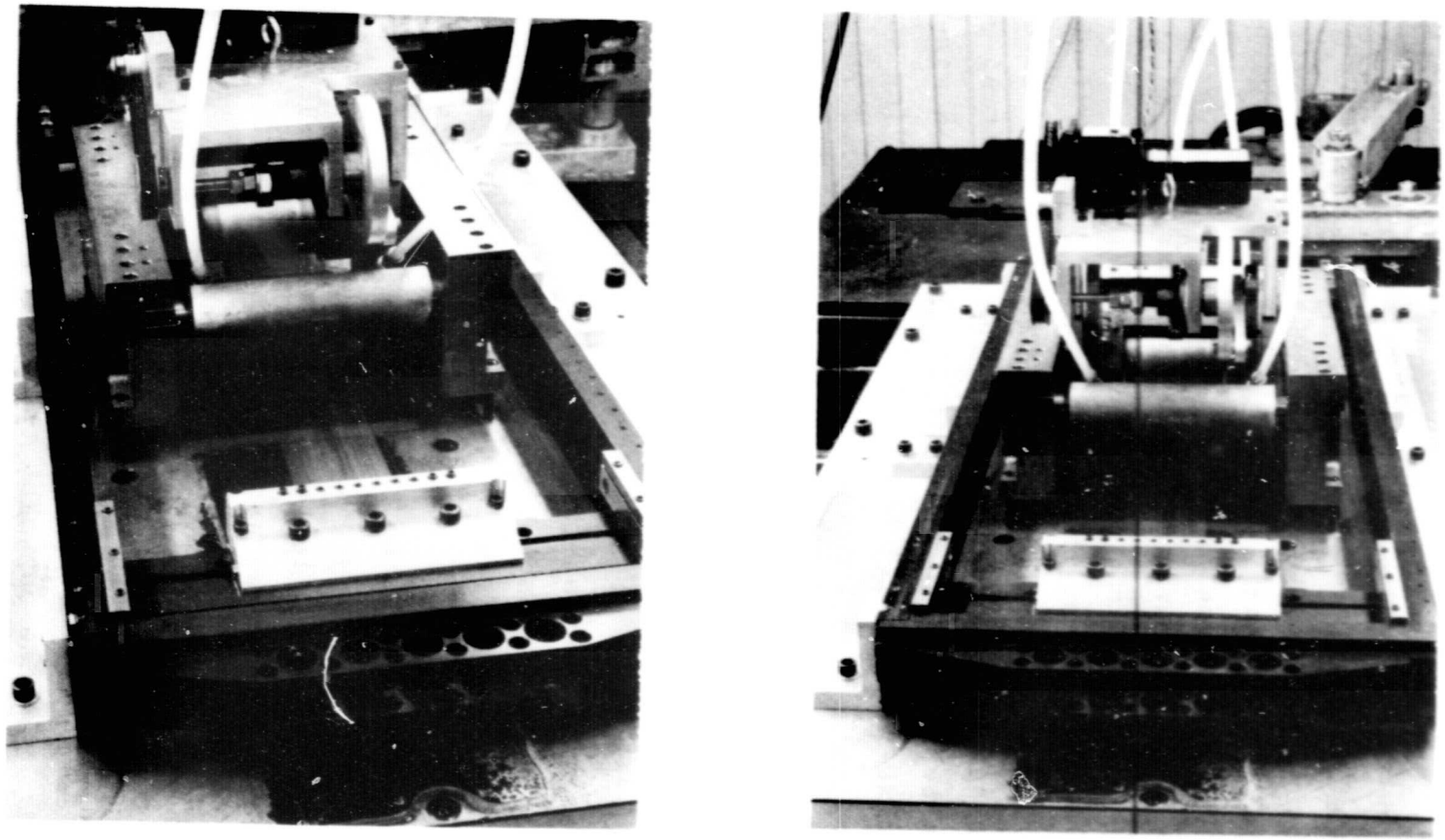

Figure 3. Two views of the high-speed slicer with light-weight bladehead

The problems that were also identified during the early testing stage were hysteresis of the feed mechanism and jerkiness in the rocking mechanism. These problems were corrected by using weights to control feed forces and by altering the rocking mechanism to achieve a smooth movement. Figure 4 shows the new rocking mechanism.

The first slicing test with these modifications was run 325-SX (details in Appendix II-A). A 10-cm diameter workpiece was sliced at 19 wafers/cm, the surface speed was 400 feet per minute with a 16-inch stroke length and 41.3 gm feed force. Very good cutting rates were achieved; such high cutting rates had never been achieved with commercially impregnated wires. The total slicing time was 11 hours, 41 minutes, giving an average cutting rate of 5.7 mils/min (0.145 mm/min). This compares to 2.33 mils/min (0.05 mm/min) obtained with similar wires before the present modification.

Even though effective slicing of 10-cm diameter silicon at 19 wafers/cm was achieved, problems were encountered when wafering was carried out at 25 slices/cm. These problems were related to vibrations transferred to the workpiece and misalignments causing wire wander. Additional shock mounts were placed on the drive mechanism in order to decrease the vibrations transferred onto the bladehead. Further, it was found that the feed mechanism was not rigid; therefore considerable vibrations were transmitted to the workpiece which contributed to wafer breakage during slicing. In addition, misalignments in the bladehead caused wire wander which also resulted in poor yields.

A new slicing head was, therefore, designed and fabricated. The salient features of this bladehead are a very high degree of rigidity and accurate alignment. A granite surface plate was used as a base on which the wirepack frame was mounted. This granite surface was used to align the reciprocating frame as well as the workpiece carriage, vertical feed

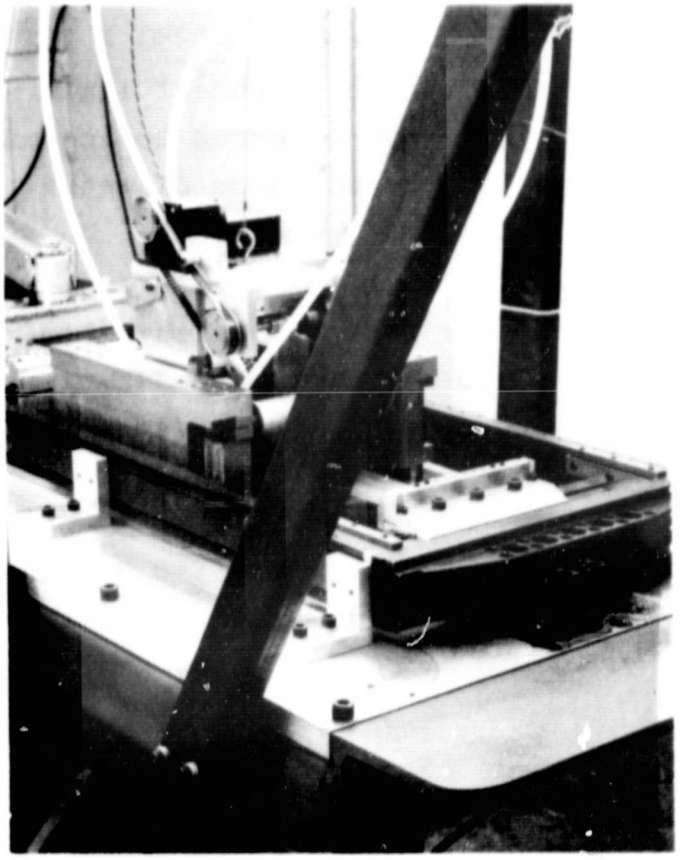

Figure 4. A view of the rocking mechanism incorporated in the high-speed slicer

and rocking assembly. Misalignments, if any, could also be measured off this class A surface from time to time. The heavy granite block also gave rigidity to the bladehead. The wirepack frame now reciprocates in a ball slide which should give it an accurate alignment during travel. The rocking mechanism was driven with an anti-backlash lead screw. A synchronous stepping motor was used to drive the rocking assembly.

In addition to the rigidity and alignment features, the wirepack frame was made lighter and enlarged to accommodate a workpiece of up to 30-cm length and 15-cm diameter. A view of this new bladehead is shown in Figure 5.

Experience with this bladehead has shown that accuracy of alignment of the various parts of the machine and transfer of vibrations to the workpiece are very significant parameters in slicing ingots at 25 wafers/cm. Other parameters observed have been the sensitivity of the rocking angle as the size of the workpiece is increased. An increase in rocking angle is necessary with larger workpieces for effective slicing. Correlation of these parameters will be discussed in a later section.

2.3 BLADE DEVELOPMENT

The key to any slicing technique is the quality of blades used. For FAST slicing diamonds are fixed onto wires. The usual procedures practiced in the industry for fixing diamonds are pressed and sintered blades (as in in OD slicing) or plated blades (as in ID slicing). Low kerf requirements rule out the use of pressed and sintered blades. Two approaches were pursued for fixing diamond on wire, viz., impregnation and electroplating. The significant advantages of impregnated blades was the ability to fix diamonds in the cutting edge only and thereby keep the kerf low.[1,5]

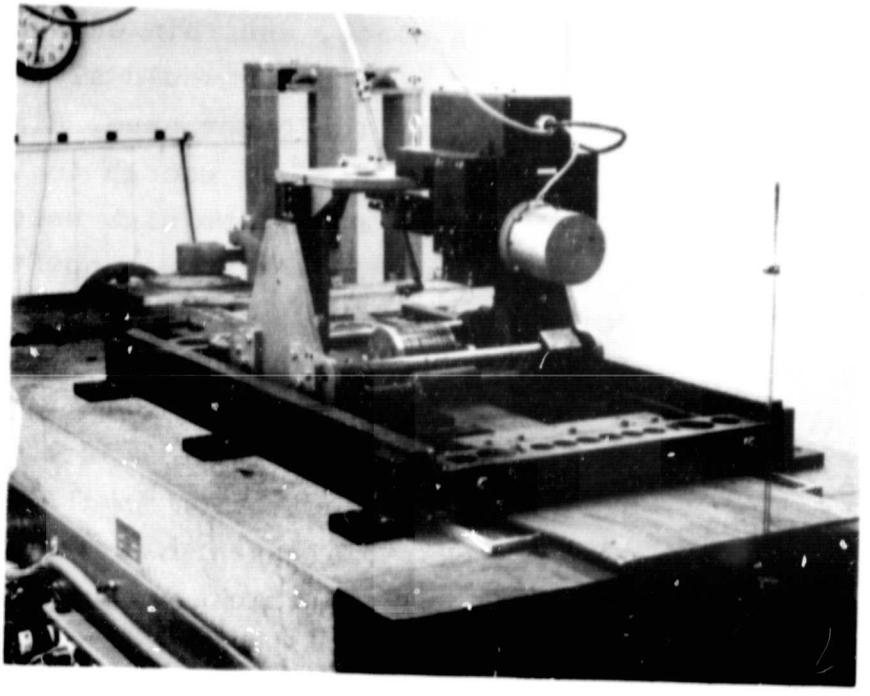

Figure 5. FAST slicer showing new bladehead

(g) suspension medium for diamonds

(h) impregnation pressure

(i) time for impregnation

(j) plating type and thickness after impregnation.

These variables are not independent but mutually interactive.

Considerable effort has been spent for optimization of these variables. For example, the copper sheath should be thick enough to hold the diamonds in place, and thin enough not to bury the diamonds. A thin copper sheath would also have a positive effect on the kerf. On the other hand, diamonds must be large enough not to be buried and small enough to give a low kerf. Impregnation pressure should be high enough to insert the diamonds into the copper and low enough not to destroy the wire. As time of impregnation is increased it aids in pushing the diamonds in the sheath; however, beyond a certain time it starts to loosen the diamonds. To get good impregnation the diamonds should be seated well into the copper sheath with high, uniform concentration on the cutting edge of all the wires. Nickel plating prevents the diamond pullout. It should have a uniform thickness on all the wires.

High strength steel and tungsten as core material were found to be adequate for impregnated wires. In the selection of size it was found that a 3 mil (0.075 mm) diameter core did not have the desired strength.[5] Wire wander was also encountered during slicing. Even though 4 mil (0.1 mm) core was used most of the optimization was carried out with 5 mil (0.125 mm) core wire.

It was found that it was possible to impregnate 45 μm size diamonds into 7.5 μm copper sheath. However, the copper was distorted. A 12.5 μm sheath was not distorted and the concentration of diamonds was high. However, after plating the diamond concentration was not as high. Impregnation of 45 μm diamonds into 12.5 μm sheath was not deep enough and diamonds

This technique needs much more development and has a lower cost potential. In the development of electroplated blades techniques of electroforming were developed where the kerf width and shape could be controlled. In view of this development emphasis was placed on plated blade approach during later stages of the program.

2.3.1 Impregnated Wires

At the start of the FAST development program impregnated wires were available commercially. These wires were 5 mil (0.125 mm) high strength steel core with a 1.5 mil (38 μm) thick copper sheath into which 45 μm diamonds are impregnated. These wires suffer diamond pull-out during silicon slicing; their life can be prolonged by nickel plating.[1] A 0.3 mil (7.5 μm) nickel plating was found to be optimum. A thicker plating buries the diamonds while a thinner plating does not prevent diamond pull-out.

In the development of impregnated blades, it is necessary to develop technique to give a high concentration of diamonds with an even distribution and good bonding to the matrix. These are essential blade requirements for efficient slicing. Initial impregnation experiments were carried out on the MBS slicer; however, during later stages an impregnation machine was designed and fabricated for making wirepacks for the high speed slicer. A high strength core wire covered by a copper sheath was used to impregnate diamonds into the wires.

The impregnation process is a multi-parameter problem. Some of the variables affecting impregnation are:

(a) wire core material
(b) size of core wire
(c) thickness of copper sheath
(d) impregnation die design
(e) size of diamond
(f) shape and type of diamond

fell out during plating. Impregnation of 30 μm diamonds into a 15.5 μm copper sheath under high forces produced satisfactory impregnation and retention of diamonds. This showed that the diamonds have to be impregnated deep into the sheath under high pressure. However, a 7.5 μm nickel plating buried the diamonds.[6] Slicing tests with a set of impregnated wires with 45 μm diamonds into 1 mil (25 μm) copper sheath and 7.5 μm electroless nickel plating showed good results in runs 335-S, 336-S and 338-S (Appendix I). A similar bladepack with 30 μm diamonds was used in runs 339-S through 341-S. A comparison of the performance of the two wirepacks showed that higher cutting rates were achieved with 45 μm diamonds.

For effective impregnation the application of diamonds on the wires was critical in achieving good concentration and uniform distribution of diamonds. Some of the variables studied were viscosity of suspension medium, concentration of diamonds, and pressure and time during spreading of the slurry. It was found that even these variables are interactive, e.g., when the viscosity was high, the diamond concentration had to be increased. With high concentration, the pressure and time had to be increased accordingly.[7] Once the diamonds were applied to the wires, they were impregnated under pressure.

A study of the effect of time of impregnation on diamond concentration showed that initially the concentration increased with time; however, after some time the diamonds were dislodged leaving the copper sheath abraded. Subsequent impregnation into this abraded copper resulted in poor impregnation and diamonds fell off the wire during handling and/or during plating.[8]

It was also found that when the diamond application resulted in low concentration, very good impregnation was achieved; a higher concentration after application resulted in poor impregnation. This may be due to the fact that the pressure is transmitted over more diamonds and therefore the pressure on each diamond is reduced. Consequently, the diamonds

are not pushed into the copper sheath. Further, the soft copper sheath is deformed, reducing the hold on the diamonds. The application and impregnation was also attempted in a single step operation, as was building up of concentration in a number of application-impregnation steps.[7]

Once the parameters were optimized and good impregnated wirepacks were fabricated efforts were made to identify whether diamond concentration is reduced because of severity of cleaning prior to nickel plating. Wire samples were taken during each cleaning step. These samples were examined by SEM and are shown in Figure 6. Close examination of 6(a) through 6(d) shows that not an appreciable amount of diamond is lost during cleaning for good impregnated wirepacks.

Comparison was also made of impregnated wires with different size diamonds. Wires impregnated with 45 μm diamonds are shown in Figure 7(a) and 60 μm size in Figure 7(b). Figure 7(a) shows that a higher and more uniform diamond concentration can be found in 45 μm size. From the photographs it is not possible to see the depth of impregnation. Slicing experiments indicate that diamond pull-out mostly occurred with 60 μm size diamonds.[7] On the other hand, nickel thickness had to be carefully controlled when smaller size diamonds were used. For example, Figure 8 shows a 45 μm diamond impregnated wire where the nickel plating buried the diamonds.

Experiments were also carried out with impregnated wires using a mixture of diamond sizes. For example, in run 424-SX a mixture of 45 μm and 60 μm diamonds was used.[7] Good cutting rates were achieved, but the yields were not high. The low yields are attributed to non-uniformity in wirepacks because of difference in protrusion of diamonds above the nickel plating with different size diamonds.

Figure 6. The effect of the cleaning baths before electroless plating: (a) first cleaning bath; (b) second cleaning bath; (c) third cleaning bath; (d) fourth cleaning bath

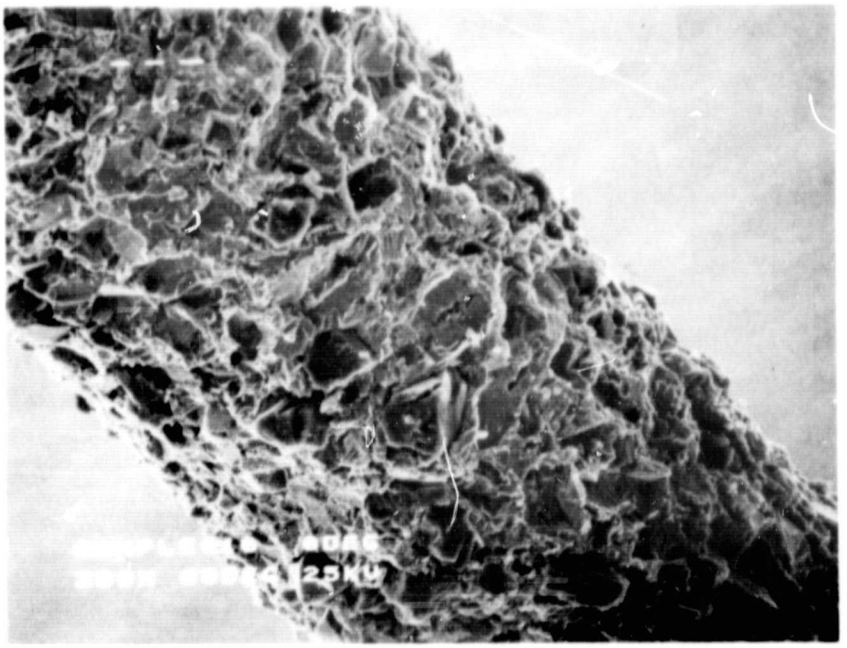

(a)

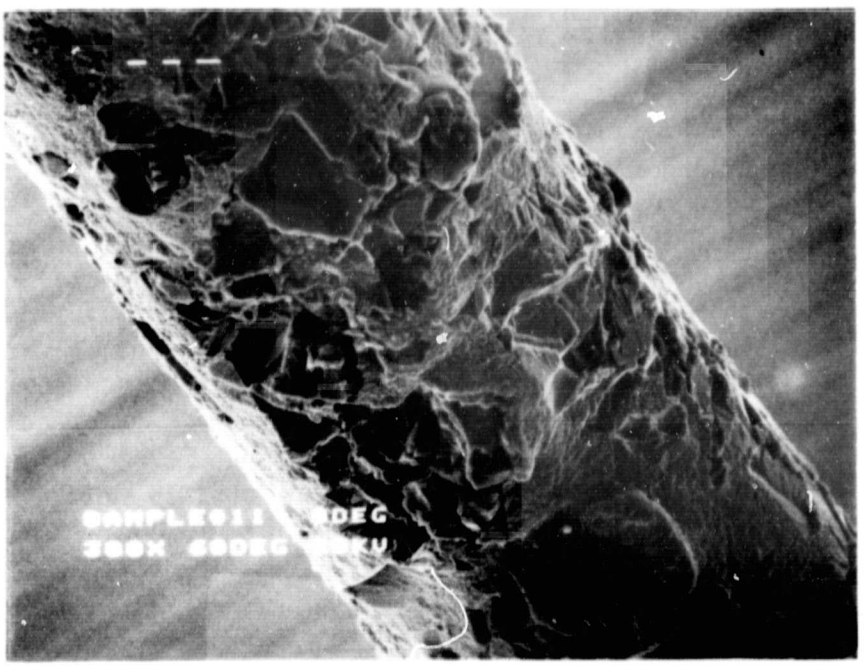

(b)

Figure 7. Impregnated wires with different sizes of diamonds: (a) 45 μm diamond; (b) 60 μm diamond

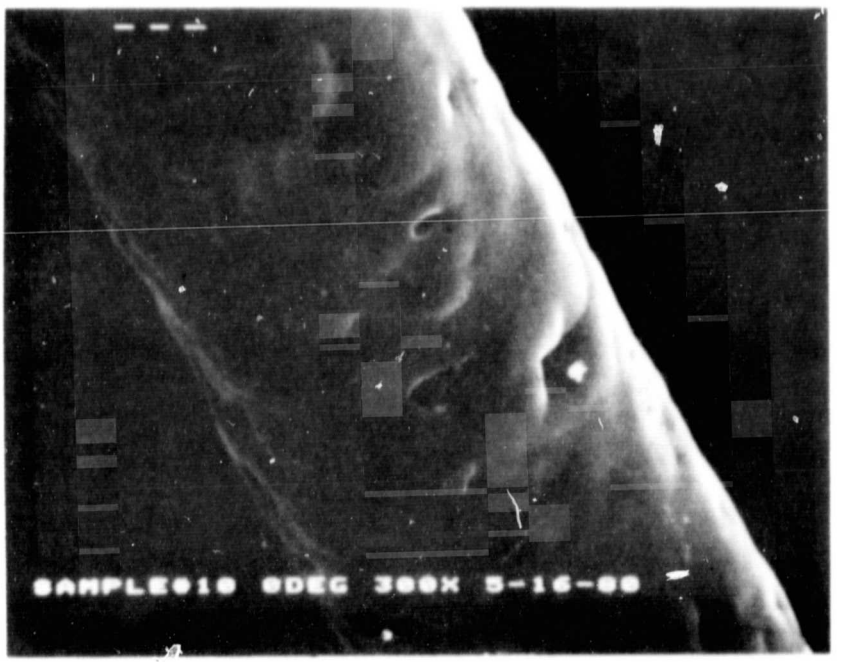

Figure 8. SEM photograph of impregnated wire with plating burying the diamonds

2.3.2 Electroplated Wires

Even though electroplating of diamonds is widely practiced in industry, problems were encountered in fixing diamonds on wires. The main difference was attributed to the high surface area to volume ratio for wires; another requirement was the high degree of uniformity in diamond concentration and plating thickness over a large area.

As mentioned earlier high strength steel and tungsten were selected as core wires for plating. Even though steel core ID blades are electroplated the high surface area to volume ratio of wires caused hydrogen embrittlement when steel core was used. These wires when stretched in the slicer showed breakage. During the initial stages, therefore, tungsten core wire was used. The problems of cleaning tungsten prior to electroplating necessitated the use of tungsten core wire with a flash of nickel. During later stages of the program it was found that the plating variables strongly affect the performance of the wirepack during FAST slicing. In order to study these variables an electroplating facility was set up by Crystal Systems. During this period cleaning procedures for pure tungsten were also developed and it was possible to use tungsten wire without the nickel flash. It was also found that it was possible to electroplate high strength steel core wires. These wires were then baked at 200°F. Such a wirepack was used in runs 473-SX through 475-SX and no wire breakage problems were encountered.

Another problem encountered with electroplated wirepacks was the non-uniformity of nickel plating over the wires. If the area of wires to be plated is considered as a rectangle, it was found that nickel buildup was heaviest near the corners of the rectangle and minimum near the intersection of diagonals. An example of non-uniform nickel buildup is shown in Figure 9.

During the initial stages the failure mechanism for wires was diamond pull-out. Work on plating problems to obtain a

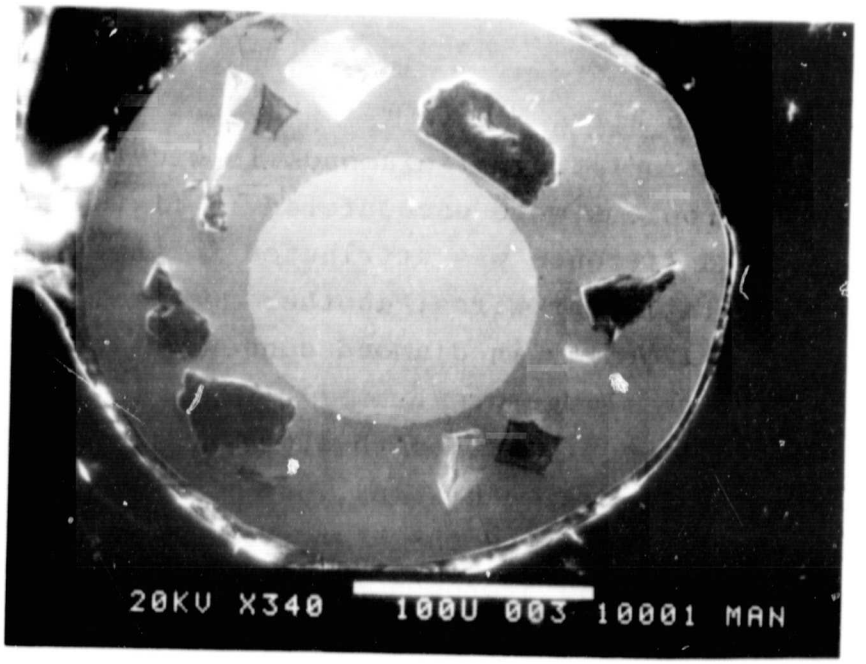

(a)

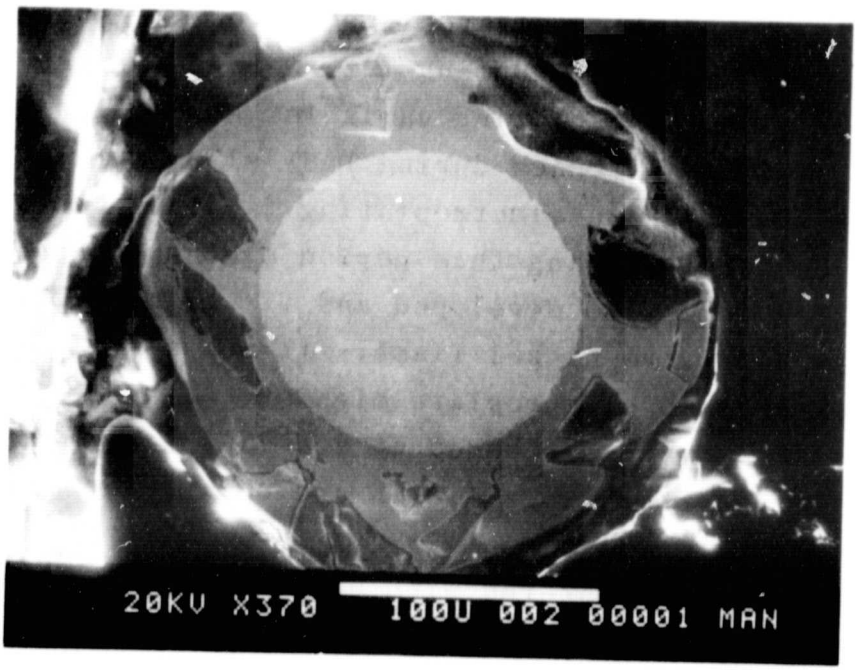

(b)

Figure 9. Cross-sectional view of wire in Figure 8 showing (a) high nickel buildup near end and (b) central area.

good bond between the diamonds and nickel matrix showed that diamond pull-out could be minimized. For example, Figure 10 shows three views of an unused wire electroplated using 45 μm diamonds. This wirepack was used to slice five 4 cm x 4 cm cross-section workpieces at 25 wafers/cm on the modified MBS slicer. Figure 11 and 12 show three views of a wire after slicing one and five workpieces respectively. It can be seen that the bonding of the diamonds was good as no diamond pull-out seems apparent.

Some comparison was made between the cutting performance of synthetic and natural diamonds.[9] It was found that under similar conditions the natural diamonds showed better slicing effectiveness. A high magnification view of 45 μm synthetic diamonds after plating on wires is shown in Figure 13. It can be seen that there are no sharp edges and the character of the diamonds is "blocky" in nature. This may explain the difference in performance.

In the electroplated wires diamonds were fixed over the entire circumference of the wire. Using a 5 mil (0.125 mm) core wire and 60 μm diamond, the kerf is too big to effectively slice 25 wafers/cm. Therefore, the largest size diamonds that could be used was 45 μm. Evaluations were carried out with 45 μm, 30 μm and 22 μm diamonds. It was found that a high concentration of diamonds could be achieved in all cases. During the initial stages it was found that the electroplated wires showed a better slicing performance as compared with the impregnated wires. The life of the electroplated wires was limited to slicing one 10 cm diameter ingot; the failure mechanism was diamond pull-out. The concentration of diamonds after slicing the first ingot was reduced significantly. An example of this behavior is evident from comparison of Figure 14 and 15 for wires prior to use and after use in run 441-SX, respectively.

Figure 10. Three views of unused electroplated wire rotated 120°

Figure 11. Three views of wire in Figure 10 after use in run 307-S

Figure 12. Three views of wire in Figure 10 after use in five runs (307-S through 311-S)

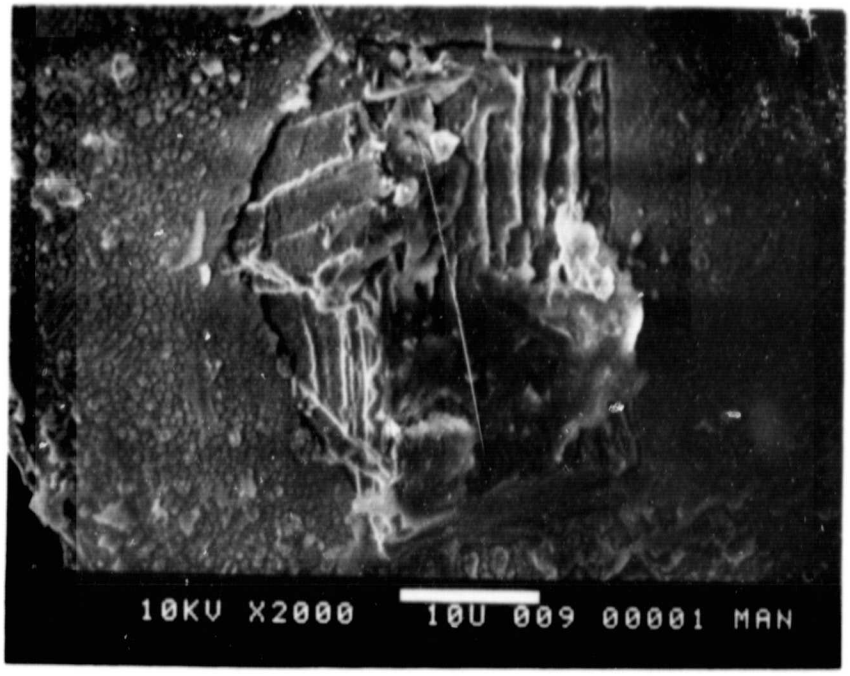

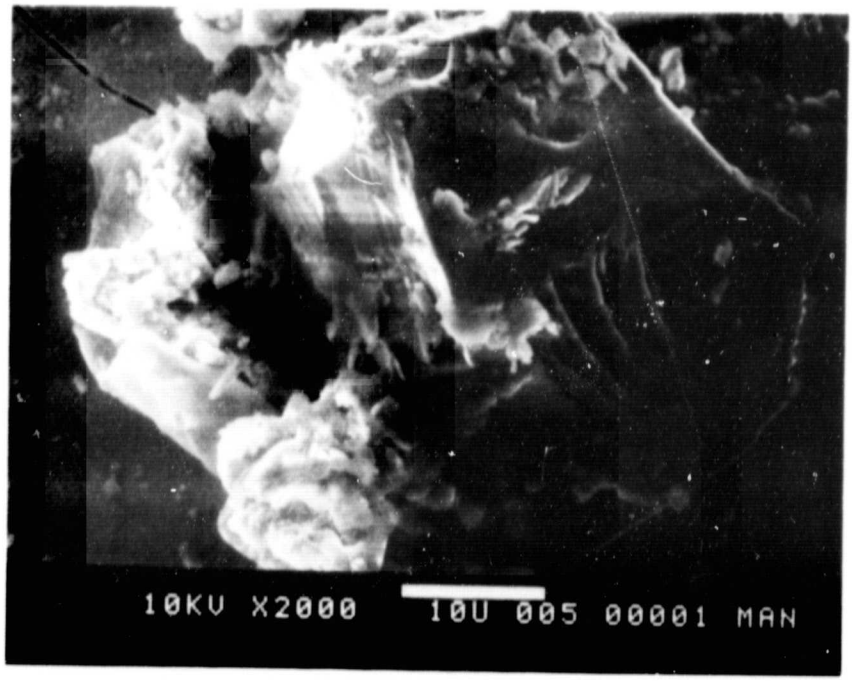

Figure 13. High magnification view of wire showing "blocky" diamonds.

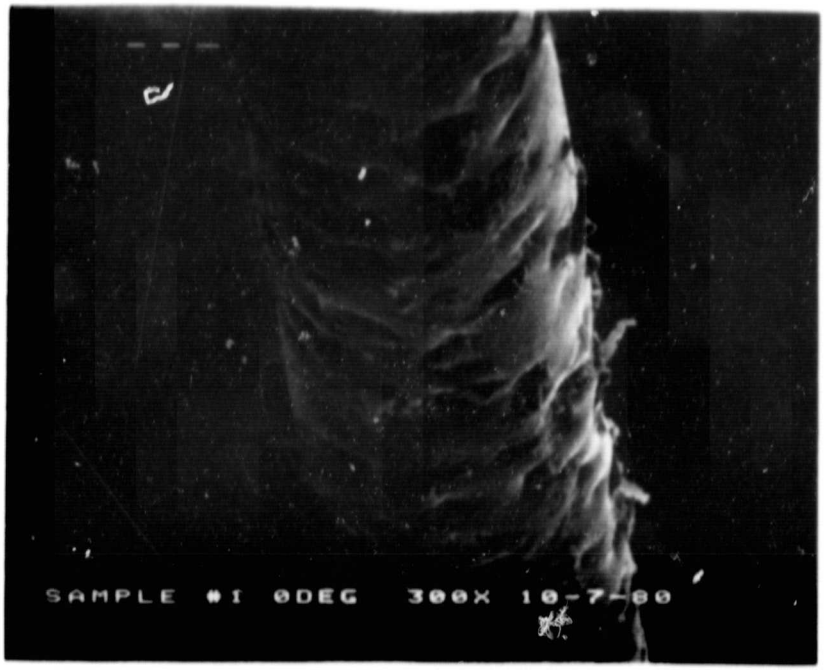

Figure 14. SEM photograph of wire before use in run 441-SX, rotated 30°

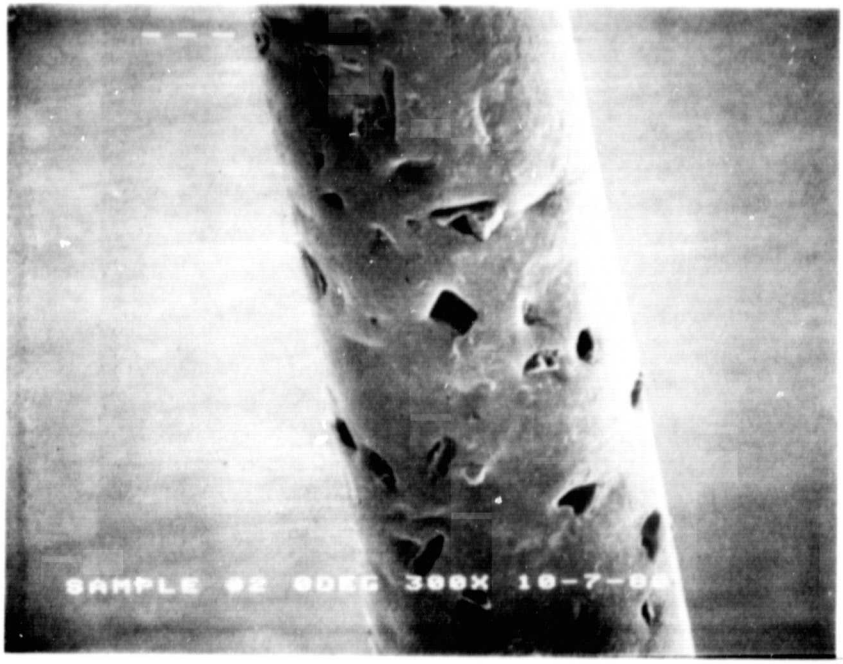

Figure 15. SEM photograph of wire after use in run 441-SX showing loss of diamonds, rotated 60°

With diamond sizes in the range of 22 to 45 μm the nickel buildup could not be changed over a wide range; it was found that for effective slicing half to two-thirds of the diamond needs to be plated with nickel. This range was a compromise between leaving enough exposed diamonds for cutting and enough nickel to hold the diamonds.

Another criterion for reducing diamond pull-out was to prevent the erosion of the nickel matrix. A mixture of 45, 30 and 15 μm diamonds was used. It was intended to have the larger diamonds for slicing and the smaller diamonds would fill in between the larger diamonds and prevent erosion of the matrix. Figure 16 shows a wire before use using a mixture of diamonds. The smaller diamonds appear to have been buried in the plating. Figure 17 and 18 show wires from the same wirepack after use in runs 437-SX and 438-SX. Examination of these wires shows that some of the smaller diamonds have been exposed and the concentration has not changed significantly even after slicing two 10-cm diameter silicon ingots. During later stages techniques were developed whereby the concentration of diamonds fixed on the wires was increased; it was, therefore, not necessary to use smaller diamonds as filler diamonds.

In order to reduce kerf, efforts were made to reduce the plating thickness. Figure 19 shows a wire plated with less nickel to fix 45 μm diamonds. This approach did not work very satisfactorily as it enhanced the diamond pull-out problem.

One of the drawbacks of electroplated wires was that the plating is wrapped over the entire circumference. With 30 μm and 45 μm diamonds the minimum kerf with 0.125 mm (5 mil) core wire is, therefore, 0.185 mm (7.4 mil) and 0.215 mm (8.6 mil) respectively. This assumes that there is no plating thickness between the bottom of the diamond and the core wire.

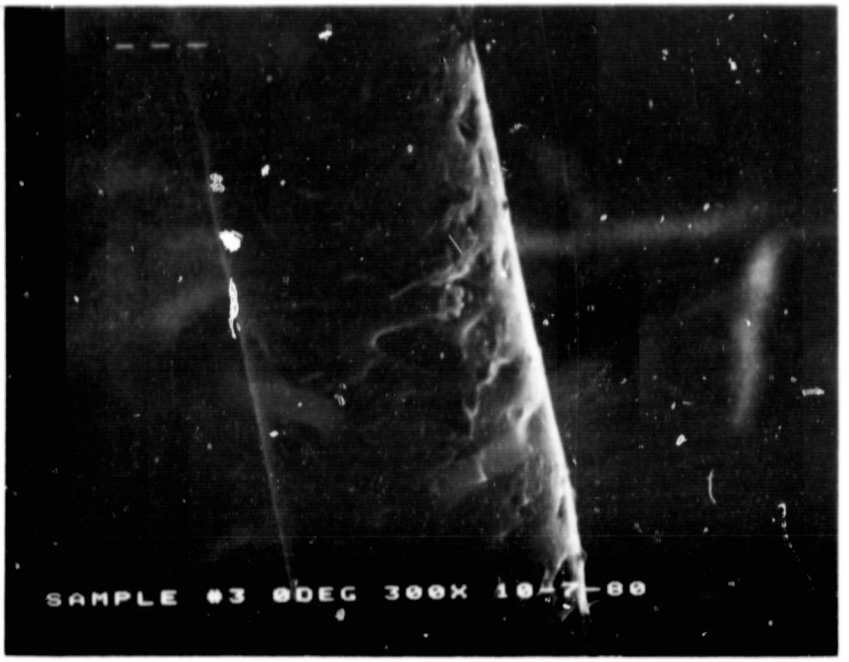

Figure 16. SEM photograph of electroplated wire before use in runs 437-SX and 438-SX showing diamonds buried in nickel

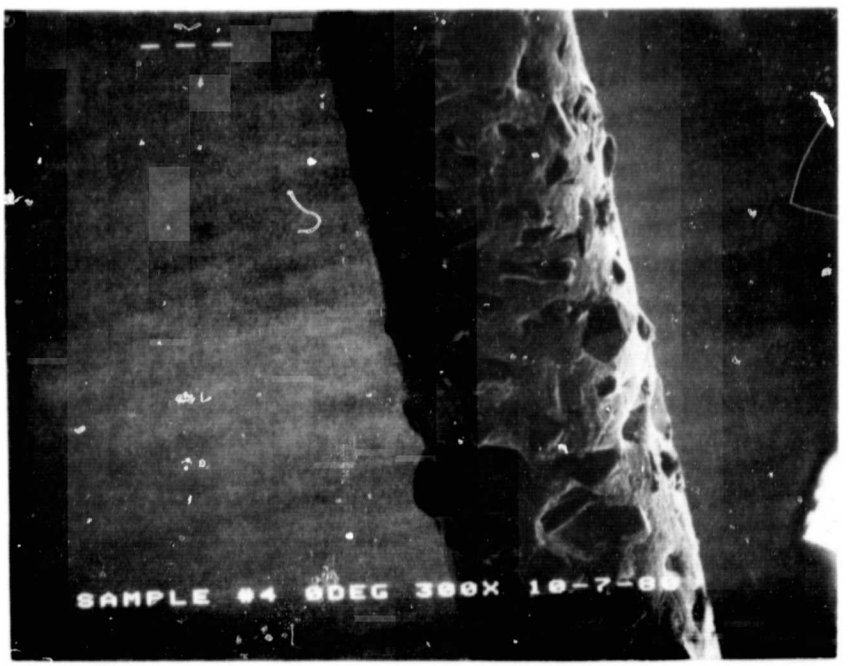

Figure 17. SEM photograph of wire used in run 437-SX showing high diamond concentration and even diamond distribution

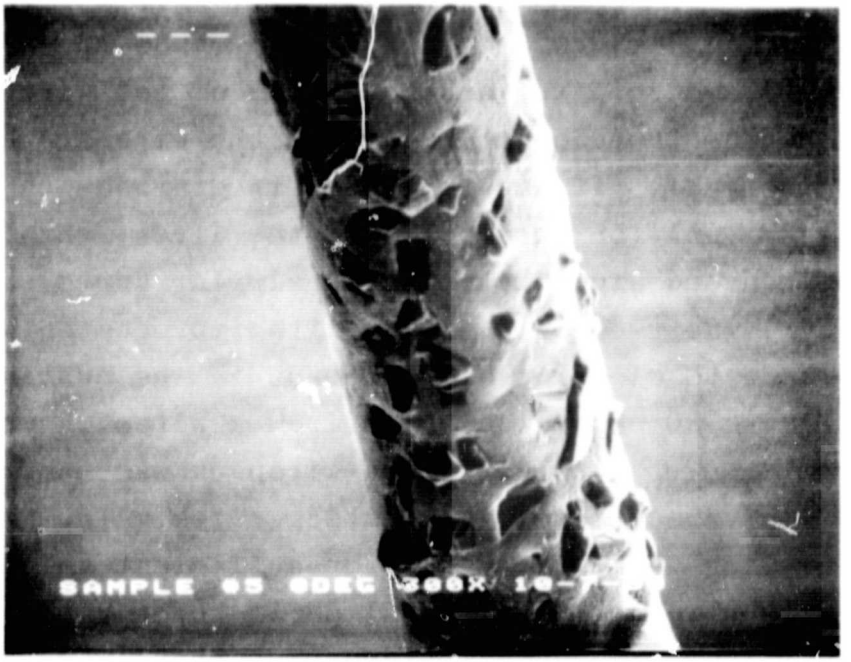

Figure 18. SEM photograph of wire used in run 438-SX showing high diamond concentration and even diamond distribution

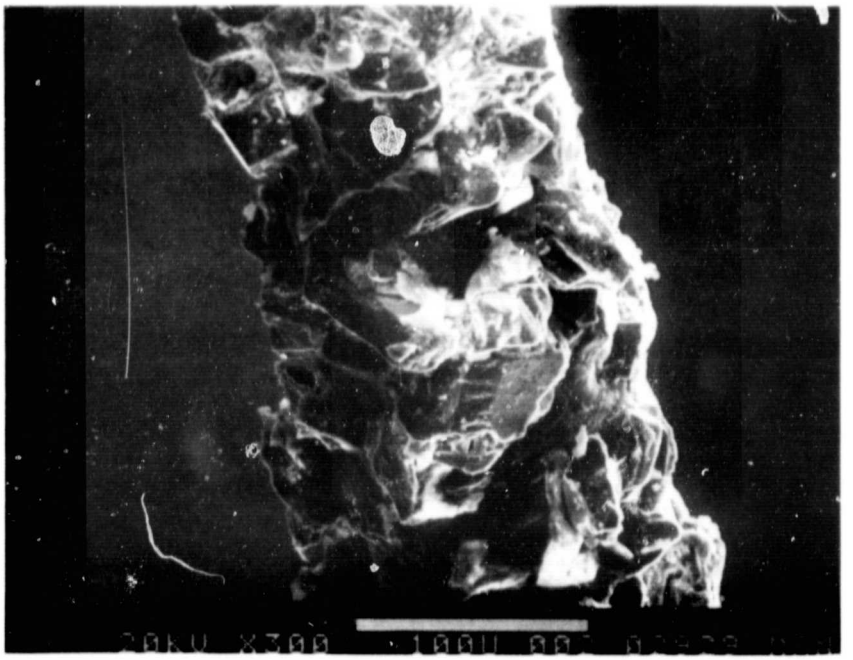

Figure 19. View of a longitudinal section of electroplated wire. The kerf was reduced by decreasing the nickel plating.

In practice the kerf is 0.225 mm (9 mil) to 0.250 mm (10 mil). The diamonds fixed at the bottom of the wire are cutting whereas those on the sides of the wire are contributing to the kerf. It was felt that if diamonds can be electroplated only on the bottom of the wires, then the kerf could be reduced significantly. A similar approach, discussed above, was used effectively with impregnated wires. Efforts were made to electroplate diamonds in the cutting edge only. Figure 20 shows two wires from a wirepack where no diamonds were plated on sides. The wirepack was used for 0.5 hour only because of low cutting rates. The area over which diamonds were plated was not sufficient to clear the wires during slicing.[10] Figure 21 shows three views of a wire section after use in run 426-SX. There was marginal clearance of these wires; some abrasion of nickel is evident in Figure 21. After slicing of one crystal, the wirepack was used to slice two more ingots in runs 429-SX and 430-SX.[11]

A comparison of diamonds electroplated over the entire circumference and in the bottom only was seen in runs 420-SX and 421-SX.[7] Figure 22 shows three views of an unused wire. During slicing in run 420-SX high cutting rates were achieved and slicing yield was 89%. SEM examination of a wire after this experiment, shown in Figure 23, shows that there appears to be no diamond pull-out. In the second slicing test (run 421-SX) high cutting rates were maintained; however, the slicing yield was lower. It was found that wafer breakage was significantly greater in the central area of the workpiece. Examination of a wire in this area showed that diamond pull-out was not a problem. Three views of the wire, Figure 24, shows that diamonds were electroplated over the entire circumference.

The technique of plating diamonds in the cutting edge only was optimized at Crystal Systems. An example of this wire is shown in Figure 25. It can be seen that a very high

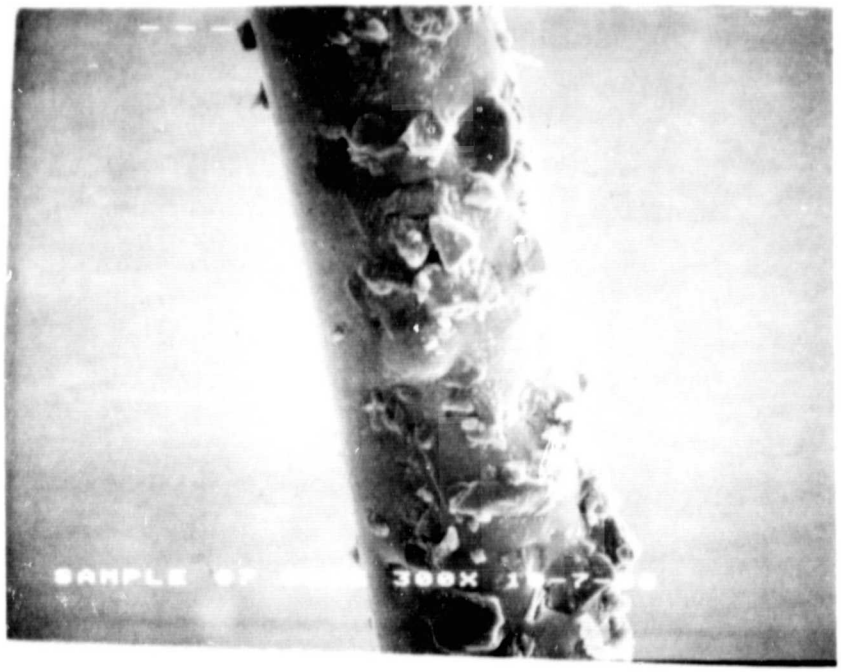

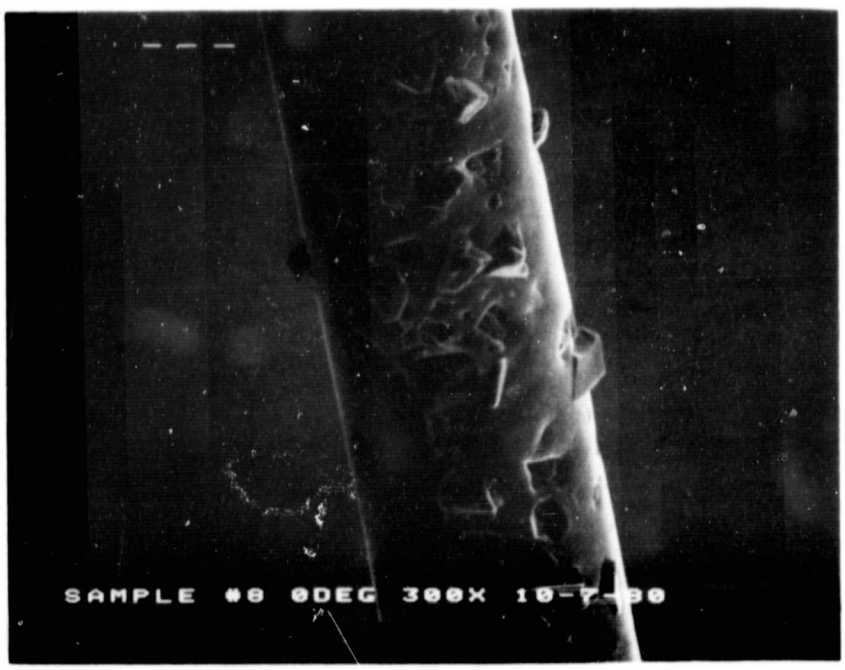

Figure 20. SEM of electroplated wires with no diamonds seen on sides

Figure 21. SEM photographs of wire used in run 426-SX (300X)

Figure 22. SEM photograph of unused wire at 120° rotation of wire. Wire was used in run 420-SX.

Figure 23. SEM photographs of a wire after first slicing test (Run 420-SX)

Figure 24. SEM photographs of a wire after second run (421-SX). This wire has diamond electroplated over the entire circumference.

Figure 25. CSI electroplated wire with diamond on one side

concentration of diamonds was achieved with enough nickel to hold the diamonds and enough diamond width to clear the wires during slicing. In spite of such progress it was not possible to eliminate the diamonds completely from the top surface over all the wires in the wirepack. The stray diamonds even though few in number caused perturbations during slicing and affected the cutting effectiveness. It was, therefore, desirable to control the kerf width precisely and eliminate diamonds completely from the top surface of the wirepack.

Electroforming techniques were developed in which diamonds are selectively plated with a predetermined kerf. Figure 26 shows an initial experiment at electroforming. The diamonds were plated on wire at a kerf of almost the size of the wire. Under these conditions it is possible to use larger diamonds in the cutting edge. Figure 27 shows the cross-section of a wire where plating was restricted to a V-groove with a 60° included angle.

A bladepack was fabricated with 60 μm diamonds plated in a 60° V-groove and used in run 461-SX to slice a 10-cm diameter silicon ingot. Very high cutting rates were achieved, 0.094 mm/min (3.7 mils/min), even though the feed forces were kept at 35.3 gm /wire. The average kerf was 0.2 mm (7.9 mils). This value is rather low for 60 μm diamond size.

While the electroforming technique was in development, efforts were continued in improving accuracy in slicing and wire life with diamonds fixed over the entire circumference of the wires. The results of runs 465-SX through 467-SX exemplify the progress made. A wirepack plated with 30 μm diamonds co-deposited over the entire circumference of the wire was used to slice three 10-cm diameter silicon ingots at 25 wafers/cm. In run 465-SX over 99% yield (222 out of a possible 224) was achieved with an average wafer thickness of

Figure 26. CSI electroforming technique to produce predetermined kerf

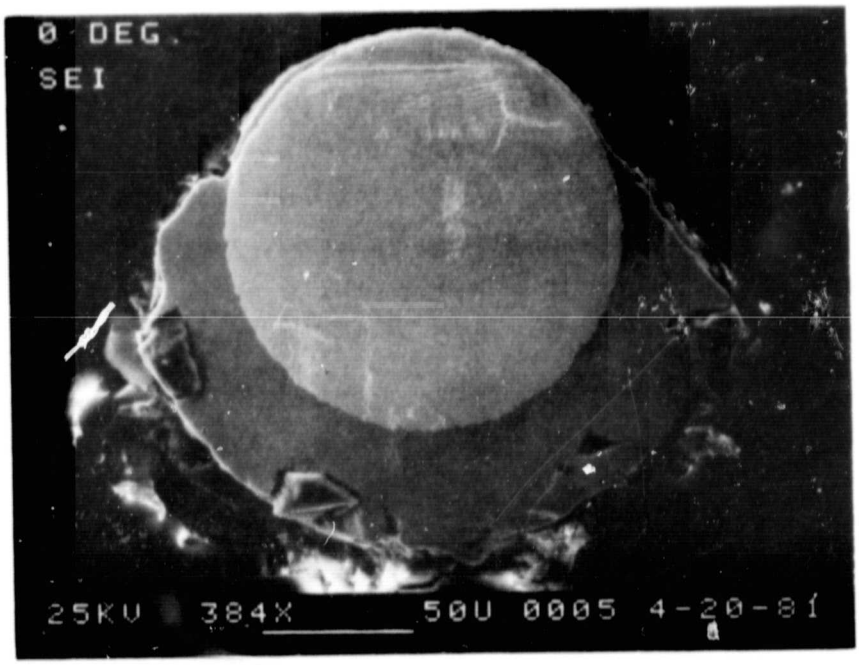

Figure 27. Cross-section of wire with plating restricted to V-groove with 60° included angle

0.196 mm (7.7 mils) and a kerf of 0.201 mm (7.9 mils). Figure 28 shows an unused section of wire. An examination of wires after each slicing run, Figure 29 through 31, showed that no significant diamond pull-out is noticeable.

It has been seen that with available techniques good characterization of the wires can be carried out and the results can be correlated to the performance of the wires. Wirepacks which show no diamond pullout or degradation also exhibit good slicing performance. However, with an examination of an unused wire it is difficult to predict the performance of the wirepack. Some basic understanding of the slicing mechanisms, degradation at the tip of a diamond, bonding of nickel-diamond, nickel core, etc., needs to be studied to predict behavior of a wirepack.

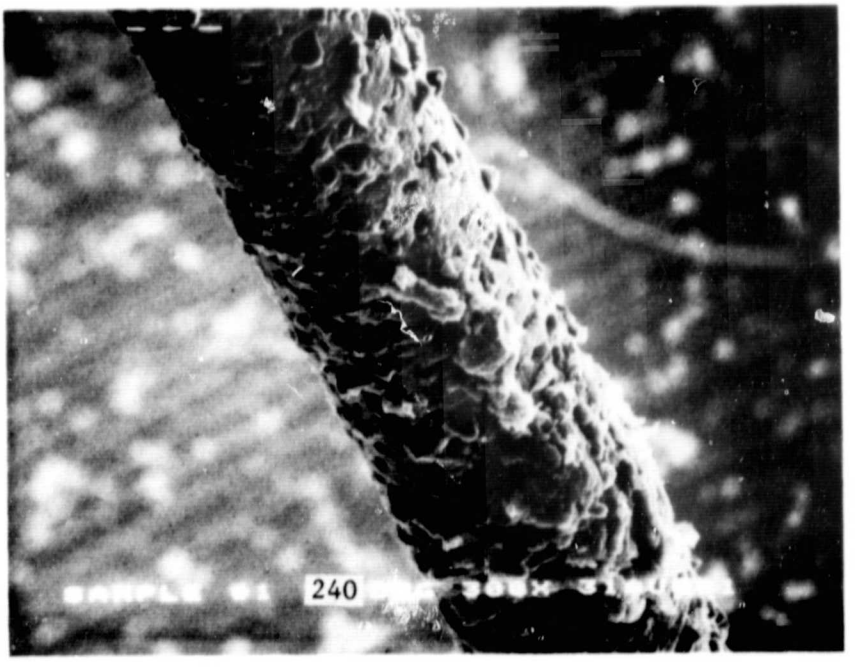

Figure 28. Two views of wire prior to use in run 456-SX.

Figure 29. Examination of a wire after use in run 456-SX

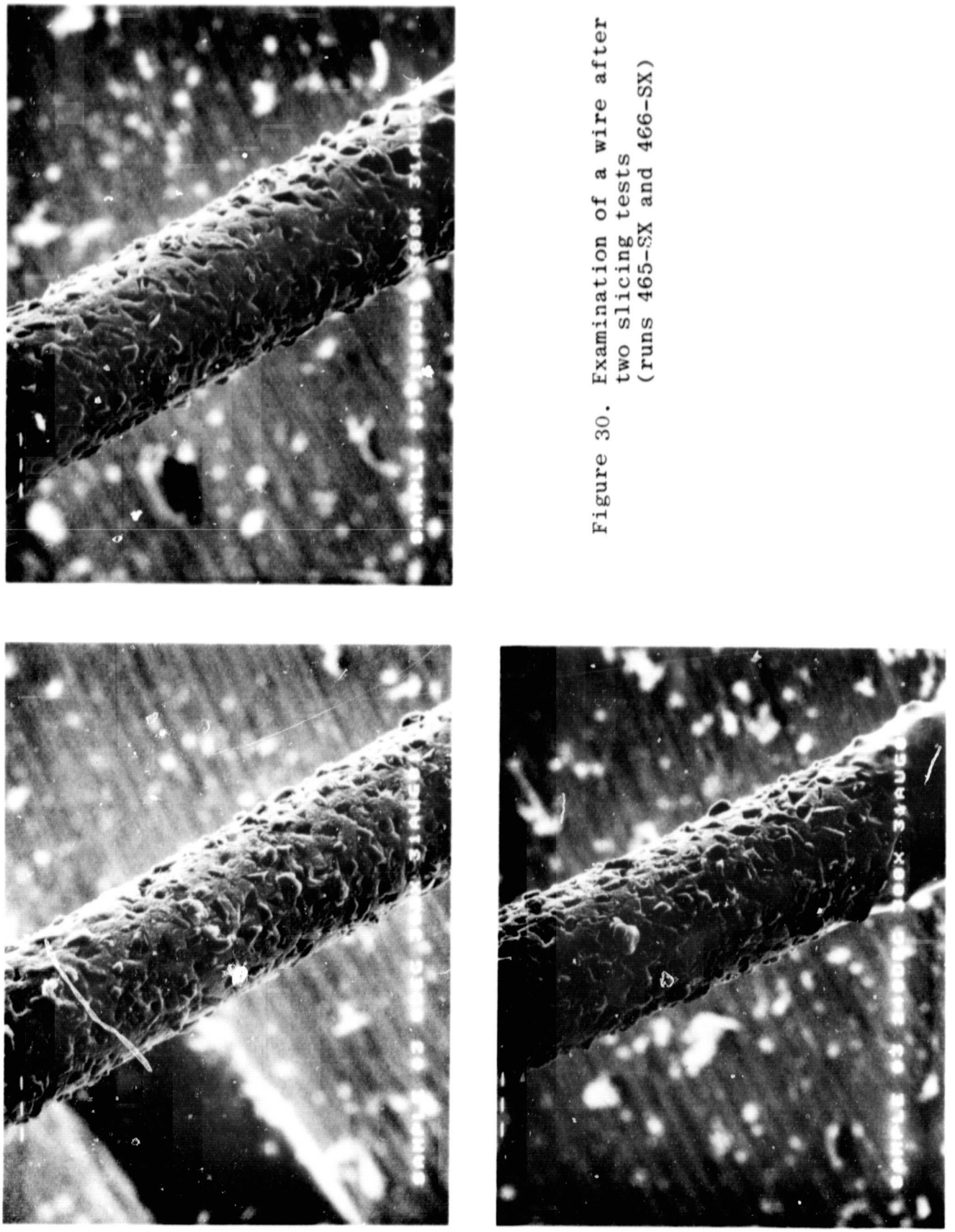

Figure 30. Examination of a wire after two slicing tests (runs 465-SX and 466-SX)

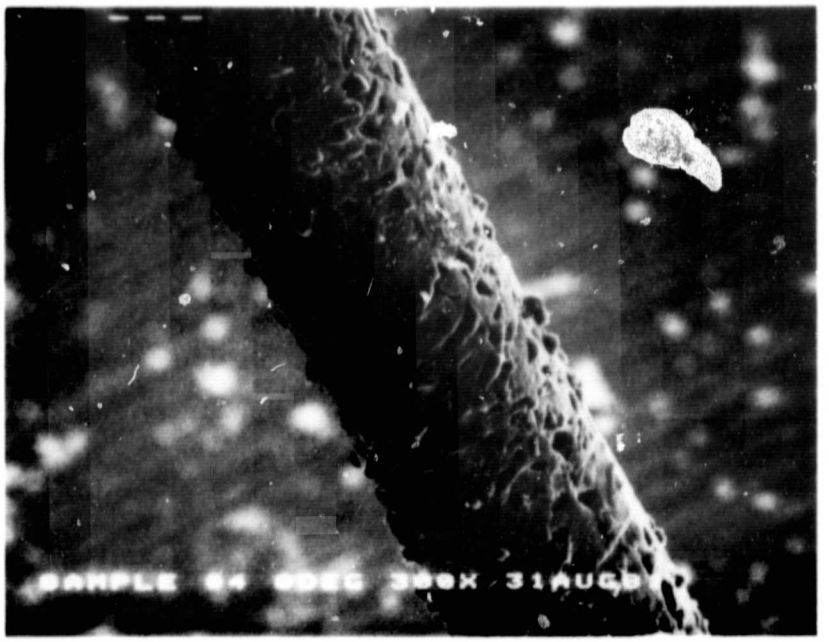

Figure 31. Examination of a wire after use in three slicing tests (runs 465-SX, 466-SX and 467-SX)

2.4 TESTING

At the start of the present phase of the program, a 4 cm x 4 cm cross-section workpiece was being sliced on the modified MBS slicer. A new high-speed FAST slicer was fabricated and one slicing experiment each was carried out with a 7.6 cm and 10 cm diameter workpiece.

During initial stages of the present program, 4 cm x 4 cm workpieces were sliced at 25 wafers/cm with the modified MBS slicer using impregnated as well as electroplated wirepacks. An example of performance with impregnated wires was in runs 305-S and 306-S. During the first slicing test 95% yield was achieved with an average slicing rate of 0.067 mm/min. The second slicing test showed 54% yield and 0.032 mm/min cutting rate. The deterioration in performance was attributed to diamond pull-out. A similar example with a set of electroplated wires was in runs 314-S through 318-S. In the first run a 100% yield was achieved and it dropped subsequently to 98, 87, 77 and 64% respectively. The slicing rates were initially 0.064 mm/min, and successively 0.051, 0.044, 0.048 and 0.060 mm/min. The improvement during the last run was because the wires were dressed prior to start of the run which probably exposed more diamonds. A comparison of these runs shows that faster cutting rates, higher yields, and longer life were achieved with electroplated wires as compared with impregnated wires. The latter approach is potentially less expensive; however, it is also less developed.

Simultaneously with slicing 4 cm x 4 cm workpiece on a modified MBS slicer development efforts were continued with 10-cm diameter ingots on the high speed FAST machine. The slicer was modified by installing a light-weight blade-head to achieve higher surface speeds. The first slicing test with this modification was run 325-SX to slice a 10-cm diameter silicon ingot at 19 wafers/cm using wires impregnated

with 45 μm diamonds. A surface speed of 400 feet per minute and a feed force of 41.3 gm was used during the test. Very good cutting rates were achieved; such high cutting rates had never been achieved with impregnated wires. The total slicing time was 11 hours, 41 minutes, giving an average cutting rate of 0.145 mm/min (5.7 mils/min). During run 328-SX this performance was repeated. Good quality wafers were sliced at an average cutting rate of 0.143 mm/min (5.62 mils/min). These cutting rates are more than 40% above the cutting rates used in economic analysis.[5] The same wirepack was again used in runs 329-SX and 330-SX. The average cutting rates achieved were 0.122 mm/min (4.82 mils/min) and 0.087 mm/min (3.44 mils/min) respectively. Figure 32 shows a plot of the depth of cut with time during runs 328-SX and 329-SX. It shows that except at the start of slicing and towards the end the cutting rate is quite linear. This demonstrates that the varying kerf length during slicing of a 10-cm diameter crystal is minimized by rocking the workpiece during FAST slicing. In regions where non-linear cutting rates are observed, the kerf length is changing rather rapidly and higher cutting rates are observed.

Also shown in Figure 32 is the data[5] for run 2-002-SX when the surface speed of the machine was 200 ft/min. Runs 328-SX and 329-SX were sliced at 400 ft/min using the same set of wires. The latter run shows the deterioration of the wires. Comparison of the data for runs 2-002-SX and 328-SX clearly shows that a significant improvement in cutting performance is achieved when surface speed is increased from 200 ft/min to 400 ft/min. By doubling the speed the average cutting rates increased from 0.059 mm/min (2.33 mils/min) to 0.145 mm/min (5.7 mils/min), a factor of 2.45.

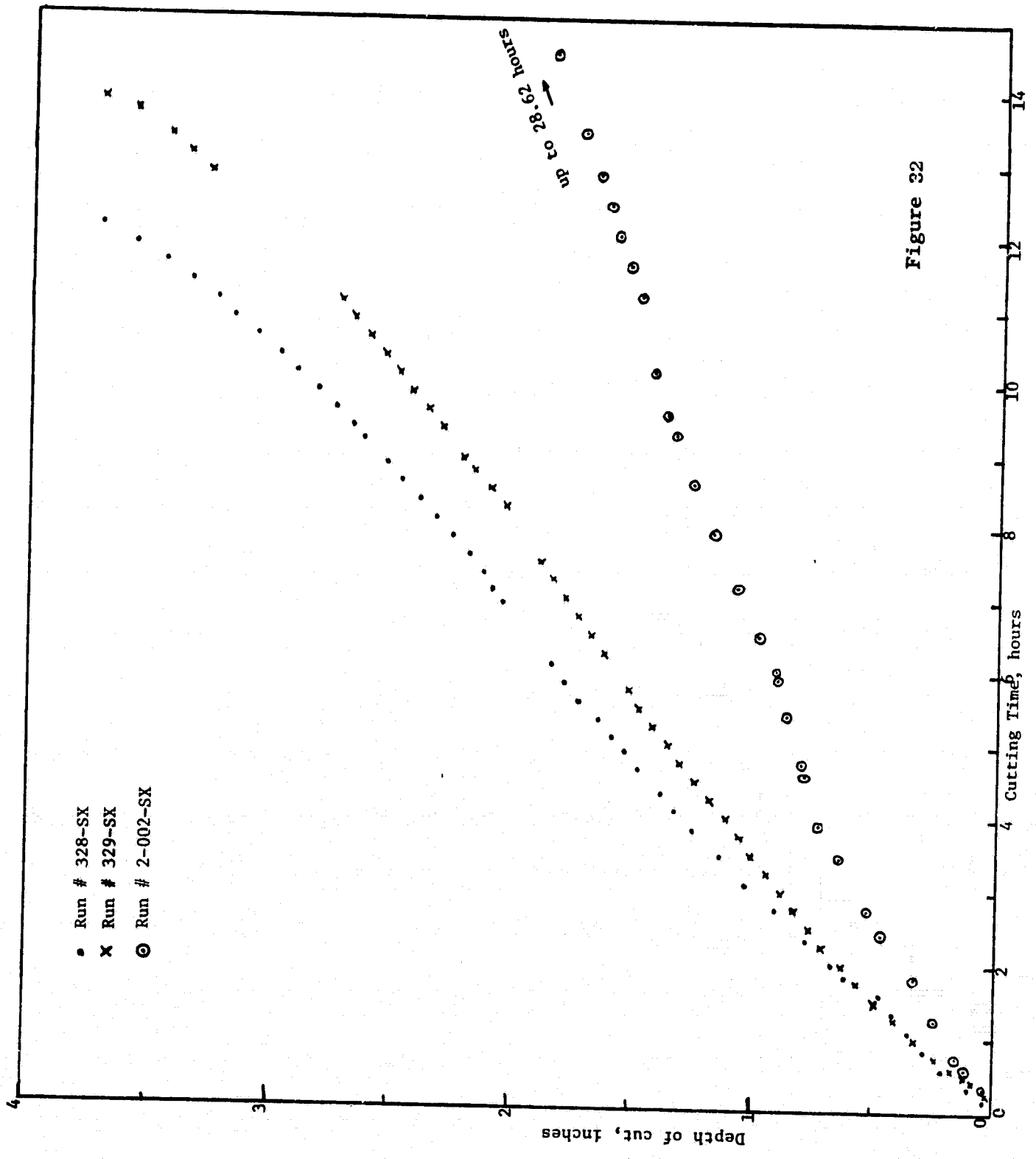

Figure 32

Other efforts to develop impregnated wires were towards using larger size diamonds. In run 422-SX, for example, 60 μm diamonds were used and in run 424-SX a mixture of 45 μm and 60 μm size were used. Other significant tests with impregnated wires were slicing of 10 cm x 10 cm cross-section workpiece in runs 403-SX, 412-SX, 424-SX and 432-SX. The cutting rates ranged from 0.040 mm/min to 0.075 mm/min and yields from 55 to 86 per cent. It was found that the limited rocking angle available for this size workpiece was affecting the slicing performance.

During blade development it was found that average slicing rate with electroplated wires was significantly higher than the impregnated wires under similar conditions. Further, diamond pull-out was more of a problem with impregnated wires. In view of this it was felt that concentration should be placed on electroplated wires as development of impregnated wires needs much more development.

A wirepack electroplated with 45 μm natural diamonds was used in runs 413-SX through 415-SX to slice 10-cm diameter ingots at 19 wafers/cm. The average slicing rates were 0.077 mm/min (3.1 mils/min), 0.050 mm/min (2.0 mils/min) and 0.050 mm/min (2.0 mils/min) respectively. The corresponding yields for the three runs were 91, 70 and 44%.

The performance of a 30 μm diamond electroplated wirepack to slice three 10-cm diameter ingots at 19 wafers/cm in runs 344-SX through 346-SX is shown in Figure 33.

As mentioned in the Blade Development section, a mixture of 45 μm, 30 μm and 15 μm diamonds was used for forming an electroplated wirepack. Such a wirepack was used in runs 433-SX through 435-SX to slice three 10-cm diameter silicon ingots at 19 wafers/cm. The performance curves are shown in Figure 34.

A number of the other variables were studied during

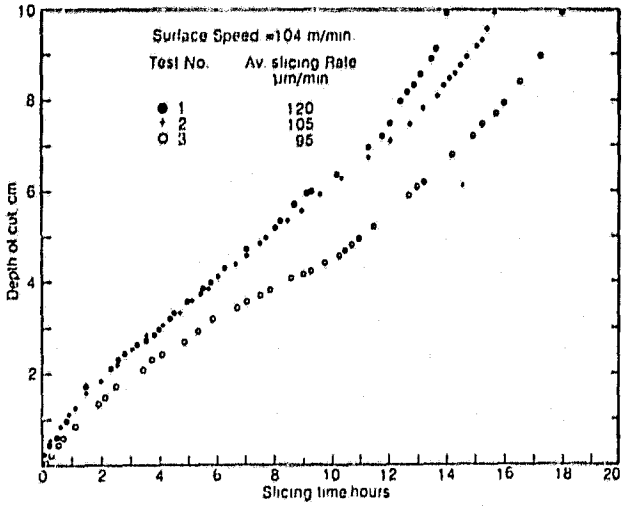

Figure 33. Slicing performance from the same wirepack using 30 µm diamonds

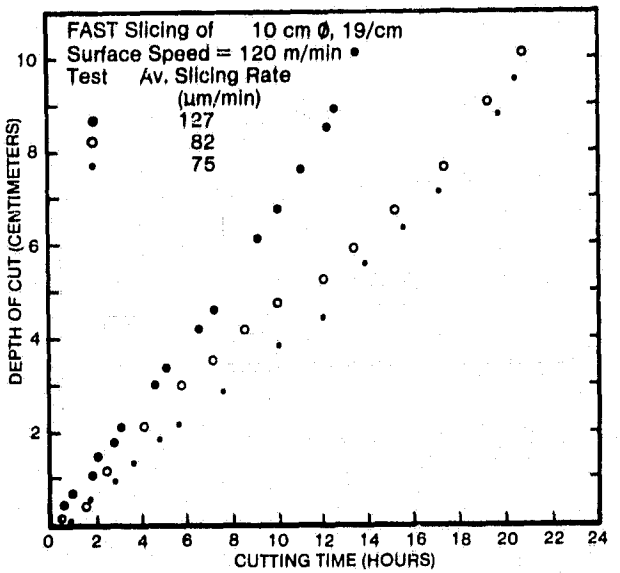

Figure 34. Slicing of three 10 cm diameter ingots using same electroplated wirepack

slicing of 10-cm diameter ingots at 19 wafers/cm, e.g., use of screened diamonds instead of micronized diamonds (run 457-SX), synthetic diamonds (run 454-SX), electroformed wirepack (run 461-SX), suitability of a steel core wire (runs 473-SX through 475-SX), prevent wire breakage by plating ductile nickel (run 459-SX), etc. A 30 μm diamond electroplated wirepack was used in runs 465-SX through 467-SX to slice 25 wafers/cm. During the first test a 99.1% yield (222 out of a possible 224) was achieved with an average slicing rate of 0.077 mm/min. In this test low feed forces of 24.4 gm /wire were used. Very good surface quality of wafers was achieved; the average wafer thickness was 0.195 mm with a kerf of 0.205 mm. During the second slicing test the average slicing rate dropped to 0.045 mm/min and the yield was only 36.2%. The average wafer thickness increased to 0.249 mm with a kerf of 0.151 mm. The data shows that during the first slicing test considerable diamonds from the sides of the wires were pulled out, thereby reducing kerf, increasing wafer thickness and decreasing the average slicing rate. The plot of the depth of cut with time is shown in Figure 35.

Another slicing test, run 464-SX, at 25 wafers/cm on 10-cm diameter workpiece, showed high slicing rates, 0.091 mm/min. In run 471-SX an 88% yield with a 0.061 mm/min average cutting rate were also demonstrated for 25 wafers/cm on a 10-cm diameter ingot.

While most of the emphasis of the program has been on 10-cm diameter ingot slicing, efforts were also made on slicing 10 cm x 10 cm square cross-section and 15 cm diameter workpieces. A 10 cm x 10 cm silicon boule was sliced at 19 wafers/cm in run 439-SX with a 96% yield and an average slicing rate of 0.1 mm/min. This cutting rate is high especially for the larger cross-section workpiece. A

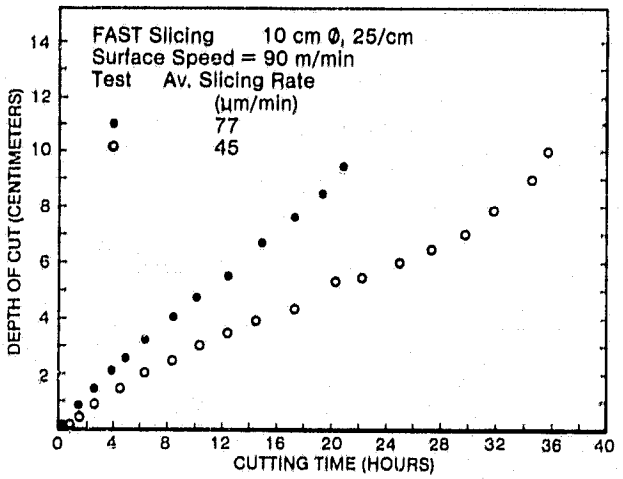

Figure 35. Slicing results of 10 cm Ø ingots at 25 wafers/in

similar demonstration was made in run 420-SX where an 89% yield and 0.085 mm/min slicing rate were achieved. Slicing of 10 cm x 10 cm silicon was also attempted at 25 wafers/cm in run 472-SX; however, the yield and slicing rate were low. It was found that in order to effectively slice a workpiece larger than 10-cm diameter, it is necessary to rock the crystal over a wider angle than could be achieved with the present slicer.

Efforts were also made to slice 15-cm diameter ingots at 19 wafers/cm. The first slicing test was in run 453-SX where the experiment was aborted after slicing about 12 cm into the 15 cm ingot. This was the first time such a large ingot was sliced by FAST. The depth of cut vs. time for this ingot is shown in Figure 36. In run 470-SX a 15-cm diameter workpiece was sliced. The average slicing rate was 0.066 mm/min (2.6 mils/min); however, the yield was poor. It was seen that the broken segments of wafers did not show much taper. During the test it was observed that once wafer breakage occurred, all the wafer fragments could not be removed because of the large kerf length. The pieces then were trapped between the wires and between the wafers and wires, thereby causing further breakage.

In run 463-SX an electroformed wirepack[12] with a 60° included angle was used to slice a 15-cm diameter workpiece. The slicing rate was 0.074 mm/min (2.9 mils/min); this is a rather high value in view of the considerably larger kerf length. A plot of the slicing performance for this test is shown in Figure 37. A similar electroformed wirepack using 60 μm diamonds was used in run 461-SX to slice a 10-cm diameter ingot. It was found that the average kerf was 0.200 mm; this is a rather low value for 60 μm diamond size.

In conclusion, it has been demonstrated that a material utilization of up to 25 wafers/cm can be achieved with over

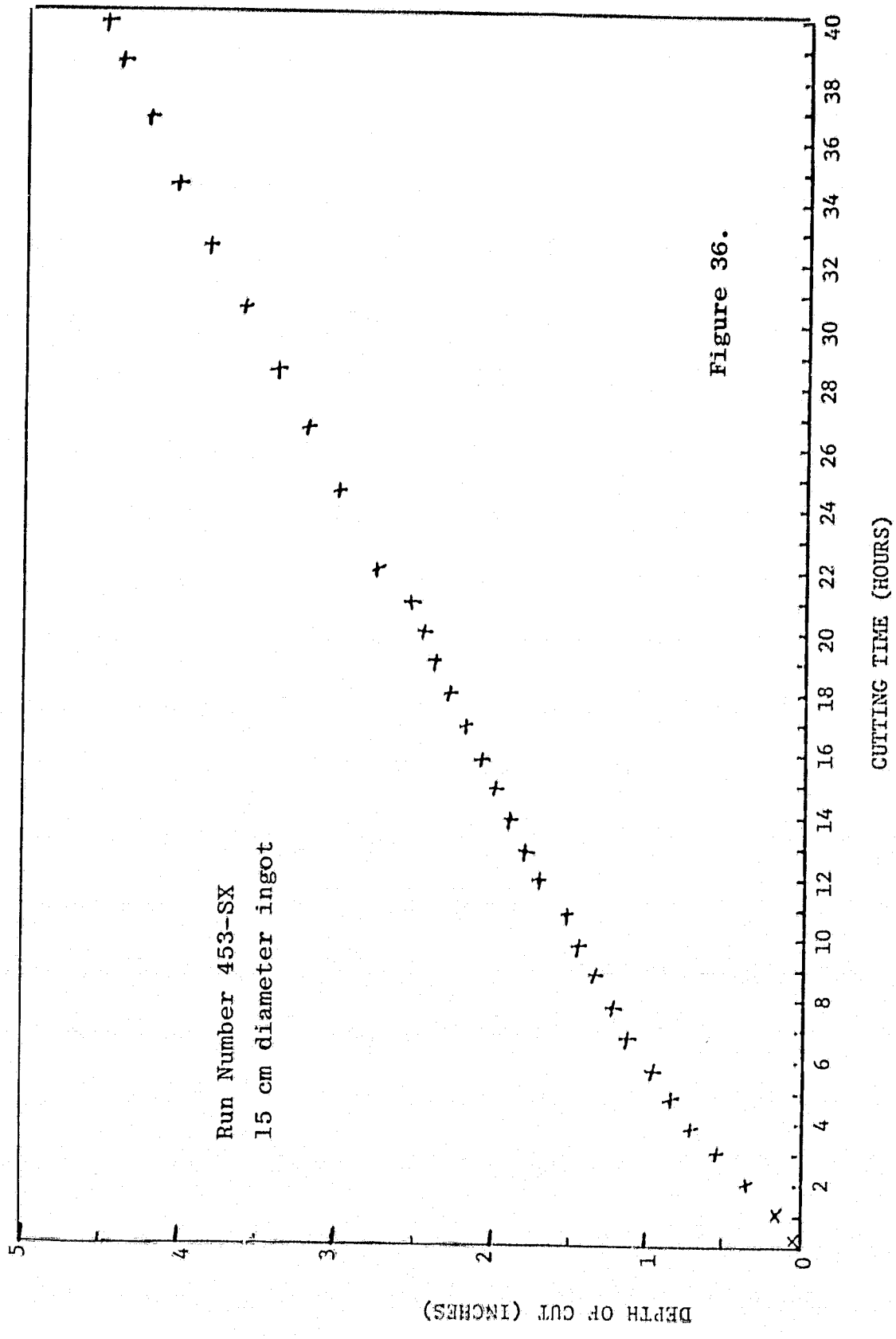

Figure 36.

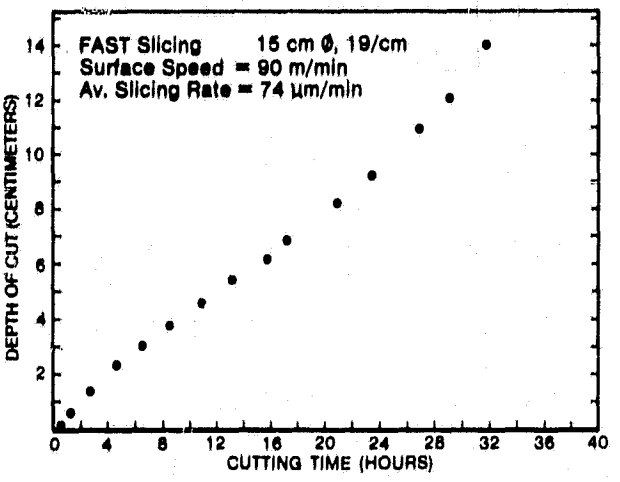

Figure 37. Slicing performance of 15 cm Ø ingot

99% yield for a 10-cm diameter ingot (0.074 mm on 15-cm diameter silicon) have been achieved. A wire life of three 10-cm diameter ingots has also been shown. New techniques have been developed in plating of wire blades which have shown potential; however, further work is necessary to explore their full effects. Machine parameters such as rigidity and rocking angle have been found to affect the testing at higher number of wafers per cm and larger workpieces. A theoretical understanding of some of these parameters is necessary to explore the full potential of the FAST technology.

Wire life of three slices through a 10 cm diameter ingot is less than the 5 and 10 slices, respectively, that is assumed in the conservative and optimistic cost analyses. The mechanism for the degradation is too subtle to be determined from SEM examination. Typical reasons for degradation are pull-out of diamonds that are cutting effectively and/or wear of diamond cutting edges. The mechanism for degradation must be understood before it can be solved. The emphasis on future work is directed towards understanding the mechanism for degradation since it is the major limitation to FAST.

2.5 ECONOMIC ANALYSIS

Two types of analyses have been made using conservative and optimistic estimates of projections for 1986. The price calculations are based on 1980 dollars and use the IPEG equation:

$$\text{Price} = \{(0.49 \times \text{EQPT}) + (135.8 \times \text{SQFT}) + (2.1 \times \text{SLAB}) + (1.3 \times \text{MATS}) + (1.3 \times \text{UTIL})\} / \text{QUANTITY}$$

where

EQPT = total equipment costs

SQFT = working area in square feet

SLAB = direct labor costs

MATS = direct materials costs

UTIL = utilities costs

FAST Slicing

It is intended to use a double-headed slicer so that two bladeheads will be used per run and two bars (30 cm x 10 cm x 10 cm) will be sliced simultaneously. The wire blades will be fabricated by nickel plating diamond on wire, since this results in the best wire life and cutting rate. The assumptions and projected add-on costs are given in Table II.

This analysis shows that the add-on cost of FAST slicing is between $5.90 and $13.13 per square meter of silicon sheet; this is considerably lower than the 1986 cost goals of $\$18.45/m^2$. If the technology is frozen at today's level, the wire life would be reduced to three slices per wire. This would cause the expendable cost to increase to $47 per run resulting in a cost of less than $\$20/m^2$.

TABLE II. IPEG Analysis for Value Added Costs of FAST Slicing Using Conservative and Optimistic Projections of Technology

	Estimate	
	Conservative	Optimistic
Equipment cost, $	30,000	30,000
Floor space, sq.ft.	80	80
Labor, units/operator	5	10
Duty cycle, %	90	95
Set-up time, hrs	1.5	1.0
Slicing rate, mm/min	0.1	0.14
Slices/cm	22	25
Slices/wire	5	10
Yield	90	95
Expendables/run, $	28	14
Motor power, h.p.	5	3
Conversion ratio, m^2/kg	0.85	1.0
Add-on Price, $\$/m^2$	13.13	5.9

2.6 CONCLUSIONS

1. The potential of FAST has been demonstrated by slicing 25 wafers/cm on a 10 cm diameter silicon ingot with over 99% yield (222 out of a possible 224).
2. A high speed FAST slicer has been designed, fabricated and tested.
3. Slicing of 10 cm x 10 cm silicon at 25 wafers/cm and 15 cm diameter workpiece at 19 wafers/cm has been demonstrated.
4. Average slicing rates as high as 0.14 mm/min have been shown during wafering of 10 cm diameter ingots.
5. Effective slicing with impregnated blades has been demonstrated.
6. Three 10 cm diameter ingots have been sliced using the same wirepack.
7. Plating procedures have been developed which do not cause wire embrittlement. This has been carried out by plating ductile nickel.
8. Hydrogen embrittlement problems with steel core wire have been solved by baking wirepacks after plating.
9. Techniques have been developed to electroplate diamonds only in the cutting edge of wires.
10. Electroforming techniques have been developed which can electroplate diamonds in predetermined shape and form.
11. During slicing of 10 cm diameter workpiece at 25 wafer/cm the average size of wafers was 0.249 mm thick with a kerf of 0.151 mm.
12. In large scale production it is expected that the add-on cost of FAST slicing will be between $5.90 and $13.13 per square meter of silicon sheet.

2.7 REFERENCES

1. F. Schmid and C. P. Khattak, ERDA/JPL 954373, Crystal Systems, Inc., Final Report (I), December 1, 1977.

2. M. H. Leipold, C. Radics and A. Kachare, "Cost of Czochralski Wafers as a Function of Diameter," JPL Publ. 80-25, February 15, 1980.

3. C. P. Khattak and F. Schmid, Proc. 2nd. Photovoltaic Solar Energy International Conf., Berlin (West), 1979.

4. T. Daud, J. K. Liu, G. A. Pollock and K. M. Koliwad, Proc. 13th IEEE Photovoltaic Specialists Conf., Washington, 1978.

5. F. Schmid and C. P. Khattak, DOE/JPL 954373, Crystal Systems, Inc., Final Report (II), June, 1979.

6. F. Schmid and C. P. Khattak, DOE/JPL 954373, Crystal Systems, Inc., Quarterly Progress Report III/3, July, 1979.

7. F. Schmid, C. P. Khattak and M. Basaran, DOE/JPL 954373, Crystal Systems, Inc., Quarterly Progress Report IV/2, July, 1980.

8. F. Schmid and C. P. Khattak, DOE/JPL 954373, Crystal Systems, Inc., Quarterly Progress Report III/4, October, 1979.

9. F. Schmid and C. P. Khattak, DOE/JPL 954373, Crystal Systems, Inc., Quarterly Progress Report III/2, April, 1979

10. F. Schmid, C. P. Khattak and M. Basaran, DOE/JPL 954373, Crystal Systems, Inc., Quarterly Progress Report IV/4, February, 1981.

11. F. Schmid, C. P. Khattak and M. Basaran, DOE/JPL 954373, Crystal Systems, Inc., Quarterly Progress Report IV/3, October, 1980.

12. C. P. Khattak, F. Schmid and M. B. Smith, "Wire-Blade Development for Fixed Abrasive Silicing Technique (FAST) Slicing," Proc. JPL/LSA Wafering Workshop, Phoenix, AZ, June, 1981.

APPENDIX II-A

SILICON SLICING SUMMARY

PRECEDING PAGE BLANK NOT FILMED

II-60 INTENTIONALLY BLANK

SILICON SLICING SUMMARY

RUN	PURPOSE	FEED FORCE/BLADE lb.	FEED FORCE/BLADE gm	AVERAGE CUTTING RATE mil/min	AVERAGE CUTTING RATE mm/min	WIRE TYPE	REMARKS
301-S	Test electroplated steel core wires	0.077	34.9	2.85	0.072	Steel core electroplated with 45 μm diamonds	Good cutting rates. Poor yield. Corrosion problems with wire.
302-S	Lifetest	0.078	35.3	2.68	0.068	Same as 301-S	Many wires broken during run due to corrosion.
303-S	Test impregnated wire with 7.5 μm sheath	0.077	34.9	1.99	0.051	5 mil, 0.125 mm W/core; 0.3 mil, 7.5 μm copper sheath; 45 μm diamond CSI impregnation. 0.3 mil, 7.5 μm nickel plated.	Good wafer quality. 90% yield.
304-S	Lifetest	0.078	35.3	0.98	0.025	Same as 303-S.	Run discontinued due to poor cutting rates.
305-S	Test impregnated wire with 12.5 μm sheath	0.077	34.9	2.64	0.067	5 mil, 0.125 mm W/core; 0.5 mil, 12.5 μm copper sheath; 45 μm diamond CSI impregnation. 0.3 mil, 7.5 μm electroless nickel plated.	Good cutting rates and wafer quality. 95% yield.
306-S	Lifetest	0.078	35.4	1.27	0.032	Same as 305-S	Poor cutting rates due to diamond pull-out. 54% yield.
307-S	Test electroplated wires	0.075	34.2	2.40	0.061	W core electroplated with 45 μm synthetic diamonds	Poor yield due to uneven nickel buildup.
308-S	Lifetest	0.075	34.2	1.60	0.041	Same as 307-S	Stroke shortened to 6" to avoid nickel buildup problem on ends. 45% yield.

SILICON SLICING SUMMARY

RUN	PURPOSE	FEED FORCE/BLADE lb.	FEED FORCE/BLADE gm	AVERAGE CUTTING RATE mil/min	AVERAGE CUTTING RATE mm/min	WIRE TYPE	REMARKS
309-S	Lifetest continuation	0.075	34.2	1.17	0.030	Same as 307-S	Lower cutting rates due to limited stroke length 40% yield.
310-S	Lifetest continuation	0.075	34.2	1.27	0.032	Same as 307-S	Cutting rates constant. 38% yield.
311-S	Lifetest continuation	0.075	34.2	1.40	0.036	Same as 307-S	Cutting rates constant. 28% yield.
312-S	Test electroplated impregnated wires	N/A	N/A	N/A	N/A	Commercially impregnated wire electroplated with nickel	Run aborted. Poor cutting performance.
313-S	Test electroplated impregnated wires	N/A	N/A	N/A	N/A	Same as 312-S	Run aborted. Diamond pull-out from wires.
314-S	Test electroplated wires	0.070	31.9	2.5	0.064	5 mil, 0.125 mm, W core electroplated with 30 μm diamonds	Very good wafer quality; 100% yield
315-S	Lifetest	0.070	31.9	2.02	0.051	Same as 314-S	Good wafer quality; 98% yield.
316-S	Lifetest continuation	0.070	31.9	1.75	0.044	Same as 314-S	Good wafer quality; 87% yield.
317-S	Lifetest continuation	0.070	31.9	1.89	0.048	Same as 314-S	Good wafer quality; 77% yield.
318-S	Life test continuation after dressing wires	0.070	31.9	2.38	0.060	5 mil, 0.125 mm W core electroplated with 30 μm diamonds	Higher cutting rates; 64% yield

SILICON SLICING SUMMARY

RUN	PURPOSE	FEED FORCE/BLADE lb.	FEED FORCE/BLADE gm	AVERAGE CUTTING RATE mil/min	AVERAGE CUTTING RATE mm/min	WIRE TYPE	REMARKS
319-S	Test plating from another source	N/A	N/A	N/A	N/A	Commercially impregnated wires electroless nickel plated, 0.3 mil, 7.5 μm	Run aborted due to poor cutting performance
320-S	Test modified plating	0.070	31.9	2.22	0.056	Commercially impregnated wire plated with a 0.3 mil, 7.5 μm nickel	Epoxy failure on mounting block. 50% yield.
321-S	Life test	N/A	N/A	N/A	N/A	Same as 320-S	Run aborted due to diamond pull-out
322-S	Test 30 μm diamond electroplated wires	0.056	25.4	3.00	0.076	5 mil, 0.125 mm W core electroplated with 30 μm diamonds	Very good quality wafers; 100% yield
323-S	Life test	0.056	25.4	1.15	0.029	Same as 322-S	Good quality wafers; 92% yield
324-S	Life test continuation	0.056	25.4	1.04	0.026	Same as 322-S	Good quality wafers; 78% yield
325-SX	Slicing of 4" Ø ingot with high speed slicer	0.091	41.3	5.70	0.145	Commercially impregnated wire plated with 0.3 mil, 7.5 μm electroless nickel	Very high cutting rates. Roller degradation observed; 21% yield
326-S	Test impregnated wire	N/A	N/A	N/A	N/A	5 mil, 0.125 mm W core, 0.7 mil, 15.5 μm copper sheath impregnated with 30 μm diamonds; 7.5 μm electroless nickel	Run aborted as diamonds were buried.
327-SX	Test 30 m diamond electroplated wire	-	-	5.19	0.13	5 mil, 0.125 mm W core, electroplated with 30 μm diamonds	Non-uniformity in plating thickness on wire.

SILICON SLICING SUMMARY

RUN	PURPOSE	FEED FORCE/BLADE lb.	FEED FORCE/BLADE gm	AVERAGE CUTTING RATE mil/min	AVERAGE CUTTING RATE mm/min	WIRE TYPE	REMARKS
328-SX	Blade life test	0.093	42.4	5.62	0.143	Commercially impregnated wire with 0.3 mil, 7.5 μm electroless nickel	Good quality wafers; 77% yield
329-SX	Life test continuation	0.095	43.0	4.82	0.122	Same as 328-SX	Lateral movement of guide roller gave poor yield (28%)
330-SX	Life test continuation	0.095	43.0	3.44	0.087	Same as 328-SX	Wire breakage due to work hardening
330-S	Test CSI impregnated blades	0.080	36.2	1.8	0.045	5 mil, 0.125 mm W core; 0.7 mil, 15.5 μm Cu sheath; 30 μm natural diamonds impregnated in cutting edge only	Very good quality wafers; 58% yield
331-S	Test electroplated blades	0.070	31.7	1.7	0.042	30 μm synthetic diamonds electroplated in cutting edge only	67% yield. Loss of cutting effectiveness with time.
332-S	Life test	0.075	34.3	0.82	0.020	Same as 331-S	Poor cutting rates
333-S	Test CSI impregnated wires	0.083	37.7	1.6	0.041	5 mil, 0.125 mm W core; 0.7 mil, 15.5 μm Cu sheath; 30 m natural diamonds impregnated in cutting edge only; 0.3 mil, 7.5 μm electroless nickel plating	Very good quality wafers; 86% yield.
334-SX	Study effect of surface speed on slicing performance using rectangular workpiece	0.084	38.3	2.13	0.054	Commercially impregnated wire with synthetic diamonds; 0.4 mil, 10 μm electroless nickel plating	Problem with ways for bladehead

SILICON SLICING SUMMARY

RUN	PURPOSE	FEED FORCE/BLADE lb.	FEED FORCE/BLADE gm	AVERAGE CUTTING RATE mil/min	AVERAGE CUTTING RATE mm/min	WIRE TYPE	REMARKS
335-S	Test CSI impregnated wires using 45 μm natural diamonds	0.078	35.8	2.31	0.057	5 mil, 0.125 mm stainless steel core; 1 mil, 25 μm Cu sheath; 45 μm natural diamonds impregnated in cutting edge only; 0.3 mil, 7.5 μm electroless nickel plating	100% yield; very good quality wafers
336-S	Life test	0.081	36.7	1.54	0.038	Same as 335-S	Good quality wafers; 74% yield. Second run with bladepack.
337-SX	Test electroplated wires	0.080	36.2	3.90	0.097	5 mil, 0.125 mm music wire electroplated with 30 μm natural diamonds	Trouble with bladehead.
338-S	Life test continuation	0.084	38.3	0.89	0.022	Same as 335-S	Third run with blade pack. 58% yield.
339-S	Test CSI impregnated wires using 30 μm natural diamonds	0.076	34.8	2.62	0.065	5 mil, 0.125 mm stainless steel core; 1 mil, 25 μm Cu sheath; 30 μm natural diamonds impregnated in cutting edge only; 0.3 mil, 7.5 μm electroless nickel plating	100% yield. Very good quality wafers.
340-S	Life test	0.080	36.2	1.54	0.038	Same as 339-S	Good quality wafers. Second run with bladepack. 73% yield.
341-S	Life test continuation	0.078	35.6	0.325	0.008	Same as 339-S	Poor cutting during third run with bladepack.

SILICON SLICING SUMMARY

RUN	PURPOSE	FEED FORCE/BLADE lb	FEED FORCE/BLADE gm	AVERAGE CUTTING RATE mil/min	AVERAGE CUTTING RATE mm/min	WIRE TYPE	REMARKS
342-SX	Test realigned bladehead	0.096	43.8	2.59	0.064	Commercially impregnated wires with 45 μm natural diamond; 0.3 mil, 7.5 μm electroless nickel	No machine problems; 50% yield.
343-S	Test commercially impregnated wire batch	0.062	28.9	1.70	0.042	Similar to 342-SX	Wafers lost at the end of run due to poor bond of ingot to plate.
401-SX	Test electroplated bladepack	0.069	31.6	2.80	0.070	5 mil, 0.125 mm W core, 45 μm natural diamonds electroplated	89 % yield.
402-SX	Lifetest	0.072	32.8	2.00	0.050	Same as 401-SX	Diamond pullout reduced cutting effectiveness, 35 % yield.
403-SX	Test CSI impregnated wire	0.070	32.0	2.50	0.062	5 mil, 0.125 mm stainless steel core; 1.5 mil, 0.037 mm Cu sheath; 45 μm natural diamond impregnated in bottom only; 0.3 mil, 7.5 μm electroless Ni.	86 % yield.
404-SX	Lifetest	0.069	31.3	-	-	Same as 403-SX	Run aborted because diamond pull-out reduced cutting effectiveness.
405-SX	Test electroplated bladepack	0.067	30.8	1.40	0.035	5 mil, 0.125 mm W core, 45 μm natural diamonds electroplated.	Diamond pull-out reduced cutting effectiveness.

SILICON SLICING SUMMARY

RUN	PURPOSE	FEED FORCE/BLADE lb.	gm	AVERAGE CUTTING RATE mil/min	mm/min	WIRE TYPE	REMARKS
406-SX	Test CSI impregnated wire		30.3	1.6	0.04	5 mil, 0.125 mm stainless steel core; 1.5 mil, 0.0375 mm copper sheath. 45 μm diamonds, electroless nickel.	78% yield. Diamond pull-out reduced cutting rate.
407-SX	Test CSI impregnated wire	0.069	31.4	2.0	0.05	5 mil, 0.125 mm stainless steel core. 0.7 mil, 0.0175 mm copper sheath. 45 μm diamonds, electroless nickel.	Run aborted due to diamond pull-out.
408-SX	Test CSI impregnated wire	0.063	28.6	1.0	0.025	4 mil, 0.1 mm stainless steel core; 1 mil, 0.025 mm copper sheath. 45 μm diamonds, electroless nickel.	Run stopped after 32 hrs. due to poor cutting rate.
410-SX	Test CSI impregnated wire	0.080	36.66	1.0	0.025	5 mil, 0.125 mm stainless steel core with 1.5 mil, 0.0375 mm copper sheath, 45 μm natural diamonds, electroless nickel plating.	Yield 67%. Poor cutting rates.
411-SX	Life test	0.070	31.71	0.9	0.022	Same as 410-SX.	Run was aborted after 13 hrs. because of diamond pull-out.
412-SX	Test CSI impregnated wire	0.071	32.50	1.6	0.040	Same as 410-SX.	Yield 82%.
413-SX	Test electroplated bladepack	0.068	31.24	3.1	0.077	5 mil, 0.125 mm W core, 45 μm natural diamonds electroplated	Yield 91%. Good cutting rates.

SILICON SLICING SUMMARY

RUN	PURPOSE	FEED FORCE/BLADE lb.	FEED FORCE/BLADE gm	AVERAGE CUTTING RATE mil/min	AVERAGE CUTTING RATE mm/min	WIRE TYPE	REMARKS
414-SX	Life test (2nd run)	0.069	31.60	2.0	0.050	5 mil, 0.125 mm diameter W wire. Co-deposited with 45 μm natural diamond (Same as 413-SX)	70% yield. Diamond still bonded to wire.
415-SX	Life test (3rd run)	0.064	29.31	2.0	0.050	Same as 413-SX	44% yield.
416-SX	Test CSI impregnated wire	0.071	32.05	2.0	0.050	5 mil, 0.125 mm stainless steel core; 1.5 mil, 0.0375 mm copper sheath. 45 μm diamonds, electroless nickel	53% yield.
417-SX	Test CSI impregnated wire	0.071	32.05	2.0	0.050	Same type as 416-SX	Run aborted after 7 hrs due to excessive blade breakage.
418-SX	Test CSI impregnated wire	0.059	26.96	-	-	Same type as 416-SX	Run was aborted after 4 hrs due to excessive blade breakage.
419-SX	Test CSI impregnated wire	0.073	33.14	3.0	0.075	Same type as 416-SX	55% yield.
420-SX	Test codeposited bladepack	0.071	32.35	3.4	0.085	5 mil, 0.125 mm wire, co-deposited with 45, 30, 15 μm diamonds	89% yield.
421-SX	Life test	0.071	32.55	2.7	0.067	Same as 420-SX	37% yield. Wire wander was observed.

SILICON SLICING SUMMARY

RUN	PURPOSE	FEED FORCE/BLADE lb	FEED FORCE/BLADE gm	AVERAGE CUTTING RATE mil/min	AVERAGE CUTTING RATE mm/min	WIRE TYPE	REMARKS
422-SX	Test CSI impregnated wire	0.071	32.35	2.0	0.05	5 mil, 0.125 mm stainless steel core; 1.5 mil, 0.037 mm copper sheath, 60 µm diamonds, electroless nickel	Run aborted due to diamond pullout.
423-SX	Test CSI impregnated wire	-	-	-	-	5 mil, 0.125 mm stainless steel core; 1.5 mil, 0.0375 mm copper sheath, 45 µm diamonds, electroless nickel	Run aborted as the diamonds were buried in the plating.
424-SX	Test CSI impregnated wire	0.070	31.[illegible]	2.7	0.067	Same as above except 45/60 µm diamonds	64% yield.
425-SX	Test CSI impregnated wire	-	-	-	-	Same type as 423-SX	Run aborted due to diamond pullout.
426-SX	Test codeposited bladepack	0.071	32.35	3.0	0.075	Same type as 420-SX.	53% yield. Poor yield due to insufficient clearance of wires.
427-SX	Test CSI impregnated wire	0.071	32.55	1.7	0.04[illegible]	Same type as 423-SX	43% yield. Wire wander was observed.
428-SX	Test CSI impregnated wire	0.046	21.06	2.7	0.067	5 mil, 0.125 mm stainless steel core; 1.0 mil, 0.0250 mm cu sheath, 45 µm diamonds, electroless nickel plating.	Run aborted due to diamond pullout.

SILICON SLICING SUMMARY

RUN	PURPOSE	FEED FORCE/BLADE lb	FEED FORCE/BLADE gm	AVERAGE CUTTING RATE mil/min	AVERAGE CUTTING RATE mm/min	WIRE TYPE	REMARKS
429-SX	Life test (2nd run) to test codeposited bladepack	0.062	27.28	1.3	0.032	Same as 426-SX (5 mil, 0.125 mm wire codeposited with 45, 30, 15 μm diamonds)	33% yield. Diamonds on wire not sufficient to clear wires. Low feed forces used to minimize vibrations from abrasion.
430-SX	Life test (3rd run)	0.072	32.94	2.3	0.052	Same as 426-SX	27% yield. Higher cutting rates achieved when feed forces were restored.
431-SX	Test new bladehead	0.054	24.56	-	-	5 mil, 0.125 mm W wire codeposited with 45, 30, 15 μm diamonds	Significant improvements because of rigidity and accurate alignment of new bladehead
432-SX	Test CSI impregnated wire	0.071	32.55	2.9	0.072	5 mil, 0.125 mm stainless steel core; 1.5 mil, 0.0375 mm copper sheath, 45 μm diamonds, electroless nickel	75% yield; loss of wafers during last inch of cut.
433-SX	Test codeposited bladepack	0.071	32.55	5.1	0.127	5 mil, 0.125 W wire, codeposited with 45, 30, 15 μm diamonds	83% yield with good surface quality
434-SX	Life test	0.073	33.34	3.3	0.082	Same as 433-SX	53% yield

SILICON SLICING SUMMARY

RUN	PURPOSE	FEED FORCE/BLADE lb.	FEED FORCE/BLADE gm	AVERAGE CUTTING RATE mil/min	AVERAGE CUTTING RATE mm/min	WIRE TYPE	REMARKS
435-SX	Life test (3d run)	0.073	33.68	3.0	0.075	Same as 433-SX	43% yield.
436-SX	Test CSI impregnated wire	0.071	32.16	2.7	0.067	5 mil, 0.125 mm stainless steel core; 1.5 mil, 0.0375 mm copper sheath, 60 μm diamonds, electroless nickel	40% yield.
437-SX	Test electroplated bladepack	0.054	24.85	4.0	0.100	5 mil, 0.125 mm W wire codeposited with 45, 30, 15 μm diamonds	52% yield.
438-SX	Life test (2nd run)	0.060	27.18	5.0	0.125	Same as 437-SX	37% yield.
439-SX	Test electroplated bladepack	0.054	24.70	4.0	0.100	5 mil, 0.125 mm W wire codeposited with 45, 30, 15 μm diamonds	96% yield.
440-SX	Life test (2nd run)	0.060	27.62	3.8	0.095	Same as 439-SX	48% yield.

SILICON SLICING SUMMARY

RUN	PURPOSE	FEED FORCE/BLADE lb	FEED FORCE/BLADE gm	AVERAGE CUTTING RATE mil/min	AVERAGE CUTTING RATE mm/min	WIRE TYPE	REMARKS
441-SX	Test codeposited bladepack	0.069	31.60	3.7	0.092	5 mil, 0.125 mm W wire, codeposited with 45, 30 μm diamonds	48% yield. Diamond pull out caused blade wander.
442-SX	Test codeposited bladepack	0.066	30.01	3.4	0.085	5 mil, 0.135 mm W wire, codeposited with 45, 30 μm diamonds	55% yield. Loss of wafers during last inch of cut.
443-SX	Test co-deposited bladepack	0.070	32.14	3.5	0.087	5 mil, 0.125 mm W wire, co-deposited with 45 and 30 μm diamonds	38% yield
444-SX	Test co-deposited bladepack (25 wires/cm)	0.044	19.9	-	-	5 mil, 0.125 mm stainless steel core; 0.1 mil, 2.5 μm Cu sheath; codeposited with 45 and 30 μm diamonds	Run aborted due to wires jumping from the grooves of support rollers and diamond pullout
445-SX	Test co-deposited bladepack	0.072	32.7	2.9	0.074	5 mil, 0.125 mm W core, co-deposited with 45 and 30 μm diamonds	48% yield; diamond pull-out reduced cutting effectiveness
446-SX	Test CSI co-deposited blade-pack	0.070	31.6	3.8	0.096	5 mil, 0.125 mm W wire, co-deposited on one side with 45 μm diamonds	49% yield
447-SX	Test CSI co-deposited blade-pack	0.072	32.5	[illegible]	0.066	5 mil, 0.125 mm W wire, co-deposited on both sides with 45 μm diamonds	91% yield

SILICON SLICING SUMMARY

RUN	PURPOSE	FEED FORCE/BLADE lb	FEED FORCE/BLADE gm	AVERAGE CUTTING RATE mil/min	AVERAGE CUTTING RATE mm/min	WIRE TYPE	REMARKS
448-SX	Test CSI co-deposited blade-pack	0.072	32.5	3.7	0.094	5 mil, 0.125 mm W wire, co-deposited on both sides with 45 μm diamonds	80% yield
449-SX	Life test (2nd run)	0.079	35.8	2.8	0.071	Same as 448-SX	74% yield
450-SX	Life test (3rd run)	0.082	37.0	2.4	0.061	Same as 448-SX	38% yield; sudden wafer breakage due to loosening of work-piece
451-SX	Test CSI codepos-ited 64/in blade-pack	0.063	28.5	2.15	0.055	5 mil, 0.125 mm W wire codeposited with 45 μm diamonds all around	Run aborted due to loss of water coolant system which caused wafer breakage
452-SX	Life test (2nd run)	0.062	28.3	2.9	0.074	Same as 451-SX	18% yield. A lot of breakage during handling.
453-SX	Slice 6-inch Ø crystal	0.071	32.4	1.9	0.048	5 mil, 0.125 mm W wire codeposited with 45 μm diamonds all around	Run aborted after 5 inches of cut.

SILICON SLICING SUMMARY

RUN	PURPOSE	FEED FORCE/BLADE lb	FEED FORCE/BLADE gm	AVERAGE CUTTING RATE mil/min	AVERAGE CUTTING RATE mm/min	WIRE TYPE	REMARKS
454-SX	Test performance of EDC synthetic diamonds	0.071	32.4	2.1	0.053	5 mil, 0.125 mm W wire co-deposited all around with 325/400 mesh EDC synthetic diamonds at CSI	Very good surface quality of wafers. 37% yield.
455-SX	Slicing of 10 cm x 10 cm cross-section workpiece	0.073	33.2	2.1	0.053	5 mil, 0.125 mm W wire co-deposited all around with 45 μm natural diamonds at CSI	Very low kerf-- approximately 6.4 mils. 54% yield.
456-SX	Slicing of 10 cm x 10 cm cross-section workpiece	0.072	32.6	1.8	0.046	5 mil, 0.125 mm W wire co-deposited in cutting edge with 45 μm natural diamonds at CSI	Average kerf 6.8 mils. 52% yield.
457-SX	Slicing with screened diamonds	0.121	55.0	2.9	0.074	5 mil, 0.125 mm W wire co-deposited all around with 325/400 mesh natural diamonds at CSI	73% yield
458-SX	Life test (2nd run)	0.084	38.1	3.6	0.091	5 mil, 0.125 mm W wire co-deposited all around with 325/400 mesh natural diamonds at CSI (same as 457-SX)	38% yield; some wires broken during slicing
459-SX	Prevent wire breakage by changing plating solution	0.084	38.0	3.1	0.079	5 mil, 0.125 mm W wire co-deposited all around with 45 μm natural diamonds at CSI	99% yield; no wire breakage

SILICON SLICING SUMMARY

RUN	PURPOSE	FEED FORCE/BLADE lb.	FEED FORCE/BLADE gm	AVERAGE CUTTING RATE mil/min	AVERAGE CUTTING RATE mm/min	WIRE TYPE	REMARKS
460-SX	Life test (2nd run)	0.084	38.0	2.1	0.053	Same as 459-SX	71% yield; 6.9 mils average kerf
461-SX	Test electro-formed wirepack	0.078	35.3	3.7	0.094	5 mil, 0.125 mm W wire electroformed to co-deposit 60 µm natural diamonds in a 60° V-groove	81% yield; 7.9 mils average kerf
462-SX	Life test of electroformed wirepack (2nd run)	0.097	43.8	3.6	0.091	5 mil, 0.125 mm W wire electroformed to co-deposit 60 µm natural diamonds in a 60° V-groove at CSI (same as 461-SX)	24% yield; some wires broken because of wire wander
463-SX	Slicing of 15 cm diameter ingot with electroformed wirepack	0.084	38.0	2.9	0.074	5 mil, 0.125 mm W wire electroformed to co-deposit 60 µm natural diamonds in a 60° V-groove	20% yield; wire wander observed
464-SX	Slicing of 25 wafers/cm	0.075	34.2	3.6	0.091	5 mil, 0.125 mm W wire co-deposited with 45 µm natural diamonds	34% yield; 7.3 mils average kerf, nickel buildup was heavier on outer wires
465-SX	Slicing of 25 wafers/cm	0.053	24.2	3.0	0.076	5 mil, 0.125 mm W wire co-deposited with 30 µm natural diamonds	99.1% yield; average wafer thickness 7.7 mils
466-SX	Life test (2nd run)	0.063	28.6	1.8	0.046	Same as 465-SX	36% yield; wafer breakage in slicing the second half of ingot

SILICON SLICING SUMMARY

RUN	PURPOSE	FEED FORCE/BLADE lb.	FEED FORCE/BLADE gm	AVERAGE CUTTING RATE mil/min	AVERAGE CUTTING RATE mm/min	WIRE TYPE	REMARKS
467-SX	Life test (3rd run)	0.063	28.7	1.3	0.033	Same as 465-SX	Run aborted because of low cutting rates
468-SX	Slicing of 10 cm x 10 cm ingot 25 wafers/cm	-	-	-	-	5 mil, 0.125 mm W wire co-deposited with 30 μm natural diamonds	Run aborted as crystal was hitting guide rollers
469-SX	Slicing of 10 cm x 10 cm ingot 25 wafers/cm	0.054	24.4	-	-	Same as 468-SX	Run aborted due to improper tracking of wires
470-SX	Slice 15 cm diameter ingot	0.072	32.6	2.6	0.066	5 mil, 0.125 mm W wire electroplated with 45 μm natural diamonds all around	Wafer breakage due to entrapment of wafer fragments between wires
471-SX	Slice 10 cm diameter ingot 25 wafers/cm	0.054	24.4	2.4	0.061	5 mil, 0.125 mm W wire electroplated with 30 μm natural diamonds all around	88% yield; average wafer thickness 7.8 mils
472-SX	Slice 10 cm x 10 cm ingot 25 wafers/cm	0.054	24.4	1.3	0.033	5 mil, 0.125 mm W wire electroplated with 30 μm natural diamonds all around	46% yield
473-SX	Test suitability of steel core wire	0.072	32.6	3.5	0.089	5 mil, 0.125 mm steel core with Cu flash, electroplated with 45 μm natural diamonds. Baked at 200° F for 5 hours.	99.4% yield; no wire breakage
474-SX	Life test (2nd run)	0.072	32.8	1.7	0.043	Same as 473-SX	63% yield; no wire breakage
475-SX	Life test (3rd run)	0.075	34.0	2.6	0.066	Same as 473-SX	37% yield; diamond pull-out observed

PART III

PAPERS AND PUBLICATIONS

Low-Cost High-Efficiency Silicon by Heat Exchanger Method and Fixed Abrasive Slicing Technique

C. P. Khattak and F. Schmid

2nd Photovoltaic Solar Energy
International Conference

Berlin - April 1979

Proceedings of the 2nd Photovoltaic Solar Energy International Conference, Berlin (West), 23-26 April 1979, pp. 106-113.

LOW-COST, HIGH-EFFICIENCY SILICON BY HEAT EXCHANGER METHOD AND FIXED ABRASIVE SLICING TECHNIQUE

C. P. Khattak and F. Schmid

Crystal Systems, Inc.
35 Congress Street
Salem, MA, USA 01970

Summary

The Heat Exchanger Method (HEM) has been adapted for growth of silicon crystals. Ingot cracking was the major problem. It has been overcome with the development of a silica crucible with a graded structure. Conditions for vacuum processing have been established. This has eliminated the use of the expensive high-purity argon. Solar cells fabricated from HEM silicon have shown conversion efficiencies of up to 15% (AM1). It has been demonstrated HEM produces silicon at low costs without compromising the quality of the material. It is the only technique which yields square cross-section, single-crystal silicon. This allows high solar-cell packing efficiency in arrays and thereby further cost reductions.

A modified multi-blade slurry machine has been used to establish the concept of multi-wire Fixed Abrasive Slicing Technique (FAST). In this approach diamond is fixed on wires and reciprocated to slice silicon. Twenty-five wafers per linear cm giving a conversion ratio of 1.08 square meters of wafer per kilogram of ingot has been demonstrated. These wafers do not exhibit edge chipping and have a surface damage of 3-5 μm. A high-speed slicer has been designed and fabricated for multi-wire FAST slicing. Workpieces of up to 10 cm diameter have been sliced.

Projected economic analysis of HEM casting and FAST slicing show an add-on cost of $10.62 per square meter of wafer.

1. INTRODUCTION

The technical feasibility of photovoltaic technology has been demonstrated for space applications. The main hindrance to adaptation for terrestrial applications is the high cost of photovoltaic arrays. One of the costly steps is conversion of polycrystalline silicon to sheet form. Important criteria to achieve cost reductions are low-cost processing, high quality product, high throughput, and efficient material utilization. The best quality silicon available in large quantity for solar application is grown by the Czochralski method. However, to be cost effective it is necessary to demonstrate multicharge throughput (1). A low-cost directional solidification technique, Heat Exchanger Method (HEM), has been used for commercial production of 32 cm diameter, 50 kg sapphire (2-5). This method has been adapted for growth of silicon crystals (6,7). Solar cells fabricated from HEM silicon have shown high conversion efficiencies, and large ingots will result in high throughput. In addition the shape of the ingot is determined by the shape of the crucible. Square cross-section crystals have been cast to achieve high packing density of wafers in a solar array. Growth of large square ingots by HEM satisfies the important criteria necessary for meeting the cost reductions.

For any ingot technology to be cost effective it has to be combined with an efficient slicing method. Kerf loss and ingot utilization (kerf plus slice) are major considerations in reducing silicon sheet cost. Internal diameter (ID) technology has been commercially utilized in the semiconductor industry where the cost of silicon is only a small proportion of the device. An economic analysis (1) of silicon slicing has indicated that ingot utilization considerations limit the cost reduction potential of ID technology. This analysis has also shown that expendable materials costs (slurry and blades) dominate the wafering costs of multi-blade slurry (MBS) technique. A recent comparison (8) of the ID, MBS and multi-wire slurry (MWS) slicing techniques has shown that the lowest kerf

widths are obtained with MWS slicing. However, the cost of wire and slurry increases the expendable materials expenses The multi-wire Fixed Abrasive Slicing Technique (FAST) concept uses fixed diamond abrasive on wire for slicing silicon. This technique combines the economic advantages of ID, MBS and MWS techniques. Expendable materials costs are low as in ID slicing, capital equipment and labor costs are low as in MBS slicing, and material utilization is high as in MWS. The FAST approach has been demonstrated to produce 25 wafers/cm on 4 cm x 4 cm cross-section workpiece and has now been extended to slicing 10 cm diameter silicon ingots.

2. HEAT EXCHANGER METHOD (HEM)

The HEM is a simple directional solidification technique (2). A seed crystal is placed at the bottom of the crucible which is seated on a high temperature heat exchanger. After evacuation to 0.1 torr, heat is provided by the graphite resistance furnace. The seed is prevented from melting by forcing gaseous helium through the heat exchanger. HEM is, therefore, the only directional solidification technique in which there is independent control of the temperature gradients in the solid and liquid with no moving parts. This method is low in capital equipment costs, labor, expendables, and energy costs. These parameters determine the cost of processing.

One of the major problems associated with solidification of silicon in silica crucibles is cracking of the ingot (9). Silicon forms a tenacious bond with silica at high temperatures and the differential thermal expansion coefficients result in cracking of the ingot during cooldown (6). This problem was solved with the development of graded silica crucibles (7,10). Figure 1 shows a 10 cm x 10 cm square ingot and etched cross-section. It can be seen that essentially the whole ingot is single crystal.

Early experiments in silicon solidification in HEM showed that the meltstock was coated with silicon carbide

Figure 1. Square ingots produced by HEM

when it was heated to high temperatures. Thermodynamic calculations showed that SiC formation was associated with use of graphite retainers in contact with silica crucibles in vacuum (11). These reactions become operative at the melt point of silicon when the pressure is reduced below about 30 torr. Under these conditions the solidified silicon ingots were saturated with carbon. It was demonstrated that when molybdenum retainers were used, preventing direct contact of graphite and silica in the furnace chamber, carbon levels in silicon were reduced by 50 percent.

Solar cells, 2 cm x 2 cm, from HEM silicon were fabricated by Spectrolab, Sylma, CA, using their standard production process. Some of the cells were textured and back-surface-field was applied to them. The ingots were sliced into 350 μm thick wafers and chemically polished to 225 μm thickness. Textured cells were thinned using a 30% NaOH solution, and then texture etched in a 1½% NaOH solution. After cleaning, wafers were diffused in phosphine gas at 850°C yielding a diffusion depth of about 0.4 μm. Front and back contacts were vacuum deposited Ti-Ag and AR coating was Ta_2O_5. The data for one of the ingots, 3.2-3.7 Ω-cm resistivity, are shown in Table I and that for textured and BSF cells in Table II. It is apparent that solar cells with up to 15% AM1 conversion efficiency can be fabricated from HEM silicon. This is comparable to production cells from Czochralski silicon.

TABLE I. DATA ON HEM SILICON SOLAR CELLS

#	AMO I_{sc} (mA)	AMO V_{oc} (mV)	AMO η	CFF	AM1 η
1	128	568	10.4	0.77	12.2
2	137	573	11.5	0.79	13.5
3	136	572	11.3	0.79	13.3
4	134	569	11.0	0.78	13.0
5	136	573	11.5	0.80	13.5
6	133	567	10.8	0.77	12.7
7	133	569	11.0	0.79	13.0
8	132	568	10.8	0.78	12.7
Control	140	612	12.4	0.78	14.5

TABLE II. DATA ON BSF AND TEXTURIZED HEM SILICON SOLAR CELLS

#	AMO I_{sc} (mA)	AMO V_{oc} (mV)	AMO η	CFF	AM1 η
1	148	583	12.2	0.77	14.2
2	156	591	12.8	0.75	15.0
3	156	587	11.6	0.69	13.5
4	156	587	12.5	0.74	14.6
5	157	591	12.4	0.72	14.5
6	148	577	11.5	0.73	13.4
7	149	583	12.0	0.75	14.0

3. FIXED ABRASIVE SLICING TECHNIQUE (FAST)

The concept of FAST was demonstrated using a modified Varian 686 MBS slicer (10). The necessity of grooved, guide rollers on both sides of the workpiece and the desirability to keep the kerf length uniform during experimental slicing limited the workpiece size to 4 cm x 4 cm cross-section.

Tungsten or high strength steel wire, 125 μm diameter, was used. Diamonds were fixed onto the wire by electroplating with nickel or by impregnation into a copper sheath on the wire. It was found that the impregnated wires suffered diamond pull-out; however, their life was extended by nickel plating after impregnation. Kerf losses were reduced by fixing diamonds only in the cutting edge. Twenty-five wafers per cm were sliced with 90-100% yields at a feed force of 35 gms per wire and surface speed 30 meters per min. Some of the salient features demonstrated in this program were slicing of thin wafers, 100 μm thickness, and kerf widths as low as 160 μm. The wafers sliced with FAST did not exhibit edge chipping. Tapered sections were examined by optical microscopy for surface damage. A typical micrograph of a (111) silicon wafer with a 5.8° tapered section is shown in Figure 2. Near the surface etch pits were piled up and their extent was less than 5 μm.

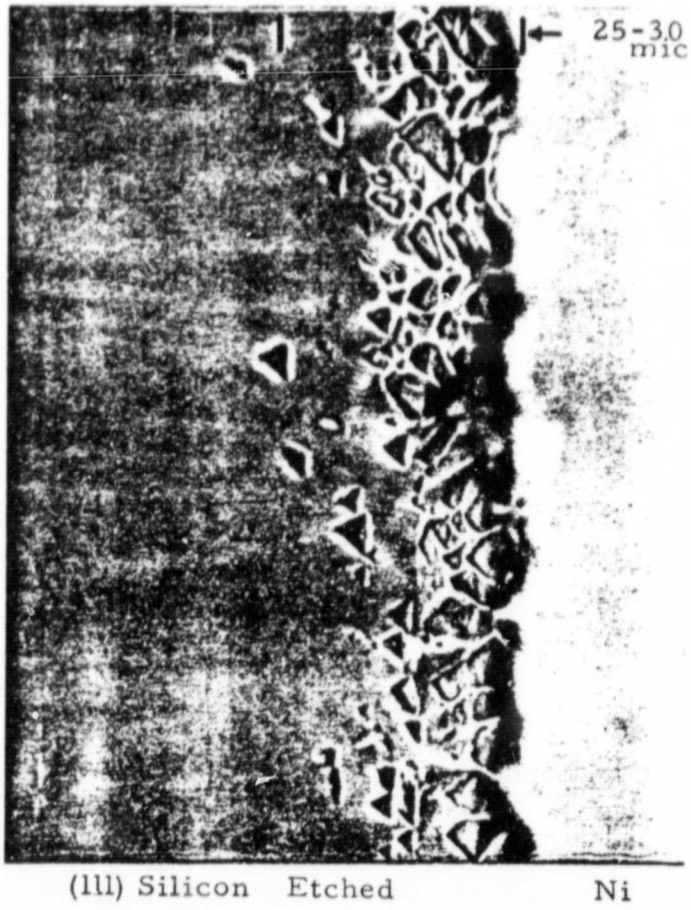

Figure 2. Optical micrograph (1000X) of a tapered section on a wafer. The dimension is magnified 10X because of the 5.8° wedge. The maximum extent of surface damage is 3 μm.

The modified MBS slicer has a massive 100 kg bladehead that cannot be reciprocated rapidly to achieve surface speeds necessary for efficient slicing with diamond abrasive. A high surface speed slicer was designed and fabricated for FAST slicing (Figure 3). Essential features of this machine are lightweight bladehead, longer stroke,

sensitive feed mechanism, counterbalanced drive, crystal rocking assembly and vibration isolation of the drive unit (12). Initial slicing of a 10 cm diameter workpiece at 65 meters per minute surface speed gave 97% wafer yield and average slicing rates of about 60 μm/minute. This demonstrated that higher surface speeds increased the cutting effectiveness and cutting rate.

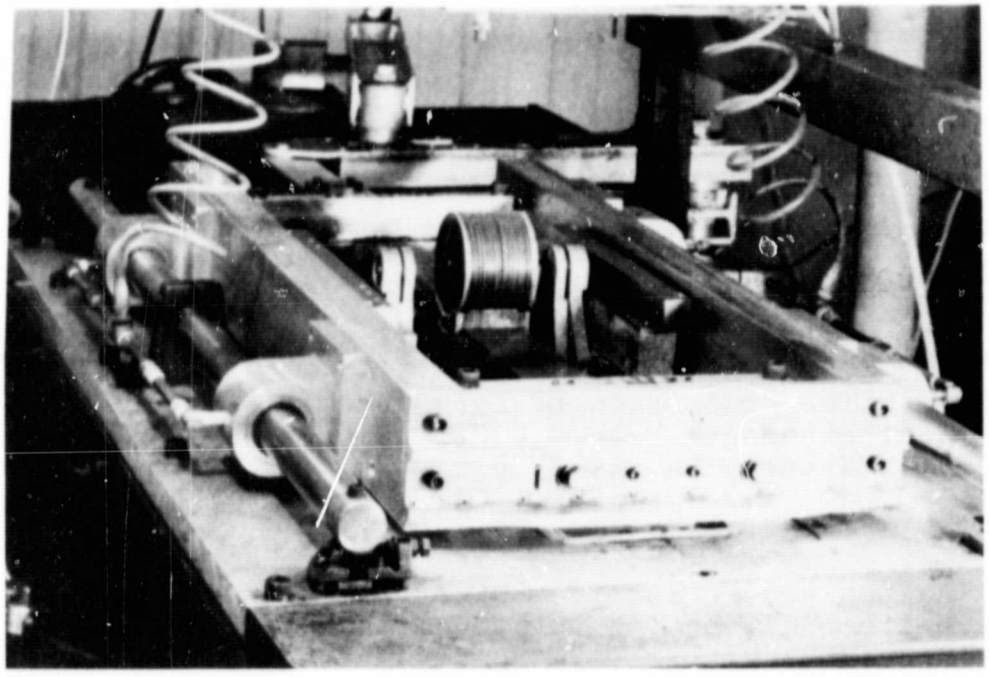

Figure 3. View of the high speed slicer for FAST after slicing a 10 cm diameter silicon ingot.

4. ECONOMIC ANALYSIS

Both HEM and FAST are low-cost processes which do not compromise quality of the product produced. The essential features have been demonstrated and scale-up is necessary.

It is intended to cast 30 cm cube ingots by HEM. These ingots will be sectioned into nine 30 cm x 10 cm x 10 cm bars which will be sliced using FAST into 10 cm x 10 cm wafers. Using the SAMICS approach (13) the cost of converting polycrystalline silicon into sheet form will be $10.62 per square meter (14), in 1975 dollars.

Acknowledgment

This paper presents results of research performed for the Low-cost Solar Array Project, Jet Propulsion Laboratory,

California Institute of Technology, sponsored by the U. S. Department of Energy through an interagency agreement with the National Aeronautics and Space Administration.

References

1. K. M. Koliwad, M. H. Leipold, G. D. Cumming and T. G. Digges, Jr., "Economic Analysis of Low-cost Silicon Sheet Produced from Czochralski Grown Material," IEEE Photovoltaic Specialists Conference, Baton Rouge, LA (1976).
2. F. Schmid and D. Viechnicki, J.Am.Ceram.Soc. 53, 528 (1970).
3. F. Schmid and D. Viechnicki, Solid State Technology 16, 45 (1973).
4. D. Viechnicki and F. Schmid, J.Cryst.Growth 26, 162 (1974).
5. F. Schmid, "The Production of Large Scatter-free Sapphire by the Heat Exchanger Method," Proc.Electro-Optics/Laser 1978 Conf., Boston, MA (1978) p. 2.
6. C. P. Khattak and F. Schmid, Am.Ceram.Soc.Bull. 57, 609 (1978).
7. C. P. Khattak and F. Schmid, "Directional Solidification of Crack-free Silicon Ingots by Heat Exchanger Method," Proc. 13th IEEE Photovoltaic Specialists Conf., Washington, D.C. (1978) p. 137.
8. H. Yoo, R. G. Schwartz and P. A. Iles, "Analysis of ID Saw Slicing for Low-Cost Solar Cells," ibid., p. 147.
9. S. L. Zerfoss, R. Johnson and P. H. Egli, Trans.Faraday Soc. (1949).
10. F. Schmid and C. P. Khattak, "Heat Exchanger-Ingot Casting/Slicing Process," Final Report--Phase I, ERDA/JPL 954373-77/4, Dec. 1, 1977.
11. F. Schmid, C. P. Khattak, T. G. Digges, Jr., and L. Kaufman, J. Electrochem. Soc. 126 (1979).
12. F. Schmid and C. P. Khattak, "Heat Exchanger Method--Ingot Casting; Fixed Abrasive Method--Multi-wire Slicing (Phase II)," Quarterly Progress Report No. 2, DOE/JPL 954373--78/1. April 7, 1978.
13. R. G. Chamberlain, "SAMICS Workbook," JPL 5101-15, Sept. 1977.
14. F. Schmid and C. P. Khattak, "Heat Exchanger Method--Ingot Casting; Fixed Abrasive Method--Multi-wire Slicing (Phase II)," Quarterly Progress Report No. 3, DOE/JPL 954373-78/2, July 15, 1978.

SILICON SLICING BY FIXED ABRASIVE SLICING TECHNIQUE

F. Schmid and C. P. Khattak

The Electrochemical Society

May 1979

Abstract No. 63

SILICON SLICING BY FIXED ABRASIVE SLICING TECHNIQUE

F. Schmid and C. P. Khattak
Crystal Systems, Inc.
35 Congress Street, Salem, MA 01970

One of the major cost factors in silicon ingot technology adaptation for terrestial photovoltaic application is in slicing boules into wafers. The most developed industrial practice is the Internal Diameter (ID) slicing. This method utilizes diamond cutting. The diamond stands up for long periods, hence, the cost of expendable materials is low. However, the ID technology as practised today has poor material utilization. The Multiblade Slurry (MBS) method has low equipment and labor costs but its expendable material costs are high. Recently Multiwire Slurry (MWS) technology has shown very good material utilization, but its expendable material costs are even higher than MBS. The multi-wire Fixed Abrasive Slicing Technique (FAST), still in advanced development stage, combines the low expendable material costs of ID method, the low labor and equipment costs of MBS and high material utilization of MWS.

FAST approach utilizes fixed diamond on wire for slicing. A multi-wire bladepack is tensioned in a bladehead and reciprocated over the workpiece. This concept was demonstrated for silicon slicing by modifying a commercially available MBS machine. Having established the concept various parameters were studied for effective slicing. Based upon this experience it was felt that some of the salient features of a FAST slicer are rocking of the workpiece and high speeds of reciprocation of the bladehead. Rocking of the workpiece minimizes the contact length between the blades and the workpiece, thereby transmitting higher effective pressures. Diamond cuts effectively at high speed as it is in a dragging mode at low speeds. High reciprocation speeds can be achieved by using a lightweight bladehead. A higher speed slicer using these concepts was designed and fabricated.

The key to any slicing is in the blade, hence blade development was pursued. Electroplated and impregnated diamond wires were used. Technology was developed to impregnate diamonds only in the cutting edge to reduce kerf and cost of diamonds. These wires also gave better accuracy and reduced wander.

The combination of machine development and blade development has resulted in slicing twenty-five wafers

per cm yielding over one square meter of wafer per kilogram of silicon ingot. It has been shown that slices as thin as 100 μm can be sliced and kerf can be reduced to as low as 160 μm.

Tapered sections prepared on FAST sliced silicon wafers have shown that there is pile-up of dislocations and microfissures near the surface. The extent of the surface damage incorporated in the wafers is 3-5 μm which is lower than that obtained by any other slicing technique.

This paper presents results of research performed for the Low-Cost Solar Array Project, Jet Propulsion Laboratory, California Institute of Technology, sponsored by the U.S. Department of Energy through an interagency agreement with NASA.

Silicon Crystal Growth in Vacuum

C. P. Khattak and F. Schmid

The Electrochemical Society

May 1979

Abstract No. 62

SILICON CRYSTAL GROWTH IN VACUUM

C. P. Khattak and F. Schmid
Crystal Systems, Inc.
35 Congress Street, Salem, MA 01970

The most developed process for silicon crystal growth is the Czochralski (CZ) method which has been in production for over two decades. In an effort to reduce cost of single crystal silicon for photovoltaic applications, a directional solidification technique, Heat Exchanger Method (HEM), was adapted. Materials used in HEM and CZ furnaces are quite similar (heaters, crucibles, insulation, etc.) To eliminate the cost of high purity argon, it was intended to use vacuum operation in HEM. Two of the major problems encountered in vacuum processing of silicon are crucible decomposition and silicon carbide formation in the melt.

Crucible decomposition results from the reaction of silicon with the silica crucible to form gaseous silicon monoxide ($Si + SiO_2 \rightarrow SiO$). This reaction proceeds to the right under vacuum operation. Under 0.1 torr pressure, typical vacuum for HEM furnace, the crucible would be decomposed. However, turbulence is eliminated in a static system such as HEM with no movement of crucible, heat zone or crystal. Convection is also minimized by stabilizing temperature gradients, i.e., growth from the bottom of crucible upwards. The SiO formed is, therefore, not removed readily from the reaction interface. Silicon crystals have been grown in silica crucibles under 0.1 torr pressure by the HEM with minimum crucible decomposition.

Thermodynamic analysis of various reactions has shown that carbon monoxide is formed as a result of contact of silica crucible and graphite retainers. These reactions are pressure sensitive and become operative below 30 torr The carbon monoxide thus formed would react with silicon to form silicon carbide. Experimentally it has been seen that when graphite retainers were in contact with silica crucibles, silicon carbide was observed on the surface of the melt and the cast ingot. Infra-red measurements showed that the silicon was saturated with carbon. When the graphite retainers were replaced with molybdenum no silicon carbide was observed on the surface of melt and cast ingots. The carbon levels in silicon were reduced by about 50%.

Silicon carbide impurities have detrimental

electrical effects for solar cell applications. In the CZ approach high carbon levels result in breakdown of crystallinity. This is contradistinct in the HEM where single crystallinity has been maintained even when silicon was saturated with carbon. It is postulated that silicon carbide floats to the surface of melt and does not impinge on the growing solid-liquid interface.

So far it has not been possible to process silicon in vacuum by CZ method because of crucible decomposition and silicon carbide impurities formation. It has been shown via HEM that both of these problems can be solved. The vacuum operation eliminates the use of high purity argon blanket, improves thermal symmetry and reduces convective currents. It has been seen that the silicon cast in vacuum by HEM has a lower oxygen content than that cast from CZ.

This paper presents results of research performed for the Low-Cost Solar Array Project, Jet Propulsion Laboratory, California Institute of Technology, sponsored by the U.S. Department of Energy through an interagency agreement with NASA.

Low-Cost Conversion of Polycrystalline Silicon into Sheet by HEM and FAST

C. P. Khattak and F. Schmid

14th IEEE Photovoltaic Specialists Conference

San Diego, CA

January 1980

LOW-COST CONVERSION OF POLYCRYSTALLINE SILICON INTO SHEET BY HEM AND FAST*

C. P. Khattak and F. Schmid

Crystal Systems, Inc.
Salem, MA 01970

ABSTRACT

The combination of Heat Exchanger Method (HEM) and multi-wire Fixed Abrasive Slicing Technique (FAST) offers one of the lowest cost processes for conversion of polycrystalline silicon into sheet form--$14.87 per square meter add-on cost. The product is rectangular cross-section, single crystal wafer with low surface damage. Cubic crystals of 20 cm size weighing up to 16.3 kg have been solidified by HEM. Some of the significant developments in the HEM process were development of a graded crucible to prevent ingot cracking, vacuum processing to reduce argon costs and improved heat extraction through a hole in the bottom of the crucible. Slicing of 10 cm diameter silicon by FAST has shown high throughput, long wire blade life and reduced kerf. Both HEM and FAST have advanced from a laboratory stage towards optimization prior to commercialization.

INTRODUCTION

The main hindrance to adaptation of photovoltaic technology for terrestrial applications is the high cost of solar arrays. One of the costly steps is conversion of polycrystalline silicon to sheet form. To achieve significant cost reductions it is necessary to produce sheet at high throughput with low expendable materials cost and low processing costs. In addition, the sheet must produce a high power density, i.e., high conversion and packing efficiency. The last feature is especially important as it reduces the cost of subsequent steps. Two new technologies, the Heat Exchanger Method (HEM) and multi-wire Fixed Abrasive Slicing Technique (FAST), have been adapted to produce silicon sheet for photovoltaic applications (1-3). All essential features have been demonstrated and presently the emphasis is on scaleup.

The Heat Exchanger Method (HEM), a directional solidification technique, is the only directional solidification technique which produces square cross-section, single-crystal silicon. Solar cells fabricated from HEM silicon have shown conversion efficiencies up to 15% (AM1), comparable in performance to production cells from Czochralski silicon (3). Although HEM is a low-cost process, the quality of silicon for solar cell application is not compromised. In addition, the square cross-section of the ingots will give a higher packing density of wafers in the array. Easy scaleup in size of ingots by HEM accounts for high throughput of the process. Silicon ingots of 20 cm cube, 16.3 kg, have been solidified with over 85% single crystallinity.

The multi-wire Fixed Abrasive Slicing Technique (FAST) uses diamond as a fixed abrasive on wire to slice silicon ingots (4). The attractive features of this method are low equipment, labor and expendable materials costs, and high material utilization. It was necessary to design and fabricate a new machine for slicing with wire. The reciprocating, high-speed slicer has been used to slice 19 wafers per cm from 10 cm diameter crystals.

Impregnated and electroplated wires have been developed for slicing silicon. Diamond pull-out is the main limitation on cutting life of the wires. Improvements in plating the wire and diamond have prolonged the life of wires.

The combination of HEM and FAST technologies offers one of the lowest add-on costs of converting polycrystalline silicon into sheet without compromising the quality of the product. A projected add-on cost of $14.87 per square meter (1980 dollars) has been calculated to meet 1986 DOE goal of less than $0.70 per watt (5).

Heat Exchanger Method (HEM)

A schematic of a HEM furnace is shown in Figure 1. A seed crystal is centered at the bottom of a silica crucible placed on a high temperature heat exchanger. After loading the

*This paper presents results of research performed for the Low-Cost Solar Array Project, Jet Propulsion Laboratory, California Institute of Technology, sponsored by the U. S. Department of Energy through an interagency agreement with the National Aeronautics and Space Administration.

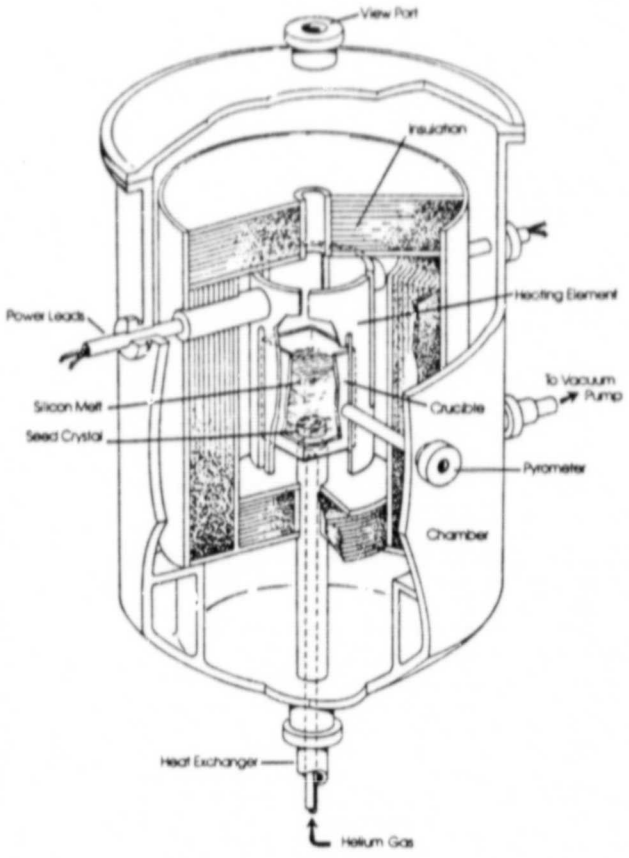

Figure 1. A schematic of an HEM furnace

crucible with polycrystalline silicon the furnace is evacuated to 0.1 torr and heat is provided by the graphite resistance heater. The seed is prevented from melting by forcing gaseous helium through the heat exchanger. The gradients in the solid are, therefore, controlled by the flow of helium, while those in the liquid are determined by the furnace temperature. Independent control of these gradients without the movement of crystal, crucible or heat zone is an important feature of HEM. A well-insulated furnace reduces the energy costs and vacuum processing eliminates expensive high-purity argon costs. The simplicity of equipment, low labor, expendable material and energy costs, therefore, make HEM a very low-cost process.

A slip-cast, high-purity silica crucible of square cross-section is heat-treated to develop a graded structure. The inside surface is high density to prevent melt penetration, whereas the outside surface is low-density to cause delamination of the crucible during the cool-down cycle in order to prevent cracking of the grown ingot (6). The crucible is, therefore, fired to high density during the heat-up cycle. An expensive step of vacuum heating the crucible to glass formation temperature prior to crystal growth is eliminated, thereby achieving cost reductions in crucible costs.

In vacuum processing of silicon it is essential to prevent direct contact of graphite and silica; otherwise it would lead to formation of silicon carbide impurities (7). A molybdenum retainer fabricated from sheet is used to support the crucible. The reuse of this retainer further reduces the expendable materials costs. The gettering property of molybdenum combined with vacuum processing has shown that HEM silicon has lower oxygen content than Czochralski silicon (8).

The HEM process relies on extraction of heat through the crucible by the heat exchanger. The increased flow of helium to promote growth of the crystal reduces the temperature of the heat exchanger. The thermal properties of silica are such that as the temperature is decreased, it becomes more insulating (9), thereby hindering the extraction of heat. A hole is cut in the bottom of the crucible through which a graphite piece is inserted. Heat extraction is, therefore, through the graphite rather than silica. The large differences in conductivities of silica and graphite ensure that heat extraction from the melt is through the seed-graphite to the heat exchanger, thereby promoting single crystallinity. The minimal direct contact of silica crucible with graphite and direct contact of silicon seed and graphite insert form silicon carbide (7) in a localized area, which seals the joint and prevents melt penetration.

The growth of 10 cm cube ingots by HEM has been reported earlier (3). During the scale-up phase 15 cm cube, 8 kg, and 20 cm cube, 16.3 kg ingots were solidified. Figures 2 and 3 show the ingots and typical single crystallinity. It can be seen that over 85% single crystallinity has been achieved. Even in areas where breakdown has occurred, very large, orientated grains have been formed. Solar cells formed from these areas did not show deterioration in performance (10).

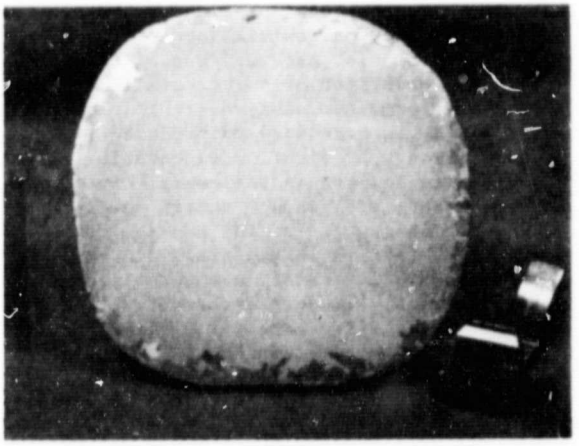

Figure 2. Polished and etched section of a 15 cm cube ingot showing single crystallinity

Figure 3. A 20 cm cube ingot along with an etched section of a 20 cm x 20 cm square cross-section silicon boule

Fixed Abrasive Slicing Technique (FAST)

The multi-wire FAST technology combines the low expendable material cost feature of ID technology, low equipment and labor costs of multi-blade slurry (MBS) and high material utilization of multi-wire slurry (MWS) process. FAST has the potential of adding lowest processing costs of all slicing processes; however, it is a new technology. Besides development of the technique efforts have to be made in the area of associated process and equipment such as slicing machine, wire blade development, etc. For example, based upon work with a modified MBS a high speed FAST slicer was designed, fabricated and tested (3). The essential feature of this slicer was that it had a light-weight reciprocating bladehead which allowed high surface speeds, 65 meters per minute compared to 30 meters per min. for the modified MBS slicer. In order to study the effect of high surface speeds, another light-weight bladehead was installed which allowed surface speeds of up to 130 meters per minute. Figure 4 shows a plot of the depth of cut as a function of time for 10 cm diameter silicon ingots sliced at two different surface speeds. A comparison of data from Tests A and C shows that by doubling the surface speed the average slicing rate increased from 59 μm/min to 145 μm/min, a factor of 2.45. Test B was carried out using the same wirepack as Test A for a second slicing life test. The average slicing rate for Test B was 122 μm/min, a slight decrease showing deterioration of the wire blades.

An interesting feature of the plots shows that except near the start and finish of the slicing tests, the slicing is quite linear with time even though the kerf length is changing appreciably. This shows that with rocking of the workpiece the effect of changing kerf length is minimized.

An important requirement of FAST is that the wires in a wirepack have uniform diamond concentration and tension and are equally spaced. Two types of wires have been developed for FAST slicing, viz. electroplated and impregnated wires. In the electroplated wires a high strength core wire is plated in an electro-nickel plating bath where diamonds are in suspension. During the plating operation a very high concentration of diamonds are entrapped onto the wires. Figure 5 shows a SEM examination of such a wire. The problem encountered with these wires was the non-uniform thickness of nickel at different positions in the wirepack. Maximum nickel buildup was found at the ends of the wirepack with minimum plating at the center. This problem was corrected by altering the placement of anodes in the plating bath. Figure 6 shows the slicing test carried out using the same electroplated wirepack. The diamond size used was 30 μm and the surface speed of the FAST slicer was 104 meters per minute. The average slicing rate for tests 1, 2 and 3 were 120, 105 and 95 μm/min respectively.

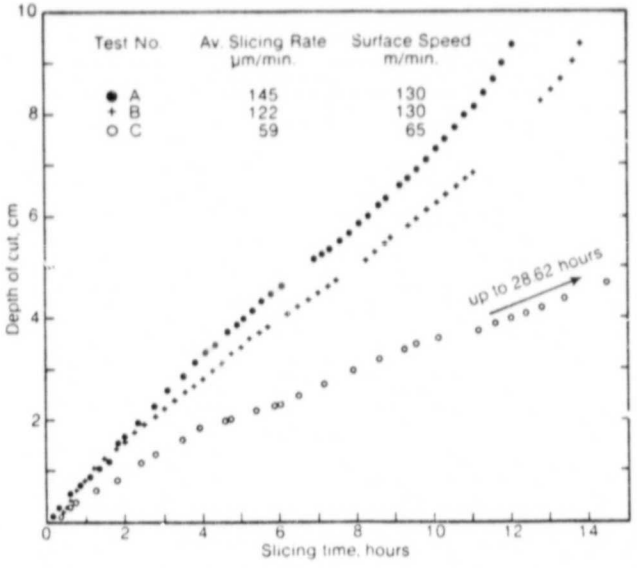

Figure 4. A plot of depth of cut with time during slicing of 10 cm diameter silicon crystal at different surface speeds

In the impregnated wires diamonds are impregnated into a soft copper sheath on high strength core wires. Techniques have been developed so that diamonds are impregnated into the bottom, cutting edge of the wires only. Diamonds are fixed into the wires of a wirepack in an impregnation unit. Aside from reducing the diamond costs the feature of diamonds in the bottom only reduces kerf and adds to the accuracy of slicing. Kerf is reduced because the amount of circumference of the wire impregnated with diamonds is controlled so that the wire clears the workpiece. The diamonds on the sides of the wires do not aid the slicing; however, they add to the kerf. The absence of diamonds on the top of the wires seats them well into the grooves of the guide rollers, thereby adding to the

accuracy of the slicing. Under such circumstances the degradation of the rollers is also reduced.

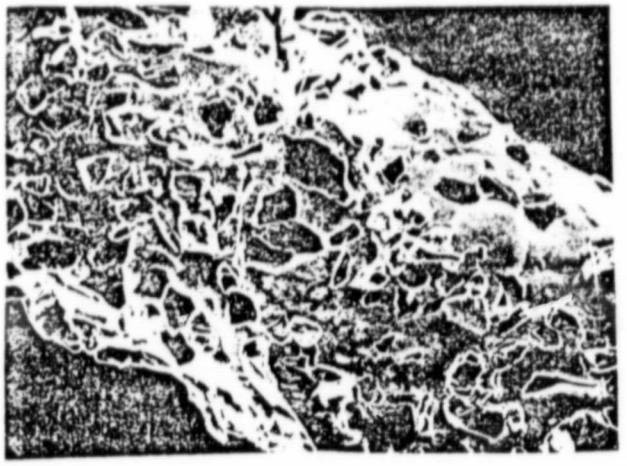

Figure 5. SEM examination of an electroplated wire showing high diamond concentration

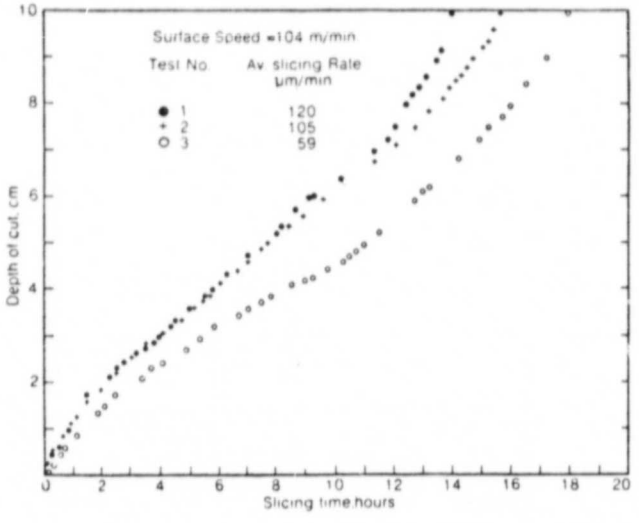

Figure 6. Slicing test of 10 cm diameter silicon ingots using the same electroplated wirepack

The multi-wire FAST method has shown high throughput, long wire life, low kerf and low expendable material cost features. In addition, it has shown high accuracy of slicing and low surface damage in the sliced wafers. FAST is a new technology and is now in an optimization and scale-up stage.

Economic Analysis

Both the HEM and FAST technologies are low-cost processes and together they have potential of giving one of the lowest add-on costs of converting polycrystalline silicon into sheet form. The wafers produced are square 10 cm x 10 cm cross-section with minimum surface damage. The projected add-on costs for HEM and FAST are $6.24 and $6.48 per square meter of sheet (1980 dollars) respectively with the combination yielding $14.87 per square meter (5). The additional step of sectioning large HEM ingots into 10 cm x 10 cm bars for FAST slicing has also been incorporated in the cost analysis. Variation of slicing parameters such as slicing rate does not show significant cost impacts.

REFERENCES

1. C. P. Khattak and F. Schmid, Am.Ceram.Soc. Bull.57, 609 (1978).
2. C. P. Khattak and F. Schmid, "Directional Solidification of Crack-free Silicon Ingots by Heat Exchanger Method," Proc.13th IEEE Photovoltaic Specialists Conf., Washington, D.C. (1978), p.137.
3. C. P. Khattak and F. Schmid, "Low-Cost, High Efficiency Silicon by Heat Exchanger Method and Fixed Abrasive Slicing Technique," Proc. Photovoltaic Solar Energy Conf., Berlin (1979).
4. F. Schmid and C. P. Khattak, "Heat Exchanger-Ingot Casting/Slicing Process," Final Report, Ph.I, ERDA/JPL 954373-77/4 (1977).
5. F. Schmid and C. P. Khattak, "Heat Exchanger Method--Ingot Casting/Fixed Abrasive Method--Multi-wire Slicing (Ph.II)," Qtrly. 3, DOE/JPL 954373-78/2 (1978).
6. J. Hino and H. E. Stauss, "Melting of Undoped Silicon Ingots," J.Metals 4, 656 (1952).
7. F. Schmid, C. P. Khattak, T.G.Digges,Jr. and L.Kaufman, J.Electrochem.Soc.126, 935 (1979).
8. F. Schmid and C. P. Khattak, "Heat Exchanger Method--Ingot Casting/Fixed Abrasive Method--Multi-wire Slicing (Ph.II)," Qtrly. 4, DOE/JPL 954373-78/3 (1978).
9. R. W. Powell, C. Y. Ho and P. E. Liley, "Thermal Conductivity of Selected Materials," Natl.Bur.Stands., NBS-8, Category 5, 99-106 (1966).
10. H.I.Yoo, P.A. Iles, and D.P.Tanner, "Silicon Solar Cell Process Development, Fabrication and Analysis," Annual Report, DOE/JPL 955089--79/4 (1979).

Origin of SiC Impurities in Silicon Crystals Grown from the Melt in Vacuum

F. Schmid* and C. P. Khattak

Crystal Systems Incorporated, Salem, Massachusetts 01970

T. G. Digges, Jr.[1]

Jet Propulsion Laboratory, Pasadena, California 91103

and Larry Kaufman

Manlabs, Incorporated, Cambridge, Massachusetts 02138

Reprinted from JOURNAL OF THE ELECTROCHEMICAL SOCIETY
Vol. 126, No. 6, June 1979
Printed in U.S.A.

Reprinted from JOURNAL OF THE ELECTROCHEMICAL SOCIETY
Vol. 126, No. 6, June 1979
Printed in U.S.A.

Origin of SiC Impurities in Silicon Crystals Grown from the Melt in Vacuum

F. Schmid* and C. P. Khattak

Crystal Systems Incorporated, Salem, Massachusetts 01970

T. G. Digges, Jr.[1]

Jet Propulsion Laboratory, Pasadena, California 91103

and Larry Kaufman

Manlabs, Incorporated, Cambridge, Massachusetts 02138

ABSTRACT

A main source of high carbon levels in silicon crystals grown from melt under reduced pressures and contained in silica crucibles supported by graphite retainer/susceptor has been identified by thermodynamic analysis. The calculations have been verified by experimental results and the carbon level can be reduced by approximately 50% with the use of molybdenum retainers.

The heat exchanger method (HEM) developed to grow large sapphire crystals (1-3) has been extended to the growth of silicon crystals (4). In this method the seed is placed at the bottom of the crucible and the temperature in the melt increases upwards. This suppresses convection that causes temperature and concentration fluctuations at the solid-liquid interface (5).

Early experiments indicated that SiC particles were found in crystals solidified by the HEM (6). However, even with the presence of SiC particles, large grains have been grown with limited interface breakdown during solidification. This observation was contradistinct to Czochralski (CZ) growth where interface breakdown due to SiC is followed by twin/polycrystalline growth (7).

The basic elements of the HEM and the CZ growth furnaces and the processes are quite similar (heaters, crucibles, insulation, etc.). A silica crucible loaded with the charge and set in a graphite retainer is placed in the furnace. The chamber is evacuated, and after melting the charge crystal growth is achieved. In the HEM process, the chamber is typically evacuated during growth to 0.1 Torr. For CZ growth an argon blanket is used and the chamber pressure can vary from 10 Torr to 1 atm (8). In early experiments with HEM growth it was quite surprising that high carbon concentrations were found in the silicon ingots. The purpose of this paper is to explain the origin of this carbon concentration and to present thermodynamic and experimental results that support the conclusions.

Reactions between Graphite and Silica

Silicon, oxygen, and carbon are used in the HEM in the form of silicon melt stock, silica crucibles and graphite furnace parts, and retainers. A thermodynamic evaluation has considered possible reactions between these three reactants and the salient reactions are reported.

Carbon has been observed in silicon crystals as silicon carbide. Silicon melt stock and graphite parts are not in direct contact; therefore, the following reactions between graphite and silica crucible were studied

$$2C + SiO_2 \rightarrow SiC + CO_2 \quad [1]$$

$$3C + 3SiO_2 \rightarrow SiC + 2CO_2 + 2SiO \quad [2]$$

$$4C + 2SiO_2 \rightarrow SiC + 3CO + SiO \quad [3]$$

$$3C + SiO_2 \rightarrow SiC + 2CO \quad [4]$$

In addition to the reactions forming SiC two additional reactions were considered

$$C + SiO_2 \rightarrow SiO + CO \quad [5]$$

$$C + 2SiO_2 \rightarrow 2SiO + CO_2 \quad [6]$$

Using the data in Table I, reactions [1]-[6] have positive free energy changes at atmospheric pressure and in the temperature range 1600°-1750°K (Table II) with those reactions that produce CO_2 tending to be more positive. The least positive free energies at atmospheric pressure are given by Eq. [4] and [5]. For reaction [5] the standard free energy of formation, $\Delta G°$, using data in Table I, is

$$\Delta G° = 162900 - 81T$$

Also

$$\Delta G = \Delta G° + RT \ln K$$

where R is the gas constant, T is temperature in degrees Kelvin, and K is the equilibrium constant for the reaction. Since equimolar ratios of SiO and CO are formed, their partial pressures are

$$p_{SiO} = p_{CO} = \tfrac{1}{2}\, p$$

where p is the total pressure. Under equilibrium conditions, $\Delta G = 0$, hence

$$\log p \text{ (atm)} = 9.15 - 1.78 \times 10^4/T$$

or

$$\log p \text{ (Torr)} = 12.03 - 1.78 \times 10^4/T$$

These equations are used to plot the curve (line) along with $\Delta G = 0$, *i.e.*, C + SiO_2 is in equilibrium with SiO + CO. The line separates the range of T, p space in which C + SiO_2 has a lower free energy than

Table I. Standard free energy of formation, $\Delta G°$, in the temperature range 1300°-1800°K (Source: Manlabs-NPL Data Bank)

Compound*	$\Delta G°$ (cal/mol)
SiC (solid)	$-16200 + 3T$
CO (gas)	$-28300 - 20T$
CO_2 (gas)	-94700
SiO_2 (solid)	$-218300 + 43T$
SiO (gas)	$-27100 - 18T$

* Note: T = °K.

* Electrochemical Society Active Member.
[1] Present address: Virginia Semiconductor, Incorporated, Fredericksburg, Virginia 22401.
Key words: carbon, thermodynamics, transport, pressure.

III-26 INTENTIONALLY BLANK

Table II. Standard free energy change for various reactions as a function of temperature

	Reaction	ΔG (calories) 1600°K	1650°K	1700°K	1750°K
[1]	$2C + SiO_2 \rightarrow SiC + CO_2$	41,400	39,400	37,400	35,400
[2]	$3C + 3SiO_2 \rightarrow SiC + 2CO_2 + 2SiO$	133,900	125,800	117,700	109,600
[3]	$4C + 2SiO_2 \rightarrow SiC + 3CO + SiO$	48,800	40,750	32,700	24,650
[4]	$3C + SiO_2 \rightarrow SiC + 2CO$	16,500	11,500	7,500	3,500
[5]	$C + SiO_2 \rightarrow SiO + CO$	33,300	29,250	25,200	21,150
[6]	$C + 2SiO_2 \rightarrow 2SiO + CO_2$	92,500	86,400	80,300	74,200
[10]	$2C + SiO \rightarrow SiC + CO$	−17,800	−17,750	−17,700	−17,650
[11]	$3C + 2SiO \rightarrow 2SiC + CO_2$	−9,700	−7,600	−5,500	−3,400
[12]	$C + SiO \rightarrow Si + CO$	−4,400	−4,500	−4,600	−4,700

SiO + CO from a second range of T, p space where SiO + CO has a lower free energy than C + SiO_2. These ranges and the $\Delta G = 0$ equilibrium curve (line) are marked in Fig. 1. Similar data for Eq. [4], also plotted in Fig. 1, show that SiC may be formed by the reaction of carbon and silica, but do not explain how SiC is transported across the crucible wall into the silicon. This leads to the conclusion that SiC is formed by reaction of a gaseous reaction product.

It should be noted that in the HEM furnace the system pressure is measured about 6 in. outside the hot zone. Even though it may not represent the exact pressure in the hot zone, it is a good indication of the operating pressures in the hot zone.

Reactions Involving Reaction Products

In the above analysis it was found that the reaction between the materials in the HEM furnace did not explain the formation of silicon carbide. Further the reactions that produce CO_2 have a higher free energy than those involving CO. Examination of the reaction

$$C + CO_2 \rightarrow 2CO \qquad [7]$$

shows that it proceeds strongly to the right at 1700°K and pressures near 1 Torr (*i.e.*, 10^{-3} atm). Thus CO will be the dominant reactant. This conclusion would be further emphasized if graphite were to react with oxygen in place of CO_2 in Eq. [7].

Another vapor species expected in the HEM furnace is SiO. This is formed by the reaction of molten silicon with the silica crucible (9, 10)

$$Si + SiO_2 \rightarrow 2SiO \qquad [8]$$

The equilibrium vapor pressure of gaseous SiO as a function of temperature for this reaction is plotted in Fig. 2.

The reaction involving the two dominant vapor species, CO and SiO, has been examined

$$CO + 3SiO \rightarrow SiC + 2SiO_2 \qquad [9]$$

and the results plotted as a function of pressure and temperature in Fig. 3. It can be seen that under the operating experimental conditions, this reaction does not proceed to the right.

Examination of the following reactions between graphite and SiO show that in two cases SiC is formed

$$2C + SiO \rightarrow SiC + CO \qquad [10]$$

$$3C + 2SiO \rightarrow 2SiC + CO_2 \qquad [11]$$

$$C + SiO \rightarrow Si + CO \qquad [12]$$

The free energy of these reactions at atmospheric

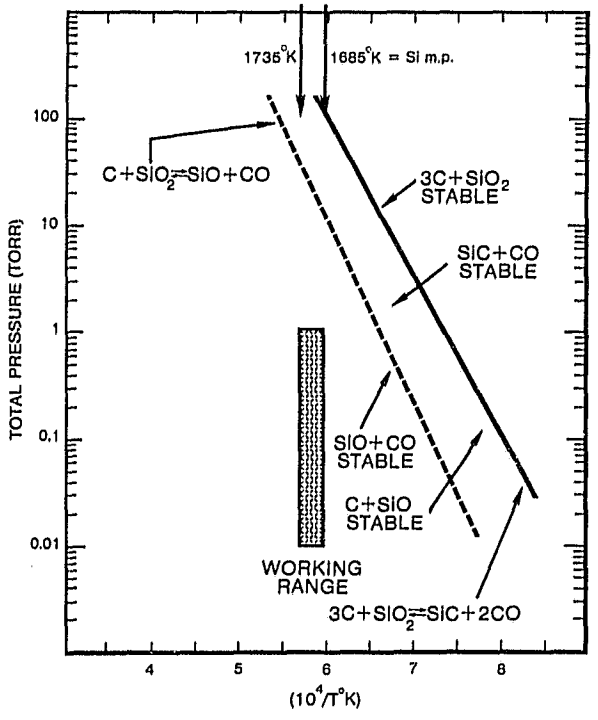

Fig. 1. Calculated pressure-temperature relations for reaction of graphite and silica to form silicon carbide, silicon monoxide, and carbon monoxide.

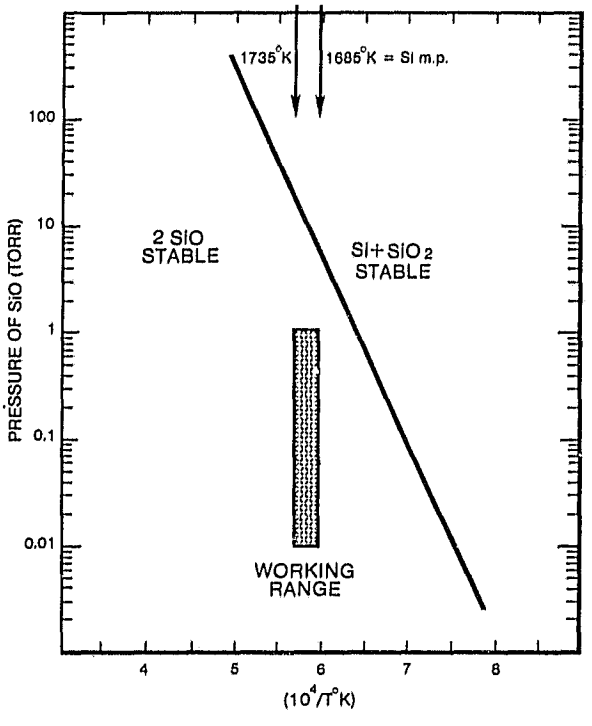

Fig. 2. Equilibrium vapor pressure of gaseous SiO as a function of temperature for the reaction Si (condensed) + SiO_2 (condensed) → 2SiO (gas).

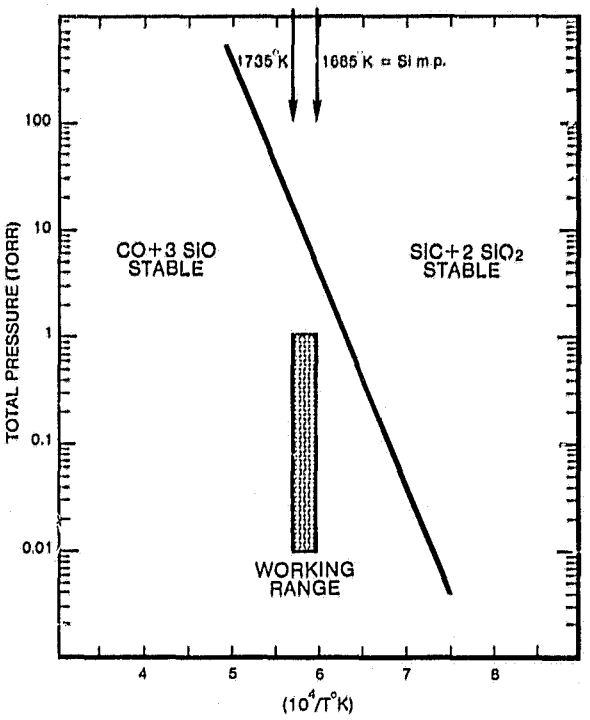

Fig. 3. Equilibrium total pressure of CO and SiO as a function of temperature for the reaction $CO + 3SiO \rightleftharpoons SiC + 2SiO_2$.

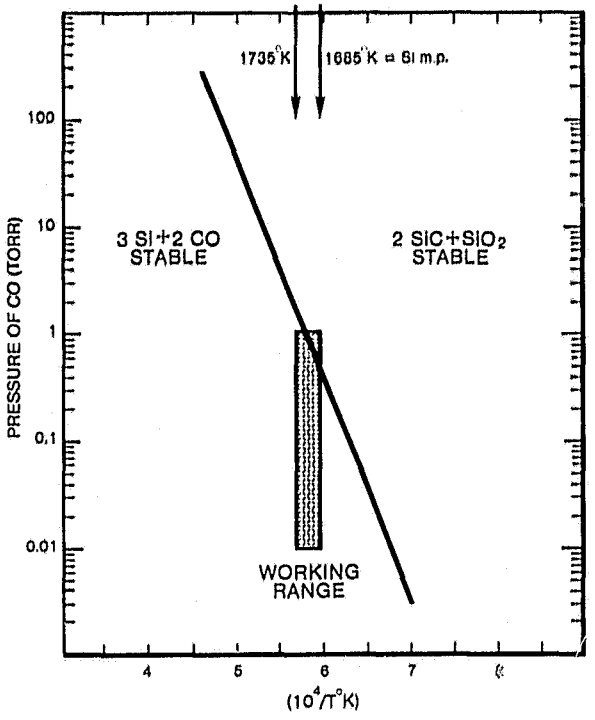

Fig. 4. Equilibrium pressure of CO as a function of temperature for the reaction $2CO + 3Si \rightarrow 2SiC + SiO_2$.

pressure is negative (Table II). This will result in coating of the furnace parts with SiC, yet no contamination of the silicon.

The following reactions involving CO and Si were studied

$$Si + CO \rightarrow SiC + \tfrac{1}{2} O_2 \quad [13]$$

$$3Si + 2CO \rightarrow 2SiC + SiO_2 \quad [14]$$

$$2Si + CO \rightarrow SiC + SiO \quad [15]$$

Reaction [13] yields a positive free energy at atmospheric pressure. Considering the pressure and temperature dependence of this reaction, the reactants will be stable in the experimental operating conditions (10). The stability range of reaction [14] shows that the reactants are stable (Fig. 4). The standard free energy of reaction [15], $\Delta G°$, using data in Table I can be represented by Eq. [16] where T = °K

$$\Delta G° = -17{,}000 + 5T \text{ (calories)} \quad [16]$$

This reaction proceeds to the right at 1700°K. The free energy of the reaction, ΔG, utilizing the usual free energy relationship, can be calculated from

$$\Delta G = \Delta G° + RT \ln K \quad [17]$$

Assuming unit activity in the condensed phase and p_{SiO}, p_{CO} (the partial pressures of SiO and CO respectively), Eq. [17] can be written as

$$\Delta G = -17{,}000 + 5T + 1.987T \ln (p_{SiO}/p_{CO}) \quad [18]$$

If the equilibrium fraction of SiO can be represented by x, then

$$x = \exp\left(\frac{17{,}000 - 5T}{1.987T}\right) \Big/ \left[1 + \exp\left\{\left(\frac{17{,}000 - 5T}{1.987T}\right)\right\}\right] \quad [19]$$

The corresponding fractions of the vapor species at different temperatures are shown in Table III. Therefore, a major source of silicon carbide formation in silicon can come from reaction [15]. The vapor pressure of carbon over graphite is less than 10^{-11} Torr at the melting point of silicon and can, therefore, be ignored. The formation of CO, besides a vacuum leak and reaction of absorbed gases on graphite parts, is from reactions [4] and [5]. This appears to be the most likely source for transport of C to the silicon.

Reactions [1]-[15] and Table I cover 9 of the 12 reactions cited by Coldwell (11). The three remaining reactions discussed in Coldwell's paper and ignored here deal with the reduction of SiO_2 and/or SiO by carbon to form silicon. These reactions are unlikely in the T, p range under consideration here. The present analysis is concerned with a wide range of pressure in contrast to Coldwell's discussion which is confined to 1 atm conditions.

Experimental Verification

The above thermodynamic analysis indicates that SiC in HEM grown silicon is attributable to the reaction of CO and Si. A major source of CO is from reactions [4] and [5], interaction of silica crucible with graphite retainer. This was verified indirectly by experiment. A graphite piece was sandwiched between two pieces of single crystal silicon with polycrystalline silicon around them. The furnace was heated close to the melting point of silicon and cooled. It was found that a silicon carbide layer was formed in areas where the graphite was in contact with the silicon crystals and also a light layer was found in the immediate vicinity. The pieces far removed from the graphite piece

Table III. Equilibrium fraction of CO and SiO at various temperatures in reaction [15]

T (°K)	$x = p_{SiO}/P_t$	% CO	% SiO
1650	0.935	6.5	93.5
1687	0.928	7.2	92.8
1700	0.925	7.5	92.5
1750	0.915	8.5	91.5

$p_t = p_{SiO} + p_{CO}$.

showed no evidence of SiC. In this experiment the graphite piece was not in contact with silica, hence reactions [4] and [5] were suppressed. In another run when the charge was heated in a silica crucible held in a graphite retainer and cooled, the entire melt stock was coated with SiC.

Experimental evidence of SiC formed in HEM grown silicon is shown in Fig. 5 and 6. Silicon carbide has accumulated at the solid liquid interface. The sample has been etched with CP-4. The groove represents a boundary where spontaneous nucleation and freezing from the top of the liquid has met the advancing interface solidifying from the bottom towards the top. In this growth a graphite retainer was used and the operating pressure was 0.1 Torr. The precipitates were identified by x-ray dispersive analysis. Infrared measurements indicated a concentration of carbon in the (3.5-4.1) $\times$ 10^{17} atoms/cm^3 range which is close to the solid solubility limit near the melting point of silicon (12). The entire top surface of the solidified ingot was covered with SiC. A similar experiment carried out with a molybdenum retainer indicated a carbon concentration of (1.5-3.1) $\times$ 10^{17} atoms/cm^3 for twelve samples. The top surface of the ingot was clean and shiny with no evidence of the SiC layers. The replacement of graphite retainer with molybdenum resulted in lower carbon levels in silicon. This eliminated the contact of graphite with the silica crucible. As far as reactions involving O_2, H_2 and water absorption in graphite, they will not be changed significantly because the HEM is carried out in a resistance heated furnace which has all graphite parts (*e.g.*, heater, liner, insulation, etc).

Fig. 5. Optical photograph (320$\times$) showing the freeze line described in text.

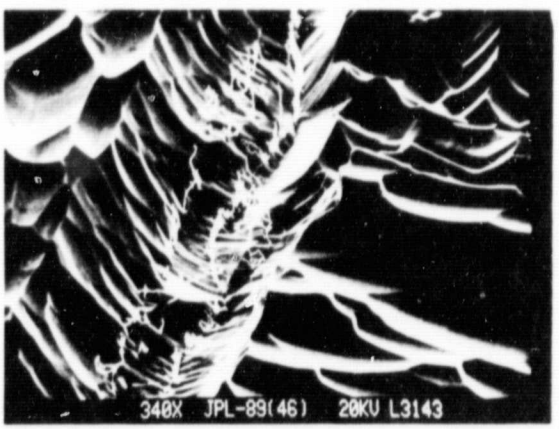

Fig. 6. SEM photograph (340$\times$) illustrates details of dendrite growth. Energy dispersive analysis of a single dendrite showed it to be SiC.

Conclusions

Evidence of high carbon levels in HEM grown silicon have led to a proposed mechanism for the cause of silicon carbide formation. It is associated with the use of graphite retainers in contact with silica crucibles under reduced pressures. High carbon levels in silicon have been reported to cause breakdown in crystallinity in CZ (7, 13) as well as in ribbon growth (14). The electrical effects of SiC inclusions have been detrimental in solar cell devices (15). The origin of high carbon levels in silicon processed in vacuum is because of reactions between silica crucibles and graphite retainers. If the graphite retainers are replaced by molybdenum, these reactions do not take place, and thereby the carbon levels in the silicon can be considerably reduced.

Acknowledgment

This paper presents results of research performed for the Low-Cost Solar Array Project, Jet Propulsion Laboratory, California Institute of Technology, sponsored by the U.S. Department of Energy through an interagency agreement with the National Aeronautics and Space Administration.

Manuscript submitted June 22, 1978; revised manuscript received Sept. 6, 1978.

Any discussion of this paper will appear in a Discussion Section to be published in the December 1979 JOURNAL. All discussions for the December 1979 Discussion Section should be submitted by Aug. 1, 1979.

Publication costs of this article were assisted by Crystal Systems Incorporated.

REFERENCES

1. F. Schmid and D. Viechnicki, *J. Am. Ceram. Soc.*, **53**, 528 (1970).
2. F. Schmid and D. Viechnicki, *Solid State Technol.*, **16**, 45 (1973).
3. D. Viechnicki and F. Schmid, *J. Cryst. Growth*, **26**, 162 (1974).
4. C. P. Khattak and F. Schmid, *Am. Ceram. Soc. Bull.*, **57**, 609 (1978).
5. K. M. Kim, A. F. Witt, and H. C. Gatos, *J. Mater. Sci.*, **6**, 1036 (1971).
6. T. G. Digges, Jr., M. H. Liepold, K. M. Koliwad, G. Turner, and G. D. Cumming, 12th IEEE Photovoltaic Specialists Conference, Baton Rouge, La. (1976).
7. F. W. Voltmer and F. A. Padovani, in "Semiconductor Silicon 1973," H. R. Huff and R. R. Burgess, Editors, p. 75, The Electrochemical Society Softbound Symposium Series, Princeton, N.J. (1973).
8. C. P. Chartier and C. B. Sibley, *Solid S... Technol.*, **18**, 42 (1975).
9. H. D. Erasmus and J. A. Persson, *Trans. Electrochem. Soc.*, **95**, 316 (1949).
10. F. Schmid and C. P. Khattak, ERDA/JPL 954373, 8th Quarterly Progress Report, October 1977.
11. D. M. Coldwell, *High Temp. Sci.*, **8**, 309 (1976).
12. R. G. Newman and J. Wakefield, "Metallurgy of Semiconductor Materials," Interscience Publ., New York (1962).
13. S. N. Rea and P. S. Gleim, ERDA/JPL 954475, Final Report, p. 29, April 1977.
14. T. F. Ciszek, *Mater. Res. Bull.*, **7**, 731 (1972).
15. C. V. Hari Rao, H. E. Bates, and K. V. Ravi, *J. Appl. Phys.*, **47**, 2614 (1976).

Single Crystal Growth of Upgraded Metallurgical Silicon by HEM for Photovoltaic Applications

C. P. Khattak, F. Schmid and L. P. Hunt

The Electrochemical Society

May 1980

SINGLE CRYSTAL GROWTH OF UPGRADED METALLURGICAL SILICON BY HEM FOR PHOTOVOLTAIC APPLICATIONS

C. P. Khattak and F. Schmid
Crystal Systems, Inc., Salem, MA 01970

L. P. Hunt
Dow Corning Corporation, Hemlock, MI 48626

ABSTRACT

Commercially available metallurgical grade (MG) silicon has high B and P content which cannot be reduced significantly by directional solidification. It has been demonstrated that by choosing high purity raw materials for an experimental Submerged Electrode Arc Furnace, most of the impurities can be reduced to 10 ppmw each, except for Al and Fe (50-100 ppmw). The B and P content of this upgraded metallurgical grade (UMG) silicon was 3 ppmw. Directional solidification of UMG silicon by the Heat Exchanger Method (HEM) has produced 16 cm x 16 cm cross-section ingots with nearly single crystal structure. This is believed to be the first time a single-crystal structure has been achieved after a single directional solidification of arc-furnace silicon. The main problem encountered during directional solidification was SiC impurities dispersed through the structure; their amount was reduced by in situ slagging. Solar cells fabricated from UMG silicon that was directionally solidified twice by HEM have shown up to 12.33% (AM1) conversion efficiency.

Introduction

The feasibility of photovoltaic technology has been demonstrated for space applications. For terrestrial use, however, the high cost of modules is a major deterrent to commercialization of photovoltaics. In present-day photovoltaic modules, the cost of the crystalline silicon starting wafer represents at least one-half of the finished module cost. In spite of extensive efforts to develop alternative materials, it appears that for at least five years crystalline silicon will be the major photovoltaics material. To make photovoltaics competitive as a source of energy, the cost of crystalline silicon material must be greatly reduced.

Lowering the cost of silicon material has to be achieved without significantly reducing the potential of the material for production of high efficiency solar cells. Currently available solar panels employ solar cells made from single crystals grown using expensive, semiconductor-grade silicon meltstock. In the preparation of semiconductor-grade silicon, the starting point is typically metallurgical silicon, a material produced in quantity for the aluminum and steel industry. This starting material, available at purity levels of 98 to 99%, sells for approximately $1.20 per kg. Costs rise rapidly, however, as the metallurgical silicon is converted first into a halide, then distilled, and finally reduced to semiconductor-grade, polycrystalline silicon in a so-called Siemens process. The resulting product sells for $50 to $75 per kg in today's market. Moreover, the process employed in the preparation of semiconductor-grade polysilicon is energy intensive.

Calculations based upon directional solidification of metallurgical silicon have shown that most impurities are reduced to ppb range. Boron and P are not significantly reduced because of near unity segregation coefficients. It has been demonstrated that use of high-purity raw materials in an experimental Submerged Electrode Arc Furnace (formerly referred to as Direct Arc Reactor, DAR) produced silicon with metallic impurities of less than 10 ppmw each, except for Al and Fe (50-100 ppw). Of significance was the low B and P concentrations. Combining this upgraded metallurgical silicon (UMG) as a meltstock and a Heat Exchanger Method (HEM) directional solidification, nearly single crystal structure was achieved. Segregation of impurities was achieved with build up in the last material to freeze--near the crucible wall. A high concentration of silicon carbide particles was seen in the structure; however, it did not break down the crystallinity. In some cases large SiC particles caused twin formation in localized areas. The concentration of these particles was reduced by in situ slagging techniques. Solar cells fabricated from the HEM solidified UMG silicon have demonstrated 12.33% conversion efficiency.

The combination of UMG silicon produced from the arc furnace and HEM technology has a potential of substantially reducing silicon materials cost for photovoltaic applications.

Silicon Meltstock

Commercially available metallurgical grade (MG) silicon is made by carbonaceous reduction of silica. Typical impurities (1) in MG silicon are shown in Table 1. Aside from

Al and Fe most of the other impurities are in the range of 20-200 ppmw. Using this meltstock as starting material and literature values (2) for equilibrium segregation coefficients, the data in Table 1 shows that considerable refinement can be achieved by directional solidification. Most of the impurities are reduced to less than 1 ppmw level except for Al, B and P. The latter elements have high segregation coefficients.

Table 1. Typical impurities in MG silicon, C_L; segregation coefficients of elements, k; and amount expected after directional solidification, C_s

Element	C_L ppmw	k	$C_s = C_L \times k$ ppmw
Al	1000	3.0×10^{-2}	30.0
B	25	0.8	20.0
Ca	850		
Cr	20	1.1×10^{-5}	0.0002
Cu	60	8.0×10^{-4}	0.0480
Fe	6300	6.4×10^{-6}	0.0403
Mg	50	3.2×10^{-5}	0.0002
Mn	140	1.3×10^{-5}	0.0018
Ni	50	1.3×10^{-4}	0.0065
P	50	0.35	17.5
Ti	90	2.0×10^{-6}	0.0002
V	200	4.0×10^{-6}	0.0008
Zr	30	1.6×10^{-8}	<0.0001

A systematic evaluation (3) of the raw materials that are used for the production of MG silicon has shown that carbon reducing materials were found to be the major source of contamination (4). The most commonly used reductants are bituminous coal, petroleum coke, and wood chips. Some silicon producers also use charcoal. The raw materials availability to some extent accounts for the variation of the final product. The use of high-purity raw materials in an experimental Submerged Electrode Arc Furnace has increased the purity of silicon (5,6). The highest purity (99.99% silicon) was achieved by using the reductant consisting of carbon black powder formed into pellets using sucrose as a binder. This silicon had metallic impurity concentrations of less than 10 ppmw each except for Al and Fe (50-100 ppmw). Emission spectrographic analysis of two batches is shown in Table 2. Boron and P were determined by electrical resistivity measurements after multiple float zoning of the silicon. Typical carbon content was about 0.5%. This high level is associated with the use of a small experimental arc furnace; in a production furnace the carbon levels are

expected to be an order of magnitude less, typical values in MG silicon. The experimental upgraded metallurgical grade (UMG) silicon is tapped from the arc furnace in air at about 1700°C and, therefore, contains carbon, silicon carbide and silica as part of the sample. Material from experiment 1 in Table 2 was only crushed and screened to remove fines, whereas that from experiment 2 was further acid-etched in order to reduce the oxide layer on the silicon. The latter material was further hand-sorted to remove obvious pieces of carbon and/or silicon carbide. Both types of UMG silicon are described later--unetched sample is from experiment 1, while etched sample is from experiment 2.

Table 2. Analysis of UMG silicon produced in two experiments. All values are in ppmw.

Impurity	Experiment 1	Experiment 2
Al	100	70
B	3	3
Ca	40	50
Cr	10	10
Cu	5	5
Fe	50	80
Mn	10	10
Mo	10	10
Ni	10	10
P	7	3
Ti	10	10
V	10	10
Zr	10	10

The HEM Process

The Heat Exchanger Method (HEM) is a directional solidification technique. This process has been adapted for the growth of large, square cross-section, single-crystal silicon ingots (7-9). A schematic of the HEM furnace is shown in Figure 1. A seed crystal is placed at the bottom of a silica crucible which is seated on a high temperature heat exchanger. After evacuation to 0.1 torr, the charge is heated by a graphite resistance furnace. The seed is prevented from melting by forcing gaseous helium through the heat exchanger. After sufficient meltback of the seed is achieved, growth proceeds by increasing the flow of helium and/or decreasing furnace temperature. The gradients in the solid are controlled by the flow of coolant through the heat exchanger while those in the liquid by the furnace

temperature. HEM is, therefore, the only directional solidification technique in which there is independent control of the temperature gradients in the solid and liquid with no moving parts.

The directional solidification results in overall purification of the meltstock. As growth proceeds, the area of the solid/liquid interface increases, thereby minimizing the effect of increasing impurities in the liquid ahead of the interface. The solid/liquid interface is surrounded by liquid, hence no steep temperature gradients exist. Even SiC particles trapped by the growing interface do not necessarily cause breakdown of crystallinity (10). This is an advantage over Czochralski growth where twinning and/or polycrystalline growth results from contaminants floating on the liquid surface (11).

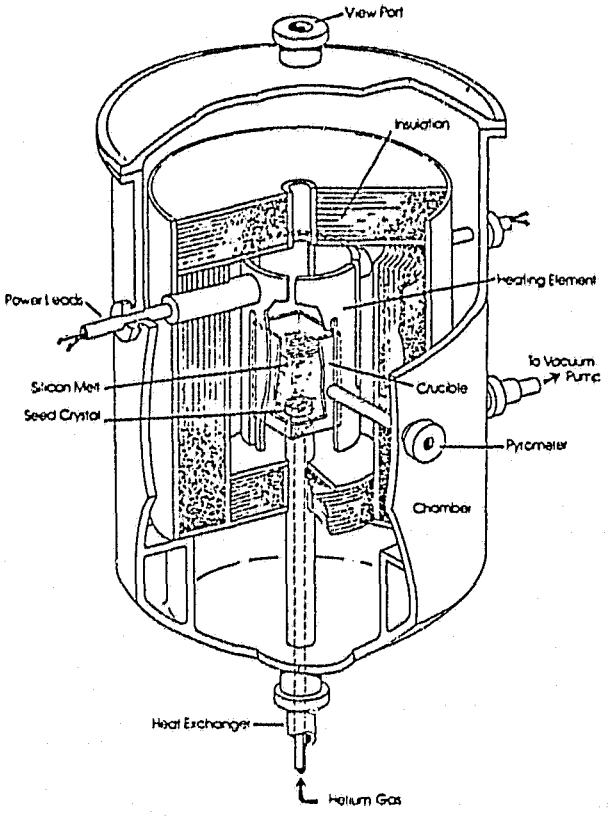

Figure 1. Schematic of HEM Furnace

When low-purity silicon meltstock is used, the lighter impurities will float on the surface of the melt, and, therefore, not interfere with the solid/liquid interface. Purification by slagging techniques can also be adopted as the slag layer will also float on the surface of the melt.

The technical advantages of HEM combined with the economic advantages, such as low equipment, labor, energy and expendable materials costs, make this technology attractive for use in reducing the materials cost of solar cells.

Directional Solidification of UMG Silicon

A 5.5 kg ingot of 16 cm x 16 cm cross-section was solidified in a silica crucible by HEM using etched UMG

silicon. A layer of contaminants was seen floating on the surface of the melt throughout the 7.75 hour solidification period; the amount decreased with time. This is an indication that some of the impurities are being removed under the vacuum operation. A slab was sectioned from the center of the ingot. The ground and etched section of the first experiment is shown in Figure 2. It can be seen that nearly single crystal structure was achieved. The twin formation in the central area originates from a particle which has been identified as SiC by x-ray diffraction. Macroscopic examination of the section also showed that SiC particles have accumulated at the bottom of the ingot as well as dispersed throughout the ingot; in some cases twins were formed but it did not break down the single-crystal structure.

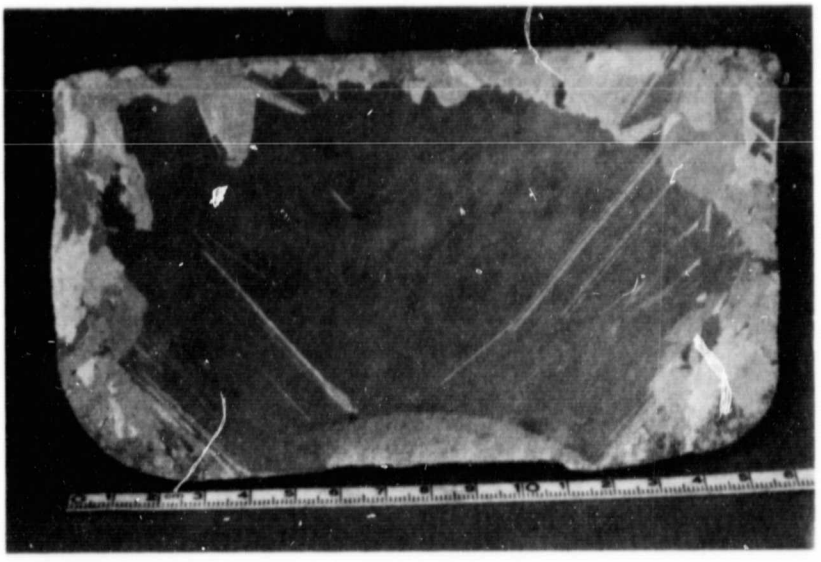

Figure 2. An etched section of a 16 cm square ingot solidified by HEM using UMG silicon

Two samples from the ingot were analyzed for impurities using Spark-Source Mass Spectrographic Technique; one of the samples was taken from the middle of the ingot while the second was taken from the edge. The results are shown in Table 3. A review of the data shows that significant purification and effective segregation have been achieved. Most of the impurities in the central region were below detectability limits of the Mass Spectrographic Technique. The resistivity of the ingot was measured to be between 0.15 and 0.20 ohm-cm.

The main problem encountered in the directional solidification of UMG silicon was the presence of SiC particles that are known to cause shunting of solar cells (12). Slagging with silica can reduce the SiC particles. Some of the reactions that proceed to the right in an HEM environment (13,14) are

$$SiC + 2SiO_2 \rightarrow 3SiO + CO$$
$$SiC + SiO_2 \rightarrow SiO + CO + Si$$
$$2SiC + SiO_2 \rightarrow 3Si + 2CO$$
$$SiC + SiO_2 \rightarrow 2Si + CO_2$$
$$SiC + SiO_2 \rightarrow C + 2SiO$$

In these cases a gaseous species will be formed leading to removal of SiC.

Table 3. Spark-source Mass Spectrographic analysis of two samples from an HEM solidified ingot using UMG silicon. All values are in ppba.

Impurity	Position in ingot		Impurity	Position in ingot	
	Middle	Edge		Middle	Edge
Ag	<6	<6	Nb	<3	<3
Al	1000	600	Ni	<30	<30
B	8000	-	P	3000	-
Co	<10	<10	Pd	<10	<10
Cr	<5	10	Sn	<5	<5
Cu	20	20	Ta	<10	30
Fe	<30	800	Ti	5	20
Mg	<5	50	V	<3	3
Mn	<5	400	W	<3	<3
Mo	<10	50	Zn	<5	<5
Na	3	40	Zr	<20	<20

In order to study this effect unetched UMG silicon with the adherent silica was used as meltstock. Some high purity silica powder was also added to the charge. During solidification a slag layer was observed on the melt surface. Some stirring of the melt was also observed. This is attributed to formation of gaseous species from the reactions between SiC and SiO_2. A cross-section of this ingot is shown in Figure 3. It can be seen that nearly single-crystal structure was achieved with most of the SiC particles accumulated near the bottom and top of the ingot.

Test solar cells (2 cm x 2 cm) were fabricated from a double HEM solidified ingot using standard cell processing procedures at Spectrolab, Inc. The range of conversion efficiency of the 22 cells processed and tested was 3.8-12.3% (AM1) with two cells above 12% and 12 above 8%. The remaining showed shunting effects. The current-voltage

characteristic of the best cell is shown in Figure 4.

Economic Analysis

The combination of UMG silicon with HEM directional solidification can have a large impact on the cost of producing silicon material for solar cells. The projected manufacturing cost of UMG silicon (5) is $3.93/kg and the add-on cost of HEM solidification (8) is $6.24/kg. The combination of the two technologies is expected to yield single-crystal, square cross-section silicon ingots at slightly more than $10/kg. This is significantly less than the $14/kg DOE goal for silicon meltstock alone to meet $0.70/watt photovoltaic power. All dollar values are in 1980 dollars.

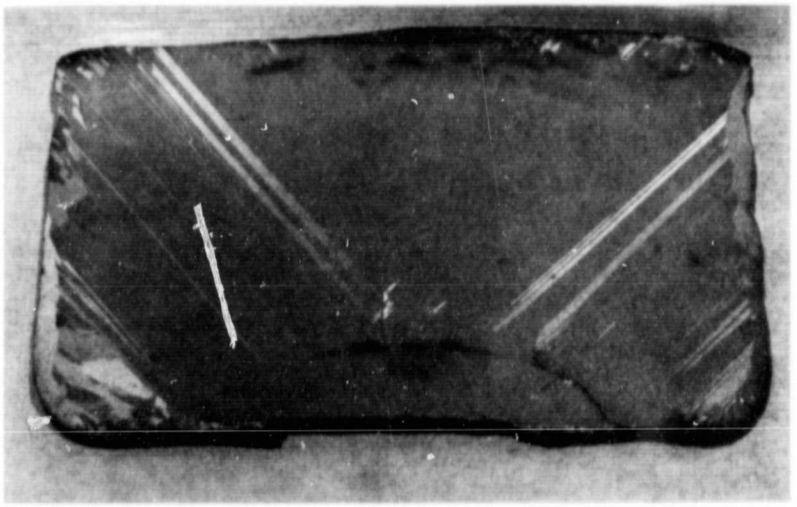

Figure 3. Nearly single crystal structure achieved with HEM solidification of UMG silicon and in situ slagging

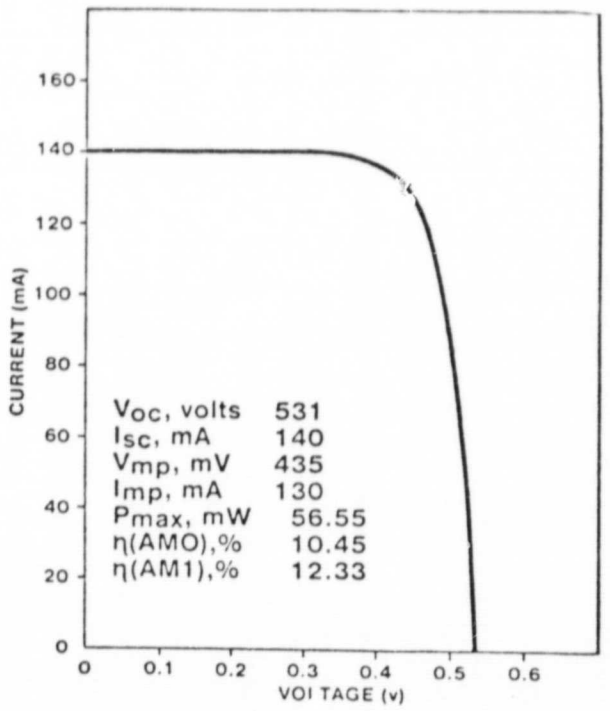

Figure 4. Solar cell data (AMO) on 2 cm x 2 cm HEM cast UMG silicon

Conclusion

It has been demonstrated that by using high purity raw materials in a Submerged Electrode Arc Furnace the MG silicon can be produced with most of the impurities below 10 ppmw each, except for Al and Fe (50-100 ppmw). It is significant that the B and P content can be reduced by using high

purity carbonaceous reductants.

Solidification of UMG by HEM has shown that nearly single-crystal ingots can be produced. The use of Czochralski technique had produced single-crystal structure only on the second pull. The main problem encountered for photovoltaic applications is the SiC particles dispersed in the structure. These particles being heavier than molten silicon sink to the bottom of the melt. However, because of particle morphology the particles float or are even suspended in the melt. SiC does not break down the structure but causes shunting of the devices. It has been shown that concentration of the particles is reduced by slagging techniques.[1] The source of these contaminants is the high carbon content of the UMG meltstock which is associated with a small furnace operated under experimental conditions. Solar cells fabricated from HEM solidified UMG silicon have shown conversion efficiencies up to 12.33% (AM1).

The combination of UMG silicon and HEM solidification offers considerable cost savings in producing silicon material for solar cells. The potential of the processes has been demonstrated. It is also important that the techniques developed and the material produced are specifically for the photovoltaic industry. There is no conflict with the semiconductor industry which can afford to pay higher prices for similar material.

Acknowledgment

This paper presents results of research supported in part by the Low-cost Solar Array Project, Jet Propulsion Laboratory, California Institute of Technology, sponsored by the U. S. Department of Energy through an interagency agreement with the National Aeronautics and Space Administration.

The authors wish to thank J. Minahan of Spectrolab, Inc., for solar cell fabrication and evaluation.

REFERENCES

1. L. P. Hunt, V. D. Dosaj, J. R. McCormick and L. D. Crossman, "Production of Solar-Grade Silicon from Purified Metallurgical Silicon," Record 12th IEEE Photovoltaic Specialists Conf., p. 125 (IEEE, New York) 1976.
2. For example, R. H. Hopkins et al, DOE/JPL-954331, Phase III Summary and 7th Quarterly Report, January 1980.

3. Dow Corning Corporation, DOE/JPL Contract No. 954559.
4. V. D. Dosaj, L. P. Hunt and A. Schei, "High-Purity Silicon for Solar Cell Applications," J. Metals, p. 8, June 1978.
5. L. P. Hunt, V. D. Dosaj, J. R. McCormick and A. W. Rauchholz, "Advances in the Dow Corning Process for Solar-Grade Silicon," Record 13th IEEE Photovoltaic Specialists Conf., p. 333 (IEEE, New York) 1978.
6. L. P. Hunt and V. D. Dosaj, "Progress on the Dow Corning Process for Solar-Grade Silicon," Record 2nd E. C. Photovoltaic Solar Energy Conf., R. Van Overstraeten and W. Palz eds., p. 98 (D. Reidel Publ. Co., England) 1979.
7. C. P. Khattak and F. Schmid, "Directional Solidification of Crack-free Silicon Ingots by Heat Exchanger Method," Record 13th IEEE Photovoltaic Specialists Conf., p. 137 (IEEE, New York) 1978.
8. C. P. Khattak and F. Schmid, "Low-cost, High-efficiency Silicon by the Heat Exchanger Method and Fixed Abrasive Slicing Technique," Record 2nd E. C. Photovoltaic Solar Energy Conf., R. Van Overstraeten and W. Palz eds., p. 106 (D. Reidel Publ. Co., England) 1979.
9. C. P. Khattak and F. Schmid, "Low-cost Conversion of Polycrystalline Silicon into Sheet by HEM and FAST," Record 14th IEEE Photovoltaic Specialists Conf., p. 484 (IEEE, New York) 1980.
10. T. G. Digges, Jr., M. H. Leipold, K. M. Koliwad, G. Turner and G. D. Cumming, "Some Observations on the Characteristics of Low-Cost Silicon Sheets," Record 12th IEEE Photovoltaic Specialists Conf. (IEEE, New York) 1976.
11. S. N. Rea and P. S. Gelim, ERDA/JPL 954475, Final Report, p. 29, April 1977.
12. C. V. Hari Rao, H. E. Bates and K. V. Ravi, J.Appl. Phys. 47, 2614 (1976).
13. F. Schmid and C. P. Khattak, DOE/JPL 954373, Quarterly Report No. 8., October 1977.
14. F. Schmid, C. P. Khattak, T. G. Digges, Jr. and L. Kaufman, J. Electrochemical Soc. 126, 935 (1979).

5101-187
Low-Cost
Solar Array Project

DOE/JPL-1012-66
Distribution Category UC-63b

Proceedings of the Low-Cost Solar Array Wafering Workshop

(8-10 June, 1981, The Pointe, Phoenix, Arizona)

Overview of a New Slicing Method -- Fixed Abrasive Slicing Technique (FAST)

Frederick Schmid
Maynard B. Smith
Chandra P. Khattak

February 1, 1982

Prepared for
U.S. Department of Energy
Through an Agreement with
National Aeronautics and Space Administration
by
Jet Propulsion Laboratory
California Institute of Technology
Pasadena, California

(JPL PUBLICATION 82-9)

OVERVIEW OF A NEW SLICING METHOD-- FIXED ABRASIVE SLICING TECHNIQUE (FAST)*

Frederick Schmid, Maynard B. Smith and Chandra P. Khattak

Crystal Systems, Inc.
35 Congress Street, Salem, MA 01970

ABSTRACT

FAST is a new slicing technique that has been developed to slice silicon ingots more effectively. It has been demonstrated that 25 wafers/cm can be sliced from 10 cm diameter and 19 wafers/cm from 15 cm diameter ingots. This has been achieved with a combination of machine development and wire-blade development programs. Correlation has been established between cutting effectiveness and high surface speeds. A high speed slicer has been designed and fabricated for FAST slicing. Wirepack life of slicing three 10 cm diameter ingots has been established. Electroforming techniques have been developed to control widths and prolong life of wire-blades. Economic analysis indicates that the projected add-on price of FAST slicing is compatible with the DOE price allocation to meet the 1986 cost goals.

INTRODUCTION

Silicon crystals have been sliced into wafers for the semiconductor industry by the Internal Diameter (ID) and Multiple Blade Slurry (MBS) techniques. While these processes were developed for semiconductor applications, they cannot be utilized, as they exist today, for photovoltaic applications. Unlike semiconductor devices where silicon material constitutes sometimes less than one per cent of the cost, the cost of silicon wafers comprises about half the cost of a solar panel. The wafering technique to produce silicon wafers from ingot is one of the important steps towards reducing costs for terrestrial photovoltaic applications. The slicing process must be low cost and must combine minimum kerf plus slice thickness to achieve high material utilization. With improved material utilization alone, the contribution of the cost of polysilicon and crystal growth for photovoltaic power generation, dollars per peak watt, is significantly reduced. Therefore, material utilization is critical for reducing costs to make photovoltaics a reality for terrestrial applications.

Besides being most developed and commercially available, the advantages of an ingot process towards making sheet are high throughput, purification of meltstock during growth, consistent quality, simple instrumentation and control; however, material utilization and kerf in slicing limits the low-cost potential. In fact, the justification for silicon ribbon processes is based on the premise that slicing cannot be cost effective. As the cost of polysilicon meltstock is reduced to the goal of $14/kg kerf losses in slicing become less significant but material utilization is still critical. The combination of an effective slicing process with an ingot process, such as the Heat Exchanger Method (HEM), allows the economical production of square shaped

high conversion efficiency material to produce high power density modules at low cost.

SLICING TECHNIQUES

The essential parameters for a slicing technique for photovoltaic applications are (i) low-cost process, (ii) low expendable costs, (iii) high material utilization and (iv) produce high quality product. There are three commercially used wafering processes, *viz.*, ID, MBS and Multiple Wire Slurry (MWS) techniques. A comparison of the parameters for these wafering methods is shown in Table I. It can be seen that the advantages are low expendable material costs in ID, low equipment and labor costs in MBS, and high material utilization in MWS; however, the ID is limited by material utilization, and MBS and MWS by their high expendable materials costs. A new slicing technique under development, the Fixed Abrasive Slicing Technique (FAST), combines the low expendable material advantage of ID, low equipment and labor costs of MBS and high material utilization of MWS.

TABLE I. A Comparison of the Essential Parameters of Wafering for Different Slicing Techniques

Parameter	ID	MBS	MWS	FAST
Equipment costs	High	Low	High	Low
Labor supervision	Medium	Low	High	Low
Throughput	Medium	Medium	Low	High
Expendable costs	Low	High	Very high	Low
Material utilization	Low	Medium	High	High
Surface damage	High	Medium	Medium	Low

In the FAST process (1) a multiple-wire bladepack is stretched in a frame and reciprocated on rails. Diamond is fixed onto the wires and used as an abrasive for slicing silicon. Diamond has been demonstrated to be an effective abrasive for silicon via the ID process and, therefore, the expendable materials costs are kept low. The simplified equipment concept of reciprocating bladehead keeps the FAST slicer costs low and this has been proven by the MBS. The best material utilization of wire slicing (2) is also incorporated in FAST. This feature is possible with wire because once the wire cuts through it no longer contacts the workpiece, hence less clearance is necessary. This reduces kerf and also make it possible to slice thinner wafers. In the MWS the silicon being sliced is completely lost when a wire breaks. For the FAST approach, a broken wire results in loss of two wafers it is contacting. In addition to the above advantages to FAST the surface damage of the sliced wafers is lower (3) than that reported for other slicing technologies (4).

FAST is a new slicing technique that has been developed to slice ingots more effectively. Work has been carried out in three areas, *viz.*, machine development, blade development and testing.

FIXED ABRASIVE SLICING TECHNIQUE (FAST)

Machine Development

Initially a MBS slicer was used for evaluation of FAST slicing. Prior work reported in literature showed very limited success with slicing using diamond plated flat blades and wires. In the development of FAST it was found that the slicing is heavily dependent on pressure at the diamond tips during slicing. Effective slicing was not achieved with diamond plated wires used in a conventional MBS setup because of insufficient pressure at the cutting edge. Significant improvement was achieved when the crystal was rocked. Under this condition the kerf length or contact between the wire and the workpiece was minimized thereby maximizing the pressure at the diamond tips used in slicing. The MBS slicer was further modified by changing the feed system; the feed forces required for wire slicing were considerably lower than used in MBS slicing, hence a more sensitive and reproducible feed mechanism was incorporated. Grooved guide rollers were also installed on either side of the workpiece so that the feed force could be increased as well as to improve the slicing accuracy. With all the modifications to MBS equipment the workpiece size was limited to 4 cm x 4 cm cross-section. The concept of FAST was proven by demonstrating (i) slicing 25 wafers/cm at high yields, (ii) slicing wafers to a thickness as low as 100 μm, (iii) reducing kerf width to as low as 160 μm, (iv) absence of any edge chipping in sliced wafers and (v) surface damage depth of 3-5 μm (3).

Experience with the modified MBS slicer showed some essential parameters which could not be incorporated. A new high speed slicer was designed and fabricated. The essential features of this machine were lightweight bladehead, longer stroke, sensitive feed mechanism, crystal rocking assembly, variable guide roller position and vibration isolation of the drive unit. A schematic of the bladehead is shown in Figure 1. This unit is designed to accommodate up to 30 cm long and 15 cm diameter workpiece. The lighter bladehead and longer stroke allowed faster reciprocation and, consequently higher surface speeds; 130 meter/min has been achieved with this unit as compared to 30 meters/min with the modified MBS unit. A more rigid support system minimized vibrations at these high speeds.

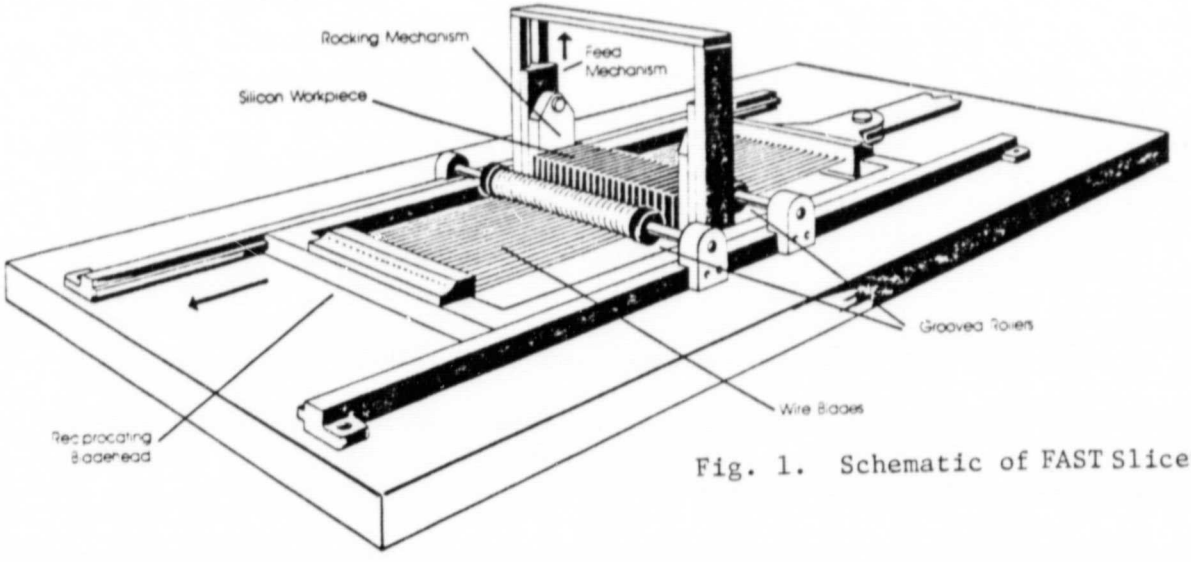

Fig. 1. Schematic of FAST Slicer

The prototype slicer designed is a two-bladehead unit linked to a single drive unit. The two bladeheads will be reciprocated 180° out of phase so that the acceleration forces will be counterbalanced equal and opposite, thereby cancelling each other. This will allow even higher speeds, less vibration and more effective slicing.

Blade Development

In order to slice effectively it is imperative to have a good blade; for FAST slicing it is important to develop effective wire blades. More detailed information on this aspect is discussed in another paper of this conference (5). In the initial stages of FAST development the only fixed abrasive wires available were diamond impregnated wires (6). Testing with these wires showed that they suffered diamond pull-out. Nickel plating of commercially available wires prolonged their life.

A wire-blade development program was, therefore, initiated to produce fixed-abrasive wires for FAST slicing. Two types of approaches were pursued, *viz.*, impregnated blades and electroplated blades. In the former case diamonds were pushed into a soft copper sheath on a high strength core; this wire was then nickel-plated to prevent diamond pull-out. Techniques were developed to impregnate diamonds in the cutting edge only--the bottom half-circumference of the wire. Significant advances were made but this approach needs much more development.

Prior to this program there was no source of electroplated wires. Even though plating of ID blades is carried out in the industry the large surface area-to-volume ratio in the case of wires presented problems. Electroplated wire-blade development has involved optimization of type and size of wire core; coatings on the wire substrate; nature, type and size of diamonds; plating baths, etc. (5). Techniques have also been developed to electroform the diamond plating to reduce kerf and achieve long life of the wirepacks (5).

Testing

The present work is a report on slicing of 10 cm diameter, 10 cm x 10 cm cross-section and 15 cm diameter silicon workpieces at 19 wafers/cm. With 10 cm diameter even 25 wafers/cm have been demonstrated.

One of the first variables studied by FAST was the surface speed. Figure 2 shows slicing tests of 10 cm diameter as a function of surface speed. A comparison of data from Tests A and C shows that by doubling the surface speed the average slicing rate increased from 59 μm/min to 145 μm/min, a factor of 2.45. Test B was carried out using the same wirepack as Test A for a second slicing life test. The average slicing rate for Test B was 122 μm/min, a slight decrease showing deterioration of cutting effectiveness. The data in Figure 3 is for slicing tests using a mixture of 15, 30 and 45 μm diamond size electroplated wirepack spaced at 19 wires/cm and shows a life of three 10 cm diameter ingots at an average cutting rate of 127, 82 and 75 μm/min. The surface speed during this experiment was 120 meters per minute.

Figure 4 shows the slicing test carried out using the same electroplated wirepack. The diamond size used was 30 μm and the surface speed of the FAST

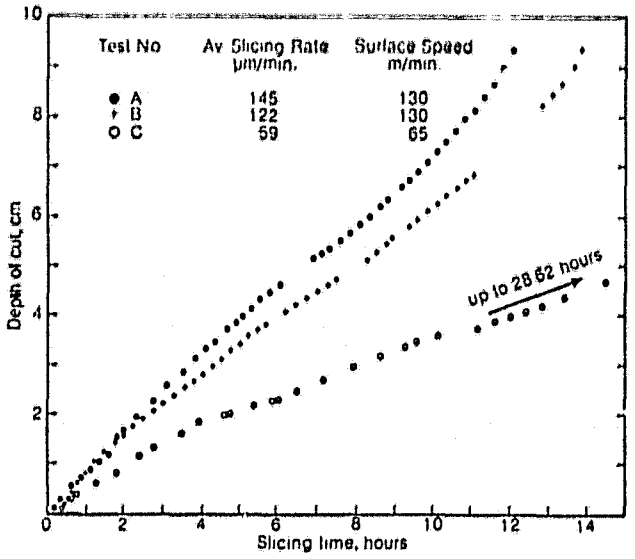

Fig. 2. Slicing performance showing the effect of surface speed

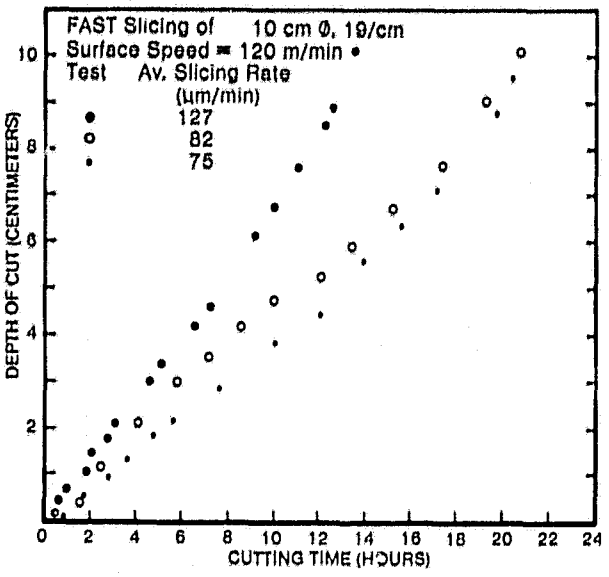

Fig. 3. Slicing of three 10 cm Ø ingots using same electroplated wirepack

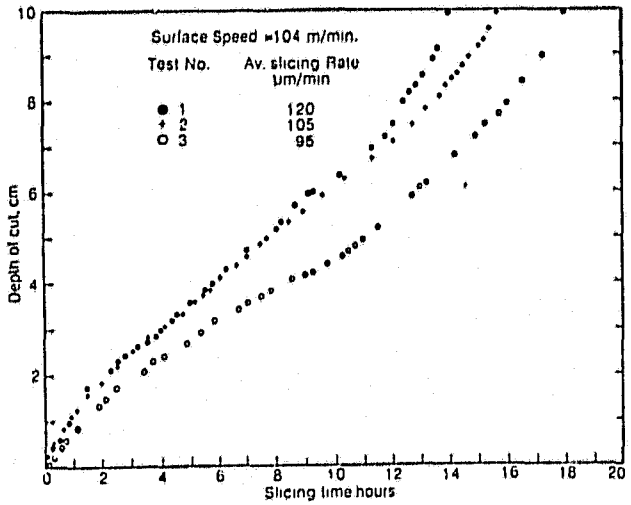

Fig. 4. Slicing performance from the same wirepack using 30 µm diamonds

slicer was 104 meters per minute. The average slicing rate for tests 1, 2 and 3 were 120, 105 and 95 µm/min respectively.

A similar test with wires impregnated with 45 µm diamonds showed an average slicing rate of 72 µm/min on a 10 cm diameter workpiece. These wires could not be used for a second slicing test; in fact toward the end of the first test wafer breakage was observed which was attributed to loss of cutting effectiveness.

In order to reduce the kerf width for slicing 25 wafers/cm a 30 µm diamond electroplated wirepack was used. During the first test a 99.1% yield (222 out of 224, 10 cm diameter wafers) was achieved with an average slicing rate of 77 µm/min. In this test low feed forces of only 24.4 gms/wire were used. Very good surface quality of wafers was achieved and the average wafer thickness of 0.195 mm with a kerf of 0.205 mm. During the second slicing test the average slicing rate dropped to 45 µm/min and the yield was only 36.2%. The average wafer thickness increased to 0.249 mm with kerf of 0.151 mm. The data shows that during the first slicing test considerable diamonds from the sides of the wires were pulled out, thereby reducing kerf, increasing wafer thickness and decreasing the average slicing rate. The plot of the depth of cut with time is shown in Figure 5.

Slicing tests with 15 cm diameter silicon workpiece were also carried out. For the larger kerf length 60 µm natural diamonds were electroformed into a

V-shape so that the diamonds were fixed only in the cutting edge of the wires. The average slicing rate was 74 μm/min. This is considerably higher wafering rate especially in view of the larger kerf length. During the test some wire wander was observed because the diamonds on the top surface of the wires could not be completely eliminated. The non-uniform nature of the top surface caused perturbation and, therefore, the wires did not seat well in the guide rollers. The data for this run is shown in Figure 6.

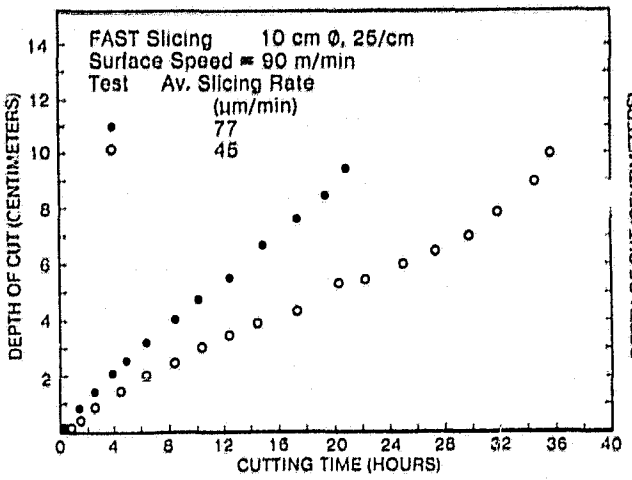

Fig. 5. Slicing results of 10 cm Ø ingots at 25 wafers/cm

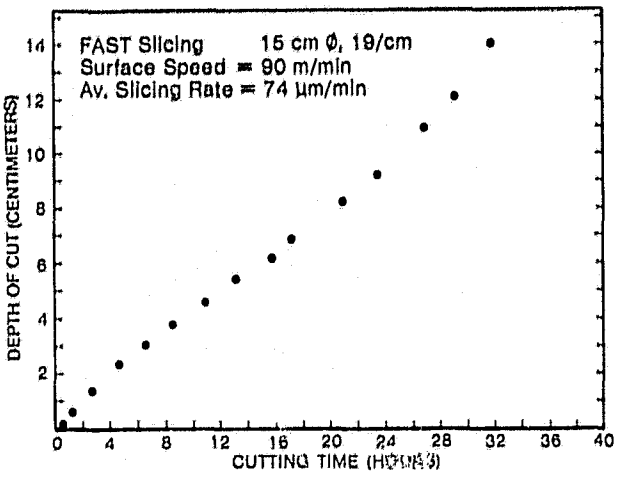

Fig. 6. Slicing performance of 15 cm Ø ingot

ECONOMIC ANALYSIS

The economic analysis has been carried out to estimate the projected add-on price of FAST slicing using IPEG methodology (7). It is intended to use a FAST slicer with two bladeheads reciprocating 180° out of phase. Each bladehead will slice a 10 cm x 10 cm x 30 cm bar to produce wafers of 10 cm x 10 cm cross-section. Two types of scenarios were developed, a conservative and an optimistic case, to estimate the projected price. The assumptions and the final add-on price are shown in Table II. Even in the conservative case the final value is less than half of the price allocation (8) for ingot technologies to meet DOE price goal of $0.70/peak watt in 1986.

CONCLUSION

The Fixed Abrasive Slicing Technique (FAST) combines the low expendable materials advantage of ID, low equipment and labor costs of MBS and high material utilization of MWS. Besides FAST produces a wafer which shows no edge chipping and with a surface damage of only 3-5 μm. This new slicing technique was initially developed by modifying a MBS slicer. After establishing the proof of concept a high speed slicer was designed and fabricated.

Techniques were developed to produce wirepack with equal spacing and tension. The wire-blade development program has involved impregnation and electroplating techniques. It has been shown that diamonds can be fixed only in cutting edges of wires. With electroforming it has been possible to control the shape and size of the plating.

Slicing effectiveness has been demonstrated on 10 cm and 15 cm diameter ingots. It has been possible to slice 25 wafers/cm on 10 cm diameter ingots and 19 wafers/cm on 15 cm diameter ingots. A blade life of slicing three 10 cm diameter ingots has been demonstrated.

Projected economic analysis has shown that the FAST technique will be able to slice silicon ingots effectively to meet the DOE price allocation for 1986 goal of $0.70 per peak watt.

TABLE II. IPEG ANALYSIS FOR VALUE ADDED COSTS OF FAST SLICING USING CONSERVATIVE AND OPTIMISTIC PROJECTIONS OF TECHNOLOGY

	Estimate	
	Conservative	Optimistic
Equipment cost, $	30,000	30,000
Floor space, sq.ft.	80	80
Labor, units/operator	5	10
Duty cycle, %	90	95
Set-up time, hrs	1.5	1.0
Slicing rate, mm/min	0.1	0.14
Slices/cm	22	25
Yield	90	95
Expendables/run, $	28	14
Motor power, h.p.	5	3
Conversion ratio, m^2/kg	0.85	1.0
Add-on Price, $\$/m^2$	13.13	5.9

*Supported in part by the LSA Project, JPL, sponsored by DOE through agreement with NASA.

REFERENCES

1. F. Schmid and C. P. Khattak, ERDA/JPL 954373, Final Report (Phase I), December 1977.

2. M. H. Leipold, C. Radics, and A. Kachare, "Cost of Czochralski Wafers as a Function of Diameter," JPL Publication 80-25, February 15, 1980.

3. C. P. Khattak and F. Schmid, Proc. 2nd. Photovoltaic Solar Energy International Conf., Berlin (West), (1979).

4. T. Daud, J. K. Liu, G. A. Pollock and K. M. Koliwad, Proc. 13th IEEE Photovoltaic Specialists Conf., Washington (1978).

5. C. P. Khattak, F. Schmid and M. B. Smith, Proc. JPL/LSA Project Wafering Workshop, Phoenix, AZ, June 1981, to be published.

6. Laser Technology, Inc., No. Hollywood, CA.

7. Interim Price Estimation Guidelines, JPL Document 5101-33, September 10, 1977.

8. Aster, R. W., "Price Allocation Guidelines, January 1980," JPL Publication 80-51, January 15, 1980.

5101-187
Low-Cost
Solar Array Project

DOE/JPL-1012-66
Distribution Category UC-63b

Proceedings of the Low-Cost Solar Array Wafering Workshop

(8-10 June, 1981, The Pointe, Phoenix, Arizona)

Wire-Blade Development for Fixed Abrasive Slicing Technique (FAST) Slicing

Chandra P. Khattak
Frederick Schmid
Maynard B. Smith

February 1, 1982

Prepared for
U.S. Department of Energy
Through an Agreement with
National Aeronautics and Space Administration
by
Jet Propulsion Laboratory
California Institute of Technology
Pasadena, California

(JPL PUBLICATION 82-9)

WIRE-BLADE DEVELOPMENT FOR FIXED ABRASIVE SLICING TECHNIQUE (FAST) SLICING*

Chandra P. Khattak, Frederick Schmid and Maynard B. Smith

Crystal Systems, Inc.
35 Congress Street, Salem, MA 01970

ABSTRACT

A low-cost, effective slicing method is essential to make ingot technology viable for photovoltaics in terrestrial applications. The Fixed Abrasive Slicing Technique (FAST) is a new slicing process which combines the advantages of the three commercially developed techniques. In its development stage FAST has demonstrated cutting effectiveness of 10 cm and 15 cm diameter workpieces by slicing 25 and 19 wafers/cm respectively. Even though significant progress has been made in the area of wire-blade development it is still the critical element for commercialization of FAST technology. Both impregnated and electroplated wire blades have been developed; techniques have been developed to fix diamonds only in the cutting edge of the wire. Electroplated wires show the most near-term promise; hence the emphasis has been placed on this approach. With plated wires it has been possible to control the size and shape of the electroplating--this feature is expected to reduce kerf and prolong the life of the wirepack.

INTRODUCTION

The Fixed Abrasive Slicing Technique (FAST) makes most ingot technologies viable for photovoltaic applications. Compared with current wafering methods --Internal Diameter (ID), Multiple Blade Slurry (MBS) and Multiple Wire Slurry (MWS) processes--the FAST approach offers the potential of lowest add-on cost (1). FAST uses diamond fixed on wires in a multiple-wire pack configuration for slicing silicon. This new technique was made feasible by developing a method for making bladepacks with equal wire spacing and tension and a higher speed reciprocating slicer. The development of FAST is being discussed in another paper at this conference (2). At the present time a preprototype slicer designed for FAST slicing is being optimized. Significant progress has been made in the area of wire blade development but it is still the critical element for commercialization of FAST technology.

For any ingot technology to be cost effective for photovoltaic applications, it has to be combined with a low-cost slicing method. Kerf loss and ingot utilization (kerf plus slice) are major considerations in silicon sheet cost. An economic analysis (3) of silicon slicing has indicated that the ingot utilization considerations limit the cost reduction potential of the ID technology. This analysis also showed that the expendable materials costs, slurry and blades, dominate the wafering costs of MBS. Demonstration tests (4) of MWS method has shown that lowest kerf widths are obtained with wire slicing. However, the cost of the wire is even more than the slurry costs, thereby increasing the expendable materials costs of MWS even more than the MBS process.

In FAST a pretensioned, fixed-diamond, multiple-wire pack is reciprocated similar to the MBS process to slice through the workpiece. The multi-wire FAST approach combines the economic advantages of ID, MBS and MWS techniques. Expendable materials costs are low as in ID slicing, capital equipment and labor costs are low as in MBS slicing, and material utilization is high as in MWS wafering.

ADVANTAGES AND REQUIREMENTS OF FAST WIREPACKS

Aside from the economic advantages, there are technical advantages of using multi-wire FAST approach:

(1) Due to the symmetry, wires do not torque the wafers after slicing as in the case of flat blades; this allows for less clearance and, therefore, reduced kerf width.

(2) In case of wire breakage only two wafers contacting that wire are lost.

(3) The diamonds fixed on the wire prevent wire wear, hence wire and abrasive cost is minimized.

(4) No fatigue problems occur because wire is not wrapped around rollers.

(5) Wires are cheap to fabricate to a higher dimensional accuracy and uniformity.

(6) No corrosion problems occur since the wires are nickel or copper plated.

(7) Wires can be pretensioned to higher stresses.

(8) Wires do not buckle under high feed forces.

(9) Slicing is carried out under low feed forces resulting in low surface damage.

(10) Wafers produced show no edge chipping problems.

The essential requirements of wirepacks used for FAST slicing are:

(1) The wires must be clamped to prevent slippage and must be with equal tension and spacing in the bladepack.

(2) Wire core must have high yield strength and modulus for minimum deflection.

(3) Diamonds must be fixed on wire with high, uniform concentration.

(4) Prevent erosion of the matrix holding the diamonds.

(5) Diamonds must exhibit long life and high cutting rates.

(6) Wire diameter must be minimum to reduce kerf.

(7) Minimized wander for accurate slicing.

(8) Prevent corrosion between the matrix holding the diamonds and the core material.

In the above tabulation the first requirement is related to fabrication

of wirepack and the rest relate to properties of wire, matrix and procedures for fixing diamonds onto wires. Simple fabrication procedures have been developed which give the wires equal spacing and tension with no problems of cumulative errors. After evaluation of various core materials (5) a selection was made to use high strength steel, stainless steel and tungsten. High strength steel and stainless steel wires were selected based on high yield strength and tungsten on the basis of its high modulus. Most of the work was carried out with a 5 mil (0.125 mm) tungsten wire because of its high modulus and corrosion resistance.

Two approaches were pursued in fixing diamonds, *viz.* impregnated wires and electroplated wires. In the former case diamonds were impregnated into a soft copper sheath on the core wire, whereas in the latter case diamonds were fixed by electroplating.

IMPREGNATED WIRES

Commercially available impregnated wire (6) was 5 mil (0.125 mm) stainless steel core with a 1.5 mil (37.5 μm) copper sheath impregnated with 45 μm natural diamonds. Slicing with this wire showed that cutting effectiveness was lost within approximately 0.25 inch depth of cut. Examination of the wires showed considerable diamond pull-out. Electroless nickel plating of these wires reduced the diamond pull-out considerably. It was found that nickel plating thickness of 0.3 mil (7.5 μm) produced best results; a nickel layer of 12.5 μm was sufficient to bury the diamonds. A wafering experiment of a 10 cm diameter silicon workpiece with 114 parallel wires spaced at 19/cm with these wires showed an average slicing rate of 2.33 mils/min (0.059 mm/min) and produced a 96.5% yield.

Impregnation techniques developed within Crystal Systems showed that it was possible to impregnate diamonds in the cutting edge of the wires only in an area less than the bottom half circumference of the wires. Figure 1 shows a cross section of such a wire. Natural diamonds of 45 μm size were impregnated into a 1.5 mil (37.5 μm) copper sheath on a 5 mil (0.125 mm) stainless steel core wire. A 0.3 mil (7.5 μm) electroless nickel layer was plated after impregnation. Slicing tests using wirepacks with diamonds impregnated in the cutting edge only improved the average slicing rate to about 3 mils/min (0.075 mm/min) and reduced the kerf. This approach also allowed use of 60 μm diamonds without significantly adding to kerf. The advantages of diamonds in the cutting edge only are:

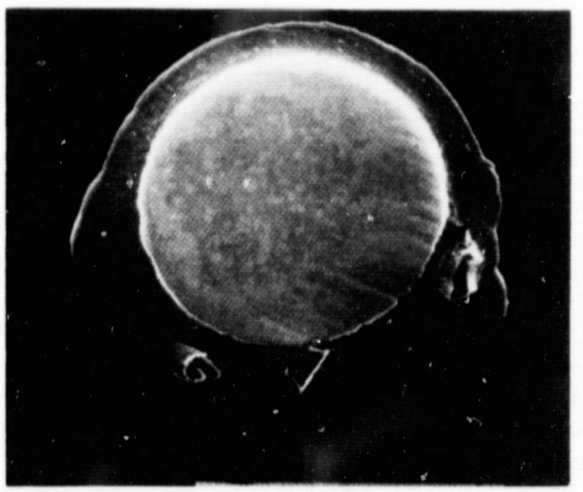

Fig. 1. Cross-section of wire with diamonds impregnated in cutting edge only

(1) Lower kerf.

(2) Use larger diamonds.

(3) Ability to add more than one layer with marginal increase in kerf.

(4) Minimize degradation of guide rollers in the FAST slicer.

(5) Better seating of the wires in the grooved guide rollers.

(6) Improved accuracy of slicing because of absence of diamonds on the sides of the wires.

(7) Minimize wire wander when diamonds in the cutting edge are somewhat "dulled".

Even though significant progress has been made with impregnated wires considerable effort has to be devoted towards achieving high concentration of diamonds with good uniformity and preventing diamond pull-out during slicing.

ELECTROPLATED WIRES

At the start of this program electroplated wires were not commercially available. Initial work was carried out in cooperation with various plating vendors.

Choice of Core Wire

It was found that the core wire used as a substrate was very important to achieve plating with a good bond between the nickel matrix and the core substrate. Plating on steel caused embrittlement which resulted in considerable wire breakage during slicing. Difficulties in cleaning procedures prior to plating of tungsten necessitated the use of a thin nickel flash on the core wire prior to use as a substrate. Figure 2 shows the longitudinal and cross-section of electroplated wires using (A) a copper flash and (B) a nickel flash on tungsten core wires. It can be seen that the longitudinal sections show a high concentration of diamonds. Examination of the cross-sections shows corrosion problems in the copper flash layer which is not existent in the case of the nickel flash wire. No such problems were evidenced in plating directly onto a stainless steel substrate (Figure 3). Emphasis was placed on using nickel flash tungsten core 5 mil (0.125 mm) in diameter; recently procedures were developed in plating copper-flash, high-strength steel wires without embrittlement problems.

Choice of Diamonds

With fixed diamond it is very important to establish a speed-pressure relationship at the diamond tip for effective slicing. Rocking of the workpiece in FAST increases the pressure by decreasing the contact length; however, the diamond type and size needs to be optimized. Both natural and synthetic variety are available. In the synthetic type the choice is blocky, explosively formed, EDC, Man-Made (7), etc. The various varieties also include tough and friable; while the former stand up to slicing conditions without breakdown, the latter breaks down and exposes new surfaces for higher cutting rates. Under similar conditions of slicing to date the natural diamonds gave better results than the blocky type. An SEM of the two varieties is shown in Figure 4.

Besides the diamond type a choice has also to be made for diamond size. The larger particles are desirable for long life and higher cutting rates;

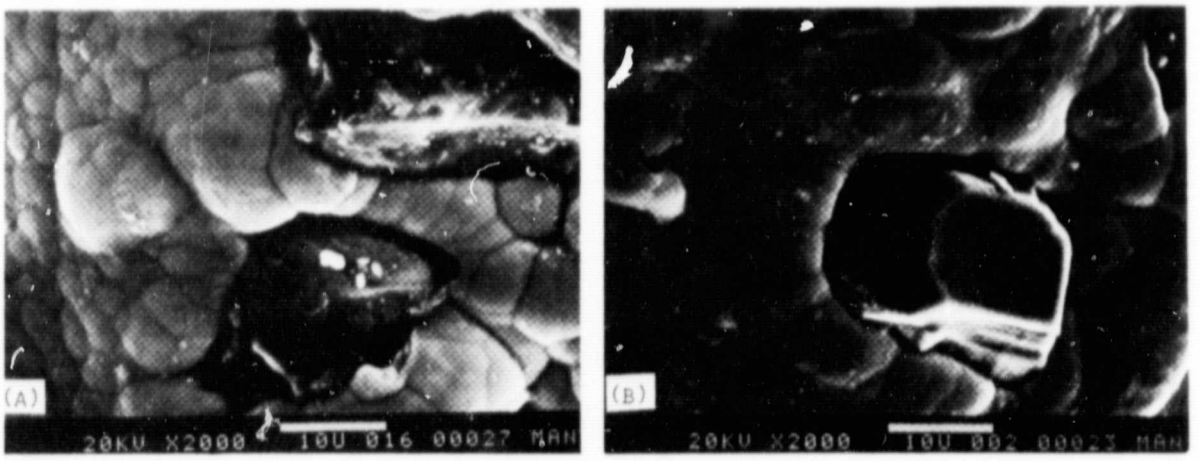

Fig. 4. SEM examination of electroplated wires with (A) natural diamonds showing sharp edges and (B) synthetic diamond showing blocky characteristic

however, they have larger kerf. The choice in particle size is, therefore, limited to the 22 μm to 60 μm range. Effective slicing has been demonstrated for the entire range with diamonds electroplated over the entire circumference. The lowest kerf of 6.2 mils (0.157 mm) was achieved with 22 μm diamonds. Best material utilization by slicing 25 wafers/cm on 10 cm diameter silicon was demonstrated by using 30 μm diamonds. The longest life wafering three 10 cm diameter ingots with the same wirepack has been with 45 μm size. Very limited experiments have been conducted with 60 μm diamonds plated over the entire circumference because the large kerf makes it impractical to slice 19 and 25 wafers per cm of silicon length with a 10 cm diameter workpiece.

With larger diamond particles or when low concentration is achieved by electroplating, the swarf generated during slicing tends to erode the matrix thereby pulling off diamonds from the wires. The concentration of diamonds to prevent erosion has to be such that the inter-particle distance is less than the size of the particle. Electroplating of wirepacks with 45 μm diamonds and small amounts of 30 μm and 15 μm diamonds has shown improved slicing effectiveness. The larger diamonds tend to slice and the smaller ones act as fillers to prevent erosion of matrix. This condition can be achieved by using screened rather than micronized diamonds. Examination of the swarf has shown the mean particle size to be about 0.5 μm and is not dependent on the size of diamonds in the range studied.

ELECTROFORMING

In order to effectively slice silicon for photovoltaic applications the wirepack fabricated should combine (i) low kerf, (ii) high density of spacing of wires, (iii) high slicing rate, (iv) long life of the wirepack and (v) high yields during slicing. The first two criteria are possible by using small diamonds; however, for the next two criteria larger diamonds may be desirable. For example, where 45 μm diamonds were plated all over the circumference of the wire, the minimum kerf achieved was about 8 mils (0.2 mm), whereas it was 6.2 mils (0.157 mm) with 22 μm size. In impregnated wires where diamonds were impregnated only in the cutting edge of the wires a compromise was arrived at

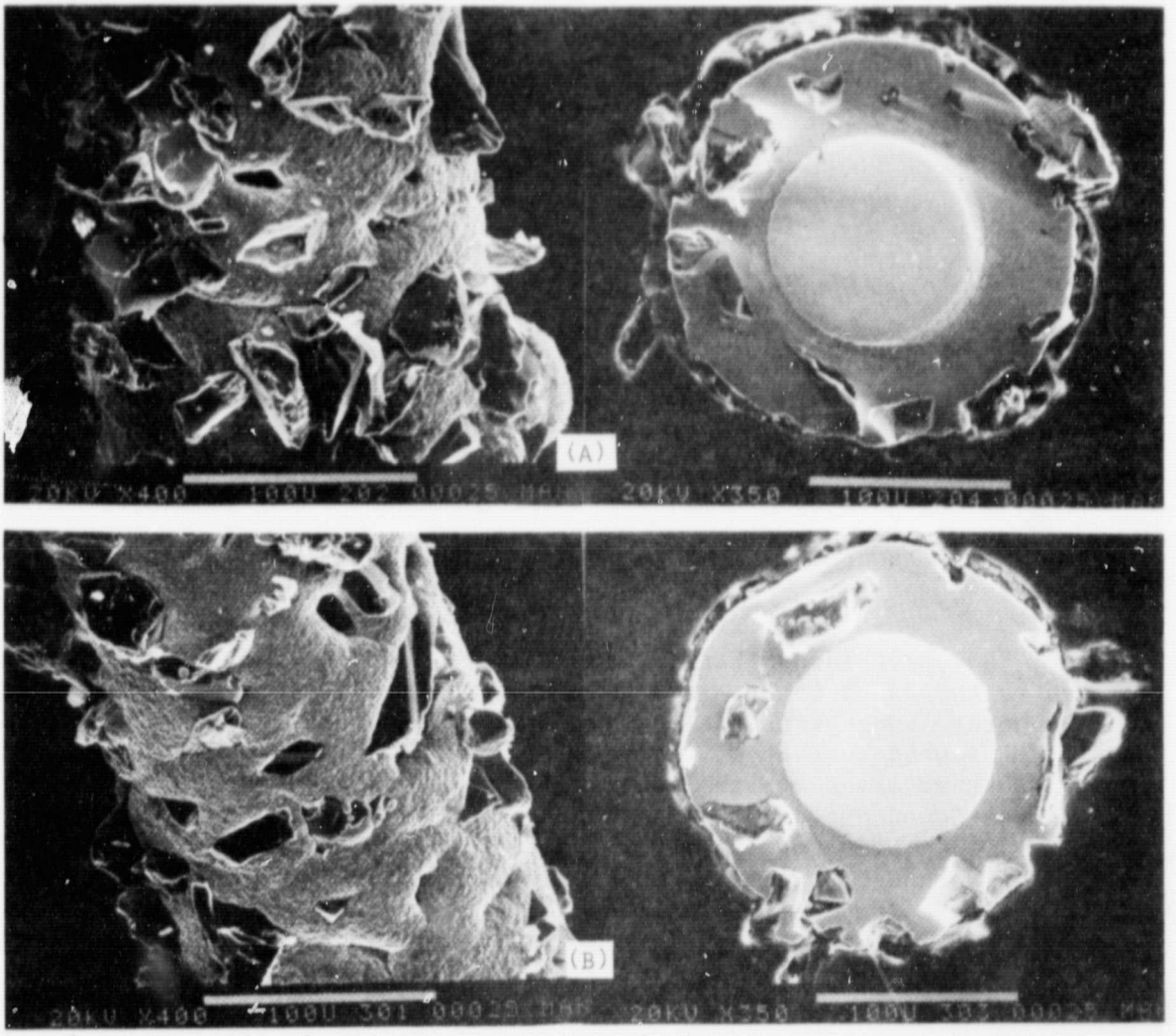

Fig. 2. Longitudinal and cross-section of electroplated wires using tungsten core with (A) copper flash and (B) nickel flash

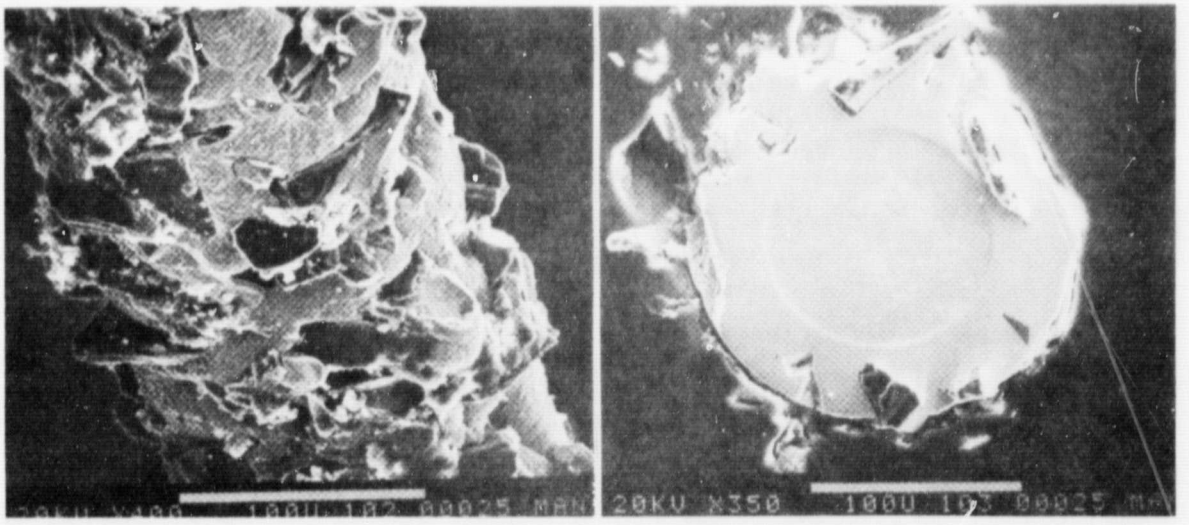

Fig. 3. Longitudinal and cross-section of an electroplated wire using stainless steel core

where larger diamonds could be used without significant increase in kerf. Techniques were developed where diamonds were electroplated in the cutting edge only and, therefore, benefits could be derived by using larger diamonds and maintaining a low kerf.

Masking of the wires during electroplating produced a flat top surface of the wires which did not seat in the guide rollers and, therefore, caused wire wander. Techniques were developed at Crystal Systems to electroplate diamonds and nickel in a form of desired shape and size, *i.e.*, electroform the plating. Figure 5 is three views of a wire rotated 120° where diamonds are electroplated by the electroforming technique. Figure 6 is a cross-section of a wire which was electroplated preferentially in a 60° V-groove. Under these conditions larger size diamonds can, therefore, be electroformed in any desired shape and size. If smaller diamonds are used plating only on the cutting edge allows more than a single layer of diamonds to be plated and the kerf width can still be controlled to the desired size.

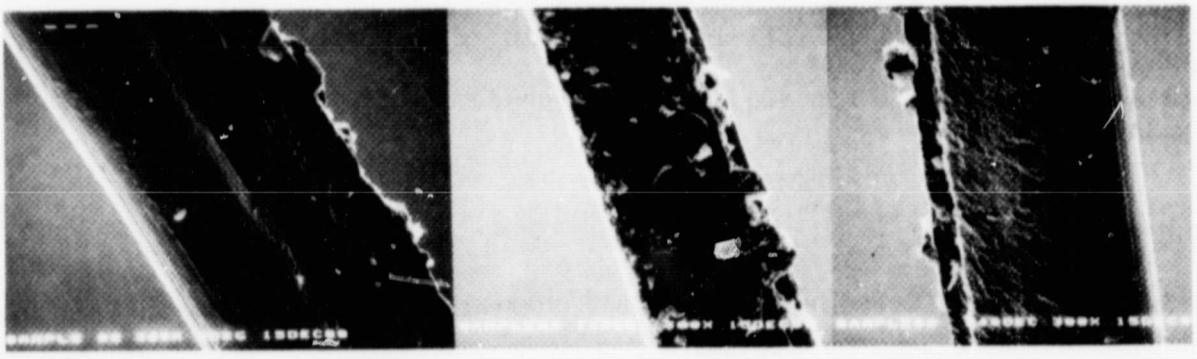

Fig. 5. Three views of an electroformed wire showing preferential plating on cutting edge only

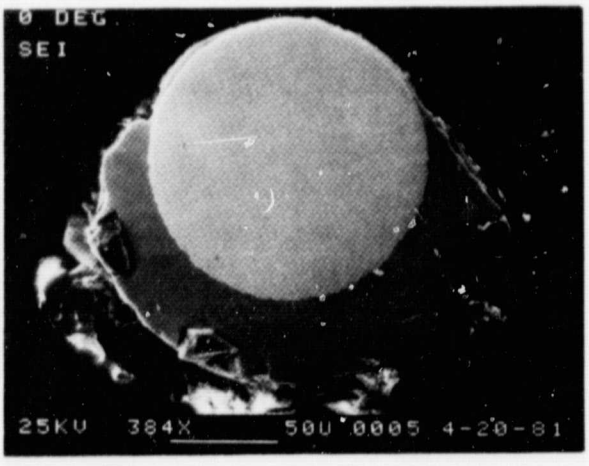

Fig. 6. Cross-section of an electroformed wire with plating in desired shape and form

RESULTS

The feasibility of using FAST for photovoltaic applications has been demonstrated. Wire-blade development has been found to be critical to commercialization of FAST. Control of the diamond plating on wires has shown effective slicing of 10 cm diameter silicon ingots at 25 wafers/cm with 224 wires in a wirepack at an average slicing rate of 3.03 mils/min (0.077 mm/min), and over 99% yield (2). It has been shown that the slicing rate is a strong function of the reciprocating speed of the bladehead; average cutting rates of 5.7 mils/min (0.145 mm/min) have been demonstrated. Wirepack life of wafering three 10 cm diameter silicon ingots has been shown. Effective slicing of 10 cm x 10 cm and 15 cm diameter cross-section ingots has also been carried out.

Electroforming techniques have been demonstrated on individual wires. Tooling for performing these tests on wirepacks has recently been received in-house; it is expected that this approach will increase the life of the wirepack considerably as well as optimize other slicing parameters.

*Supported in part by the LSA Project, JPL, sponsored by DOE through agreement with NASA.

REFERENCES

1. H. Goldman and M. Wolf, DOE/JPL 954796, Quarterly Report, November 1978.

2. F. Schmid, M. B. Smith, and C. P. Khattak, Proc. JPL/LSA Project Wafering Workshop, Phoenix, AZ, June 1981, to be published.

3. K. M. Koliwad, M. H. Leipold, G. D. Cumming and T. G. Digges, Jr., Proc. 12th IEEE Photovoltaic Specialists Conf., Baton Rouge, LA (1976).

4. C. P. Chen, "Multi-Wire Slurry Wafering Demonstrations," DOE/JPL Publ. 78-37, February 22, 1978.

5. F. Schmid and C. P. Khattak, ERDA/JPL 954373, Final Report (Phase I), December 1977.

6. Laser Technology, Inc., No. Hollywood, CA.

7. EDC and Man-Made are trademarks of DeBeers and General Electric Company, respectively.